Catalytic Reforming of Higher Hydrocarbon Fuels to Hydrogen:

Process Investigations with Regard to Auxiliary Power Units

Zur Erlangung des akademischen Grades eines

DOKTORS DER NATURWISSENSCHAFTEN

(Dr.rer.nat.)

Fakultät für Chemie und Biowissenschaften

Karlsruher Institut für Technologie (KIT) – Universitätsbereich

genehmigte

DISSERTATION

von

Dipl.-Chem. Torsten Kaltschmitt

aus Leimen (Baden)

Dekan: Prof. Dr. Martin Bastmeyer

Referent: Prof. Dr. Olaf Deutschmann

Korreferent: Prof. Dr. Jan-Dierk Grunwaldt

Tag der mündlichen Prüfung: 20.Juli 2012

2012

Meinen Eltern

“Wenn du schnell gehen willst, geh allein.

Wenn du weit gehen willst, geh mit anderen“

(südafrikanische Weisheit)

Abstract

This thesis discusses the investigation of the catalytic partial oxidation on rhodium-coated honeycomb catalysts with respect to the conversion of a model surrogate fuel and commercial diesel fuel into hydrogen for the use in auxiliary power units. CPOx on monolithic catalysts allows the autothermal production of large quantities of hydrogen at millisecond contact times. Various logistic fuels can be converted efficiently to hydrogen, allowing the supply of fuel cells by means of the today's infrastructure.

A new fuel feeding concept was developed and is introduced for the management of high-boiling logistic fuels. Defined transition of the liquid fuel into the gaseous phase even for temperatures above the auto-ignition point and mixing with a multitude of reactants allows the investigation of defined technical reformer parameters under accurate boundary conditions with time-resolved resolution. The set-up allows transient and steady-state experiments under varying reaction conditions with computer-assisted reproducible precision and reliability.

Two different problems arising during the CPOx reaction of higher hydrocarbons have been evaluated. Beginning with isooctane as model fuel, the significance of gas-phase reactions in the catalytic partial oxidation at short contact times and high temperatures was identified and studied in experimental and numerical terms. Special attention was given to the formation of coke precursors downstream the oxidizing catalyst zone. Two different kinds of carbon deposition zones deriving from different carbon formation pathways were identified during the slightly fuel-rich operated CPOx reaction, initiated by thermal cracking reactions of unconverted fuel as a function of temperature, feed composition, and residence time.
Furthermore, die influence of certain amounts of both water and carbon dioxide were investigated over a broad range of concentrations for a CPOx reformer operating with isooctane. The experiments investigate the change in the chemical behavior for the reformer unit, when tail-gas is partly recycled from a fuel cell's exhaust gas due to practical issues. The specific impact of water and/or carbon dioxide on the reformer's behavior can be interpreted by the water-gas shift chemistry and, in parts, by steam reforming. Syngas composition is not dramatically affected but the formation of soot precursors can

significantly be reduced, preventing the reformer from coking, even at decreased fuel conversion. However, tail-gas recycling shifts the occurrence of soot precursors towards lower C/O ratios, which is untypical for isooctane CPOx.

Commercial diesel fuel was investigated for most interesting C/O regimes in CPOx operation. Pulse-free fuel feeding without pre-combustion allows the detailed and time-resolved investigation of a logistic hydrocarbon fuel more with respect to the chemical reaction. The results revealed a rather close operation window for diesel fuel and coke formation was assigned to methane cracking even at reaction conditions, where no soot precursors were present, at temperatures close to 1450 K.

Kurzfassung

Die hier vorgelegte Dissertation behandelt die Untersuchung der katalytischen Partialoxidation (CPOx) an mit Rhodium beschichteten Wabenkörpern bezüglich der Umsetzung eines Modelkraftstoffes sowie Dieseltreibstoff zu Wasserstoff für den Einsatz in mobilen Stromerzeugern. Die katalytische Partialoxidation erlaubt die autotherme Erzeugung großer Mengen an Wasserstoff bei nur wenigen Millisekunden Kontaktzeit. Die effiziente Umsetzung verschiedenster Kraftstoffe hin zu Wasserstoff erlaubt die Versorgung von Brennstoffzellen mittels der heutigen Versorgungsnetze.

Es wurde ein neues Konzept für die Bereitstellung und Handhabung von schwerflüchtigen Kraftstoffen entwickelt, mit dem eine Überführung des Kraftstoffes in die Gasphase auch oberhalb der Zündtemperaturen unter definierten Bedingungen möglich ist. Das gleichzeitige Mischen mit verschiedensten Reaktivkomponenten erlaubt die zeitaufgelöste Untersuchung chemischer Prozesse von nachgestellten, relevanten Betriebszuständen von technischen Reformen unter genau definierten Randbedingungen. Die Anlage erlaubt die betriebssichere Durchführung sowohl instationärer als auch stationärer Betriebszustände mit computergestützter, wiederholbarer Genauigkeit.

In dieser Arbeit wurden zwei Probleme der katalytischen Partialoxidation höherer Kohlenwasserstoffe untersucht. Beginnend mit dem Modelkraftstoff Isooktan wurde die Bedeutung von Gasphasenreaktionen, welche innerhalb der katalytischen Partialoxidation bei kurzen Kontaktzeiten und hohen Temperaturen auftreten, experimentell und numerisch untersucht. Besonderes Augenmerk lag hierbei auf der Bildung von Kohlenstoff-Vorläuferverbindungen flussabwärts der im Katalysator auftretenden Oxidationszone. Es wurden zwei unterschiedliche Kohlenstoffablagerungsbereiche identifiziert, welche auf verschiedene Kohlenstoffbildungswege zurückzuführen sind. Beiden Ablagerungen geht die thermische Zersetzung von unverbrauchtem Kraftstoff unter leicht kraftstoffreichen Betriebsbedingungen voran, die als Funktion der Temperatur, der Edukt-Zusammensetzung sowie der Verweilzeit untersucht wurde.
Weiterhin wurde der Einfluss der Zugabe von Wasser und Kohlenstoffdioxid zum Eduktstrom eines mit Isooktan betriebenen CPOx Reformer untersucht. Die Experimente

veranschaulichen den Einfluss von teilweise rückgeführtem Abgas einer Brennstoffzelle auf das chemische Verhalten des Reaktors über einen weiten Konzentrationsbereich, wobei der Haupteinfluss von sowohl Wasser als auch Kohlenstoffdioxid mit Hilfe der Wassergas-Shift Reaktion erklärt werden kann. Die Ergebnisse zeigen nur einen geringen Anteil an Wasserdampfreformierung. Die Abgasrückführung zeigt einen nur mäßigen Einfluss auf die Synthesegaszusammensetzung, mindert jedoch die Bildung von Kohlenstoff-Vorläuferverbindungen in erheblichem Maße trotz verminderter Kraftstoffumsetzung. Dadurch können Kohlenstoffablagerungen innerhalb des Reformers vermindert werden. Allerdings treten die jeweiligen Vorläuferspezies bereits bei niedrigeren C/O Verhältnissen auf, als es für einen mit Isooktan betriebenen Reformer typisch ist.

Die Bereitstellung von kommerziellem Dieselkraftstoff konnte realisiert und die Umsetzung im Bereich relevanter C/O Verhältnisse für die katalytische Partialoxidation untersucht werden. Eine fluktuationsfreie Zuführung von Dieselkraftstoff erlaubte dessen detaillierte und zeitaufgelöste Untersuchung. Die durchgeführten Untersuchungen zeigen ein sehr enges Betriebsfenster für Dieselkraftstoff auf, mit Betriebstemperaturen von maximal 1450 K am Katalysatorausgang. Die Bildung von Kohlenstoffablagerungen kann auf thermische Zersetzung von Methan zurückgeführt werden in Bereichen, in denen keine Vorläuferverbindungen aufgetreten sind.

Table of content

1 Introduction 1
1.1 Hydrogen as Future Energy Carrier 1
1.2 Concept of an Auxiliary Power Unit (APU) 4
2 Objectives of this Work 10
2.1 Influence of Gas-phase Reactions Downstream the Catalyst (Study 1) 12
2.2 Tail-gas Recycling for a Simulated SOFC Anode Exhaust Gas (Study 2) 14
2.3 Diesel Fuel Handling under Defined Pulse-free Boundary Conditions (Study 3) 15
3 Fundamentals of Heterogeneous Catalysis relevant for this Work 18
3.1 Introduction 18
3.2 Modeling of Heterogeneous Catalysts in Chemical Reactors 20
3.2.1 Chemical Reactions 22
3.2.2 Mean-Field Approximation 24
3.2.3 Reactive Flow-field 26
3.2.4 Coupling of Chemical Reactions with the Flow-field 29
3.2.5 Detailed Modeling and its Limitations 31
4 Experimental Setup 32
4.1 Concept for Feeding High-boiling Fuel into the Reactor 32
4.2 Description of the Reactor Unit 36
4.3 Catalysts used 41
4.3.1 Monolithic Supports 41
4.3.2 Model Catalyst 42
4.4 Analytical Set-up 45
4.4.1 Fourier Transformation Infrared Spectroscopy 45
4.4.2 Mass Spectrometry 47
4.4.3 Paramagnetic Oxygen Detection 48
4.5 Method of Internal Standard for Total Flow Determination 49
4.5.1 Total Flow Determination 49
4.5.2 Error Consideration 52
4.6 Used Materials 54
4.7 General Start-up of the Reactor and Ignition of the Catalytic Reaction 55
5 Influence of Gas-phase Reactions Downstream the Reforming Catalyst (Study 1) 57

5.1 Accomplishment of Study 1 ... 57
5.2 Modeling Approach ... 60
5.3 Results and Discussion ... 62
5.4 Summary and conclusion for Study 1 ... 70
6 Tail-gas Recycling of a Simulated SOFC Anode Exhaust Gas (Study 2) ... 72
6.1 Accomplishment of Study 2 ... 72
6.2 Results ... 74
6.2.1 Effect of H_2O as a Co-feed – Case 1 ... 74
6.2.2 Effect of CO_2 as a Co-feed – Case 2 ... 87
6.2.3 Effect of H_2O and CO_2 as a Co-feed – Case 3 ... 88
6.3 Discussion ... 89
6.3.1 Effect on Reactor Outlet Temperature ... 89
6.3.2 Effect on Main Product Distribution ... 90
6.3.3 Effect on Formation of Side-Products (Methane, Ethylene, Propylene) ... 94
6.3.4 Effect on Coke Formation ... 104
6.4 Summary and Conclusion for Study 2 ... 110
7 Catalytic Partial Oxidation of Diesel Fuel (Study 3) ... 112
7.1 Accomplishment of Study 3 ... 113
7.2 Results and Discussion ... 116
7.2.1 Experiments with 80 % Nitrogen Dilution – Case 1: ... 117
7.2.2 Experiments with Synthetic Air Mixture – Case 2: ... 124
7.3 Summary and Conclusions for Study 3 ... 128
8 Summary and Overall Conclusions with Regard to the APU Concept ... 130
9 References ... 136
A. List of abbreviations ... ii
B. List of symbols ... iii
C. Auxiliary Power Unit ... vi
C.1. Fuel Requirements for APUs ... vi
C.1.1. Primary Fuels Derived from Coal ... ix
C.1.2. Primary Fuels Derived from Crude Oil ... ix
C.1.2.1. Liquefied Petroleum Gas ... xi
C.1.2.2. Gasoline ... xi
C.1.2.3. Diesel Fuel ... xii
C.1.2.4. Kerosene ... xv
C.1.3. Primary Fuels Derived from Natural Gas ... xv

C.1.3.1. Propane / Butane and LPG xvii
C.1.3.2. Methanol xviii
C.1.3.3. Ethanol xix
C.1.4. Primary Fuels Derived from Biomass xx
C.1.4.1. Biodiesel xxi
C.2. Fuel Processing in APUs – Fuel Processors xxiv
C.2.1. Pre-treatment of the Primary Fuel – Desulfurization and Pre-reforming xxiv
C.2.2. Conversion of the Primary Fuels to Hydrogen xxvii
C.2.2.1. Steam Reforming (SR) xxix
C.2.2.2. Catalytic Partial Oxidation (CPOx) xxxii
C.2.2.3. Autothermal Reforming (ATR) xxxiv
C.2.3. Product Clean-up and Optimization – Water-gas Shift and CO Polishing xxxviii
C.3. Fuel cells in APUs xli
C.3.1. Solid Oxide Fuel Cells xliii
C.3.2. Proton Exchange Membrane Fuel Cells xliv
C.4. Balance of Plant xlv
D. Mechanism M1 and M2, Surface Mechanism xlviii
E. Scientific publications and conferences l
E.1. Publications l
E.2. Conference oral presentations l
E.3. Poster presentations li
F. Curriculum vitae lii

1 Introduction

1.1 Hydrogen as Future Energy Carrier

The increasing energy demand in the world is almost completely covered by energy that is produced from fossil fuel-based hydrocarbons. The consumption of hydrocarbons can be tracked back to the invention of the steam engine by Thomas Newcomen in 1712, making it possible, for the first time, to convert carbon or hydrocarbons into mechanical power [1]. Ongoing industrialization tremendously increased the demand for energy. Coal as a solid energy carrier was complemented by liquid crude oil and natural gas. Although changing the state of the energy carrier from solid to gaseous, the number of hydrogen atoms it contained changed from zero to four. However, the increasing production of energy out of hydrocarbon sources is accompanied by the release of large amounts of pollutants, and in particular, from the greenhouse gas carbon dioxide. With the appearance of the rising automobile industry, demands for hydrocarbon fuels increased, accompanied by increasing pollutant emissions. The Environmental Protection Agency (EPA) in the US identified six main pollutants deriving from the combustion of gasoline in internal combustion engines – nitrogen dioxide, ozone, sulfur dioxide, particulate matter, carbon monoxide, and lead.

While most greenhouse gases, such as carbon dioxide and methane, are mainly produced from burning hydrocarbon fuels, nitrogen dioxide, carbon monoxide, and lead are mainly contributed to by vehicles emissions [2]. Greenhouse gases accelerate the climate change on Earth, while pollutants cause health problems such as cancer, heart problems and other diseases such as asthma. Therefore, the liberation of pollutants and greenhouse gases has to be significantly reduced as, otherwise, life on Earth may become unsustainable [2].

Following the historical change of energy carriers from solid to gaseous, rising in hydrogen content respectively, it becomes obvious that hydrogen can become the energy carrier of the future, as it does not lead to any carbon dioxide emissions [1]. Since hydrogen, as the most abundant element in the universe, is chemically bound and not available by nature, hydrogen must be produced. Therefore, Züttel et al. [1] pose the question, “what are the possible sources of energy for a hydrogen-based society”? They give the answer that nuclear

fusion of hydrogen is the only source of primary energy on a geological timescale, which produces heat and electricity. However, due to massive technical problems, this has not been achieved yet. Besides the question for the primary source for hydrogen production, hydrogen is still considered to have a high potential as an alternative fuel due to nearly zero emissions of pollutants and water is the only by-product when burned. Today, hydrogen is generated from a variety of energy sources, such as natural gas or gasoline, and when using renewable sources such as biomass, solar or wind, hydrogen would be available in a virtually unlimited quantity [2].

To introduce hydrogen as an alternative energy carrier in modern society, and in particular as an alternative fuel for internal combustion engines, thus avoiding pollutant emissions, several challenges have to be faced and overcome. As stated by Johnston *et al*. [2] and Dunn [3], five different factors have to be mentioned with regard to the slowing adoption of hydrogen in today´s infrastructure: the production, storage, distribution, safety, and the public perception of hydrogen. As already mentioned, hydrogen has to be produced. Furthermore, produced hydrogen has to be stored for on-demand use, but its low density turns this to a challenging task. Today´s solutions are not suitable with regard to economic aspects. Transition to hydrogen as a fuel requires an extensive infrastructural distribution network for end-user supply or it has to be performed onsite at the fueling station. Decentralized production is less effective due to high energy demands. Still, however, hydrogen is transported via pipelines or large tanker trucks. The latter is not cost effective for large-scale distribution, but otherwise, pipelines have significant initial capital costs which have to be paid in advance. Handling hydrogen can be dangerous due to its flammability over a wide concentration range and its tendency for leakage.

Hydrogen, as the most common element in the universe, is chemically bound on Earth in large amounts and has to be released from a broad variety of feedstock. These include, besides water, all hydrocarbon sources, ranging from natural gas, oil, and coal to biomass. Today, the most important criteria for the production of hydrogen and, therefore, the choice of feedstock are capital and maintenance costs, efficiency of the conversion, flexibility of the process in design and operation, safety and hazard risk management, and in general the minimization of waste production [4]. Various technologies are available for the production of hydrogen and will be presented only in a short general overview at this point. Thermal

conversion processes are the by far most utilized processes, with steam reforming leading the way. About 50 million tons of hydrogen are produced annually and most results from steam reforming [4, 5]. Several reforming technologies are performed in industry and will be discussed in Chapter C.2.2 with regard to their usage in mobile applications. However, despite the fact that hydrogen is a clean energy carrier, large amounts of the greenhouse gas carbon dioxide are emitted when hydrogen is produced from a hydrocarbon source. This is quite similar to the conventional combustion process, e.g., of fossil fuels in cars. If hydrogen is to become the future energy carrier, even if produced from biomass, the sequestration of carbon dioxide must be considered [5]. Splitting water by electrolysis is an alternative pathway for hydrogen production. However, due to the strong bonds in water molecules, a theoretical 39.3 kWh of electrical energy is needed to split one kilogram of water [1], and only about 3 % of the world´s hydrogen production is covered by electrolysis [5]. The most common process producing hydrogen by electrolysis is the chlor-alkali process for the production of chlorine, in which hydrogen is only a by-product. Several electrolysers are available on the market, producing hydrogen out of water with efficiencies of about 65 – 75 % [5]. Electricity can either be taken from the grid or directly produced from renewable sources, such as wind and solar energy. For the latter, hydrogen can also severe as energy storage to even unsteady power generation. Furthermore, solar energy can be used to perform most of the thermal conversion processes for hydrocarbon feedstock.

Today, hydrogen is used as a raw material in industry, especially in the refinery, than as an energy carrier. Changing the energy carrier to hydrogen, electrolysis will gain more importance, especially when electrical energy is generated from renewable sources.

In general, hydrogen is generated on-site and transported via pipelines. However, a key condition for the transition from the fossil fuel-based energy carriers towards hydrogen is the development of a safe, efficient, and compact storage technology. Today´s fuel cell applications are powered mainly with pure hydrogen, either compressed in a pressurized gas tank or, hydrogen from liquefied hydrogen, stored in cryogenic tanks. For mobile applications such as vehicles, the storage of hydrogen in a solid material is considered to be potentially superior to liquid or compressed gaseous storage [6]. A lot of research is performed in the field of hydrogen solid-state storage. But there is still a lack of suitable materials concerning hydrogen storage capacity, cost, and thermodynamics. However, the

key requirements for a practical storage material are a high storage density, favorable sorption thermodynamics and kinetics, prolonged cycleability and lifetime. Today, such materials are not available on the market at economical production costs. To introduce hydrogen as a future energy carrier without having the infrastructural technologies and logistics in the next years, the on-board production of hydrogen from a fossil fuel has the potential and can strike a balance between the well-known and accepted fossil fuel energy carriers and hydrogen as one possible energy carrier of the future.

The on-board production of hydrogen from fossil fuels is challenging due to the needs of a fuel processor system that effectively converts a hydrocarbon fuel into hydrogen for the use in fuel cells. This approach has been pursued by many researchers for several years. Several concepts were presented and are still under development, facing the problems of efficient hydrogen production and competing with the common ordinary fossil fuel-based technologies. One concept regards the so-called auxiliary power unit (APU) system, dealing with the on-board production of hydrogen from a logistic fuel for the use in fuel cells for electricity production in the power range of 1 – 5 kW. This concept will be explained in the following chapter and serves as the technical background for the experimental investigations within this thesis.

1.2 Concept of an Auxiliary Power Unit (APU)

The use of auxiliary power units based on various fuel cell types has the potential of providing electrical energy with high efficiencies, compared to the conventional power generation with electric generators. The APU system is independent from the vehicles internal combustion engine and is therefore not constrained by the Carnot´s rule. This enables an APU to be more efficient in electricity production, which is a prioritized issue in the automotive industry due to fuel economy and emission abatement.

Stringent environmental legislations and the increasing costs for automotive fuels call for new and innovative technologies, especially in the automotive sector. For instance, heavy-duty trucks idle about 20 – 40 % of their operating time [7], resulting in increased emissions, particulates, and the environmental harmful greenhouse gas carbon dioxide. Electronic

devices and comfort systems, e.g., TVs, microwave ovens, air conditioning, consume more energy than is provided by the vehicles batteries. Idling the engine is performed for power generation only. Operating a system that is decoupled from the vehicles engine would results in a better energy utilization of the fuel and simultaneously help to decrease emissions and particulates [7]. Various logistic fuels have been reported to be appropriate for fuel processors, e.g., LPG, methanol or natural gas. A more detailed overview of various fuel types and their production is given in Chapter C.1.1 - C.1.4.

Hydrogen is the only convertible chemical fuel for most fuel cells, apart from methane and methanol. A lot of research was performed on the development of direct methanol fuel cells or the conversion of methanol into hydrogen [8]. Nevertheless, for mobile applications, in particular for vehicles, an additional storage tank would be required, resulting in additional vehicle weight, cost, and an extension of the existing infrastructure for fuel provision.

Pure hydrogen could also be used as on-board fuel. In this case, no fuel processor would be necessary. For commercialization of fuel cell vehicles fueled with pure hydrogen, the present hydrogen storage systems for automotive applications cannot match the operating range of conventional vehicles with internal combustion engines that are fueled with a fossil fuel [8] due to the low-energy density of hydrogen [9]. Furthermore, as for methanol, an additional storage tank with increased safety issues would be necessary on-board, which would also again increase costs and vehicle weight.

However, for the integration of fuel processor fuel cell systems in today's infrastructure, the system must be able to convert a commercially available fuel, such as gasoline or diesel fuel, into hydrogen. The concept shall be explained in more detail on the basis of **Figure 1-1**.

The primary fuel, which is available on-board and also used for the internal combustion engine, is primarily desulfurized to prevent all downstream parts, especially the reformer and the fuel cells, from sulfur contamination and the resulting poisoning. Depending on the fuel, desulfurization can be costly and size intensive. The desulfurized fuel can then either be pre-reformed or fed directly to the reformer unit. In the pre-reformer, hydrocarbons greater than C_{2+} in the fuel are converted to a mixture of hydrogen, carbon monoxide, parts of carbon dioxide, and methane [10]. Coke formation in the reformer unit and downstream parts is partly prevented as heavier hydrocarbons have been removed from the stream. Furthermore, gas mixtures containing only C_1 hydrocarbons can be fed directly to high-

temperature fuel cells for direct internal reforming [11-13]. Alternatively, the fuel or pre-reformate is then mixed with air and converted to a hydrogen-rich gas mixture in a reformer unit. The most common reforming processes are catalytic partial oxidation, steam reforming, and their combination, autothermal reforming [7, 14]. In most cases, steam has to be provided to the reformer, either for the reaction or for coke prevention. As already mentioned in Chapter 2.3, the evaporation of a logistic liquid fuel for the reformer unit is complicated. When the boiling range of the fuel overcomes the auto-ignition temperature, evaporation and reforming of the fuel are difficult. Several techniques have been presented in literature [15-22] with more or less stable long-term operation [7]. Therefore, the prime challenge in designing reformer units handling liquid hydrocarbon fuels is creating a perfect mixture of fuel and oxidant upstream the catalyst, while preventing the mixture from igniting. The mixing chamber must provide full evaporation with fast dynamic response on the system's demands, and must furthermore provide a homogeneous flow profile for the catalyst [8].

The produced hydrogen-rich reformate can be fed directly to the fuel cell when high-temperature fuel cells are implemented, e.g., SOFCs or MCFCs. CO does not poison the active sites of the anode and is, due to WGS, internally converted with water to hydrogen [23], and the same is true for CH_4. When low-temperature fuel cells are used, e.g., the popular PEMFC, CO has to be removed due to poisoning of the platinum sites in the anode. Several technologies are available. Most common are water-gas shift reactors that operate in both high- and low-temperature regimes and provide efficient CO removal down to about 1 vol%. Further purification is achieved with preferential oxidation or the selective methanation of carbon monoxide. Values below 10 ppm in CO content can be realized, meeting the requirements for PEMFCs. For further efficiency increase, membrane filters for hydrogen enrichment can be implemented in the system.

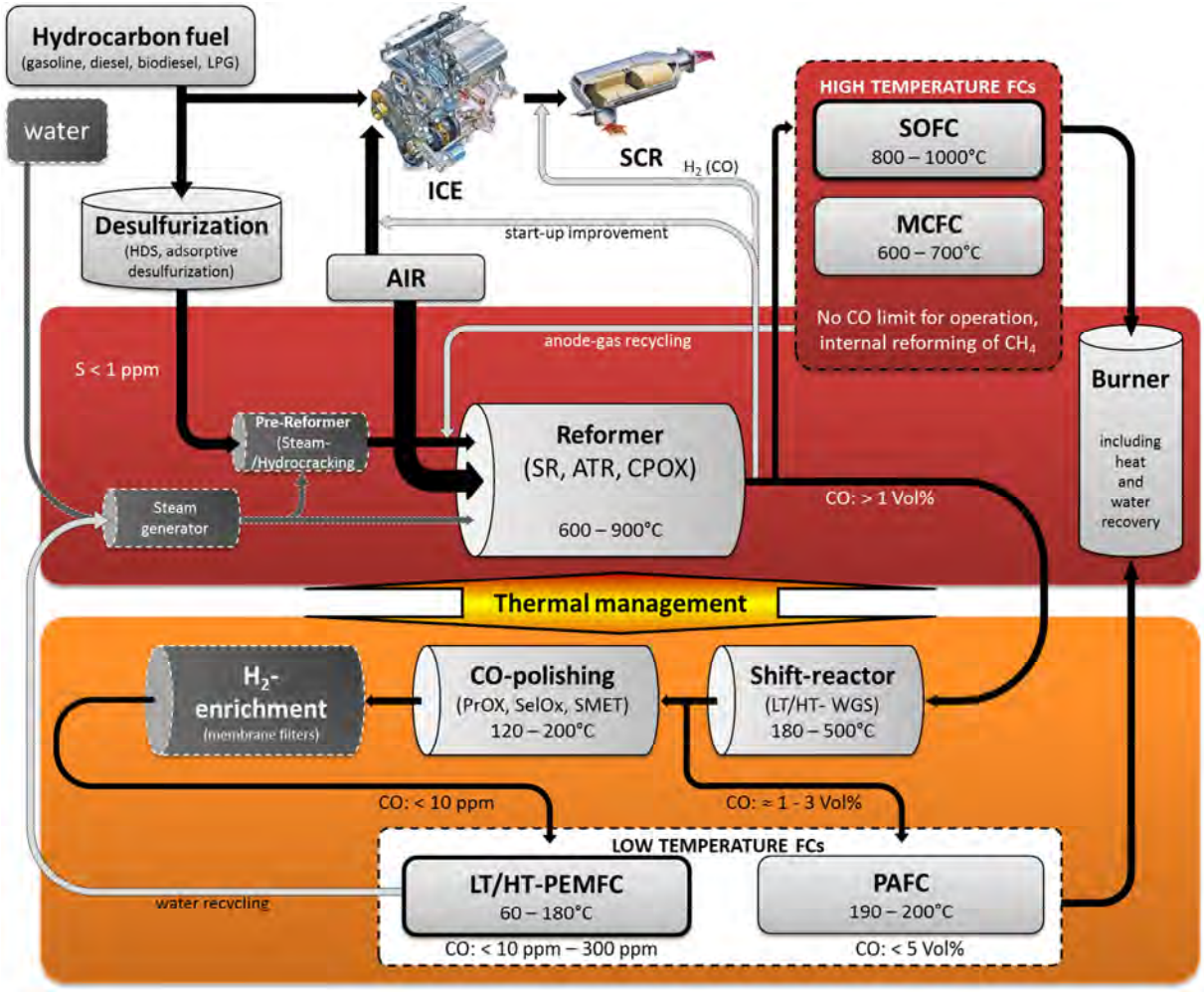

Figure 1-1: Detailed concept chart of an APU, including pre-treatment of the hydrocarbon fuel (desulfurization, pre-reforming), the conversion of fuel to hydrogen-rich gas mixtures (Reformer), direct use in high-temperature fuel cells (upper right), CO removal (HT/LT WGS, CO-polishing), hydrogen enrichment and use in low-temperature fuel cells (bottom middle). Blackened parts are not necessary in general; their usage depends on the process demands based on fuel source and hydrogen quality. Greyed lines indicate fuel processor integration in the APU / vehicle. For efficiency improvement and energy recuperation, a significant focus has to be put on thermal management, as different temperature regimes are present in a fuel processor (indicated in red (HT) and orange (LT)).

The flue gas coming from the fuel cell stacks is generally burned in a catalytic burner as only parts of the provided hydrogen are converted into electrical energy and water [24]. Hydrogen conversion is in the range of about 75 – 92.5 % [8]. Therefore, hydrogen, carbon monoxide, and unconverted hydrocarbons can, to a certain level, be present in the exhaust gas of the fuel cell stack. The combustion of the flue gas provides further heat for the fuel processor system.

The waste water from the burner as well as the water coming from both the anode and cathode side of a low-temperature fuel cell can be recycled and used once more in the reforming process. In case of high-temperature fuel cells, the exhaust gas can be partly recycled to the reformer inlet to improve the reformer efficiency [25] or is burned for heat supply. In practice, various configurations, depending on the chosen reformer concept, can be realized with different levels of integration and process intensification. Nevertheless, independent from the final concept design, the fuel processor has to meet certain aspects. The fuel processor should be constructed in a compact and light-weight design to meet very strict cost targets. Furthermore, reliable performance must be guaranteed also in frequent startup and shutdown cycles during one day, with changing demands for hydrogen production, ranging between 5 – 100 % of the processor's capacity.

In addition to a more efficient production of electrical energy compared to the electric generator, an on-board fuel processor offers further advantages. When a hydrogen source is available on-board, the hydrogen can be used for issues regarding exhaust gas after-treatment. The removal of NO_x emissions is often performed with the method of selective catalytic reduction (SCR) to meet legislative regulations, e.g., Euro V and Euro VI in the EU. The selective reduction is performed with small inorganic molecules, mainly H_2, CO, and NH_3, reducing NO_x to nitrogen and water on a catalytic surface. A commercial technology for lowering NO_x emissions is the use of NH_3-SCR with the commercial available additive AdBlue®, a 32.5 % aqueous solution of urea for utility vehicles [26, 27]. The provision of H_2 online without the need of further storage capacities would therefore improve the overall efficiency of exhaust gas aftertreatment.

A second advantage that shall be mentioned is the use of APUs in the automotive industry. Several research groups have shown that, due to significant emissions reduction of pollutants and particulates, the feeding of a gas mixture containing synthesis gas to the injection system of the engine significantly improves the cold start-up phase of a compression ignition engine [28-30]. Nevertheless, in most studies, only a small fuel reformer is placed in the exhaust gas recirculation (EGR) loop behind the engine's exhaust stream, which reforms part of the exhaust gas with small amount of engine fuel to a mixture of syngas, methane, and carbon dioxide (REGR). REGR is then re-fed to the preheated engine inlet and burned in the chamber. Providing a synthesis gas that is used for combustion improvements and on-top for the production of electrical energy with high efficiency would

result in an efficient usage of the initial fuel's energy content and help to reduce fuel consumption in general.

In summary, it can be stated that on-board hydrogen generation from logistic fuels is a challenging task including heat and energy recuperation reformer design as well as the development of sulfur tolerant, long-term stable catalysts. Choosing the right reforming process strongly depends on the type of primary fuel used and the type of fuel cell stack as well as on the desired power output and the used catalyst [31].

2 Objectives of this Work

Catalytic partial oxidation (CPOx) is a promising technology for the reforming of liquid hydrocarbon fuels to hydrogen or synthesis gas for the usage in fuel cell applications. One field of modern industrial interest in CPOx are compact and autothermal operating reformers for the production of hydrogen and synthesis gas from liquid hydrocarbon fuels, such as gasoline, diesel, and kerosene. These so-called auxiliary power units (APU) represent an efficient on-board technique for electricity supply via fuel cells as well as primary and secondary measures for reduction of NOx emissions in conventional combustion processes [32] and for the improvement of the cold start-up phase of internal combustion engines. Furthermore, the formation of smoke emissions can simultaneously be significantly reduced [28, 29, 33]. The concept of the auxiliary power unit is discussed in more in detail in Chapter 1.2, as the APU is the underlying technological application for the work presented in this thesis. Investigations within this work deal with different kinds of chemical problems that may arise during the operation of an APU, especially when a commercial logistic fuel is used for the production of hydrogen. These conventional fuels are attractive due to their high energy density, their widespread production, distribution, and their retailing infrastructure [34, 35]. Future technologies can benefit from these advantages; no further improvement or development of alternative energy distribution facilities and networks has to be carried out as the distribution and on-board storage of, for instance hydrogen, present technical problems. The on-board fuel is converted into a hydrogen-rich syngas, which can be achieved by different routes. Among the three reforming routes, i.e., steam reforming (SR), partial oxidation (POx), and autothermal reforming (ATR, combination of SR and POx) [7], steam reforming is less attractive for mobile applications due to slow start-up and endothermic operation [9]. The main routes to reform hydrocarbons into hydrogen are presented in more detail in Chapter C.2.2 and shall only be mentioned briefly at this point. In contrast, CPOx of logistic fuels offers a high throughput and an autothermal route for the supply of large amounts of hydrogen at short contact times (10^{-2} to 10^{-4} s). **Equation 2-1** shows the catalytic partial oxidation of isooctane, which was used in this work as reference fuel for gasoline in studies 1 and 2. For the last Study 3, which was carried out with

commercial diesel fuel, a sum formula was estimated, representing the averages composition of the fuel.

$$C_8H_{18} + 4O_2 \rightarrow 8CO + 9H_2$$

Equation 2-1

The produced synthesis gas from, e.g. the catalytic partial oxidation is then directed to a fuel cell for the conversion of chemical to electrical energy. Various types of fuel cells are available on the market, but only a few can be expected to meet the requirements for on-board conversion of the electrochemical fuel.

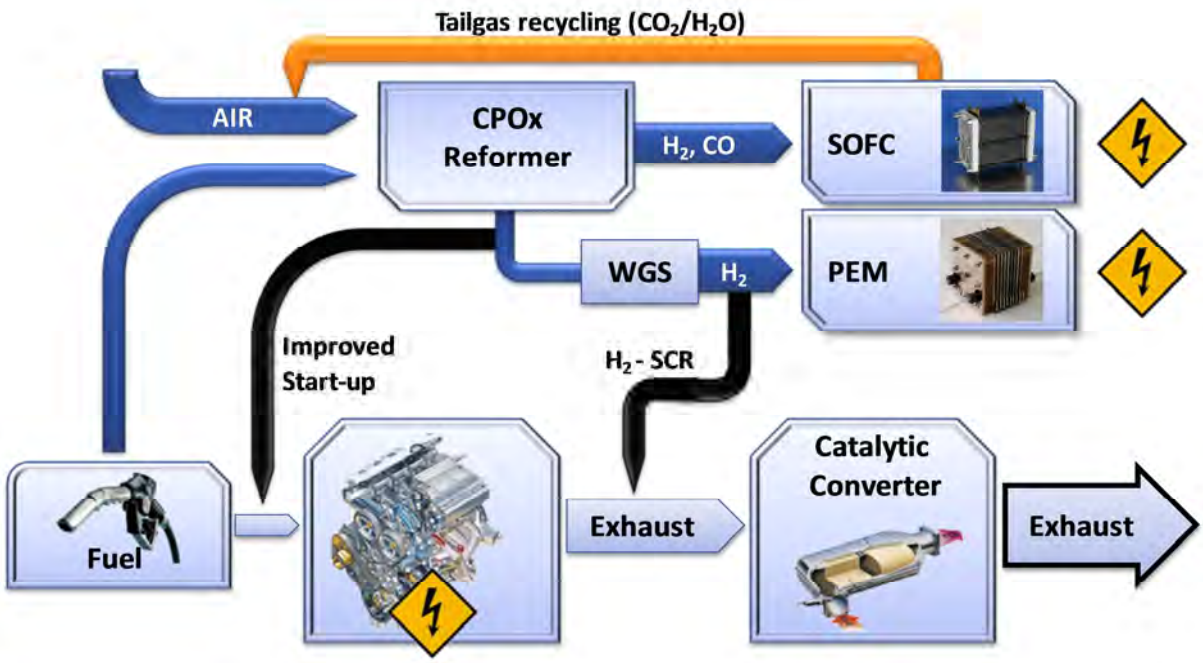

Figure 2-1: Concept drawing of an APU. The bottom path shows the conventional principle of a today's automobile with internal combustion engine (ICE), generator, and exhaust gas after-treatment. The electricity production is performed by the generator, driven by the ICE. The upper path describes the combination of CPOX reformer and fuel cell stack with additional options for start-up and emission control improvement. Reprinted from [36] with permission from ACS.

A short review about available fuels on the market may be suitable for on-board fuel reforming is presented in Chapter C.1. Since two different types of fuel cells are very

common in the field of mobile applications in the range of 1-10 kW, only these two types will be discussed in more detail in Chapter C.3. Aside from proton exchange membrane (PEM) fuel cells, solid oxide fuel cells (SOFC) are under consideration for mobile application. In contrast to PEMFCs, SOFCs do not require an additional fuel processing system for CO cleaning (Chapter C.2.3) and, in fact, can even be operated with a certain amount of hydrocarbons in the feed [37-39]. Nevertheless, an upstream desulfurization of the fuel has to be taken into account in both cases, as the reformer itself is sensitive to sulfur because the reforming catalysts contains precious metal. This topic will be discussed in more detail in Chapter C.2.1. A scheme of an APU is shown in **Figure 2-1**. For higher efficiency and long term stability of such APUs, a fundamental understanding of the chemical processes is essential as it paves the way for commercialization. Even though high fuel conversion and hydrogen selectivity, both > 90 %, can be achieved by using Rh-coated catalysts [34, 40], the successful technical realization may depend on several technical and chemical issues. The latter provided the inspiration for the work presented in this thesis and will be explained in more detail in the next sections.

2.1 Influence of Gas-phase Reactions Downstream the Catalyst (Study 1)

The reformers that are used in APU systems often consist of monolithic structures with pore diameters on the order of one millimeter and are coated with noble metal catalysts such as rhodium or platinum. Aside from the heterogeneous conversion on the catalytic surface, homogeneous reactions in the gas-phase may be significant at the operating temperatures of approximately 1000 K, in particular for the logistic fuels that contain higher hydrocarbons. Coking and aging of the catalyst as well as coke formation downstream the reformer from precursors formed in the reformer are major challenges in the practical realization of on-board reformers and APUs. The formation of coke precursors is contributed to homogeneous gas-phase reactions [41], in particular at fuel rich operating conditions, i.e., molar C/O ratios above unity.

The formation of hydrogen by CPOx of hydrocarbons over rhodium is generally accepted to follow the indirect route, which means that, at first, total oxidation of the hydrocarbon

occurs until most of the oxygen is consumed, at least near the catalytic surface, and then, the remaining fuel is steam-reformed [42-45]. Numerically predicted [46] and experimentally determined [47] axial species profiles implicate complete fuel conversion within the first millimeters of the catalyst channel for lean conditions (C/O < 1.0), with H_2, CO, H_2O, and CO_2 being the only products. However, at C/O > 1.0, an increasing amount of by-products such as methane, olefins, and aromatics, is detected [34, 48], the latter two of which indicate thermal decomposition (pyrolysis) of the fuel in the gas phase [41]. A recent study on CPOx of isooctane revealed the on-set of homogeneous conversion at a point in the reactor at which oxygen is almost completely consumed and coke is accumulated on the catalyst [49]. At this location, the mixture consists of synthesis gas, steam, CO_2, and some remaining fuel. Since the product stream cannot be instantaneously cooled down beyond the catalyst, homogeneous gas-phase reactions may continue beyond the catalyst, leading to thermal cracking of the hydrocarbon species and thereby to the formation of smaller, unsaturated hydrocarbons. In case of CPOx of methane, Burke and Trimm investigated the coking behavior downstream the catalyst zone with and without nitrogen-cooled product gas stream at different pressures. Coke was observed at about 750 kPa but was avoided, even up to 1500 kPa, when gas-phase cooling was employed [41]. Consequently, a study on the impact of gas-phase chemistry on conversion and selectivity of CPOX reformers must be carried out at the conditions occurring in the downstream part of the catalyst and in the post-catalyst zone.

Therefore, an experimental study focusing on the impact of gas-phase reactions occurring downstream the oxidation zone in a CPOx reformer was performed for isooctane as reference fuel. To highlight the problem of gas-phase reactions in more detail, a reference case will be discussed (catalytic case), which was operated at slight fuel-rich conditions using the honeycomb catalyst with rhodium, as described in Chapter 4.3.2. Then, the homogeneous conversion of the product stream, simulated by a mixture of syngas, total oxidation products, and remaining fuel, is experimentally and numerically investigated in the fuel-rich region downstream the catalyst (non-catalytic case). The gas mixture compositions are derived from the results obtained by the catalytic case experiment. Numerical simulations using two different gas-phase reaction mechanisms are used to predict the axial species profiles and the product compositions, which are compared with the experimental results.

2.2 Tail-gas Recycling for a Simulated SOFC Anode Exhaust Gas (Study 2)

As already mentioned in the previous chapter, the production of synthesis gas via CPOx of hydrocarbons follows the indirect route, which means that, firstly, total oxidation of the hydrocarbon occurs until most of the oxygen is consumed, at least close to the catalytic surface, and, secondly, downstream reforming of unconverted fuel with the provided steam from the catalytic combustion takes place. This exothermic catalytic combustion provides the heat for subsequent endothermic reforming of the remaining fuel in the oxygen-free reaction zone, which results in the production of syngas [42, 50]. CPOx of methane as a model surrogate for natural gas feedstock was intensively studied over the group VIII noble metal catalysts, in particular over rhodium, for which carbon formation was not observed [50-56] on the catalytic surface. With nickel and manganese, coke formation is observed, which is mainly attributed to the endothermic methane cracking (**Equation 2-2**) and to slightly exothermic Boudouard reactions or CO-disproportion (**Equation 2-3**) [57].

$$\boldsymbol{CH_4 \rightleftharpoons C + 2H_2}$$

Equation 2-2

$$\boldsymbol{2CO \rightleftharpoons C + CO_2}$$

Equation 2-3

Using liquid hydrocarbon feeds, as it was done in this work, coke deposition on the catalyst and on surfaces downstream the catalytic structure gain more importance. CPOx of larger hydrocarbons such as isooctane, n-decane, and n-hexadecane shows increasing amounts of by-products such as methane, olefins and aromatics at molar C/O ratios above unity [15, 32, 34, 49, 58]. As indicated in the previous chapter, the formation of olefins and aromatic species indicates thermal decomposition of the fuel in the gas phase. As the reformate gas stream cannot be immediately cooled down behind the catalytic section of the reactor [41], homogeneous gas phase reactions occur in the hot outlet gas stream. These reactions may include of pyrolysis of remaining fuel, water-gas-shift (WGS) reactions, hydrogenation of unsaturated hydrocarbons, and eventually significant coke formation [59]. With regard to

the application of CPOx reformers in APUs, the concentrations of olefins in the reformate product stream should not exceed a maximum amount of a few ppm to prevent coke formation in downstream pipes and devices. However, the possibilities of cooling the reformate significantly below temperatures of 780 K to avoid pyrolytic reactions [59] may be limited as the necessary operating temperature of a SOFC stack is above 900 K [60, 61]. For lower temperatures, huge efforts are undertaken in strategies dealing with the improvement of materials for both anode and cathode, the improvement of the electrolyte thickness and the electrolyte itself, the reduction of energy consumption of the SOFC, and the usage of micro-scale technologies for a more efficient thermal management [61]. Furthermore, proton exchange membrane fuel cells can be used instead of SOFCs. Nevertheless, other problems like CO poisoning of the active sites in the membrane have to be faced and require additional fuel processing devices [62, 63].

Re-feeding certain amounts of the exhaust gas of the fuel cell stack, which consist mainly of water and carbon dioxide (in case of high-temperature fuel cells), to the reformer inlet can be one possibility to reduce coke formation aside from its potential to increase the overall efficiency of the APU. Tail-gas recycling also provides alternative C, H, and O sources for the CPOx process, which may alter the operating behavior of the reformer. In CPOX of methane, co-feeding of water and / or carbon dioxide was shown to help in adjusting the H_2/CO ratio in the product stream but also modifying the general reactor performance [52, 64, 65].

In this thesis, experimental investigations have been performed to study the main effects of carbon dioxide and steam addition on a CPOX reformer fed with isooctane as a reference fuel for gasoline.

The effects are discussed in comparison with product compositions reached in studies without tail gas recycling [49] and with thermodynamic equilibrium data.

2.3 Diesel Fuel Handling under Defined Pulse-free Boundary Conditions (Study 3)

With regard to the APU concept, investigations in literature mainly focus on model fuel surrogates for a better understanding of the chemical processes in the reformer [15, 32, 66-69]. In technical application, the reforming of heavy hydrocarbons and logistic fuels, such as diesel and kerosene, is attractive for mobile applications as these fuels are already

implemented on-board in the vehicles' structure. Due to the broad variety of the composition of logistic fuels, the reforming of a diesel fuel is difficult and is accompanied by both chemical and physical problems. The latter especially occur during the upstream evaporation and premixing with air. The handling of logistic fuels is not as easily possible as for a single component fuel, e.g. direct total evaporation in a carrier gas stream, because the auto-ignition temperature of normal alkanes decreases with increasing chain length, typically below 200 °C for $C_{>10}$ n-alkanes. Concentration gradients that arise during the evaporation range from pure fuel to pure air, which leads to regimes in which the fuel/air mixture can spontaneously ignite, especially when the temperature exceeds the auto-ignition level. Several different techniques have been reported to evaporate diesel fuel in CPOx applications, e.g. external atomization and evaporation of the fuel in the absence of air with downstream mixing [16], thin-film evaporation on hot reactor walls [15, 17], pre-mixing the diesel fuel with water for improved evaporation [18-20], exothermal pre-reactions in the form of cool flames for the evaporation of liquid hydrocarbons [21] or the injection of diesel fuel into hot combustion air [17, 22]. In most cases reported, the described methods have been shown to produce large amounts of soot or unstable operation with high risk for auto-ignition of the premixed diesel/air mixture due to prolonged residence time upstream the catalyst necessary for the evaporation process [7].

Apart from physical problems that occur when handling the fuel, chemical issues have also been reported. Feedstocks derived from petroleum are complex mixtures of linear and branched alkanes, alkenes, and aromatics. Structure and configuration of various hydrocarbon species have been investigated under CPOx conditions. Normal alkanes ranging from C_1 to C_{16} [32, 34, 70-72], branched alkanes [73], and cyclic hydrocarbons, e.g. cyclohexane [74, 75], were tested and revealed different reaction behaviors for conversion and desired reaction product selectivities. Nevertheless, in the real application, mixtures of hydrocarbons do not react directly as superposition of the single components investigated. With regards to the mixtures reactivity, which was recently studied for fuel surrogates containing ethanol [76], only trends can be identified [75]. In literature, only little information can be found that deals with the catalytic partial oxidation of logistic diesel fuel on a more fundamental chemical basis than the suitability for the fuel processor in general [77]. In most cases, water is co-fed to the diesel in order to assist the evaporation process and to avoid pre-combustion [78, 79]. However, nearly all results in literature can be

summarized to indicate that the reformer design and diesel/air mixture homogeneity are the determining factors for the development of an efficient operating diesel fuel reformer [7, 8, 77].

Handling commercial diesel fuel in reformer application has to be done with highest precision, as fast coke formation up- and downstream of the catalyst is the consequence otherwise. A new reactor setup with well-defined boundary conditions was established to guarantee a pulse-free diesel fuel inlet stream with coke-free operation upstream the catalyst by evaporating a nebulized diesel flow without significant contact to the reactor wall. The results reveal a rather small operation window for a diesel fuel/synthetic air inlet mixture due to pre-ignition for fuel-lean conditions and to strong coke formation for fuel-rich reaction conditions within a few minutes down to seconds, respectively. The results show the same trends as for earlier experiments with the model surrogate fuel isooctane and gasoline [34, 49, 75]. With regard to fuel feeding, the new reactor configuration can handle commercial diesel fuel like a single component fuel. For the first time, CPOx of diesel fuel shows the expected trends in fuel conversion and hydrogen production similar to the trends of a single component fuel, contrary to reports in literature [15].

3 Fundamentals of Heterogeneous Catalysis relevant for this Work

3.1 Introduction

The term “catalysis” first appeared in the year around the year 1835, and was defined by Jöns Jacob Freiherr von Berzelius as a group of reactions, in which one interacting component is not consumed. The phenomenon “catalysis” occurred much earlier, at the beginning of the 19th century. In 1823 Döbereiner invented the first lighter based on the formation of hydrogen from sulfuric acid catalyzed by zinc. The hydrogen was then directed to a platinum foam and ignited with the atmospheric oxygen [1, 80]. In 1909, Wilhelm Ostwald gave a first definition: “*Ein Katalysator ist ein Stoff, der die Geschwindigkeit einer chemischen Reaktion erhöht, ohne selbst dabei verbraucht zu werden und ohne die endgültige Lage des thermodynamischen Gleichgewichts dieser Reaktion zu verändern.*“ [81]. In today’s science, catalysis is the alteration of a chemical reaction in the presence of a catalyst without changes in the thermodynamic equilibrium. A catalyst is a material that is used to accelerate a chemical reaction within the meaning of this definition in order, to efficiently produce a product by lowering the potential energy of the reaction compared to the non-catalyzed route. This is achieved by the formation of bonds with the reacting molecules on the catalyst’s active site, allowing these to react under formation of a product, which is then detached from the active site, while the catalyst leaves the reaction in an unaltered way. This cycle can be repeated for several thousand times without changing the catalyst’s chemical or physical properties, so a smaller amount of catalyst is needed compared to the amount of product obtained. In summary, it can be said that a catalyst offers an alternative route for the reaction considered, which is much more complex but energetically favored. This is achieved by a decrease in the reactions activation energy, whereas the change of the Gibbs free energy ΔG between the reactants and the products remains unaffected, and therefore an acceleration of the overall reaction rate occurs. Since ΔG of the reactions remains constant, a catalyst does not affect the overall thermodynamic equilibrium of the reaction and, therefore, accelerates both the forward and the reverse reaction in the same order of magnitude [82]. Nevertheless, with the knowledge of modern

surface science, the definition by Wilhelm Ostwald is still appropriate but has to be extended in some respects. Sintering and coke formation affect the catalytic structure, leading to a loss in catalytic activity, and thus, due to the reaction conditions, the catalyst does not leave the cycle without any alteration. Furthermore, a catalyst does not accelerate a chemical reaction. It rather increases the probability of one favored specific reaction pathway compared to all the other possibilities to form the desired reaction product [81].

With catalysis, processes can be operated in the most favorable thermodynamic regime under much milder reaction conditions than for the non-catalytic ones, and therefore, catalysts are the key technology for reducing both investment and operation costs of a chemical process.
In the last century, catalysis gained more importance in nearly all areas of life. Starting with the large-scale production of ammonia by Haber and Bosch [83] and the formation of nitric acid by Ostwald, the large-scale production of fertilizer entailed a worldwide economic upswing. Today, catalysts are the workhorses for the chemical transformation of 85 – 90 % of all industrial products in the field of transportation fuels, bulk, and fine chemicals, and the reduction of waste and emissions [75, 81, 82].

When talking about catalysis, a more precise differentiation has to be made, depending on the catalysts appearance and the surrounding environment. Two main disciplines of catalysis are distinguished [82]:

- Homogeneous catalysis:

  Both catalyst and reactant exist in the same phase, which can be either the gaseous or liquid phase. Homogeneous catalysis often occurs in atmospheric chemistry, for instance, in the degradation of ozone molecules by chlorine atoms, and in the liquid phase, e.g., for complex pharmaceuticals with organometallic catalysts.

- Heterogeneous catalysis:

  Catalyst and reactant exist in different phases, i.e., the catalyst in the solid phase and the reactant in the gaseous or liquid phase.

  Commonly, the active site of a heterogeneous catalyst is its surface, e.g. a platinum wire or mesh. However, many heterogeneous catalysts in industry and especially in

the automotive exhaust gas aftertreatment are noble metals [84], their costs would be immense if the pure metal was used. In modern catalysts, the active sites are usually metal particles in the scale of only a few nanometers, supported on a porous media. This porous structure dramatically increases the available geometric surface of the catalyst, providing a high surface area where the active particles are highly dispersed. Therefore, in heterogeneous catalysis, the interaction between the surface topology, the active site, and the bulk phase, be it gaseous or liquid, are the critical physical processes which have to be looked at. Diffusion of the reactant through the porous substrate, adsorption on the surface, movement on-top of the surface, bond cleavage and product formation on the active site, desorption of products and intermediates from the surface, and diffusion back into the bulk phase are major aspects in the description of heterogeneously catalyzed reactions and are essential for the understanding of the chemical background.

In this work, the heterogeneously-catalyzed partial oxidation of higher hydrocarbon fuels is investigated with regard to the occurrence of homogeneous gas-phase reactions downstream the monolithic honeycomb catalyst. A detailed modeling approach is needed to obtain a deeper understanding of the ongoing processes on an elementary level, as, in a real reactor, a broad variety of physical and chemical processes superimpose leading to the overall reaction behavior. These processes are transport phenomena in axial and radial direction, gradients in temperature along the catalyst / reactor axis, and chemistry with homogeneous and heterogeneous reactions.
Therefore, in the following section, the basics of the description of a real reactor with detailed numerical simulation methods are presented.

3.2 Modeling of Heterogeneous Catalysts in Chemical Reactors

This chapter provides an overview of the theory of the detailed modeling approach of chemical reactors. For a more explicit discussion of the underlying mathematical fundamentals, please refer to the open science literature in academia [80, 85-88].

In technical reactors, a multitude of chemical and physical phenomena has to be taken into account because of the broad complexity of a real reactor system. Models with a global description of the reactor behavior are stretched to their limits with increasing complexity of the system. Chemical reactions occur either in parallel or are strongly interlinked with each other, which makes a global description more complicated. The transient behavior of mass and heat transport within the catalyst, diffusion of the individual species from the bulk to the surface and vice versa, and the structure of the catalytic surface additionally overlap with the technical behavior of the reactor. If global reaction mechanisms are used for the description of such complex systems, their modeling parameters are in many cases fitted to experimental data.

To gain a more detailed understanding of the chemical processes and reactions, global reaction mechanisms are not satisfactory enough [80]. Therefore, tools for detailed modeling based on elementary reaction mechanisms are under ongoing development and provide powerful solutions for the fundamental understanding of chemical reactors.

Various models have been developed, established on detailed numerical simulation, and coupled with the description of flow-fields for mass- and heat transport. **Figure 3-1** shows the individual modeling stages for a monolithic honeycomb catalyst channel, as it was used in this work. The transport of momentum, energy, and chemical species inside the channel can occur not only in axial but also in radial direction and have to be distinguished and evaluated individually. While the reactive mixture diffuses to the inner channel wall and the porous washcoat layer, gaseous species adsorb and react on the catalytic surface. The products desorb and diffuse back into the bulk flux. Transport of mass in the fluid phase is superimposed by diffusion processes in the washcoat layer, limiting the overall catalytic activity of the surface. Furthermore, when temperature is high, chemical species can react homogeneously in the gas-phase and the temperature distribution results from a combination of heat convection and conduction, heat transport in the solid materials, thermal radiation, and heat release caused by chemical reactions.

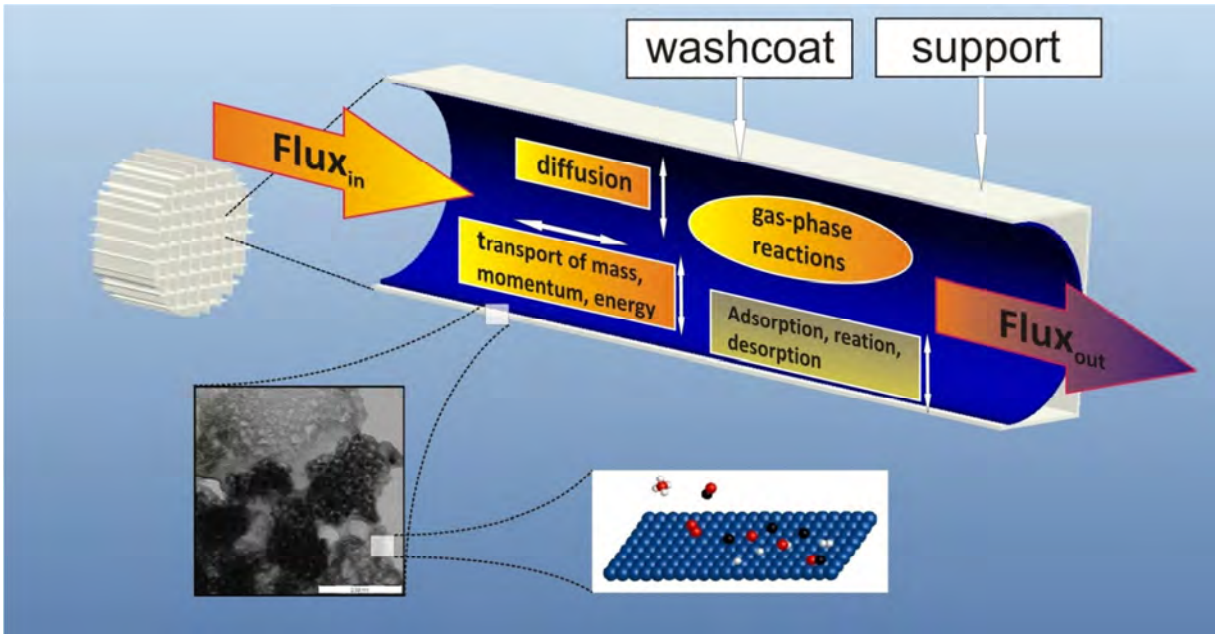

Figure 3-1: Modeling stages in a monolithic honeycomb catalyst channel.

Each stage describes its own timescale regime, ranging from femtoseconds for the elementary steps and microseconds for diffusion to the second time-scale for thermal processes.

3.2.1 Chemical Reactions

On the initial level of the detailed modeling approach, first chemical reactions are considered, which occurring both in the homogeneous gas-phase and heterogeneously on the solid surface. A chemical reaction can be generally written as

$$\sum_{i=1}^{N_g+N_s} \nu_i' A_i \rightarrow \sum_{i=1}^{N_g+N_s} \nu_i'' A_i$$

Equation 3-1

with v_i' and v_i'' as stoichiometric coefficients of the chemical species *i* and A_i as species symbol. In general, A_i can be used for gas-phase, surface and bulk species. The net stoichiometric coefficient shall be described by $v_i = v_i'' - v_i'$.

At an equilibrium, the equilibrium constant for the conversion of v_i moles can be determined to be

$$K_p = \exp\left(-\frac{\Delta_R G^0}{RT}\right)$$

Equation 3-2

Since the rate of a reaction can be interpreted as the probability for a collision of two species in the gas-phase, it depends on the species concentration and the temperature. The rate of formation or consumption of a species *i* in a chemical reaction is called reaction rate and is expressed by its change of concentration c_i with time dependence on the reaction order a_i' for species *i*

$$\frac{dc_i}{dt} = v_i k_\mathrm{f} \prod_j^{N_\mathrm{g}+N_\mathrm{s}} c_j^{a_j'}$$

Equation 3-3

When looking at elementary reactions, a_i' can be expressed by the stoichiometric coefficient v_i', as the reaction is considered on a molecular level. At a chemical equilibrium, the forward and reverse reaction rates are equal on a microscopic level,

$$v_i k_\mathrm{f} \prod_j^{N_\mathrm{g}+N_\mathrm{s}} c_j^{v_j'} = v_i k_\mathrm{r} \prod_j^{N_\mathrm{g}+N_\mathrm{s}} c_j^{v_j''}$$

Equation 3-4

and their equilibrium constant K_c can be expressed by

$$K_{\mathrm{c}} = \frac{k_{\mathrm{f}}}{k_{\mathrm{r}}} = \prod_{i}^{N} c_i^{v_i}$$

Equation 3-5

with $k_{\mathrm{f/r}}$ as the temperature-dependent reaction rate constant for forward and reverse reaction. It is derived from the Arrhenius equation describing the reaction rate constant as a function of the activation energy E_{a} and the temperature T with A as pre-exponential factor:

$$k = AT^{\beta} \cdot \exp\left(-\frac{E_{\mathrm{a}}}{RT}\right).$$

Equation 3-6

The description of a global macroscopic reaction can then be given by a set of elementary reactions R_{g} for all considered species N_{g} where forward and reverse reactions are considered as individual elementary steps. Thus, the molar reaction rate $\dot{\omega}_i$ of a gas-phase species i can be expressed by the summation over a set of reaction rates of all elementary reactions

$$\dot{\omega}_i = \frac{dc_i}{dt} = \sum_{k=1}^{R_{\mathrm{g}}} v_{ik}\, k_{\mathrm{f}k} \prod_{i=1}^{N_{\mathrm{g}}} c_i^{v'_{ik}}$$

Equation 3-7

3.2.2 Mean-Field Approximation

When a chemical reactor system is considered, not only gas-phase reactions have to be taken into account. The surface of the reactor wall and, what is more important in heterogeneous catalysis, the active sites of the catalyst, including the support, have to be taken into account for a detailed description of the system. The key for an detailed understanding of the catalytic process on the surface would be the development of quite sophisticated models with detailed reaction mechanisms based on elementary steps

occurring on the catalyst surface. However, since a catalytic surface consists of a support material, a porous media and an active site, the local constitution of the surface would be required due to the broad variety of adsorbates available. Interactions of active site and support strongly depend on their environment and are essential for the understanding of catalyzed reactions. These parameters are available only for the most simple surfaces, for instance Pt(111). Only few reactions have been successfully modeled with the approach of detailed kinetic Monte-Carlo-Simulations [89-91].

For the description of more complex surface structures, some assumptions regarding the local variation of the surface have to be made. To simplify the topology of a catalytic surface, the amount of active sites can be expressed as a surface site density, Γ, describing the amount of active sites available for a defined surface area. Concentrations are then expressed relatively to Γas the surface coverage θ_i in dependence of the number of occupied surface sides σ_i for species *i*.

$$\theta_i = \frac{c_i \sigma_i}{\Gamma}$$

Equation 3-8

This approach is called Mean-Field-approximation. Local conditions of the surface are averaged to certain cells with the negligence of the influence of directly neighboring sites, whose states are now characterized by mean-values, for instance, the concentration of species *i* as surface coverage θ_i and a certain temperature.

Under these assumptions, the molar reaction rate for heterogeneous reactions of an adsorbed species on the catalytic surface can be described analogous to the reaction rate of homogeneous gas-phase species, and a molar net production rate of either a gas-species or an adsorbed species on the catalytic surface can be given as

$$\dot{s}_i = \sum_{k=1}^{R_s} \nu_{ik} k_{\mathrm{f}k} \prod_{j=1}^{N_g+N_s+N_b} c_j^{\nu'_{jk}}$$

Equation 3-9

The binding state of adsorption is a function of the surface coverage to which the expression of the rate coefficient has to be adapted:

$$k_{\mathrm{f}_k} = A_k T^{\beta_k} \left[\frac{-E_{\mathrm{a}_k}}{RT}\right] \prod_{i=1}^{N_\mathrm{S}} \theta_i^{\mu_{i_k}} \exp\left[\frac{\epsilon_{i_k}\theta_i}{RT}\right]$$

Equation 3-10

with μ_{i_k} and ϵ_{i_k} as surface coverage dependent rate coefficients of species *i*.

3.2.3 Reactive Flow-field

Apart from the detailed description of the chemical reactions, which is summarized in Section 3.2.1and 3.2.2, the characterization of a chemical reactor depends on the description of physical processes. In this work, monolithic honeycomb catalysts and open tubes (Study 1) have been used for the investigation of catalytic reactions and shall be used as an example for the description of the flow-field.

The dynamics of a certain fluid flow field are specified by the conservation equations. For the general description of a single monolithic channel, the NAVIER-STOKES equations can be used. The NAVIER-STOKES equations are given as:

Continuity equation

$$\frac{\partial}{\partial t}\rho + \frac{\partial}{\partial x_i}\rho v_i = 0$$

Equation 3-11

Conservation of species mass

$$\frac{\partial}{\partial t}(\rho Y_s) + \frac{\partial}{\partial x_i}(\rho Y_s v_i) = -\frac{\partial}{\partial x_i} j_{si} + M_s \dot{\omega}_s$$

Equation 3-12

with j_{si} as the description for the diffusion gradients in concentration and temperature

$$j_{si} = -\rho D_s \frac{M_s}{\bar{M}} \frac{\partial}{\partial x_i} X_s - \frac{D_s^T}{\rho T} \frac{\partial}{\partial x_i} T$$

Equation 3-13

Conservation of momentum

$$\frac{\partial}{\partial t}(\rho v_k) + \frac{\partial}{\partial x_i}(\rho v_k v_i) = -\frac{\partial}{\partial x_i} p - \frac{\partial}{\partial x_i} \tau_{ij}$$

Equation 3-14

with τ_{ij} as description for the friction tensor including the dynamic viscosity coefficient η

$$\tau_{ij} = -\eta \left(\frac{\partial}{\partial x_i} v_j + \frac{\partial}{\partial x_j} v_i - \frac{3}{2} \frac{\partial}{\partial x_k} v_k \delta_{ij} \right)$$

Equation 3-15

Conservation of energy

$$\frac{\partial}{\partial t}(\rho h) + \frac{\partial}{\partial x_i}(\rho h v_i) = \frac{\partial}{\partial t} p + v_i \frac{\partial}{\partial x_i} p - \frac{\partial}{\partial x_i} q_i - \tau_{ij} \frac{\partial}{\partial x_i} v_i$$

Equation 3-16

with q_i as description for the heat flux density

$$q_i = -\lambda \frac{d}{dx_i} T + \sum_{s=1}^{N_g} h_s j_{si}.$$

Equation 3-17

This set of equations describes the dynamic laminar flow field in three dimensions. Their solution is quite difficult and requires tremendous computing time. Therefore, some simplifications are assumed. Regarding a single monolith channel, this is often approximated

by a perfect cylindrical geometry, even for non-circular cross-sections. Furthermore, the inlet flow pattern is assumed to follow this structure. The monolithic channel can be assumed to be rotationally symmetric in the axis of the channel, and external influences on the flow, e.g., gravity forces, can be neglected. This leads to the two-dimensional governing equations with the cylindrical coordinates *z* for the axial and *r* for the radial position as independent variables.

To further reduce the complexity of the system, the boundary layer approximation can be used. It is valid for high flow rates which provide a laminar flow field but are not yet turbulent and, therefore, the axial diffusive transport can be neglected in comparison to the convective axial transport. Higher-order derivatives in axial direction are eliminated, resulting in parabolic differential equations that can easily be solved. The axial direction becomes a time-like coordinate. The simplified boundary layer approximation equations are given as

Mass continuity equation

$$\frac{\partial}{\partial z}\rho u + \frac{1}{r}\frac{\partial}{\partial r}(r\rho v) = 0$$

Equation 3-18

Conservation of species mass

$$\frac{\partial}{\partial z}(\rho u Y_s) + \frac{1}{r}\frac{\partial}{\partial r}(r\rho v Y_s) = -\frac{1}{r}\frac{\partial}{\partial r}\left(r j_{s,r}\right) + M_s \dot{\omega}_s$$

Equation 3-19

Conservation of momentum (axial)

$$\frac{\partial}{\partial z}(\rho u u) + \frac{1}{r}\frac{\partial}{\partial r}(r\rho v u) = -\frac{\partial}{\partial z}p - \frac{1}{r}\frac{\partial}{\partial r}\left[\eta r \frac{\partial}{\partial r}u\right]$$

Equation 3-20

Conservation of momentum (radial)

$$\frac{\partial}{\partial r}p = 0$$

Equation 3-21

Conservation of energy

$$\frac{\partial}{\partial z}(\rho u h) + \frac{1}{r}\frac{\partial}{\partial r}(r\rho v h) = u\frac{\partial}{\partial z}p - \frac{1}{r}\frac{\partial}{\partial r}(r q_r)$$

Equation 3-22

3.2.4 Coupling of Chemical Reactions with the Flow-field

The chemical processes at the surface are coupled with the surrounding flow-field by balance equations at the gas-surface interface. Surface reactions are now considered as a boundary condition in the conservation of species mass equation. Since the production rates of species on the catalytic surface are dependent on adsorption and desorption rates and, therefore, dependent on the gaseous fluid phase, the mass transport of these has to be considered. In dependence of boundary conditions, such as temperature, pressure, and species concentrations, the net reaction rates of homogeneous gas-phase and heterogeneous surface reactions become dependent on the mass transport of species *i* and are, therefore, determined by mass balances, considering diffusive and convective mass transport terms. To get a detailed description of the reactor with axial resolution in species concentration, the equations for flow field description are coupled with the reaction rates of the occurring chemical reactions on an elementary level. In most catalysts, washcoats are applied on the catalyst support to enlarge the available surface area. The washcoat thickness varies from 10 to 200 µm and can exhibit a non-uniform distribution on the support, for instance in small channels, where the edges of a channel have thicker washcoat layers than the center of a channel wall for reasons of cohesiveness. Mass transport limitation in a porous structure lead to concentration profiles in the structure and, hence, to reaction rates

which vary with position. For a description of the washcoat´s properties, various models can be consulted that describe the mass diffusion in porous media, i.e., molecular and Knudsen diffusion. With regard to the transport limitation in porous media, the transport effectiveness factor η_i is introduced. η_i simplifies the description of washcoat models and is defined as the ratio of the mean surface reaction rate in the porous structure divided by the surface reaction rate of species *i*, $\dot{s}_i$. When a homogeneous porous medium, time-independent concentration profiles, and a rate law of first order are assumed, η_i can be calculated in dependency of the Thiele module. The Thiele module includes the washcoat thickness (L) and the species concentration $c_{i,0}$ at the fluid/washcoat interface.

$$\eta_i = \frac{\tanh(\Phi)}{\Phi}$$

Equation 3-23

$$\Phi = L \sqrt{\frac{\dot{s}_i \gamma}{D_{\mathrm{eff},i} c_{i,0}}}$$

Equation 3-24

With $F_{\mathrm{cat/geo}}$ as the ratio of catalytic active surface area to geometric surface area the reaction rate of species *i* can be expressed by

$$R_i^{\mathrm{het}} = \eta_i F_{\mathrm{cat/geo}} \dot{s}_i M_i$$

Equation 3-25

with

$$\dot{s}_i = \sum_{i=1}^{N_\mathrm{s}} \nu_{ik}\, k_{\mathrm{f}k} \prod_{j=1}^{N_\mathrm{g}+N_\mathrm{s}} c_j^{\nu'_{jk}}$$

Equation 3-26

3.2.5 Detailed Modeling and its Limitations

The approach of detailed modeling offers a way for understanding chemical processes between the reactor structure, the catalyst surface, and the chemistry of the reactive mixture. Elementary reaction steps describe the chemical behavior of each species in the overall system for defined physical boundary conditions of temperature, pressure, and concentration. Nevertheless, the quantification of these elementary reactions is difficult and in most cases, most parameters that are needed are still unknown or can only be estimated. Due to the high temperatures in the catalytic partial oxidation, not only surface reactions have to be considered, and gas-phase species can react in the reactive flow contributed to by homogeneous gas-phase reaction pathways.

The assumption of simplified models, such as the mean-field approximation, enables one to describe a technical reactor with certain accuracy on the basis of elementary reactions. The mean-field approximation was introduced, in which the site heterogeneity of a real surface complexity was averaged out by surface coverages. The certain non-uniform catalytic surface, deriving from crystal structure defects, edges, steps, impurities, and additives, is reduced and a reaction mechanism can be set up with several sub-mechanisms for different surface structures, including the washcoat properties [85, 92].

However, when a more detailed understanding of the chemistry is essential, the mean-field approximation cannot be used. Kinetic Monte-Carlo simulations can be carried out [93] to investigate a chemical process on the molecular level with a precise description of the surface. In this method a certain species *i* is considered dependent on its neighborhood, i.e., surrounding sites and molecules. Adsorption, surface reactions, desorption, and phase transitions are calculated to obtain a real-time snapshot of the catalytic process [94-96]. The CO oxidation on Pt was carried out by Kissel-Osterrieder [89] with kinetic Monte-Carlo simulations including the surrounding flow field.

4 Experimental Setup

Within this work, a new lab-scale reactor (denoted as CPOX-II) was planned, constructed, installed, and successfully set to work for the investigation of high-boiling hydrocarbon mixtures, which cannot be evaporated below auto-ignition temperature or thermal cracking. The need for this set-up arises from the lack of experimental data of commercial hydrocarbon fuel types which are normally used in technical applications. The basic concept of the planning comprised the guideline of boundary conditions of already installed reactors here at the Karslruhe Institute of Technology, which handle model fuel surrogates, in particular the CPOX-I reactor [48]. By satisfying these conditions, experimental data remain comparable with former works.

The concept of the introduced lab-scale reactor is based on the handling of commercially available fuels for detailed, time-resolved investigation with defined boundary conditions over a broad feed-composition regime. The fuel has to be efficiently mixed with the other gaseous products to be contained in the inlet stream to provide a homogeneous distribution of the inlet stream over the radial cross-section of the catalyst. Nevertheless, since oxygen and other reactive components are present, their contact must be hindered as long as possible to avoid pre-reactions in the inlet section and, thus, to guarantee a well-known inlet composition. The reactor is designed to investigate the catalytic partial oxidation of commercial hydrocarbon fuels in real-time scale [97, 98].
In the following Sections 4.1 and 4.2, the reactor for the investigation of higher hydrocarbon fuels with time-resolved ex-situ analysis is discussed in more detail.

4.1 Concept for Feeding High-boiling Fuel into the Reactor

Hartmann *et al.* introduced a reactor concept with time-resolved analysis for the investigation of CPOx with fuel surrogates [3]. This concept has been adapted and was further improved with regard to lower residence time, diversity of the available gaseous

species that can be provided, simultaneous dozing of two different kinds of liquids and the ability to provide a pulse-free, high-boiling hydrocarbon liquid, for instance diesel fuel and kerosene. The reactor handles up to eleven gaseous species: N_2, O_2, NO, CO, CO_2. H_2, NH_3, CH_4, C_2H_2, C_2H_4, C_3H_6.

The investigation of hydrocarbon species in CPOx focuses mainly on the conversion of fuel surrogate components, such as methane for LNG, isooctane (2,2,4-trimethylpentane) for gasoline, n-dodecane and n-hexadecane for diesel fuel [32]. However, commercially-available energy sources are used in industrial applications. Large-scale fuel cell power plants, for instance, are operated with natural gas, which is steam-reformed and further cleaned up to provide a clean hydrogen gas stream for fuel cell power generation [99]. Diesel fuel is mainly reformed in mobile applications (e.g., APUs) for hydrogen production because of its on-board availability on trucks. Kerosene is the fuel of choice for future on-board reforming technologies in the aircraft sector.

Diesel fuel, for instance, is a mixture of several hundreds of different hydrocarbon species with a boiling point ranging from 160°C up to 380°C [99], which is higher comparable to gasoline and kerosene. A defined evaporation is not possible below the auto-ignition point. The auto-ignition point is defined as the lowest temperature at which the fuel will spontaneously ignite in the presence of air without any external source of heat. Spraying diesel fuel offers an alternative technique to feeding diesel fuel to a CPOx reactor. Nevertheless, in literature, diesel fuel is often injected with commercially-available diesel injection nozzles [15]. These nozzles operate with a frequently triggered injection sequence, similar to the injection process in an internal combustion engine. This triggering provides a non-continuous, slightly pulsing flow of reactants and is constant over time only in average. Since CPOx with noble metal catalysts is performed at millisecond contact times, transient effects are difficult to explore when the inlet flow stream is not precisely controlled and not pulseless. The diesel fuel can be sprayed either directly on the hot catalyst surface or indirectly on the hot reactor walls, followed by evaporation. Thermal cracking of the higher-boiling fraction in diesel fuel might be a problem when using this kind of techniques, as the nozzle's spray pattern is not adapted to the reactor size.

To face these difficulties in handling high-boiling hydrocarbon surrogates including commercial available fuels, a new lab-scale reactor plant was build. In this set-up, a two-substance stainless steel nozzle was integrated in the established tube-in-tube inlet

configuration, which is reported in earlier publications [48, 100]. The nozzle operates with a carrier gas stream, which nebulizes the hydrocarbon liquid droplets, formed at the tip of the nozzle. The carrier gas is provided via a thermal mass flow controller operated at two bars pressure. The liquid hydrocarbon is provided by a micro annular gear pump and controlled by a coriolis mass flow controller at almost ambient pressure of the liquid. With this configuration, a precise dosing of a few milliliters per minute of nebulized liquid is achieved, which is necessary for a high resolution of the carbon to oxygen (C/O) ratio in the inlet stream. Resolutions down to Δ C/O = 0.05 are realized.

The carrier gas stream enters the nozzle and is pressed through a small annular slit surrounding the nozzle hole. This slit is adjustable in width, so that for each liquid flow a good spray pattern can be achieved. A schematic drawing of the reactor inlet configuration is shown in **Figure 4-1.**

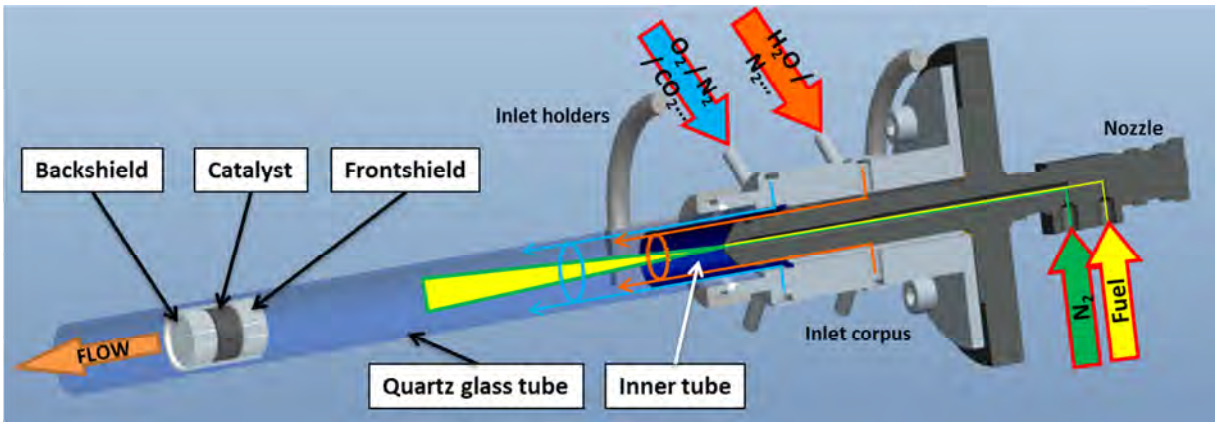

Figure 4-1: Schematic drawing of the inlet configuration: The nozzle (right) is placed in a stainless steel inlet corpus providing the liquid fuel (yellow) and the carrier gas (green). The nozzle tip ends in an inner stainless steel tube with a wall thickness of only 0.2 mm. An inner gas stream (red) keeps the nebulized fuel away from the inner tube wall and provides further non-reactive inlet stream components such as water vapor. The inner tube (dark blue) finally ends in the reactor quartz glass tube. Through a second small annular slit between inner and quartz glass tube, further gaseous components are provided containing the reactive oxygen (light blue). As a consequence of the small slit mentioned, high gas velocities are achieved, which additionally contribute to keeping the nebulized fuel away from the reactor wall.

Besides the fuel/carrier gas mixture, two independent gas streams can be provided to the inlet of the reactor. The first gas stream supplies the inner tube with a gas mixture at the

inlet temperature, e.g., inert gas, water vapor or others, keeping the fuel/carrier gas mixture away from the inner tube reactor wall. So, no considerable fuel depositions are recognized, that lead to coke formation on the reactor wall in the inlet section. The first gas stream is illustrated as red line in **Figure 4-2**. The second gas stream (illustrated as light blue lines) supplies the outer tube with the reactive, gas stream containing oxygen.

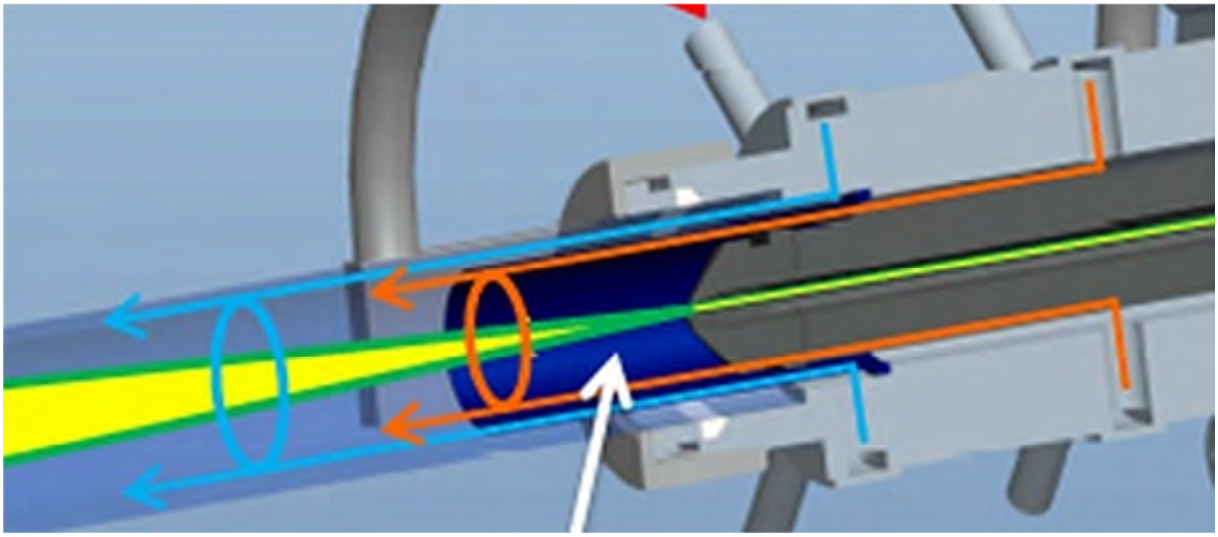

Figure 4-2: Enlarged section of the tube-in-tube configuration of Figure 4-1 (same labeling).

The outer tube is formed by the outer wall of the inner stainless steel tube and the inner wall of the quartz glass tube, which acts in parallel as reactor body. The slit formed by these two tubes is 0.85 mm in width, permitting high-space velocities at the inner reactor wall, depending on the gas stream volume flow (**Figure 4-3**). Furthermore, the nebulized liquid fuel is additionally kept away from the hot reactor wall. The total gas stream, provided as described above, hits the catalyst about 250 mm downstream in the reactor tube. Since the reactive oxygen is first mixed with the hydrocarbon containing non-reactive gas mix at the end of the inner tube and, therefore, it is guaranteed that no pre-oxidation of the hydrocarbon liquid occurs in the inlet section. All the gas streams mentioned and described are of pulse-free operation, which ensure defined inlet conditions with high-boiling hydrocarbon liquids. The description of the experimental set-up in general is given in the

next part, detailed measuring configurations are given for the three different studies in the corresponding chapter, respectively.

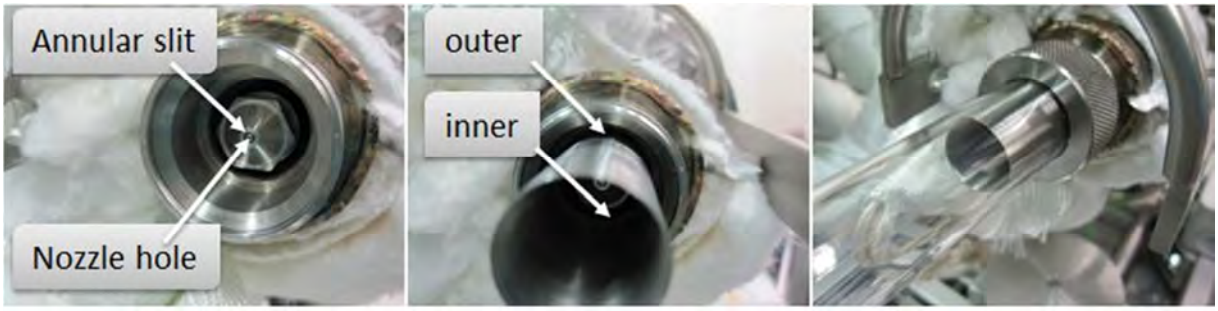

Figure 4-3: Picture of the two-substance stainless steel nozzle integrated in the tube-in-tube inlet configuration. Left: nozzle without inner tube installed. Middle: with installed inner tube. Right: complete configuration with quartz glass tube.

4.2 Description of the Reactor Unit

Due to local circumstances, additional aspects had to be taken into account during the planning and the construction of the reactor. The reactor plant operates closely to a high-power laser system, which is used for the in-situ analysis of the gas-phase in small channels above a catalytic surface in a specially-designed optical accessible reactor. Nevertheless, high-power lasers as operated in this case belong in laser category CLASS 4. Therefore, the reactor plant was constructed in that way, that nearly full remote control is available for operating the reactor. The reactor plant was constructed in a way, also to supply the mentioned optically-accessible reactor with a reactive gas mixture. In **Figure 4-4**, the schematic setup of the reactor plant is shown. It can be roughly divided into four different parts, the gas- and liquid prearrangement including mixing, evaporation and preheating as well as the reactor itself and the analytical section.

Five Eurotherm E2216 temperature indicator controllers (TIC) are used to adapt the temperature of all inlet parts online, e.g., lines providing liquid vapor, gas pre-heater (stainless steel tube heat exchanger, L = 5,5m x $Ø_i$ = 4mm), and inlet assembly in a temperature regime up to 300°C. Eurotherm E3216i TICs are used for furnace (Carbolite HST/200/E301, T_{max} = 1100°C, L = 350mm) operation, allowing the use of programmed

temperature ramps with up to eight segments. Pneumatically and magnetically actuated 3/2-way valves are used for flow directing (see **Figure 4-4**), e.g., reactor or bypass, and for protecting the analytical part in case of an emergency shutdown, while 2/2-way magnetic valves interrupt the feed flows (gaseous and liquid). Mechanical pressure shutdown devices protect the reactor against overpressure, while a membrane pump (MV 2 with CVC2000II controller, Vacuubrand) in the exhaust line keeps a constant reactor pressure when total flow rates > 5 SLPM are necessary.

The reactive gas mixture is provided via Bronkhorst thermal mass flow controllers type F-201 for gaseous species, Bronkhorst Liquiflow type L23 combined with a CEM W202A evaporator unit (also Bronkhorst), and Bronkhorst Liquiflow type L1C2 combined with a low-pulsation total evaporator [101] for smaller hydrocarbon liquids and water. All liquids are provided via pressurized vessels, using helium as pressure gas. Nevertheless, commercial diesel fuel cannot easily be dosed with thermal mass flow controllers because of its higher viscosity and changing thermal heat capacity depending on the fuel composition. Therefore, the diesel fuel is pumped with a micro annular gear pump (HNP Mikrosysteme, type MZR-4605) and controlled by Bronkhorst mini-Cori-Flow mass flow controller type M13. The micro annular gear pump has a displacement volume of only 12 µl with a pulse-less volume flow rate of 0.012 – 72 ml/min. Pressures up to 50 bars can be achieved. The controlled diesel flow is directly fed to the two-substance nozzle (Düsen-Schlick GmbH, type 970 S8 with 0.5 mm drilled hole for liquid outlet) together with a constant nitrogen carrier flow rate of 3 SLPM. Both vapor-containing feed flows, either from the CEM evaporator or the low-pulsation evaporator, can be either directed to the reactor or in the bypass, just so the pure gas mixture provided by the different Bronkhorst MFCs. For purposes of inlet mixture verification, the bypass line can be optionally directed to the analytics.

A quartz glass tube (ilmasil® PN, QSIL GmbH) is used as reactor body because of chemical inertness and high temperature stability. At both ends, an outer diameter of 1” with a wall thickness of 1.5 mm is used for the connection to the inlet and outlet section of the reactor unit, sealed with a conical shaped PTFE ring. All parts for in- and outlet, including sealing rings, are self-made at the workshops of KIT. For the middle section, a quartz glass tube with an outer diameter of 23 mm, also with 1.5 mm wall thickness, is used to achieve desired gas hourly space velocities (GHSV) at lower total gas volume flow rates. Both tube types are

molten together for gas-tightness, also at KIT. Nevertheless, since the connection endings are 1” in diameter, nearly any reactor-tube configuration can be placed inside the furnace. For instance, further reactor tubes have been constructed for the usage of packed-bed catalysts.

The product-gas mixture leaving the reactor exit is directed to an online FTIR multi gas analyzer (Multigas 2030, MKS Instruments), that detects a broad variety of IR-active species occurring during the reaction behavior of the reactor. The species are identified by their characteristic absorbed radiation that matches the frequency of the bond or group that vibrates, e.g., double bonds, triple bonds, or a carbonyl group. But since larger hydrocarbon molecules without characteristic functional group are investigated, FTIR methods only detect the sum signal of C-H vibrations for all species. For a further detailed analysis of this higher hydrocarbon species, a gas chromatograph with mass spectrometer (Thermo Finnigan, Trace GC with PolarisQ MS) with a two column configuration (Restek Rt-Q-Bond PLOT Column, 30 m, 0.32 mm ID, 10 µm and Restek ShinCarbon ST 100/120 NOC, 2 m, 0.53 mm ID) is used. Samples are taken online directly behind the reactor outlet. After the FTIR analysis, the product stream is cooled down to 5 °C with a sample gas cooler (EGK ½, Bühler technologies) to condensate steam and hydrocarbon ($C_{>3}$) species. Since the cooling is installed after the FTIR, most condensable species are detected quantitatively, e.g., water and single ring aromatics such as benzene and toluene, which are well known precursors for soot deposition. Once the condensate has been removed, hydrogen and oxygen are detected. For hydrogen, a sector field mass spectrometer (H-Sense.net, MS4 Analysentechnik) is used while a paramagnetic oxygen detector (Magnos 206, ABB) analyzes the oxygen content in the gas mixture.

For data acquisition of process parameters, e.g., temperatures, pressure, and the I/O control (analog and digital) a compact FieldPoint (cFP) module (cFP-2020, National Instruments) is installed. The cFP can be seen as a stand-alone, embedded real-time controller or Ethernet interface for PC-based, distributed I/O communication, and is equipped with eight I/O banks (2x NI cFP-TC 120 for thermocouple connection, NI cFP-AI 120 for analog signal input, NI cFP-AO 210 for analog signal output, NI cFP-DI 330 for digital status input, NI cFP-DO 403 for digital status output, 2x NI cFP-RLY 421 for switching of valves and software emergency shutdown) for hardware connections. National Instruments hardware is fully compatible with the graphical programming environment LabView® which is used for the graphical user

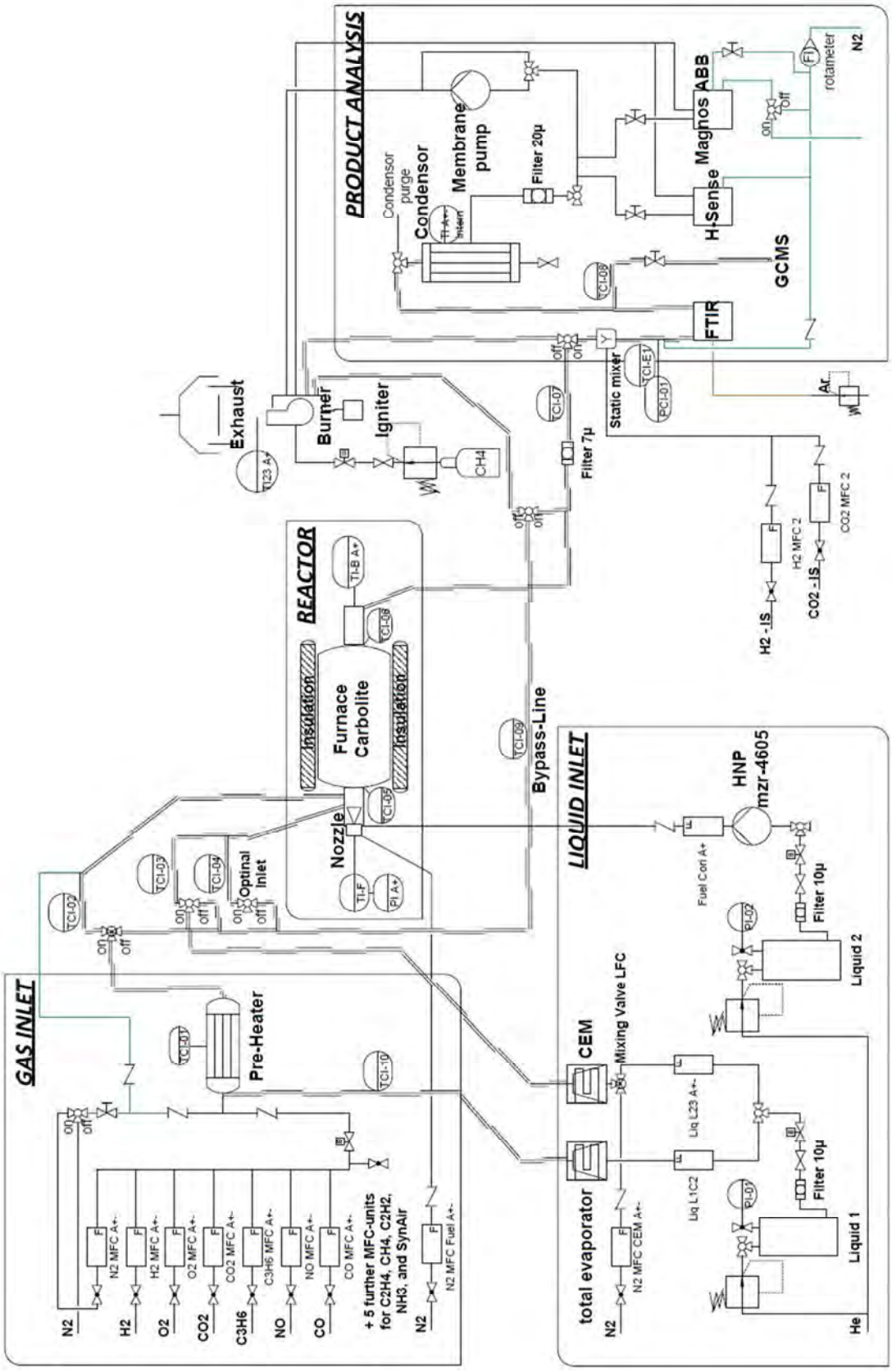

Figure 4-4: Schematic drawing of the experimental setup. Green lines symbolize the nitrogen purge gas when the reactor is offline. Brown line symbolizes the argon purge for the FTIR interferometer and optics chambers. 3/2-way-valves with on/off notation are controlled by LabView®. “On” shows the switching state, when the valve is switched on.

interface (GUI) of the reactor plant with the user. Compact and modular programming of so called virtual instruments (Vis) make it possible to control each device independently from each other, but still combined as one main GUI with full user access of each device. **Figure 4-5** shows a screenshot of the GUI for the remote control of the reactor plant. On the left, online analytic and process values are visualized; on the right, the full control of TICs, MFCs, valves and the analytic devices is located. **Figure 4-6** shows a picture of the installed reactor set-up.

Figure 4-5: Screenshot of the LabView® GUI. Left-hand side shows the online process value signal curve diagrams. Right-hand side shows the control panels for MFCs, TICs, valves, and signal curves for temperature control, data storage, and analytic devices.

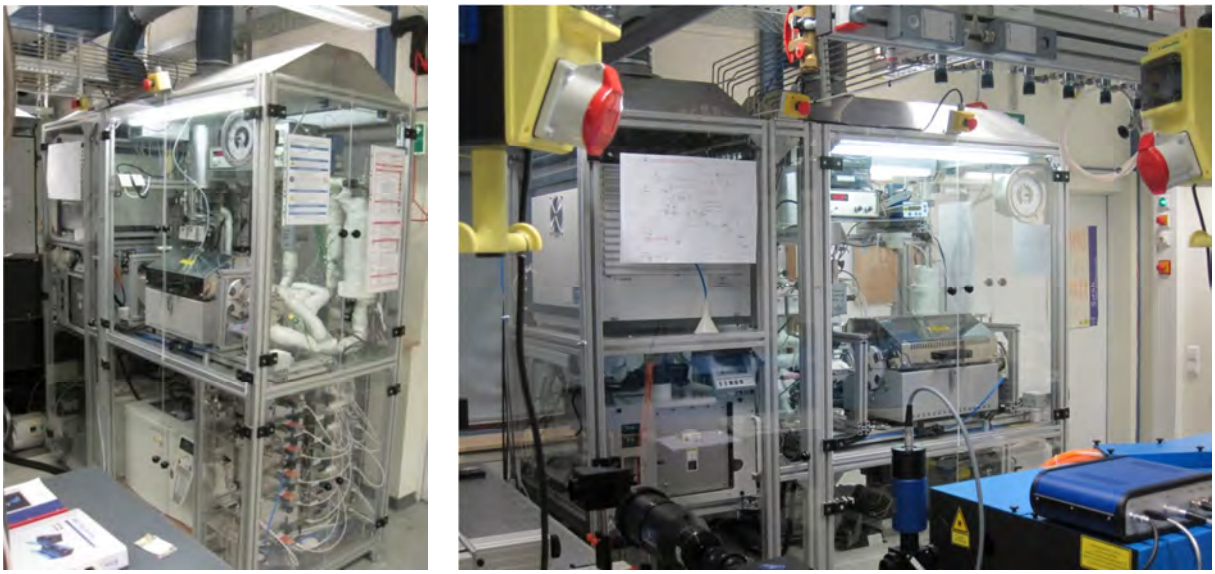

Figure 4-6: Pictures of the installed reactor set-up close to the laser system (blue device, bottom right in the right picture)

So, real-time data processing and storage is ensured even when one device has failed. The acquisition frequency for a set of data values is limited to 1 Hz, as the FTIR measures one spectral raw data file per second only. Nonetheless, a time-resolved monitoring of the investigated process is achievable, which delivers important experimental data of kinetic parameters and make the interpretation of results more precise compared to steady state analyses, typically achieved with gas chromatography.

4.3 Catalysts used

4.3.1 Monolithic Supports

Catalytic monolithic structures gained more and more importance in technical application in the last years. The demand for “process intensification”, which means reducing of the process volume and, therefore, reducing multiple step processes down to a smaller scale, is huge compared to the well-established large-size, packed-bed reaction plants. Monolithic structures combine different positive aspects compared to particulate catalysts [24, 102]. Particulates can underlie mechanical attrition due to the weight of the packed-bed itself of the motion in a fluidized bed. Rapid reaction parameter changes during transient operation provide further stress to the particle, which can induce weakening of the structural integrity and cause further attrition. Blockage of the reactor outlet can occur due to increasing pressure drop inside the system, accompanied by a loss in catalyst activity [103].

In general, a monolithic catalyst support consists of a basic structure providing structural stability, a washcoat layer for a significant increase of the surface structure, and an active site dispersed within this washcoat. In most cases, the basic structure is a thin-walled honeycomb structure, which can be formed out of a ceramic material or metal, depending on the desired purpose. Ceramic materials such as cordierite act as insulators, resulting in a very adiabatic reactor behavior [104]. Metals, in turn, act as heat conductors and are preferred for isothermal operating conditions. Cordierite is a manganese-alumina silicate with a typical composition of $(Mg,Fe)_2[Si_5Al_4O_{18}]\cdot H_2O$. Its temperature stability ranges up to 1573 K which makes it attractive for high-temperature applications with a high mechanical pressure resistance [75].

The active catalyst is incorporated in a washcoat layer which is directly deposited on the geometric catalytic surface of the monolithic structure to improve the surface to volume ratio of the original honeycomb. The washcoat itself is, in most cases, based on alumina mixed with stabilizers to improve thermal stability and to avoid sintering of the active sites inside the washcoat and the resulting decrease in catalytic activity.

Taking aspects of chemical engineering into account, honeycomb catalysts have a much smaller pressure drop in axial direction of the reactor than a packed bed, and higher space velocities can be achieved at smaller reactor sizes. In the sector of exhaust gas after-treatment, monolithic catalysts have been established over the last 30 years due to thermal stability and low pressure drop at high gas velocities. Nevertheless, in industry, monolithic catalysts are still very rare in chemical processes, compared to the classically used pellet catalysts [104]. This is due to the existence of well-established processes with a considerably smaller production volume of industrial catalyst compared to the volume of catalyst necessary for exhaust-gas after-treatment.

However, monolithic structures have advantages related to science research and to modern aspects for micro-scale reactor design, with regard to thermal management of the catalyst compared to a packed bed. Furthermore, monolithic structures provide a simple geometry which can be easily described by governing equations for momentum, mass and heat transport. Due to the small channel dimensions at the millimeter scale, a laminar flow-field is formed inside one channel, which makes the solving of the governing equations system more simple. The coupling of the flow-field with detailed reaction mechanism allows a more precise investigation of chemical reactions and helps to understand the chemical processes in a technical reaction, for instance, a reformer as used in this work [32].

4.3.2 Model Catalyst

The catalyst used for the experimental investigation of the presented data is a commercially-available honeycomb monolithic catalyst made from cordierite with 900 cpsi channel density. It is 10 mm in length with an alumina washcoat and dispersed rhodium as active site. The model catalyst specifications are given in **Table 4-1**. The catalyst was provided by the Umicore AG & Co. KG free of charge.

This catalyst is positioned between a front and a back heat shield, both 10 mm in length. The front heat shield is an alumina oxide foam, 19 mm in diameter and 10 mm in length with a porosity of 85 ppi. The back heat shield is, analogous to the catalyst, an uncoated cordierite monolithic honeycomb structure with a channel density of 600 cpsi, and is also 19 mm in diameter and 10 mm in length. The front foam provides a uniform inlet flow over the catalyst cross-section and guarantees equal inlet distribution for each channel of the monolithic structure.

Table 4-1: specification of the used catalyst; same charge of catalyst as already described by Hartmann [75].

CATALYST	**Umicore S-Type**
Honeycomb	
Material	Cordierite
Channel density [cpsi]	900
Hydrodynamic channel inner diameter [µm]	500
Wall thickness [µm]	60
Washcoat	
Material	γ-alumina oxide
Washcoat thickness [µm]	10
BET surface area [$m^2\ g^{-1}$]	51,9
Average pore diameter [nm]	13,7
Active site	
Noble metal	Rhodium
Loading [$mg\ cm^{-3}$]	1.48

Both heat shields also serve as thermocouple fixations. Therefore, a hole with 2 mm in diameter was drilled into the center of each heat shield and has a length of about nineteenth of the heat shield's lengths. Two different types of thermocouples, both with an outer diameter of 1.5 mm and 500 mm in length were used, type K (Newport OMEGA, KQXL-IM15U-450) in the front shield and type N (Newport OMEGA, NQXL-IM15U-450) in the back shield. For all catalytic experimental investigations, the complete assembly was placed in the reactor tube, being a quartz glass tube with an overall length of 500 mm, sealed with Fiberfrax® ceramic fiber paper to the glass wall to suppress bypass of the inlet mixture. The quartz glass is surrounded by a furnace, which has a length of about 350 mm, for heating and thermal insulation. The in- and outlet of the quartz glass tube are located outside the furnace and connected to the front inlet and back outlet fittings. Further insulation is provided for the blank quartz glass tube to minimize thermal heat losses over a distance of about 70 mm up- and downstream the furnace casing.

Gas hourly space velocities are calculated for the total gross volume occupied by the monolithic structure of the catalyst, in which the front alumina oxide foam and the back monolithic body are not taken into account.

4.4 Analytical Set-up

In this work, the product composition was analyzed with a variety of analytical methods. In Chapter 4.2, the individual analytic devices are mentioned, whereas in this chapter, their main function principle shall be explained with regard to quantitative analysis utilization.

4.4.1 Fourier Transformation Infrared Spectroscopy

In this work, the measure principles of the absorptive infrared spectroscopy have been used for quantification of IR-active species. IR-spectroscopy is a subcategory of molecular spectroscopy. By light absorption, molecules can be excited in their vibrational and rotational states of atoms and functional groups. In general, light with a wavelength of 0.8 – 500 µm can be used, but for the quantification of most species, the typical spectral range of 2.5 – 25 µm is used, which corresponds to a wave number of 400 – 4000 cm^{-1} [105].

Due to quantum mechanics, the adsorption of light is only possible for discrete energy values. Therein, only discrete energy states for rotation and vibration of a certain molecule are allowed, coupled with certain selection rules for energy excitation. These discrete energy states depend on the geometrical structure, bond strength, and weight of the atoms involved. The adsorption of light (photons) for vibrational excitation is the main principle of IR-spectroscopy. Photons can interact with a specific molecule by collision. Elastic collisions lead to Rayleigh scattering without energy loss and, therefore, the emitted photon has the same emission wavelength as the initial photon. Due to energy changes, inelastic collisions lead to a shift in the emission wavelength of the scattered photon. A loss of energy results in a larger photon wave length, called Stokes shift, while the uptake of energy (mainly from excited molecules, but rare) results in a shorter photon wave length, called Anti-Stokes-shift.

However, the excitation of rotational and vibrational states is coupled with a change in the molecule's dipole moment. Therefore, only molecules are IR sensitive which have a permanent or inducible dipole moment, otherwise they are Raman active [106].

In general, two types of IR-spectroscopy measurement techniques are available, dispersive and non-dispersive IR-spectroscopy devices. While non-dispersive devices (NDIR) only have

filters installed for certain spectral regions, their field of application is limited to one or only a few components detectable in parallel.

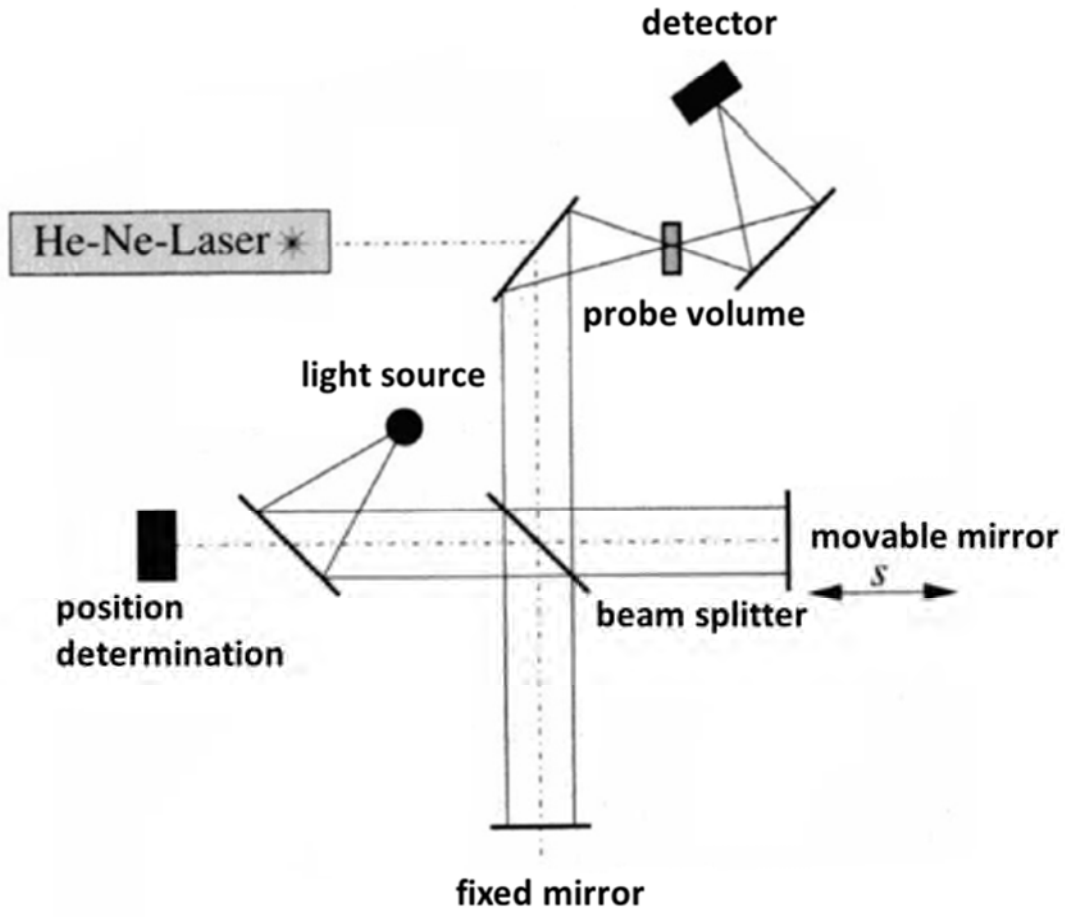

Figure 4-7: Schematic illustration of a Michelson interferometer, adapted from [107].

In contrast, dispersive devices use optical devices, such as monochromators (grids or prisms), for wave length separation and detection. However, scanning the wave length regime can be time consuming, and the spectra region of about $10 - 400\ cm^{-1}$ cannot be detected. The use of a Michelson interferometer (**Figure 4-7**) instead of monochromators results in much better spectral resolution with shorter measurement times. The initial IR beam passes the probe volume and hits a beam splitter, creating two beam lines which interfere after reflection on a fixed and a movable mirror. The intensity is detected in

dependence of the movable mirror's position (s). The signal is converted with Fourier-transformation algorithms resulting in a signal intensity as the function of the wave length for all transitions of the sample. For quantitative analysis, the law of Lambert-Beer couples the signal intensity with the concentration of the individual species in the probe volume. By setting different detection areas for certain species in the resulting spectrum, several species can be quantified simultaneously [105]. A Multigas 2030 from MKS was used for quantitative FTIR spectroscopy species determinations.

4.4.2 Mass Spectrometry

Mass spectrometry is an analytical method to separate ionic species in dependency of their masses and charge. Ionization of a gaseous sample is performed mainly with electrons of 70 eV of energy, leading to cationic species, which are accelerated with electromagnetic fields towards the separation unit. Instead of electron ionization (EI), several other ionization methods can be performed, especially for organic molecules. The high ionization energy leads to fragmentation of the molecule resulting in individual fragment patterns. To avoid complete fragmentation, soft ionization methods are available. In this work, only hydrogen was detected using EI with H-Sense mass spectrometer by MS4. The accelerated cationic species are then separated in a magnetic sector-field, due to the Lorentz force for ionic masses in a magnetic field. Ions with different masses have different trajectories with individual deflection angles. Depending on the geometry of the analyzer only certain ions leave the analyzer and are detected (**Figure 4-8**). For quantitative analysis, the intensity of the detector signal is correlated with the concentration of the considered species, in this work hydrogen.

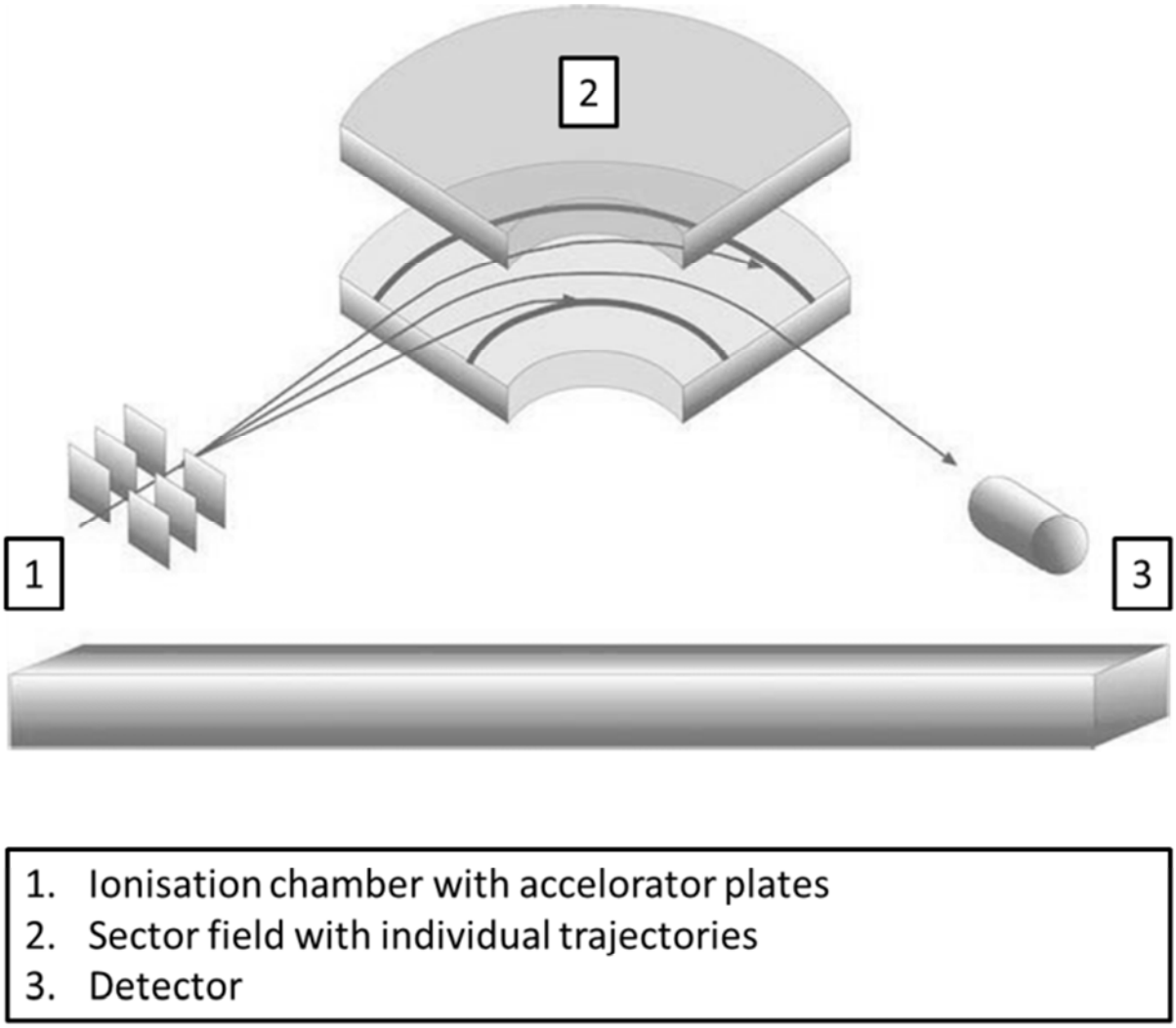

Figure 4-8: Schematic illustration of a sector field mass spectrometer, adapted from [108]

4.4.3 Paramagnetic Oxygen Detection

Oxygen can be detected due to its paramagnetic characteristics. In this work, an ABB Magnos206 oxygen analyzer was used, working according to the principle of magneto-mechanics. Herein, paramagnetic oxygen displaces a non-magnetic material out of a magnetic field, that is created by two permanent magnets. In **Figure 4-9**, two thin-walled glass marbles, low in weight and either evacuated or filled with a diamagnetic gas, are given as displaced material. The marbles are rigid-linked together and are attached to a torsion filament. The paramagnetic oxygen is attracted by the magnetic field and displaces the marbles, which results in a rotary movement that is optically detected. A conductor loop is

used to induce a magnetic field in the opposite direction of the initial one to compensate the rotary movement in dependency of the detector's signal. The current, adjusted for compensating the induced magnetic field in the conductor loop, is directly proportional to the oxygen content in the gas mixture and can be used for oxygen quantification [107].

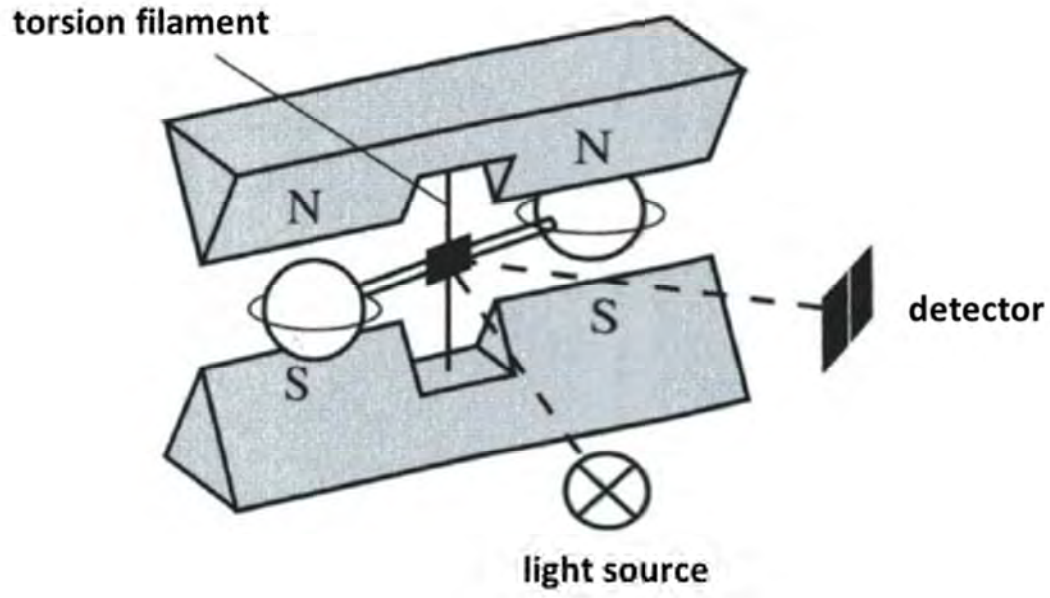

Figure 4-9: Schematic illustration of the magneto-mechanic detection principle, adapted from [107].

4.5 Method of Internal Standard for Total Flow Determination

4.5.1 Total Flow Determination

Since a hydrocarbon species with $C_{>2}$ is converted in a CPOx reaction, more moles of products are formed compared to the number of moles on the educts. **Equation C-5** and **Equation C-6** exemplarily show the CPOx reaction of a hydrocarbon species with and without oxygen contained in it. The net molar increase results in a volumetric increase compared to the volume of the total inlet flow rate. To determine the molar flow rate of a species *i* during the reaction, its concentration and the total volume flow rate have to be determined, as the molar flow rate is calculated as shown in **Equation 4-1**.

$$\dot{n}_i = \dot{V}_{tot} c_i$$

Equation 4-1

The determination of the total flow rate is performed with internal standard methods. A certain amount of carbon dioxide is pulsed directly into the product gas stream upstream the online FTIR analysis. The arising offset is determined and is aligned with the offset arising from a known total flow rate of nitrogen. The same procedure is performed with a certain amount of hydrogen for the determination of the hydrogen and oxygen flow rates, because upstream of their detection, condensable species are removed from the product stream, which results in a change of the total flow rate. The total flow rate determined for hydrogen is also used for oxygen quantification.

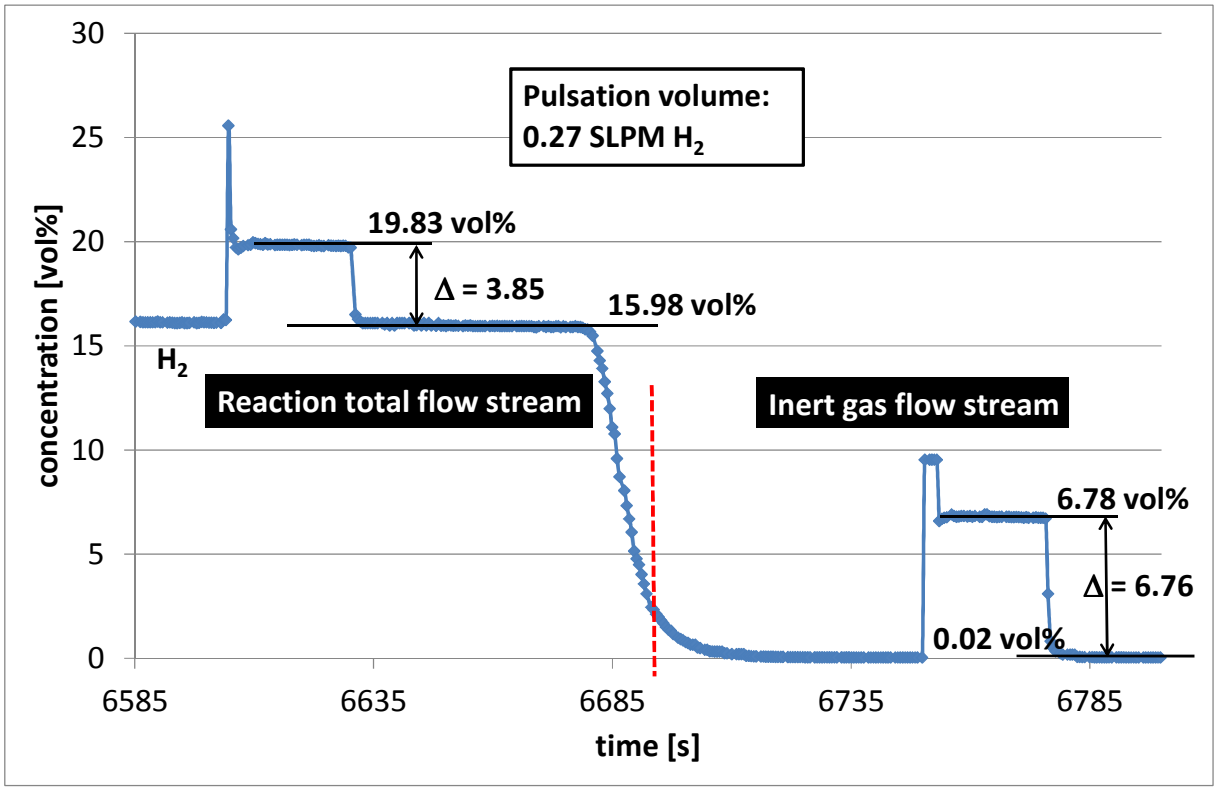

Figure 4-10: Method of internal standard for total flow determination. Shown is an exemplary pulse sequence of 0.27 SLPM H_2 into the reaction total gas stream (left) and the pure nitrogen flow (right).

Figure 4-10 exemplarily shows a pulse sequence for hydrogen with an arising offset in the concentration value. A hydrogen flow of 0.27 SLPM was pulsed into both, the reaction total gas stream and the pure nitrogen stream. Since the total flow rate of the pure nitrogen stream is known, the unknown total flow of the reaction can be calculated. For instance, in Study 2, a total flow rate for nitrogen of 3.2 SLPM was chosen.

When the total flow rate for an operating point is determined, the conversion X_i, yield Y_i and selectivity S_i of species *i* can be calculated by means of **Equation 4-2** - **Equation 4-4**, while n_k is the molar amount of the underlying educt *k*. Yield and selectivity are important parameters when comparing experimental data of chemical reactions.

In this work, yields and selectivities have been calculated on the basis of H and C atoms for each desired species *i*, respectively. For hydrogen and water, H yields and selectivities were calculated, and for all other C-containing species calculations were carried out for C yields and selectivities.

$$\boldsymbol{X_i = \frac{n_{i,0} - n_i}{n_{i,0}}}$$

Equation 4-2

$$\boldsymbol{Y_i^H = \frac{v_i^H \cdot (\dot{n}_i - \dot{n}_{i,0})}{v_k^H \cdot \dot{n}_{k,0}}}$$

Equation 4-3

$$\boldsymbol{S_i^H = \frac{v_i^H (\dot{n}_i - \dot{n}_{i,0})}{v_k^H (\dot{n}_{k,0} - \dot{n}_k)}}$$

Equation 4-4

Typically, the yields and selectivites presented in Chapter 5, 6 and 7 of this work refer to the number of C and H atoms entering the reactor of the used fuel only, as the fuel is the only species in the inlet stream that contains C and H. Beside this “fuel-based” calculation, Chapter 6 introduces a second type of yield. The chapter deals with the recycling of CO_2 and H_2O and, therefore, additional C and H sources are available in the inlet stream in parallel to

the fuel. Therefore “all-based” yields are calculated with reference to all C and H atoms entering the reactor, including CO_2 and H_2O. In Chapter 6.2, the respective references are given for the different kinds of yield calculation in each case discussed.

4.5.2 Error Consideration

As described in Chapter 4.2, the gas mixture was provided by Bronkhorst thermal mass flow controllers. Their error is stated by the manufacturer to be 2 % for the maximum value adjustable, but to be only with 0.5 % average error for the set flow rate. Their repeatability is specified as < 0.2 % for the set flow rate. However, gas flows were referenced with an external device for flow determination. For flow rates between 5 - 500 smlpm (standard milliliter per minute), a BIOS Definer 220 L, and for flow rates between 300 – 30000 smlpm, a BIOS definer 220 H was used, both having an error of 0.75 % by volume.
Liquid flow rates were determined by weight per minute with a balance, Kern PLJ720-3F with internal calibration, averaged over 12 – 15 data points. The balance’s reproducibility is stated to be 0.001 g, which is an order of magnitude smaller than the dosed process value. Average errors of liquid calibration were typically < 3 %. With these values, errors for the C/O ratio can be determined and are, of course, dependent on the flow rate of the feed stream. For the experimental conditions used in this work, the maximum errors in C/O were determined to be ΔC/O = 0.02 for C/O in the range of 0.6 – 0.85, ΔC/O = 0.03 for C/O in the range of 0.9 – 1.1, ΔC/O = 0.04 for C/O in the range of 1.15 – 1.3, and ΔC/O = 0.05 for C/O in the range of 1.4 – 1.6.
Errors for the analytic setup are given by each manufacturer. For the MKS FTIR, errors in gas concentrations are in the order of 2 % of the measured value, depending on the gas species considered. For the MS4 H-Sense, an absolute error of about 2.5 % is given.

For temperature determination, thermocouples of type N and K were used. For both, errors given by the manufacturers are 0.75 % of the measured value. However, the placement of the thermocouples, in particular the back-face thermocouple, can change the measured temperature by up to 30 K, in the front-face by up to 15 K, due to variations in catalyst and heat-shield dimensions (±0.5 mm) and to the thermal expansion of the thermocouples with

increasing reactor and furnace temperature (±3 mm). The thermal efficiency, explained in Chapter 6.3.1 in more detail, can be used to estimate the thermal losses of the reactor. Therefore, the measured gas inlet and gas outlet temperatures of the reactor are compared to the calculated adiabatic reactor temperature with regard to the enthalpy of the in- and outlet gas compositions. The adiabatic reactor temperature was calculated with the software program DETCHEM^{ADIABAT} [109]. For small C/O ratios < 0.9, thermal losses corresponding to a temperature of maximum 100 K (for C/O of 0.6) were determined, however, for C/O > 0.9, thermal losses were reduced corresponding to a temperature of less than 15 K. Furthermore, deviations from the calculated adiabatic reactor temperature can be explained by the fact that only the gas temperature at the catalyst's exit is measured, and not the surface temperature.

Major errors were caused from the fact that the total flow determination had to be performed with the method of an internal standard. Due to reaction conditions, CPOx of higher hydrocarbon species results in a net volume increase. The total flow rate downstream the reactor cannot be measured at temperatures as high as 200 °C, including all condensable species, such as water vapor. The determination of the internal standard is, therefore, dependent from the MFC's error and the error of the analytic devices. Furthermore, the dynamic behavior of the CPOx reaction causes slight fluctuations in the total volume stream, also contributing to the error of the total flow rate determination. The overall error of the total flow determination can be as high as 10 % for unstable reactor operating conditions. Typically, total flow errors were determined in the range of 1 - < 5 %.

Since, error determination is complicated in such process lab-scale reactors, attention is mostly given to the atomic balances of C, H, and O atoms. Here, the molar amounts of C, H, and O of the inlet feed-stream are compared with the quantified amounts of the outlet stream. Typically, atomic balances can be closed for each atomic species for C/O ratios < 1.2 (for isooctane) and < 0.9 (for diesel) as follows:

C: 96 _ 103 %

H: 95 - 101 %

O: 95- 105 %

At higher C/O ratios than stated above, C balances decrease below 70 % with increasing C/O due to tremendous carbon formation on the catalyst and the reactor tube. H and O balances decrease likewise.

4.6 Used Materials

Gases used in this work were stored in a gas cylinder as delivered from the manufacturers. Gases were purchased from AirLiquid Germany. Certificated test gas cylinders were purchased either from AirLiquid Germany or from basi Schöberl GmbH & Co.KG, Germany. The purity of the used gases is shown in **Table 4-2**.

Table 4-2: Purities of the chemical substances used within this work. No value can be given for the purchased diesel fuel.

Chemical of gas	Purity [%]
Nitrogen	99.999
Argon	99.999
Helium	99.999
Hydrogen	99.999
Carbon monoxide	99.997
Oxygen	99.995
Carbon dioxide	99.995
Ethylene	99.9
2,2,4-trimethylpentane	99.0
Diesel fuel	NAN

Isooctane (2,2,4-trimethylpentane) was purchased from Alfa Aesar GmbH & Co.KG, Karlsruhe, with a purity of 99 % and was used without any further purification.

The diesel fuel investigated in Study 3 was purchased from a gas station, ZG Raiffeisen, Waldhornstr. 14-16, 76131 Karlsruhe, Germany and was at that time declared as summer diesel fuel.

4.7 General Start-up of the Reactor and Ignition of the Catalytic Reaction

In this paragraph, the general start-up procedure of the reactor and the analytic setup is described. The three studies performed in this work have only a common background, but are not directly interlinked with regard to chemical understanding or experimental accomplishment. Therefore, the precise experimental description is given for each study at the beginning of the Chapter, respectively.

All presented experiments were carried out following the same operating procedure concerning the reactor plant. Before a measurement was performed, the whole reactor was preheated to the desired value and flushed with nitrogen to remove residues from the system. Residues are mainly humidity and carbon dioxide from air that entered the reactor system through the open end of the exhaust line. The instrument monitor utility of the FTIR software was used for the determination of the contamination level. The instrument monitor utility provides the possibility to check the instruments signal and detector linearity. Furthermore, a single-beam graph of the most recently collected spectrum is screen-compared with the background spectrum stored in the device at delivery. Nitrogen was purged as long as both single-beam spectra overlapped, indicating a clean background in the FTIR with comparable light intensity on the detector and therefore no residues left in the reactor. This procedure was performed every day to guarantee comparable measurement conditions for quantification of the different species. When background signals were stable, the recently collected spectra were set to a level of zero for the actual measurement, that is, all quantification values were set to zero.

In parallel, the hydrogen mass spectrometer was automatically calibrated with a certificated test gas mixture consisting of 1 vol% hydrogen in 99 % nitrogen, each with a purity of 99.999 %. This was also performed every day.

After purging the system, calibration, and checking the background signals, the desired nitrogen flow rates for the evaporators and the dilution were adjusted.

The determination of the total flow rate was performed with the method of internal standards, as described in 4.5. The reference offset for a known nitrogen flow rate was taken in Study 1 and 2 directly after the shutdown of the reaction, however, for Study 3, directly before the ignition procedure.

When the back-face thermocouple positioned directly behind the catalyst indicated values below a temperature of 523 K, the catalyst was preheated with the oxidation of hydrogen to water. Therefore, 300 ml/min of oxygen were dosed into the nitrogen stream. When oxygen was detected in the oxygen detector, 200 ml/min of hydrogen were added. The back-face temperature immediately rises and water is detected in the FTIR. When a temperature above 543 K was reached, the desired value of the fuel was adjusted. Within seconds, the reaction ignites and temperature rises sharp up, the oxygen flow rate was adapted to fit the desired C/O ratio and hydrogen was taken out of the inlet stream. The catalyst was operated for about 15 minutes at this operating point before any further adaption was performed, for instance, changes in the C/O ratio.

After the completion of a measurement, first, fuel was taken out of the inlet stream, followed directly by oxygen. The reactor cooled down in nitrogen. A carbon burn-off was performed at that point to remove any residues on the catalytic surface.

In general, the experiments in Study 1 were accomplished following the above description regarding inlet conditions preparation. Since no catalyst was used for the investigation of gas-phase reactions, no ignition procedure was necessary. The individual handling of the reactor is described in 5.1.

With regard to Study 3, this procedure had to be adapted to the special handling of diesel fuel in the reactor. The precise description is therefore given in 7.1.

5 Influence of Gas-phase Reactions Downstream the Reforming Catalyst (Study 1)

The following chapter presents the results of the investigation of gas-phase reactions, which can occur downstream of the catalytic zone in a CPOx reformer with regard to the concept of an APU. At temperatures above 823 K in the effluent, homogeneous gas-phase chemistry is relevant, especially for fuel-rich operation of the reformer. In many approaches, the fuel processor is operated at fuel-lean conditions, often with water present in the inlet to enhance fuel evaporation and to avoid coking. With regard to the efficient conversion of the fuel to hydrogen, C/O ratios about unity are favorable to obtain high selectivities in H_2 [34]. Due to transport limitations of oxygen in the initial first millimeters of the catalyst, fuel conversion is not complete, leading to the presence of small amounts of hydrocarbons in the downstream catalyst and reformer section, which could be identified to be responsible for coke formation.

5.1 Accomplishment of Study 1

In Study 1, the influence of gas-phase reactions occurring downstream of a CPOx reformer with a monolithic honeycomb catalyst was investigated. This study has already been published in:

"Torsten Kaltschmitt, Lubow Maier, Marco Hartmann, Christian Hauck, Olaf Deutschmann,

Influence of gas-phase reactions on catalytic reforming of isooctane,

Proceedings of the Combustion Institute, *Volume 33, Issue 2*, *2011*, *Pages 3177-3183".*

In the following, the results are discussed as in the article available. Reprinted (adapted) with kind permission of Elsevier. Copyright (2011) Elsevier.

Two different problems are distinguished, each of which is described separately in the experimental accomplishment and the discussion of the experimental results.

Catalytic case: The catalytic experiment in Study 1 was carried out in a CPOx reactor with the catalyst configuration described in Chapter 4.3.2, without any further modification. The inlet section was preheated to a temperature of 463 K. Furnace temperature was set to a value of 523 K to preheat the catalyst. Isooctane was used as reference fuel. The C/O ratio was calculated as ranging from 0.8 – 1.6 with a total inlet flow of 4 SLPM with a dilution of 80 vol% nitrogen. The reaction was accomplished as declared in 4.7. The determination of the internal standard offset was performed after the shutdown of the reaction.

Non-catalytic case: A quartz tube reactor with a total length of 500 mm and with an inner diameter of 20 mm was placed in the furnace as described in 4.2. The heated length of the quartz glass tube inside the furnace casing is 250 mm, the entrance is defined as z = 0 m for the simulations described in chapter 5. Two thermocouples were placed at the reactor inlet (z = 0 m) and center zone (z = 0.125 m) inside the tube. The position of the center thermocouple corresponds to the location of the catalyst exit in standard CPOx experiments [48] and equates to the highest expected temperature in the tube downstream the catalyst. Experiments without catalyst were conducted using a simulated exhaust gas of an isooctane-fueled CPOX reactor as inlet gas, which mainly consists of synthesis gas, steam, CO_2, ethylene, and the remaining fuel isooctane (Table **5**-**1**). The compositions were determined based on the experimental results of the catalytic case performed by Hartmann *et al.* [34, 75] and served as the basis for the experiments accomplished in Study 1. Since the reactions total flow rate decreases with increasing C/O due to non-stoichiometric reaction conditions, the residence time increases and is additionally given in Table **5**-**1**.

These compositions were fed to the reactor tube under isothermal conditions, and gas-phase products have been quantified for C/O = 1.0, 1.3, and 1.6. The product stream is analyzed by means described in 4.2.

Four different temperatures were used to investigate gas-phase reactions and kinetic parameters at isothermal conditions. The furnace temperature was set to 873 K (770 K), 973 K (877 K), 1073 K (993 K) and 1173 K (1108 K) for a measurement consisting of the three different C/O ratios 1.0, 1.3, and 1.6. The values in parentheses were the corresponding

temperatures measured inside the reactor tube at the position of the normally-located catalysts exit. Below a temperature of about 773 K, gas-phase reactions can be neglected.

Table 5-1: Inlet compositions given in mole fractions and residence time in s.

C/O	1	1.3	1.6
CO	2.01E-01	1.82E-01	1.68E-01
H_2	2.32E-01	2.29E-01	2.12E-01
CO_2	1.10E-02	1.18E-02	1.41E-02
H_2O	1.47E-02	8.75E-03	1.34E-02
Ethylene	0.00E+00	4.85E-04	4.41E-04
Isooctane	6.25E-05	2.77E-03	7.68E-03
Nitrogen	5.41E-01	5.65E-01	5.84E-01
τ	0.809	0.841	0.879

For each measurement the furnace was heated to 523 K and the composition of C/O = 1.0 was adjusted, following the procedure explained in 4.7. When steady state was reached, C/O was changed to 1.3 and subsequently to 1.6. After that, the furnace temperature was set to 873 K with a C/O ratio beginning at 1.0. Once steady state was reached, C/O was changed as described above. After steady state of C/O = 1.6 was reached, the reaction was shut-down and a burn-off was conducted for full removal of carbon deposits in the quartz reactor. Therefore, the reactor was heated up by a 15 K/min ramp to 973 K in 1 SLPM synthetic air (O_2:N_2 = 20:80), kept at that temperature for 5 minutes, and then cooled down to room temperature in nitrogen flow.

This procedure was repeated for temperatures from 973 K to 1173 K. A constant dilution of 3.2 SLPM nitrogen flow rate was used in all experiments, corresponding to the nitrogen feed of the referenced CPOx experiment.

5.2 Modeling Approach

The catalytic and non-catalytic conversion of isooctane in the tubular quartz glass reactor is modeled using a two-dimensional and a one-dimensional flow field description, respectively. Both simulations apply tools of the DETCHEM^{TM} software package [109], DETCHEM^{CHANNEL} and DETCHEM^{PLUG}, respectively. The DETCHEM^{CHANNEL} code was recently shown to efficiently treat catalytic reforming of logistic fuel surrogates even if thousands of reactions were implemented [67, 110-112]. The catalytic case here serves as a reference to illustrate the problem of adequate gas-phase reaction models, which were the focus of Study 1. All simulations in Study 1 were performed by Dr. Lubow Maier and are mentioned here to give a better understanding of the basic problem introduced in Chapter 2.1.

Catalytic case: The reactor is set-up in a way that, due to the thermal insulation the temperature gradient across the catalyst is small. Furthermore, uniform inlet conditions are ensured. Therefore, all channels of the monolith behave essentially alike, and only one representative channel needs to be analyzed. The flow field inside the monolith channel is laminar. This single channel is approximated by an axis-symmetric cylinder leading to the axial and radial spatial coordinates as independent variables of the flow-field simulation. Due to the short residence time in on the order of milliseconds, the transport in axial direction is mainly determined by convection implying that axial diffusion can be neglected, which reduces the elliptical structure of the steady-state Navier-Stokes equations to a parabolic one by application of a boundary-layer approximation [113]. At given inlet conditions, the boundary-layer equations are solved by integration along the axial direction with a method-of-lines procedure. The chemical reactions are modeled by detailed reaction schemes for heterogeneous and homogeneous reactions. The state of the catalytic surface is then described by the temperature and a set of locally-varying species surface coverages. Inlet and boundary conditions of the simulation of catalytic partial oxidation of isooctane over Rh

are taken from the experiment [34, 48, 49], in which a 1 cm long Rh coated monolith was used, fed with 4 SLPM isooctane/oxygen mixture at the catalyst temperature of 1080 K, C/O ratio of 1.1, and 80% N_2 dilution.

Non-catalytic case: In the simulation of the non-catalytic conversion in a heated tube, inlet and boundary conditions were chosen according to the isothermal experimental study described above and in Table **5**-**1**. A one-dimensional isothermal plug flow model was applied. The product composition of the catalytic experiment now serves as inlet feed. Since the measured catalyst exit temperature was chosen as a reference (in the center of the tube) for the operating reactor temperature in the non-catalytic experiment, the conversion that was numerically predicted by the simulation can be interpreted as an upper limit of the total conversion in the homogenous reaction zone downstream of the catalyst.

Surface reaction mechanism: In the catalytic case, a recently-developed surface reaction mechanism consisting of 56 reactions among 9 gas-phase and 17 surface-adsorbed species was used without modification [49].

Gas-phase reaction mechanisms: In both the catalytic and the non-catalytic case, detailed homogeneous gas-phase mechanisms were coupled with the flow-field description. Two different homogeneous chemistry models for isooctane were used, including aromatic (AH) and polyaromatic hydrocarbons (PAH), to better indicate the reliability of currently-available models.

Gas-phase reaction mechanism 1 (M1): This first mechanism is based on the well-known, detailed scheme developed for isooctane combustion at Lawrence Livermore National Laboratory (LLNL) [114, 115], which consists of 4238 reactions among 1034 species, most of them reversible. This mechanism was later coupled with a detailed toluene scheme from Dagaut *et al.* [116], which is discussed by Andrae *et al.* [117]. The toluene mechanism [116] has been validated by experiments of toluene oxidation in an atmospheric jet-stirred reactor, by simulation of benzene oxidation from 0.46 to 10 atm, the ignition of benzene-oxygen-argon mixtures, and the combustion of benzene in flames. The merged mechanism consisted of 8927 reactions among 1082 species.

Gas-phase reaction mechanism 2 (M2): A much smaller second mechanism was applied, as well. It is derived from various literature sources based on the work by the Dean group [118,

119], eventually leading to 3611 reactions among 420 species including the reaction pathway for aromatic and some polyaromatic hydrocarbons, such as naphthalene, anthracene, and pyrene.

5.3 Results and Discussion

Catalytic case:, The catalytic conversion of isooctane over Rh is exemplarily discussed at C/O = 1.1. At this slightly fuel rich condition, all the oxygen is consumed but conversion of the fuel isooctane is not complete. Rapid catalytic conversion of isooctane basically stops after the catalyst's first millimeter (**Figure 5-1a**). In that short entrance zone, the major products H_2 and CO, but also H_2O and CO_2 (not shown) are formed. The remaining fuel opens up a second, now homogeneous route for conversion, which is pyrolysis of the fuel and molecular-growth in the gas-phase, leading to soot precursors and deposition of carbon on the catalytic surface. At the catalyst exit, significant amounts of ethylene, acetylene, and benzene are predicted, which were also detected experimentally. However, in the experiment, gas-phase reactions may also occur downstream of the catalyst, which means that the measured data is likely to differ to a certain amount from the concentrations occurring at the catalyst exit t. The numerically-calculated surface coverage of different species along the axial direction for steady-state operation of the catalyst shows the formation of a carbon layer on the surface at $z > 1.1$ mm, leading to a deactivation of the catalytic surface in this zone (**Figure 5-2**). Since active sites are not available at $z > 1.1$ mm, the inhibiting effect of the noble metal on gas-phase conversion through radical recombination will disappear as well. Consequently, a radical pool can be built up and homogeneous pyrolysis is likely (**Figure 5-1b**).

It should be noted that, in real catalytic systems, coke formation and build-up is a transient effect overlapping with the catalytic conversion of hydrocarbon species. The simulation conducted in the present study computes the steady state without taking transient effects, such as slow build-up of coke, into account, as no model for coke formation was implemented in gas-phase kinetics. The steady-state simulation results show a carbon-covered (one monolayer) surface downstream of the reactor, which is consistent with the general experimental observation that the catalyst cokes up starting at the back end of the

catalyst in CPOx reactors using higher hydrocarbons at rich conditions. At reaction temperatures above 973 K (700°C), the simulation and experiments show significant thermal cracking of the fuel.

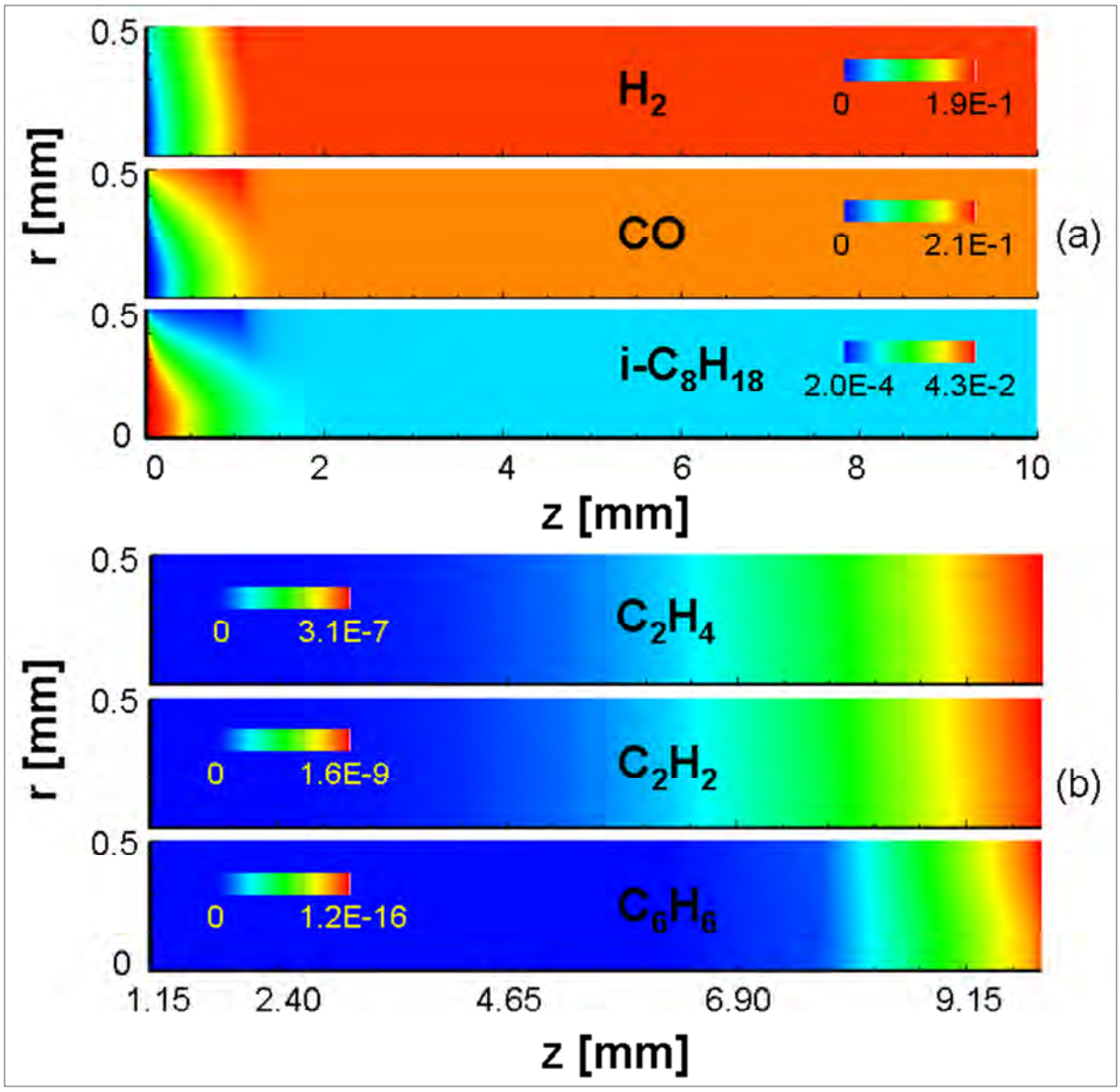

Figure 5-1: Numerically predicted mole fractions of isooctane, CO, H_2 (a) and ethylene, acetylene, and benzene (b) in the catalytic channel at C/O = 1.1, 1080 K, 80 % N_2 dilution. The symmetry axis of the channel and the gas-wall interface are at r = 0 and 0.5 mm, respectively.

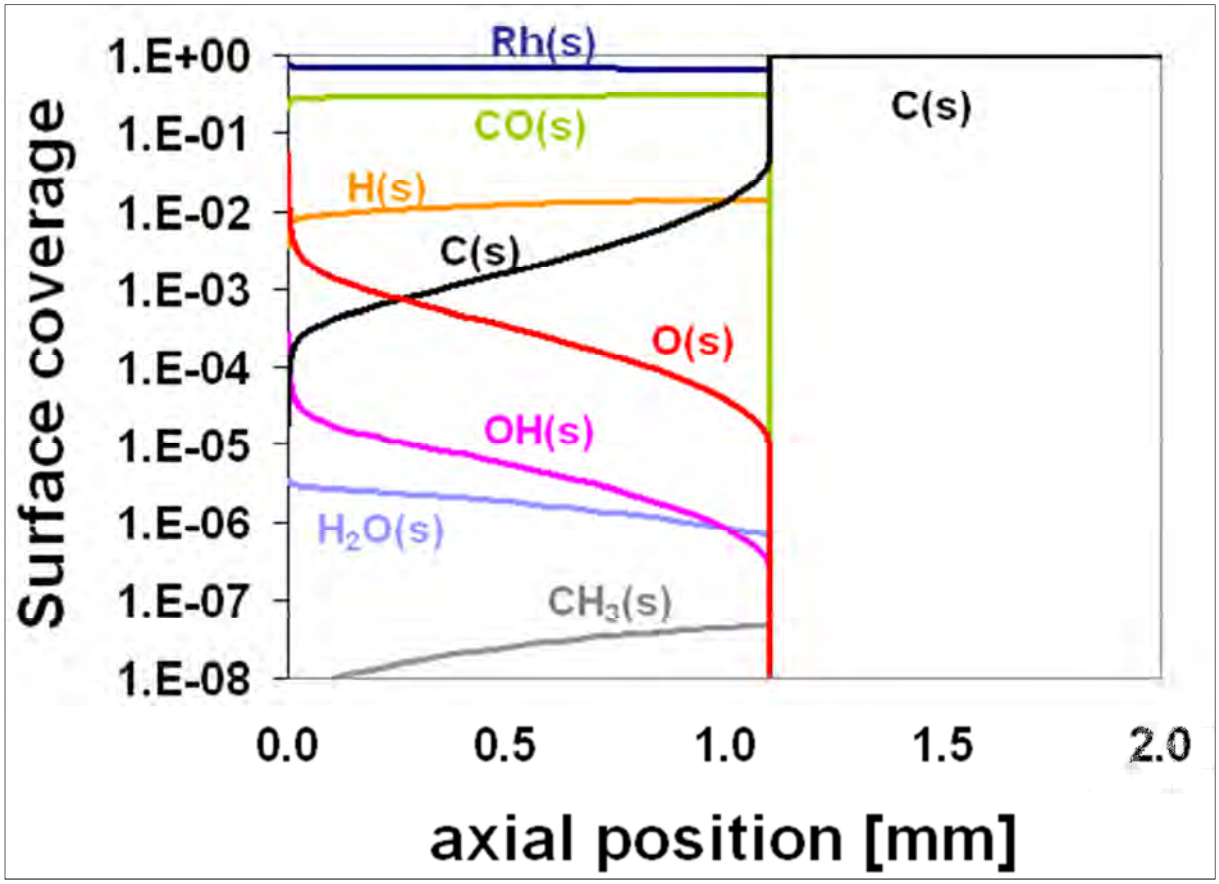

Figure 5-2: Numerically predicted surface coverage of adsorbed species as a function of axial position along the monolith channel: C/O = 1.1, 1080 K, 80 % N_2 dilution, 4 SLPM.

Non-catalytic case: The problem in catalytic reforming of isooctane at slightly fuel-rich conditions was introduced. The presence of remaining unconverted fuel at the point where all oxygen is consumed can lead to additional reactions in the gas-phase, especially at high temperatures. Therefore, the focus will now be on gas-phase reactions only and the potential homogeneous conversion of the remaining fuel in the non-active section of the catalyst and further downstream will be discussed. The numerically-predicted species profiles in the heated empty tube are shown in **Figure 5-3** at a temperature of 1108 K and rather rich conditions of C/O = 1.6. With both chemistry models (M1 and M2), the small (remaining) amount of isooctane is completely converted in the first five centimeters. However, the product composition still varies significantly; even the major products hydrogen and CO vary, and their concentrations decrease, while hydrocarbons, such as methane, ethylene, propylene, and acetylene, are produced. Propylene concentration

decreases again (z > 5cm) due to further thermal cracking, hydrogenation, and formation of aromatics and polyaromatics, eventually resulting in carbon deposition. Homogeneous conversion of hydrogen reaches 10 % at high temperature and fuel rich conditions whereas CO is only slightly converted (1 – 2 %).

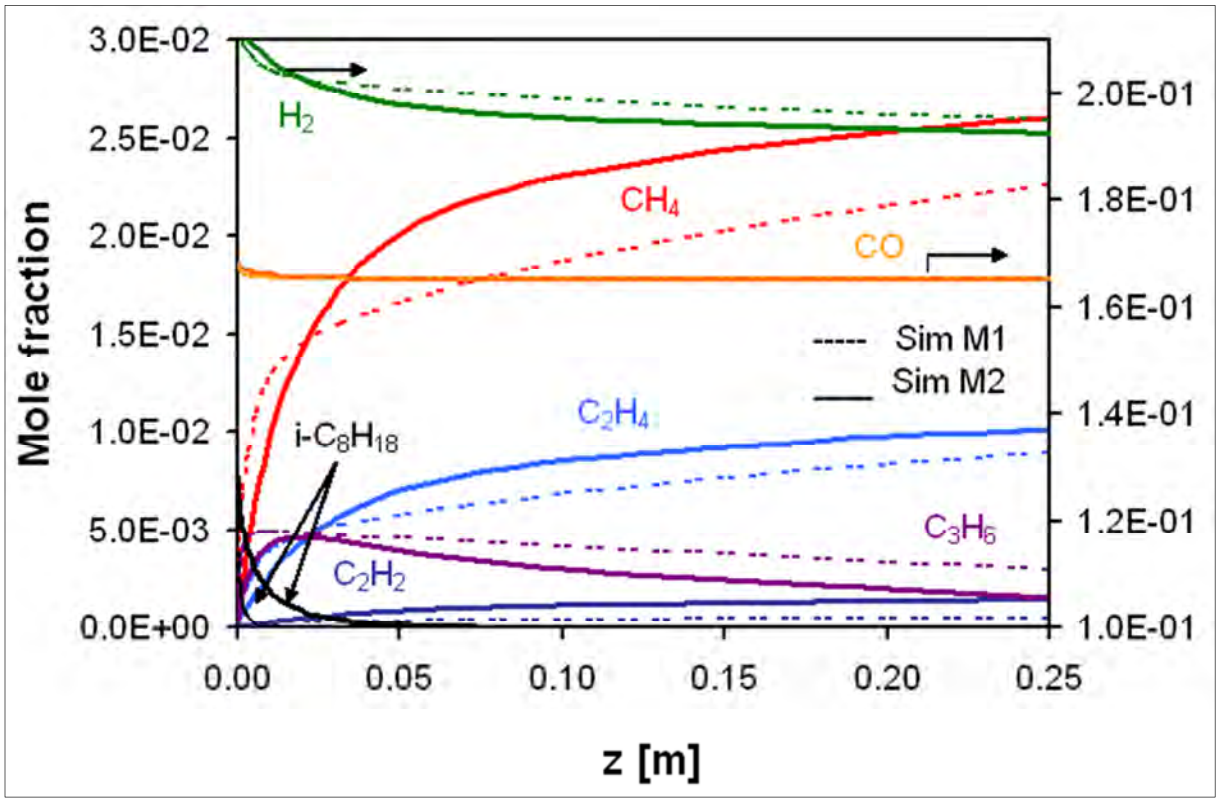

Figure 5-3: Numerically predicted fuel and product profiles with mechanisms M1 (dashed lines) and M2 (solid lines) as a function of axial position along the reactor; C/O = 1.6, 1108 K, 6 SLPM.

Experimental results confirm these trends; for all three C/O ratios studied, hydrogen and carbon monoxide concentrations are slightly reduced, while water and carbon dioxide concentrations increase (except for a gas temperature of 1108 K in case of carbon dioxide). This implies that, here, reverse water gas shift and hydrogenation reactions are significant in gas-phase chemistry. As shown in **Figure 5-4**, significant amounts of C_3-C_4 olefins (1,2-propadiene, propene, propyne, n-butene (1-buten, 2-butene), iso-butene, and 1,3-butadiene) are formed directly at the reactor entrance, resulting from thermal cracking of the remaining fuel. Ranzi *et al.* give a calculation plot for the distribution of the initial

selectivities of primary products formed in isooctane oxidation reactions [120]. At temperatures comparable to those in the experiments in this work, initial products formed are mainly decomposition products and olefinic species, as predicted from the two mechanisms M1 and M2. Ongoing cracking processes combined with acetylene and aromatic hydrocarbons formation further downstream lead to the formation of polyaromatic hydrocarbons, such as naphthalene, anthracene, and pyrene, which finally results in carbon deposition.

The way of polyaromatic hydrocarbon formation can be suggested to start from an olefinic species, followed by hydrogen abstraction of a radical species in the gas-phase. Radical polymerization with C_2-C_3 olefins starts, building-up larger hydrocarbon chains followed by cyclisation and dehydrogenation, ending-up in the formation of aromatic rings. Latter ones can undergo further accumulation resulting in polyaromatics and deposits [118]. In the upper part of **Figure 5-4** a photo of the experimental reactor tube is displayed after operation at these conditions. Two different zones of carbon deposition can clearly be distinguished, a slight carbon zone in the entrance region of the furnace and a pronounced carbon coating around the center of the reactor and downstream. The first carbon deposition results mainly from C_3-C_4 olefins leading to coke formation via alternative pathways compared to PAH mechanism, while the second carbon deposition arises from continuous PAH formation. The soot formation process in the combustion of hydrocarbons still remains a challenging problem, and the mechanism of soot formation is not fully understood. In addition to the mechanism of formation of polyaromatic hydrocarbons, some other models have been proposed, such as the polyyne model of soot formation, the mechanisms of acetylene pyrolysis and pure carbon cluster formation [121]. One of these alternative pathways can be assumed for coke formation at the first carbon zone. Krummenacher *et al.* [15] suggested a pathway for olefin formation when unconverted hydrocarbons are present after the first total oxidation zone. They do not specify, whether this pathway is for homogeneous or surface chemistry because of its difficult termination. The following scheme shows the postulated pathway for a hydrocarbon species in general and not for the used fuel isooctane. The formation is initiated by pyrolysis of the hydrocarbon, leading to two alkyl radials

$$R_1 - R_2 \rightarrow R_1 \cdot + R_2 \cdot,$$

Equation 5-1

determined by statistical C-C scission accounting for the higher bond strengths associated with methyl and ethyl. The radical can, then, undergo either β–scission to form ethylene and a smaller radical

$$RCH_2CH_2 \cdot \rightarrow R \cdot + C_2H_4,$$

Equation 5-2

or β-hydrogen elimination to form a larger stable olefin

$$RCH_2CH_2 \cdot \rightarrow RCH = CH_2.$$

Equation 5-3

It is expected that the radical continues this fragmentation under the formation of ethylene until it finally forms ethyl or propyl, ending up in ethylene or propylene by dehydrogenation

$$C_2H_5 \cdot \rightarrow H \cdot + C_2H_4$$

Equation 5-4

$$C_3H_7 \cdot \rightarrow H \cdot + C_3H_6.$$

Equation 5-5

The axial shift in the appearance of the carbon zone in both experiment and simulation likely arises from the not fully adequate assumption of an isothermal reactor, in particular at the inlet at z = 0 m. Beyond the first coking zone, no carbon deposits are found, which could be caused by carbon gasification reactions with CO_2 and water, and the fact that olefinic hydrocarbon concentrations are much smaller in this zone whereas the concentration of PAH is not yet large enough for deposit formation.

A minimal reactor temperature is obviously required for thermal cracking processes. In case of isooctane, a temperature of at least 850 K is needed to initiate gas-phase fragmentation and the formation of C_1-C_3 hydrocarbon species at the given residence time (**Figure 5-5**). Isooctane conversion is not observed below 850 K, neither in experiment nor in simulation. With rising temperature more hydrocarbon fragments are produced.

A maximum isooctane conversion of 87.5 % is observed in case of C/O = 1.6 at 1108 K. The main products for temperatures above 850 K are methane and propylene. In the simulation with mechanism M1 more C_1-C_3 hydrocarbon species are predicted than with M2. This can be related to the missing of PAH formation reactions in M1, in which only AH formation is included. In M2, C_1-C_3 hydrocarbon species are used for PAH formation, resulting in reduced species concentration profiles.

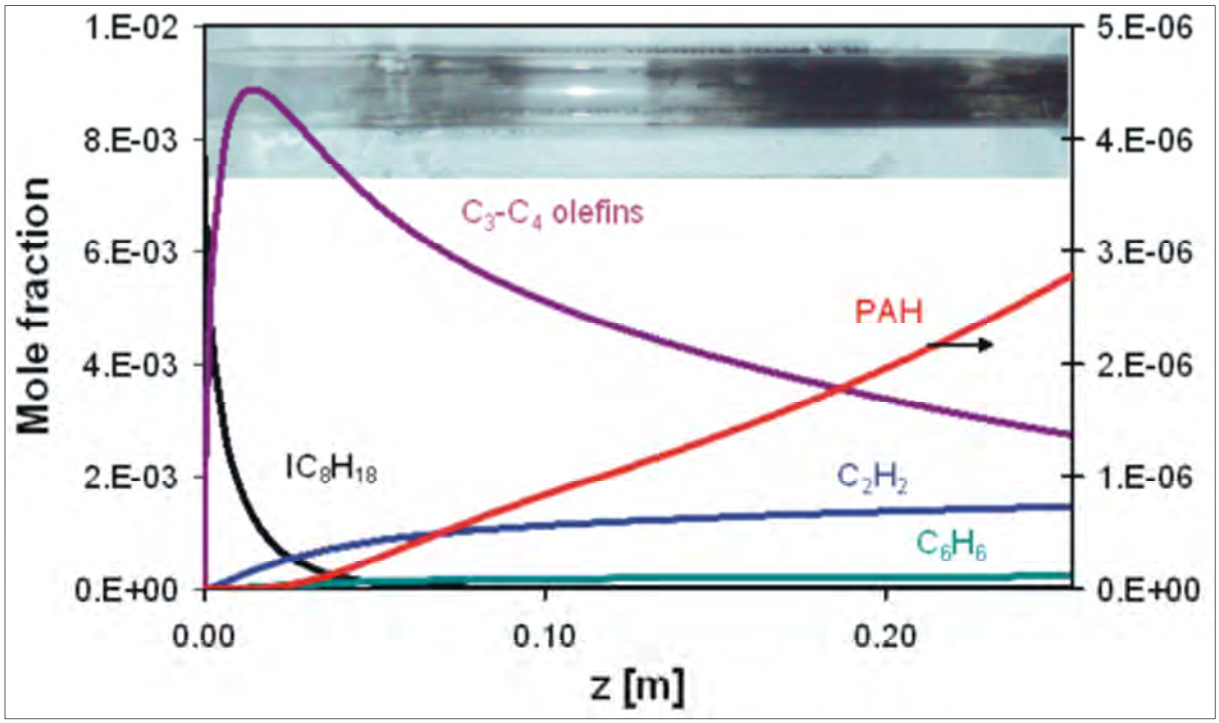

Figure 5-4: The distribution of carbon precursors along the reactor modeled with mechanism M2; C/O = 1.6, 1108 K, 6 SLPM. C_3-C_4 olefins contain 1,2-propadiene, propene, propyne, n-butene (1-buten, 2-butene), iso-butene, and 1,3-butadiene; PAH contains naphthalene, anthracene, and pyrene. Embedded photo shows the tubular quartz reactor after operation.

The experiment detects even less, which indicates that these species have a stronger tendency to form carbon depositions than predicted. When the temperature exceeds 990 K, propylene concentration decreases and more ethylene and acetylene are formed, which are not found at temperatures below 1000 K due to their high formation enthalpy. It can be estimated that the consumed amount of propylene is either used for further

methane / ethylene formation or for PAH production. Apparently, propylene is preferred to ethylene for the allocation of soot precursor species at high temperatures.

Certainly, the formation of soot precursor species and, therefore, carbon deposition does not only depend on reactor temperature but also on gas inlet composition corresponding to different C/O ratios. The higher the C/O inlet ratio, the larger the amount of soot precursors formed. Detailed species profiles in gas-phase reactions as a function of the C/O ratio at a temperature of 993 K are shown in **Figure 5-6**. Consumption of hydrogen and carbon monoxide slightly rises with an increasing C/O ratio; CO reveals a sharper decline than hydrogen for C/O < 1.3. The consumption of water and the formation of carbon dioxide points to the water-gas shift reaction taking place for C/O < 1.3. **Figure 5-6** shows that at higher fuel concentration of C/O > 1.3, water is produced but hydrogen is increasingly consumed, which is related to methanation.

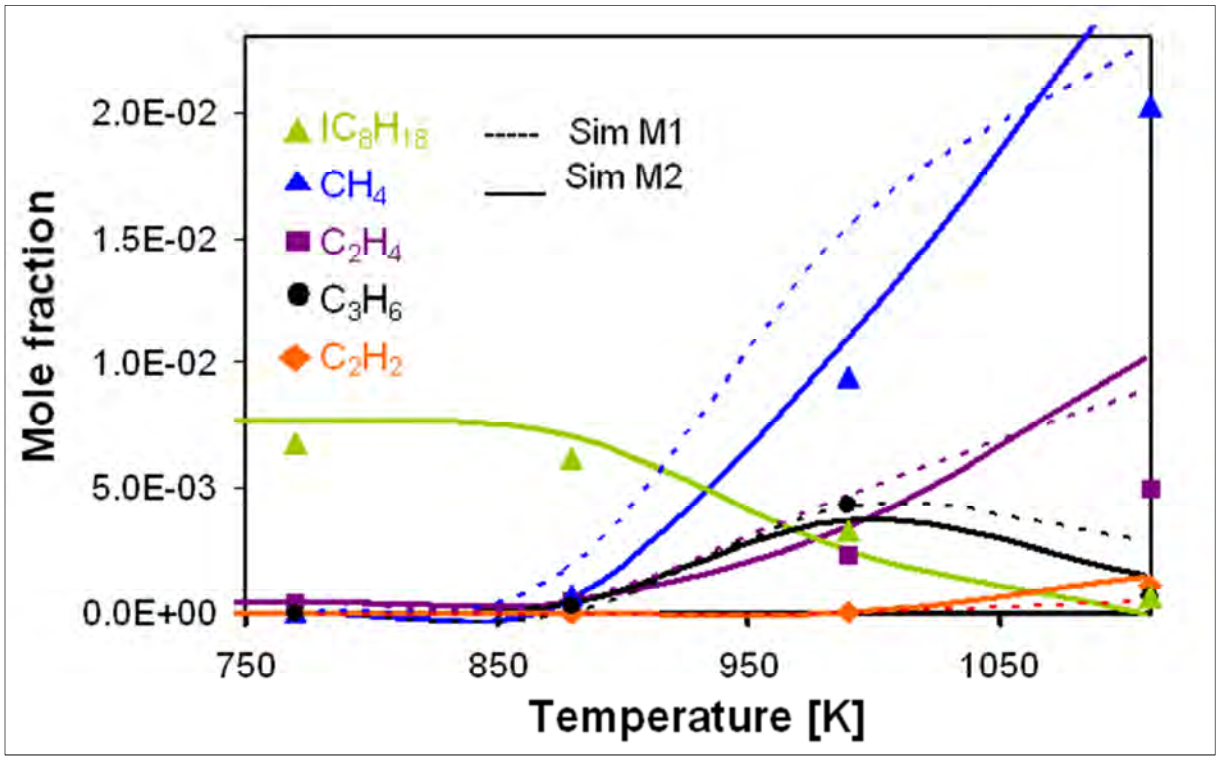

Figure 5-5: Product distribution as a function of temperature measured in the center of the reactor tube for C/O=1.6; symbols = experiment, dashed/solid lines = simulations with M1/2.

With the formation of by-products, synthesis gas is consumed by gas-phase reactions. Most of the by-products seem to derive from the fuel via olefin formation. Ethylene does not have a significant influence on gas-phase reaction chemistry as long as isooctane is provided. An increase in ethylene concentration, compared to the inlet feed, is observed for all C/O ratios and temperatures. Thermal cracking initiates fuel fragmentation at the first millimeters of the reaction zone, followed by a variety of reforming and condensations reactions, leading, on the one hand, to a decrease in syngas concentration and, on the other, hand to PAH formation and finally to carbon deposition, both of which are undesired in the applications considered.

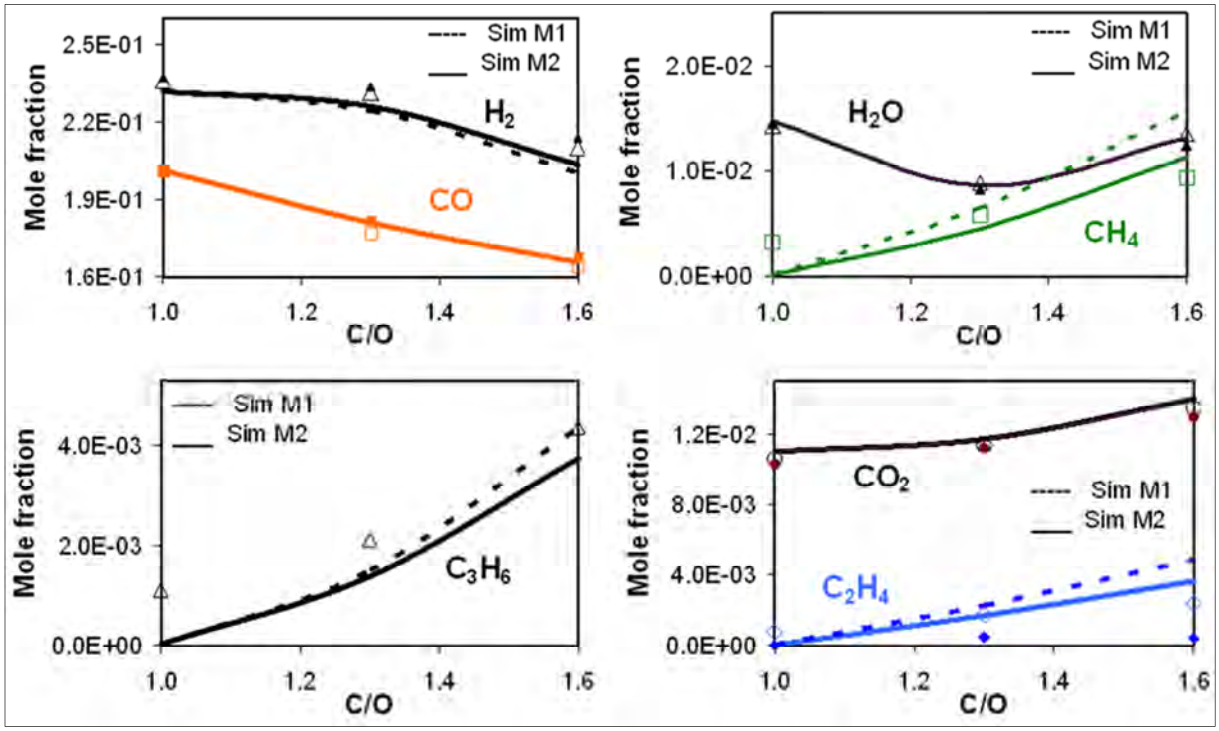

Figure 5-6: Species profiles for varying C/O ratios at 993 K; open symbols = experiment, dashed/solid lines = simulations with mechanisms M1/M2, filled symbols = inlet.

5.4 Summary and conclusion for Study 1

Isooctane was chosen as a model substance to better understand the impact of gas-phase reactions on conversion and selectivity in CPOx of logistic fuels. At fuel rich conditions, i.e.,

molar C/O ratios above unity, the catalyst is covered by carbon deposits downstream of the position at which all oxygen is consumed. In this catalyst zone and further downstream of the catalyst, gas-phase reactions play a major role in the conversion of the remaining fuel. Pure gas-phase experiments and simulations with two different, large elementary-step experiments reveal: apart from surface reactions, gas-phase reactions among a multitude of species are responsible for coke formation when unconverted fuel leaves the high-temperature oxidation zone in the catalyst. Large amounts of olefinic hydrocarbons are initially formed by thermal cracking, leading to aromatic molecules and PAHs. The presence of gas-phase reactions in the post-catalytic zone decreases the amount of hydrogen produced through methanation and hydrogenation of carbon monoxide and olefins, especially at fuel-rich conditions. The cracking of the remaining fuel increases the concentration of by-products (ethylene, acetylene, and C_3-C_4 olefins) and, consequently, of carbon deposits.

This study also reveals that experimentally-determined yields (major as well as minor products) in laboratory CPOx reactors may deviate from the local yields at the catalyst exit because the products can usually not be quenched in a sufficiently fast manner to avoid gaseous post-reactions occurring within millimeters beyond the catalyst. Here, models can be used to re-calibrate the measured data by solving the inverse problem of determining what concentration would have existed at the catalyst exit. While such an approach will be usable only in special cases, an estimation of the impact of gas-phase reactions on the conversion in catalytic reforming of gasoline and diesel fuel can support the design and optimization of technical fuel reformers.

Even though both gas-phase reaction models and the surface reaction model can predict the species profiles well, several unresolved issues remain, such as the reactions between gas-phase species and the carbon-coated catalyst and the temporal effects, e.g., the rate of loss of catalytic activity with increasing carbon deposition.

6 Tail-gas Recycling of a Simulated SOFC Anode Exhaust Gas (Study 2)

The avoidance of coke formation in CPOx reformers is still a challenge for present research to prolong the performance of the catalytic activity and the overall lifetime of the reformer. The addition of carbon dioxide and water has been shown to have less influence on the main production of syngas in case of methane reforming, since the co-feeds mainly interact via water-gas or reverse water-gas shift chemistry [122, 123]. Only the H_2/CO ratios change in correspondence to the added co-feed [57]. It should be mentioned, that most co-feeds of carbon dioxide and water have been performed in connection with CPOx of methane, and the results in this work are related to the model fuel isooctane. However, partly recycling tail-gas can also be understood as a quasi-autothermal reforming of the fuel. The amount of water for ATR is not precisely controllable and S/C ratios are lower compared to ATR (cf. Chapter C.2.2.3). Nevertheless, some advantages of ATR can be found in the presented data of Study 2.

6.1 Accomplishment of Study 2

In Study 2, the influence of a simulated recycle tail-gas was investigated. CO_2 and H_2O were partly added to the inlet stream of an isooctane fueled CPOx reformer. First, both substances were investigated independently from each other (case 1 and 2) and second, both substances were examined together (case 3).
This study has already been published online:

"Torsten Kaltschmitt, Claudia Diehm, and Olaf Deutschmann,

Catalytic Partial Oxidation of Isooctane to Hydrogen on Rhodium Catalysts: Effect of Tail-Gas Recycling,

Industrial & Engineering Chemistry Research, dx.doi.org/10.1021/ie201712d.

In the following, the results are discussed as in the article available. Reprinted (adapted) with permission of the American Chemical Society. Copyright (2012) American Chemical Society.

The catalytic experiments in Study 2 were carried out in a CPOx reactor with the catalyst configuration described in Chapter 4.3.2, without any further modification.
The inlet section was preheated to a temperature of 463 K. Furnace temperature was set to a value of 523 K to preheat the catalyst. The reaction was accomplished as declared in 4.7. The determination of the internal standard offset was performed after the shutdown of the reaction. Water vapor was provided via the low pulsation total evaporator and directly added to the total volume flow in a mixing chamber.

Catalytic experiment and notation of inlet conditions: Referring to Study 1, isooctane has been used again as reference fuel for Study 2. Herein, isooctane/oxygen feeds containing 1 – 30 vol% of steam or carbon dioxide and mixtures of these (denoted here as recycled tail gas (ReTG)) have been investigated. Steam to carbon (S/C) and carbon dioxide to carbon (CO_2/C) ratios were used to quantify the amounts of steam and carbon dioxide added, respectively. The molar C/O ratios shown in the results were calculated by the total number of carbon atoms divided by the total number of oxygen atoms contained in the feed including the recycled tail gas. In the given CO_2/C and S/C data, the amounts of CO_2 and steam, respectively, refer to the number of C atoms contained in the fuel isooctane only. All compositions have been designed to produce a total inlet flow of 4 SLPM with 80 vol% nitrogen dilution.
In the beginning, the reaction was ignited as declared in 4.7 with pure isooctane/oxygen inlet. After the reaction temperature reached a constant level, steam, carbon dioxide, or both together were set on top of the inlet composition. Measurements were carried out by keeping a constant CO_2/C - and / or S/C - ratio in one experiment (0.01, 0.05, 0.1, 0.2, and 0.3), while varying C/O from 0.72 to 1.79 (in each step, CO_2 and/or H_2O have to be adapted to keep the CO_2/C and the S/C ratio constant, respectively). The fractional numbers for the C/O ratio arise, as mentioned before, from the incorporation of the ReTG to the calculation.
A carbon burn-off was conducted after each measurement to clean the catalyst surface from carbon deposits. Therefore, the reactor was heated up by a 12.5 K/min ramp to 973 K in

1 SLPM synthetic air (O_2:N_2 = 20:80), kept at that temperature for 5 minutes, and then cooled down to room temperature in nitrogen flow.

Both after the studies of all measurements with steam addition and after all measurements with CO_2 addition a fresh catalyst was used, while the catalyst was not replaced for the different measurements at given CO_2/C and S/C but regenerated by carbon burn-off. Each measurement was performed twice with the same catalyst, respectively.

Equilibrium calculations: The Equilibrium compositions were calculated by the DETCHEM^{EQUIL} software code [109] with constant pressure under isothermal conditions using the gas temperature measured at the monolith exit. Results are supplied and compared with the experimental data in mole fractions. The adiabatic reactor temperature was calculated with the DETCHEM^{ADIABAT} software code [109], using the experimentally-measured inlet and outlet gas concentrations and the gas inlet temperature of 463 K.

6.2 Results

In the following, results are presented separately for the three cases studied: addition of H_2O, addition of CO_2, and simultaneous addition of both H_2O and CO_2. The C/O ratios given are always calculated including all C and O atoms entering the reactor, i.e., including the atoms in the added of steam and carbon dioxide. As far as product yields are concerned, two different calculation views are provided. First, the yield was calculated based on the C or H atoms contained in the fuel only (fuel-based) and, second, based on the overall C or H atoms entering the reactor (all-based). In case of hydrogen and water, H based yields, and for all other species, C-based yields are shown.

6.2.1 Effect of H_2O as a Co-feed – Case 1

The effect of H_2O was investigated for five different S/C ratios added to the reactor inlet to determine the influence of steam on a CPOx reformer with isooctane as fuel feed. S/C ratios

of 0.01, 0.05, 0.1, 0.2, and 0.3 were chosen for one set of measurements, while C/O was varied as described in Chapter 6.1. In all figures of Chapter 6, the experiments with the addition of H_2O are visualized as red lines and symbols.

Figure 6-1 reports the yields for the main products, hydrogen and carbon monoxide. For an S/C ratio between 0.05 - 0.3, a net hydrogen production is achieved, since the fuel based yields (symbols) exceed 100 %. Referenced to the overall yield, up to an S/C of < 0.1, higher amounts of hydrogen can be reached, whereas, for an S/C of 0.1, the maximum of hydrogen production shifts towards smaller C/O ratios, but remains at the same order of magnitude and decreases with rising steam co-feed. The carbon monoxide production is only enhanced for small S/C ratios < 0.1. In terms of total oxidation products (**Figure 6-2**), the yields of H_2O and CO_2 rise with increasing S/C ratio. The catalyst outlet temperature (**Figure 6-3**) decreases with rising S/C and has a negative offset of about 10 to 200 K (S/C = 0.01 to 0.3) but has the same shape as the reference.

The addition of steam to the inlet feed reduces the total amount of the soot precursors ethylene and propylene right from the smallest S/C **(Figure 6-5**) ratio. Ethylene and propylene are reduced by more than 50 % compared to the reference isooctane experiment. Methane formation reveals a different behavior. Passing an S/C ratio of 0.1, more methane is produced, increasing with rising steam co-feed (**Figure 6-5**). Giving attention to the molar flow rates (**Figure 6-6**) of C_1 - C_3 hydrocarbons, methane and acetylene are formed with increasing S/C ratio, and are shifted to lower overall C/O ratios. Ethylene and propylene show a different behavior. Their formation increases for a C/O of about 0.8 – 0.9 and decreases with raising S/C ratio, but is not noticeably shifted towards lower C/O ratios as observed for methane and acetylene formation. The amounts of ethylene and propylene become too small at high ReTG streams to be detectable. With steam as a co-feed, up to an S/C of about 0.1 in the lean area, conversion is similar to the isooctane reference (**Figure 6-3**). With rising S/C, conversion decreases but still exceeds 97 % for C/O < 0.9; at higher C/O, conversion drops and the formation of C_2 and C_3 hydrocarbons is observed.

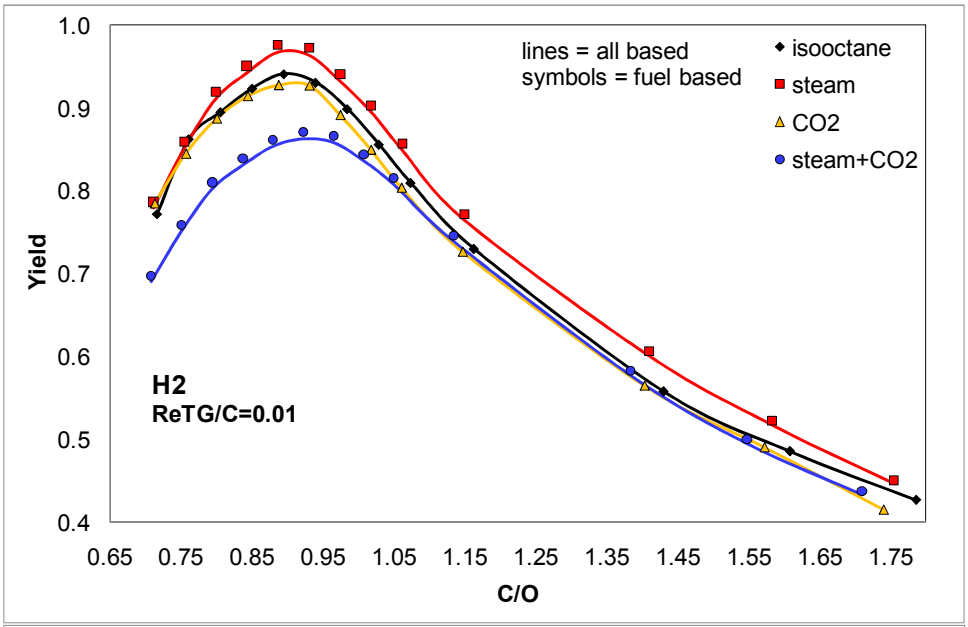
lines = all based
symbols = fuel based
isooctane
steam
CO2
steam+CO2
H2
ReTG/C=0.01
Yield
C/O
1.0
0.9
0.8
0.7
0.6
0.5
0.4
0.65 0.75 0.85 0.95 1.05 1.15 1.25 1.35 1.45 1.55 1.65 1.75

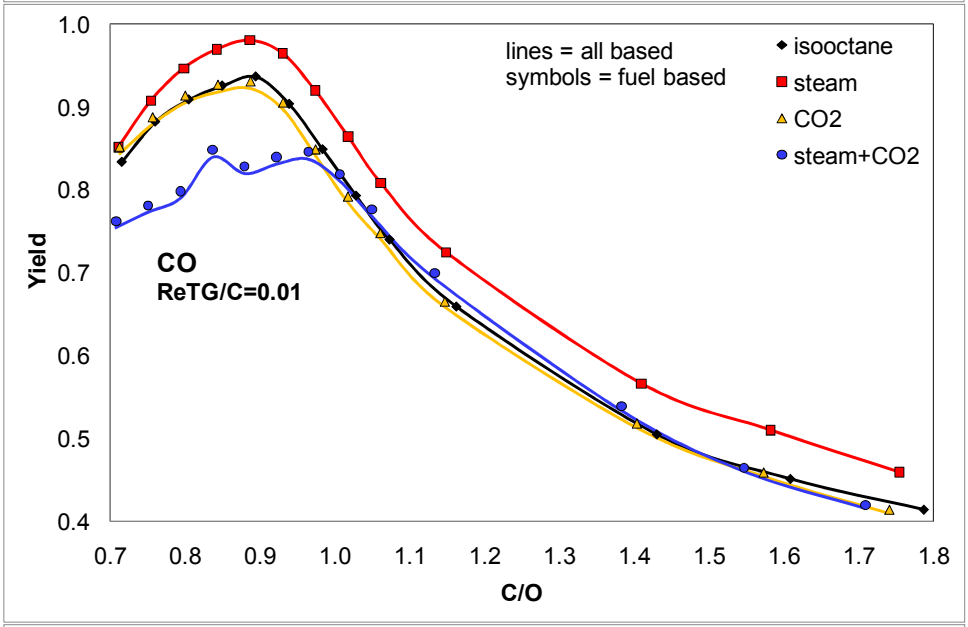
lines = all based
symbols = fuel based
isooctane
steam
CO2
steam+CO2
CO
ReTG/C=0.01
Yield
C/O
1.0
0.9
0.8
0.7
0.6
0.5
0.4
0.7 0.8 0.9 1.0 1.1 1.2 1.3 1.4 1.5 1.6 1.7 1.8

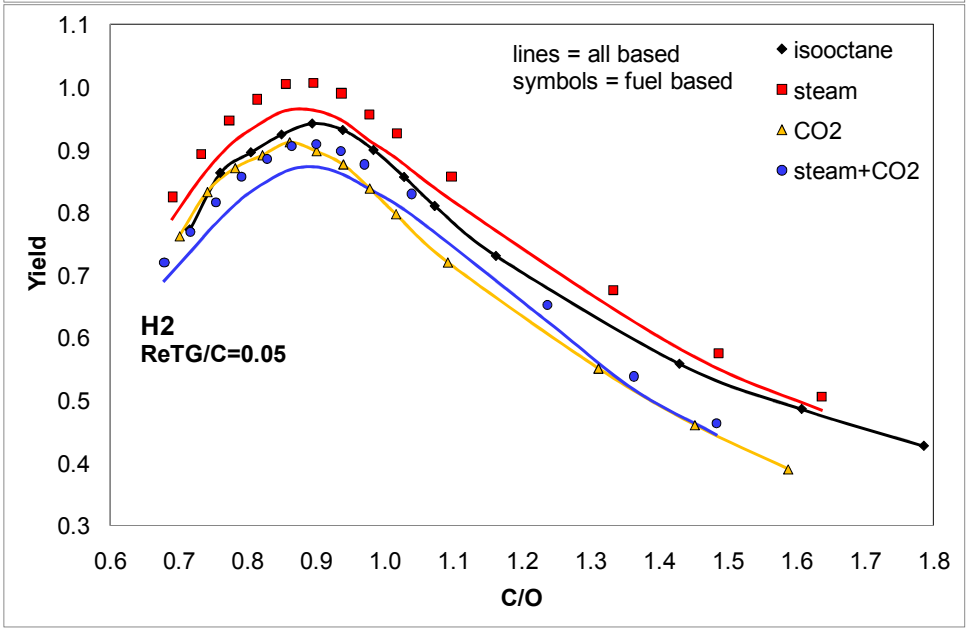
lines = all based
symbols = fuel based
isooctane
steam
CO2
steam+CO2
H2
ReTG/C=0.05
Yield
C/O
1.1
1.0
0.9
0.8
0.7
0.6
0.5
0.4
0.3
0.6 0.7 0.8 0.9 1.0 1.1 1.2 1.3 1.4 1.5 1.6 1.7 1.8

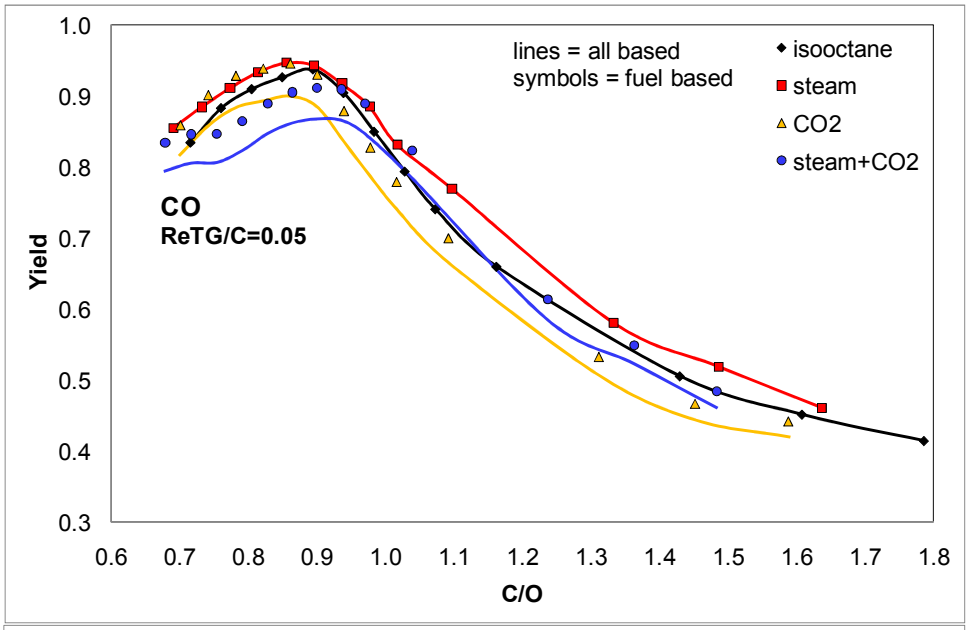
lines = all based
symbols = fuel based
isooctane
steam
CO2
steam+CO2
CO
ReTG/C=0.05
Yield
C/O
1.0
0.9
0.8
0.7
0.6
0.5
0.4
0.3
0.6 0.7 0.8 0.9 1.0 1.1 1.2 1.3 1.4 1.5 1.6 1.7 1.8

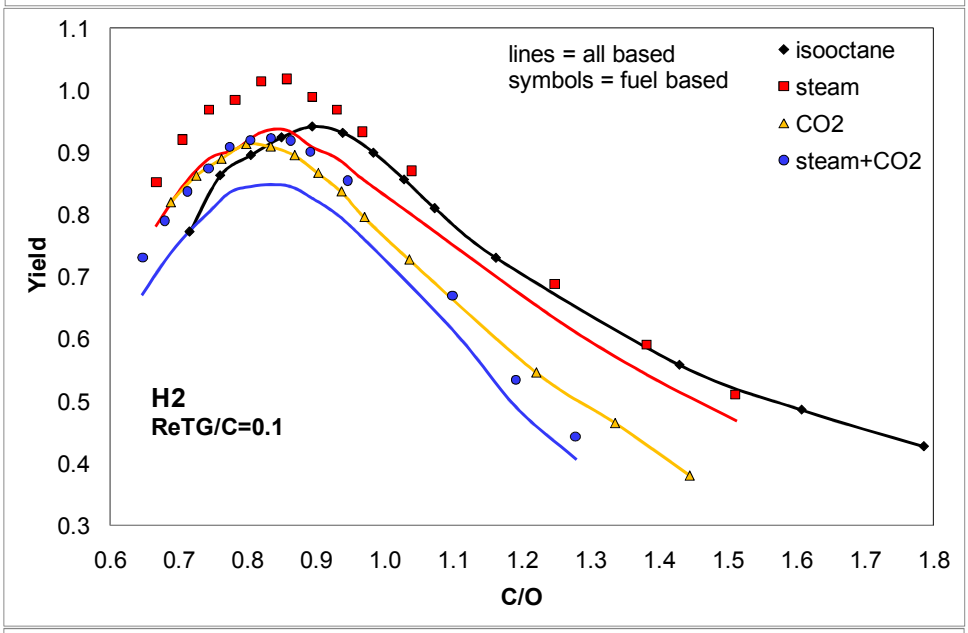
lines = all based
symbols = fuel based
isooctane
steam
CO2
steam+CO2
H2
ReTG/C=0.1
Yield
C/O
1.1
1.0
0.9
0.8
0.7
0.6
0.5
0.4
0.3
0.6 0.7 0.8 0.9 1.0 1.1 1.2 1.3 1.4 1.5 1.6 1.7 1.8

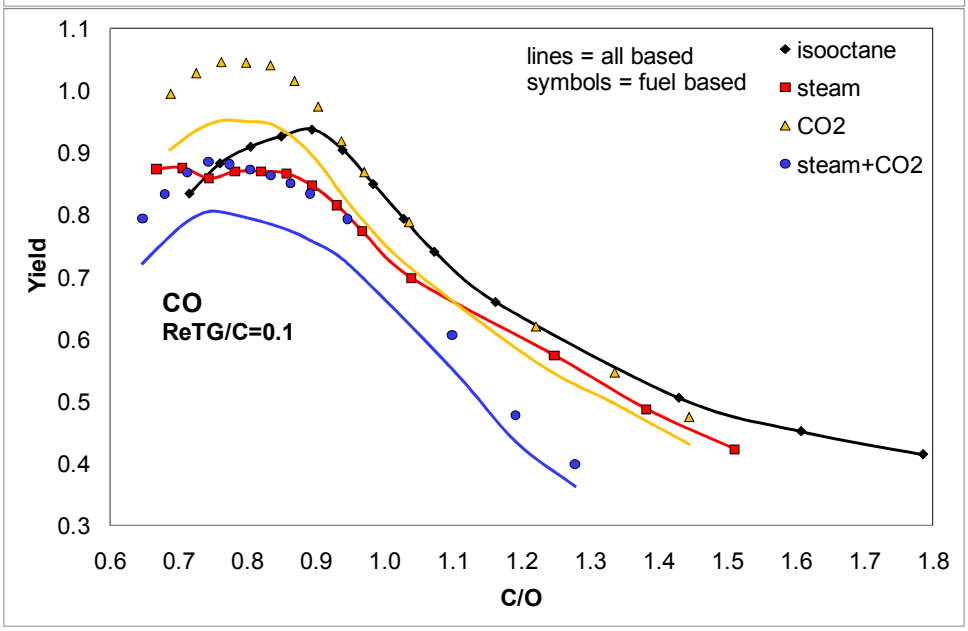
lines = all based
symbols = fuel based
isooctane
steam
CO2
steam+CO2
CO
ReTG/C=0.1
Yield
C/O
1.1
1.0
0.9
0.8
0.7
0.6
0.5
0.4
0.3
0.6 0.7 0.8 0.9 1.0 1.1 1.2 1.3 1.4 1.5 1.6 1.7 1.8

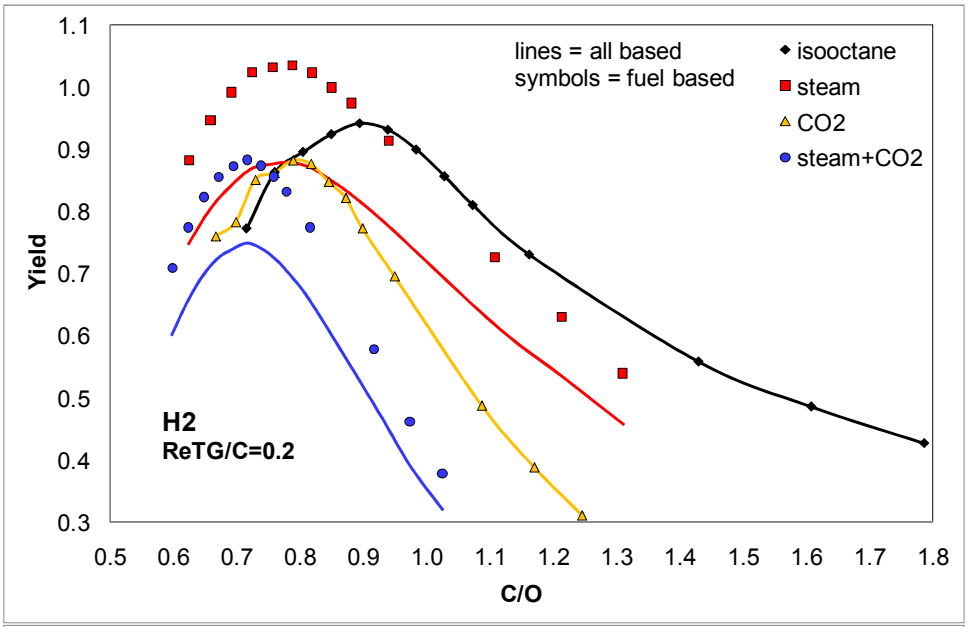
lines = all based
symbols = fuel based
isooctane
steam
CO2
steam+CO2
H2
ReTG/C=0.2
Yield
C/O

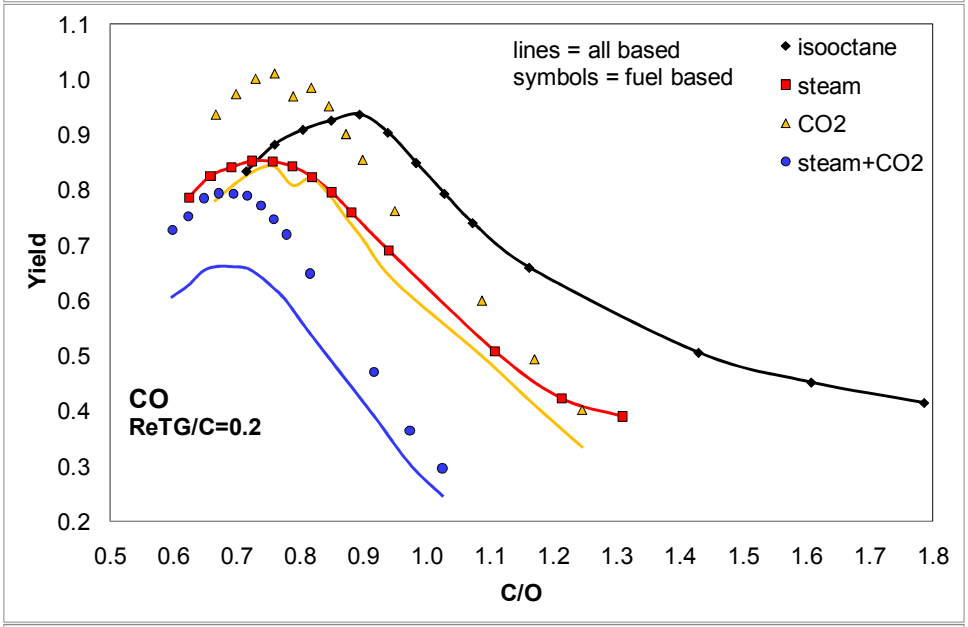
lines = all based
symbols = fuel based
isooctane
steam
CO2
steam+CO2
CO
ReTG/C=0.2
Yield
C/O

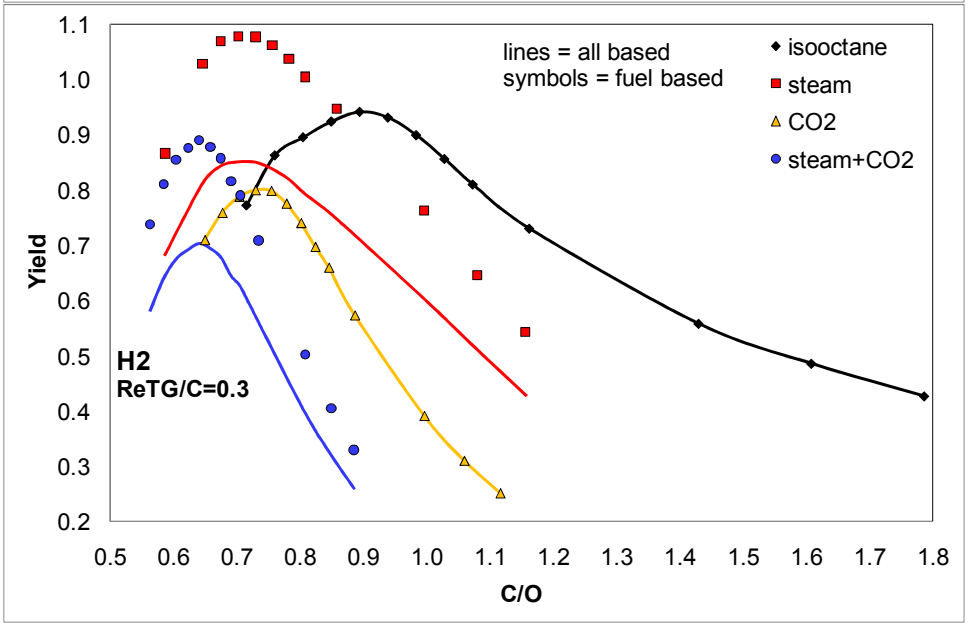
lines = all based
symbols = fuel based
isooctane
steam
CO2
steam+CO2
H2
ReTG/C=0.3
Yield
C/O

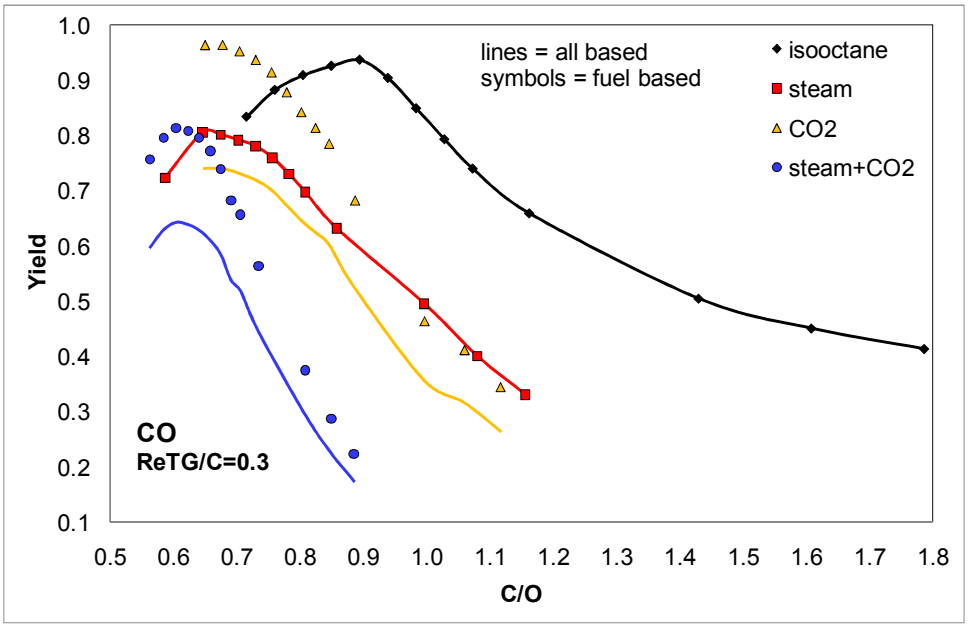

Figure 6-1: Yield of H_2 and CO for cases 1-3 and the five different ReTG/C ratios. Full lines = all-based C/H yield, symbol = fuel-based C/H yield.

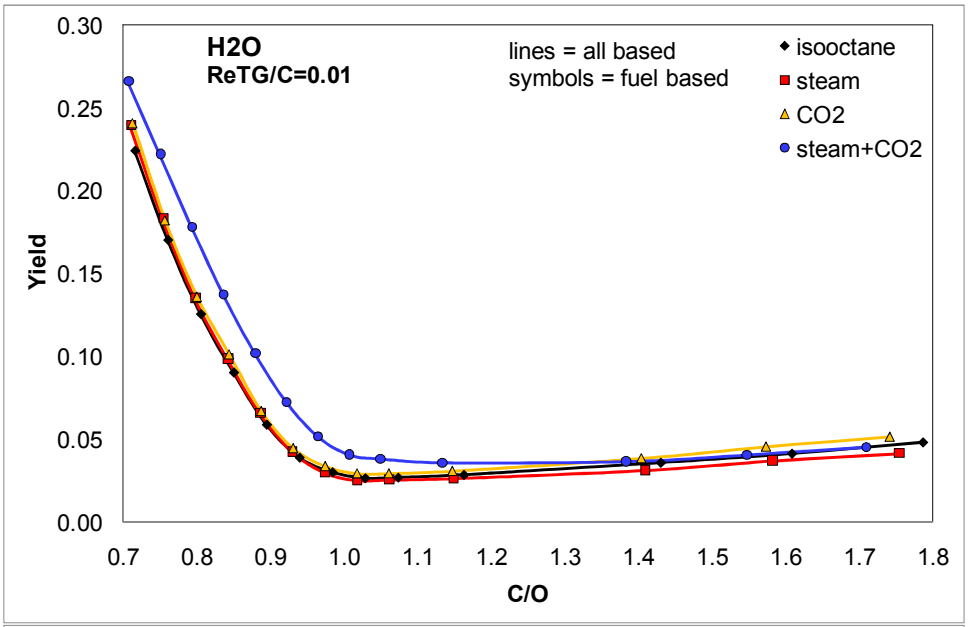
H2O
ReTG/C=0.01
lines = all based
symbols = fuel based
isooctane
steam
CO2
steam+CO2
Yield
C/O
0.30
0.25
0.20
0.15
0.10
0.05
0.00
0.7
0.8
0.9
1.0
1.1
1.2
1.3
1.4
1.5
1.6
1.7
1.8

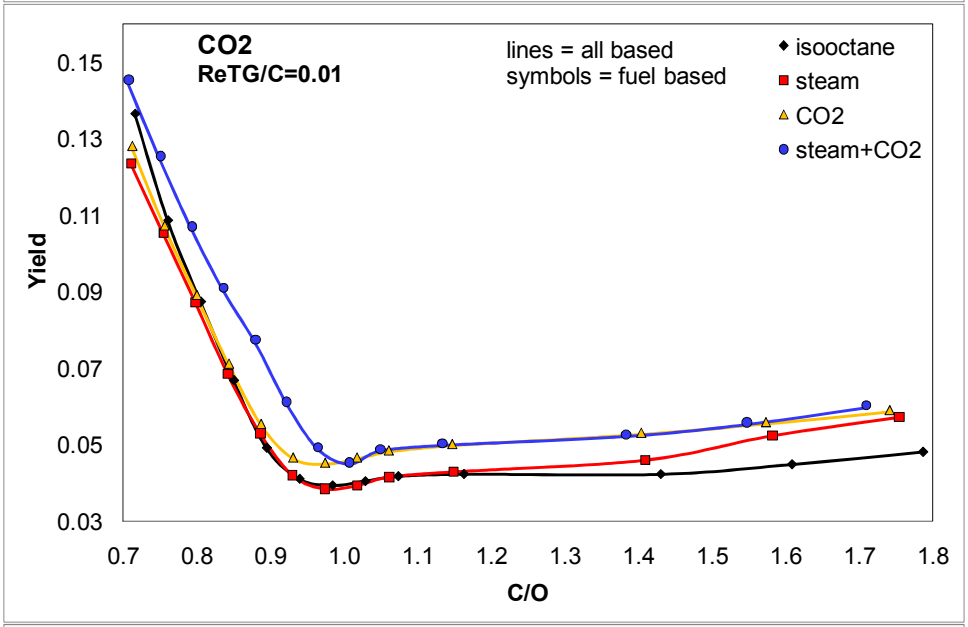
CO2
ReTG/C=0.01
lines = all based
symbols = fuel based
isooctane
steam
CO2
steam+CO2
Yield
C/O
0.15
0.13
0.11
0.09
0.07
0.05
0.03
0.7
0.8
0.9
1.0
1.1
1.2
1.3
1.4
1.5
1.6
1.7
1.8

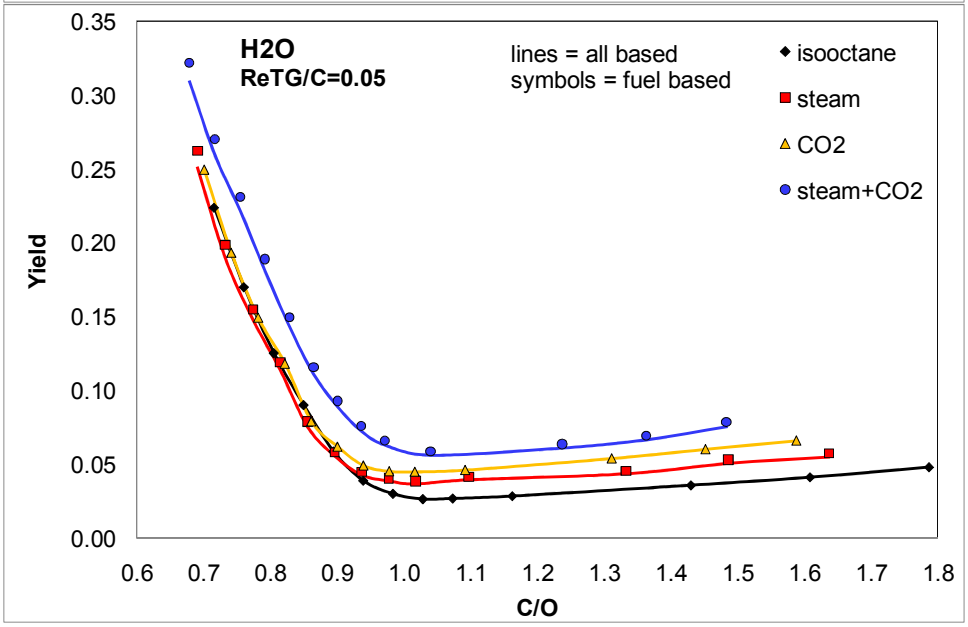
H2O
ReTG/C=0.05
lines = all based
symbols = fuel based
isooctane
steam
CO2
steam+CO2
Yield
C/O
0.35
0.30
0.25
0.20
0.15
0.10
0.05
0.00
0.6
0.7
0.8
0.9
1.0
1.1
1.2
1.3
1.4
1.5
1.6
1.7
1.8

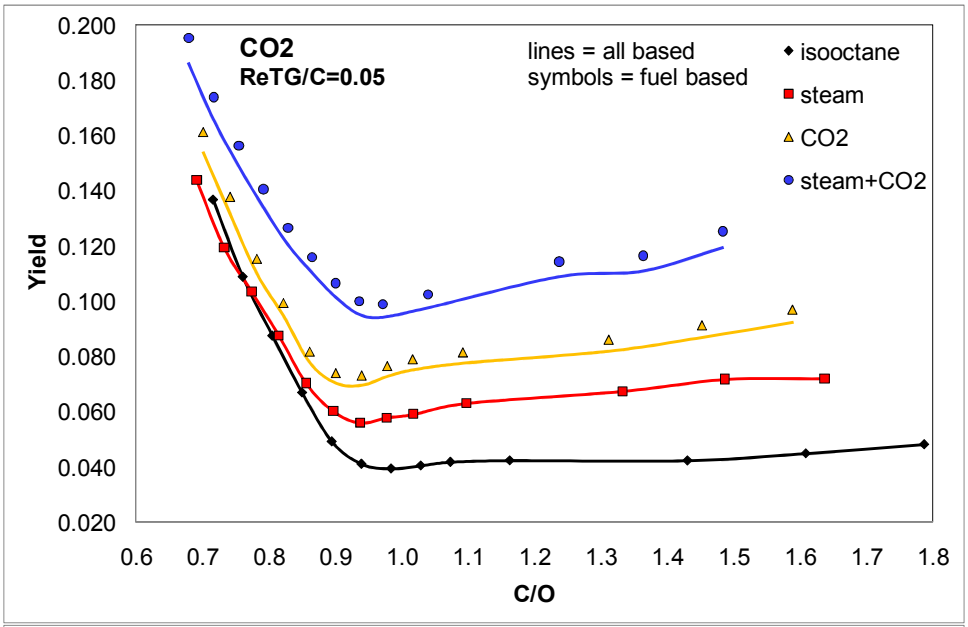
CO2
ReTG/C=0.05
lines = all based
symbols = fuel based
isooctane
steam
CO2
steam+CO2
Yield
C/O
0.200
0.180
0.160
0.140
0.120
0.100
0.080
0.060
0.040
0.020
0.6 0.7 0.8 0.9 1.0 1.1 1.2 1.3 1.4 1.5 1.6 1.7 1.8

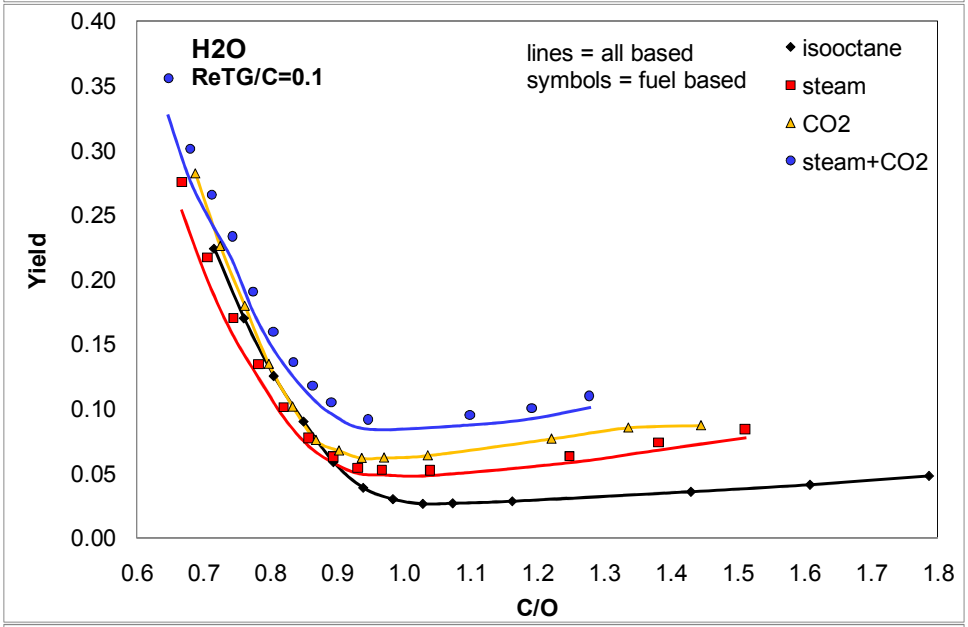
H2O
ReTG/C=0.1
lines = all based
symbols = fuel based
isooctane
steam
CO2
steam+CO2
Yield
C/O
0.40
0.35
0.30
0.25
0.20
0.15
0.10
0.05
0.00
0.6 0.7 0.8 0.9 1.0 1.1 1.2 1.3 1.4 1.5 1.6 1.7 1.8

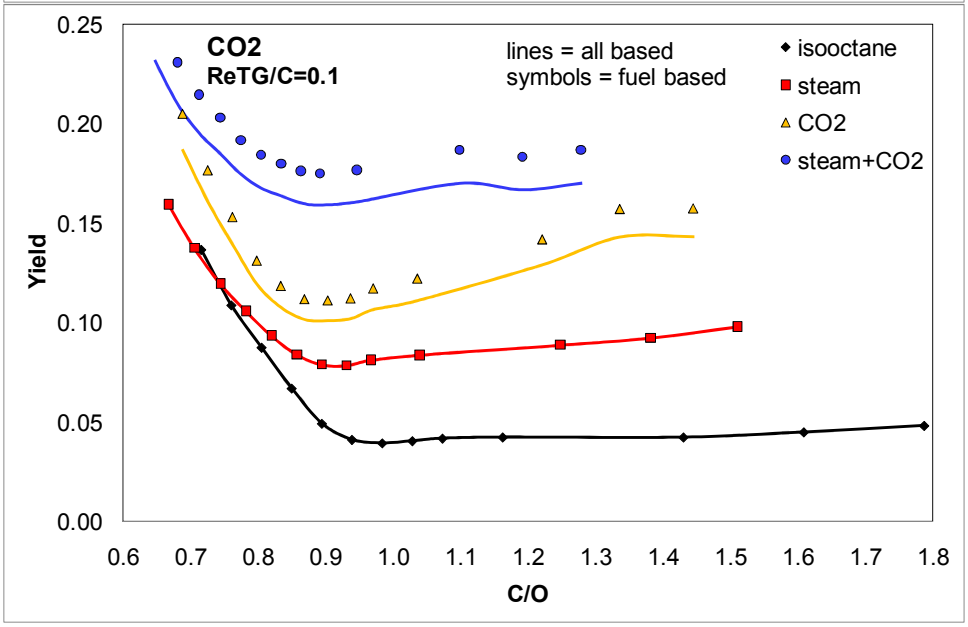
CO2
ReTG/C=0.1
lines = all based
symbols = fuel based
isooctane
steam
CO2
steam+CO2
Yield
C/O
0.25
0.20
0.15
0.10
0.05
0.00
0.6 0.7 0.8 0.9 1.0 1.1 1.2 1.3 1.4 1.5 1.6 1.7 1.8

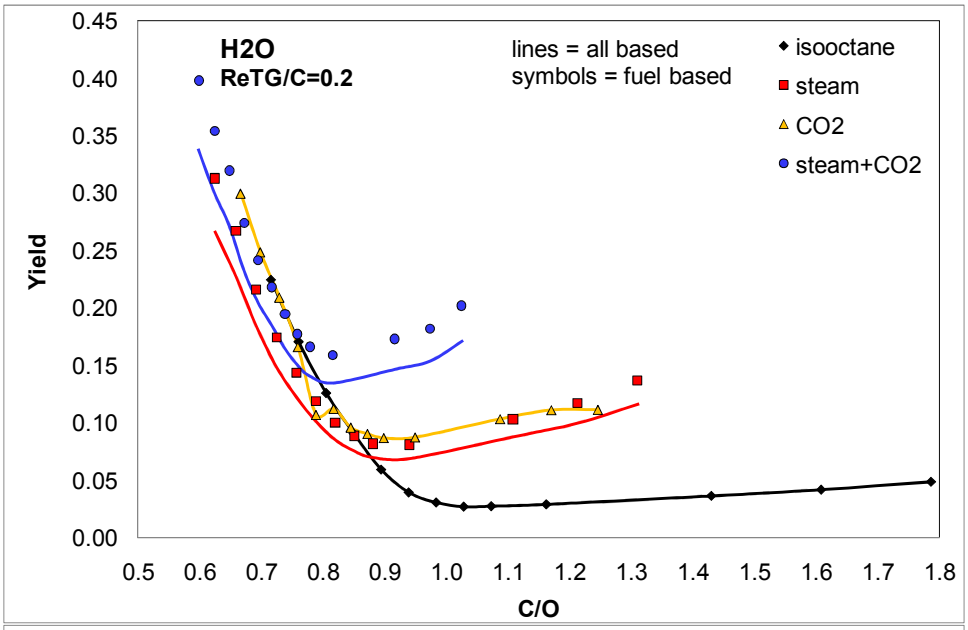
H2O
ReTG/C=0.2
lines = all based
symbols = fuel based
isooctane
steam
CO2
steam+CO2
Yield
C/O
0.00
0.05
0.10
0.15
0.20
0.25
0.30
0.35
0.40
0.45
0.5
0.6
0.7
0.8
0.9
1.0
1.1
1.2
1.3
1.4
1.5
1.6
1.7
1.8

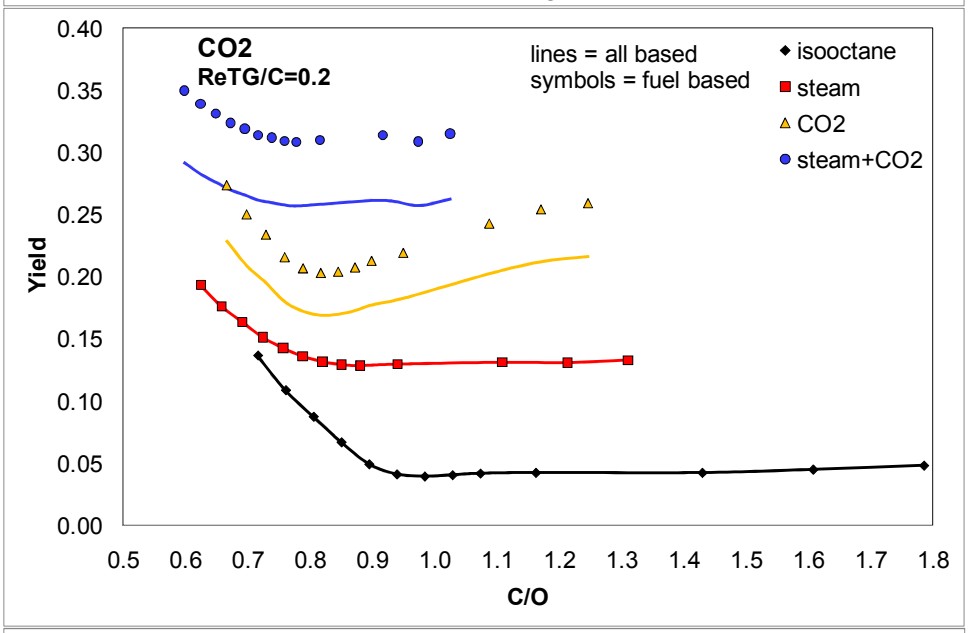
CO2
ReTG/C=0.2
lines = all based
symbols = fuel based
isooctane
steam
CO2
steam+CO2
Yield
C/O
0.00
0.05
0.10
0.15
0.20
0.25
0.30
0.35
0.40
0.5
0.6
0.7
0.8
0.9
1.0
1.1
1.2
1.3
1.4
1.5
1.6
1.7
1.8

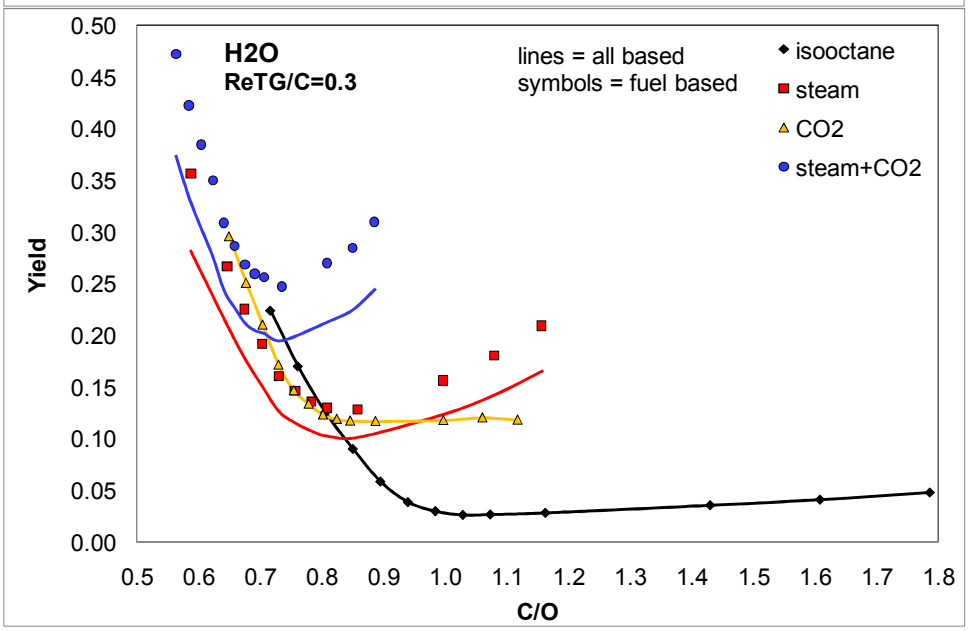
H2O
ReTG/C=0.3
lines = all based
symbols = fuel based
isooctane
steam
CO2
steam+CO2
Yield
C/O
0.00
0.05
0.10
0.15
0.20
0.25
0.30
0.35
0.40
0.45
0.50
0.5
0.6
0.7
0.8
0.9
1.0
1.1
1.2
1.3
1.4
1.5
1.6
1.7
1.8

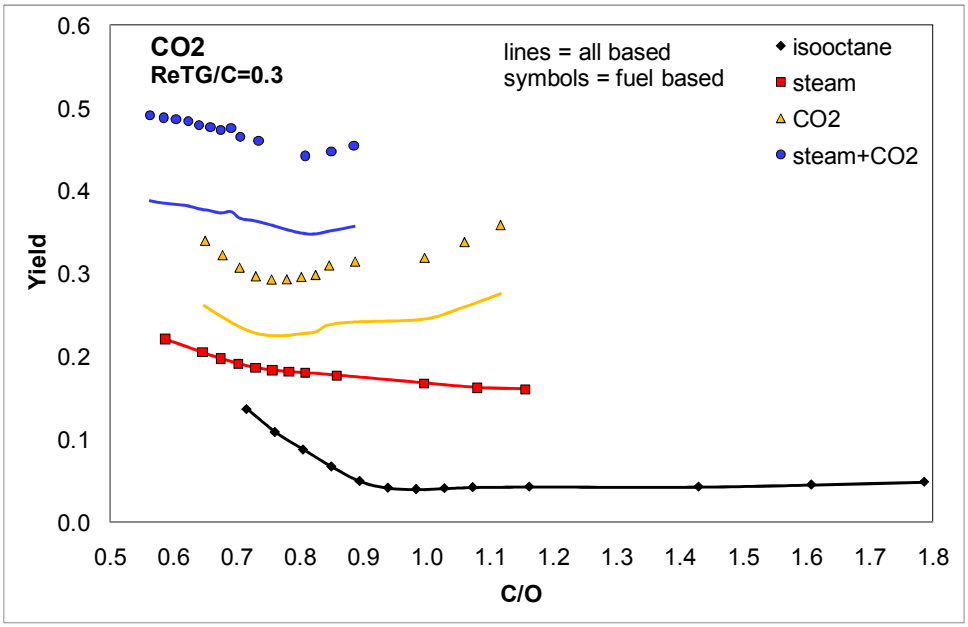

Figure 6-2: Yield of H_2O and CO_2 for cases 1-3 and the five different ReTG/C ratios. Full lines = all-based C/H yield, symbol = fuel-based C/H yield.

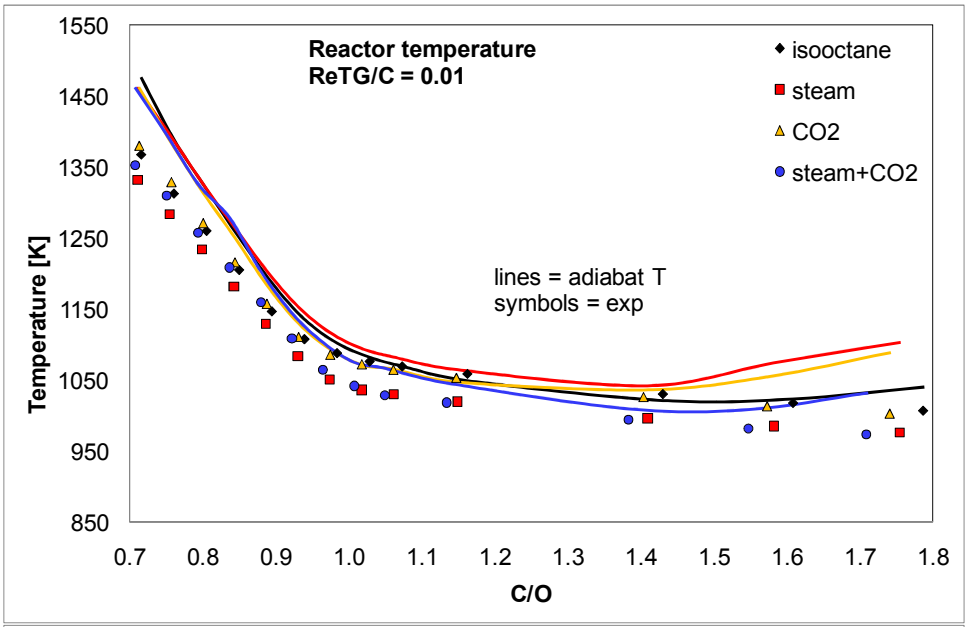
Reactor temperature
ReTG/C = 0.01
isooctane
steam
CO2
steam+CO2
lines = adiabat T
symbols = exp
Temperature [K]
1550
1450
1350
1250
1150
1050
950
850
0.7
0.8
0.9
1.0
1.1
1.2
1.3
1.4
1.5
1.6
1.7
1.8
C/O

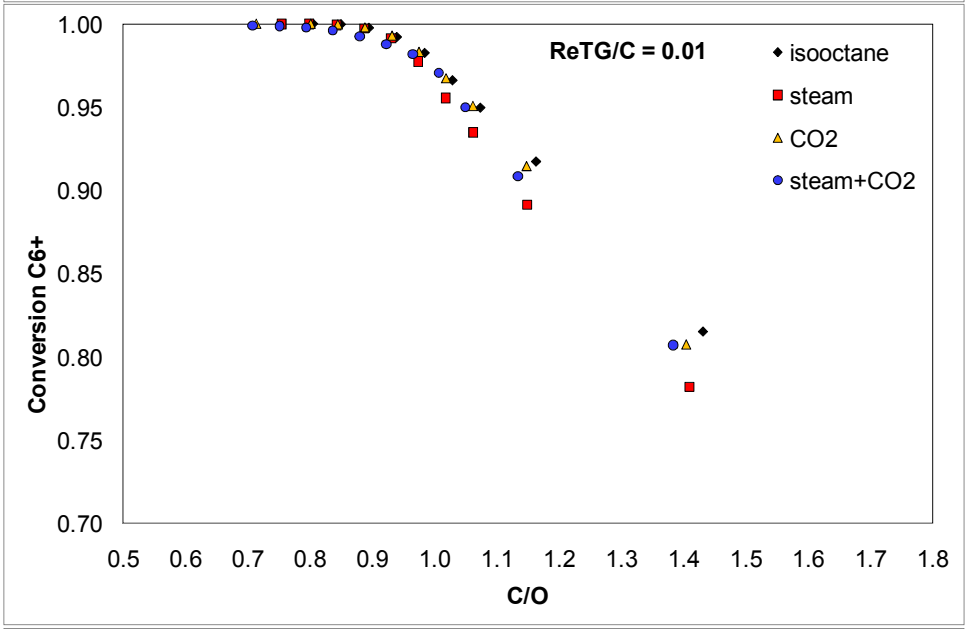
ReTG/C = 0.01
isooctane
steam
CO2
steam+CO2
Conversion C6+
1.00
0.95
0.90
0.85
0.80
0.75
0.70
0.5
0.6
0.7
0.8
0.9
1.0
1.1
1.2
1.3
1.4
1.5
1.6
1.7
1.8
C/O

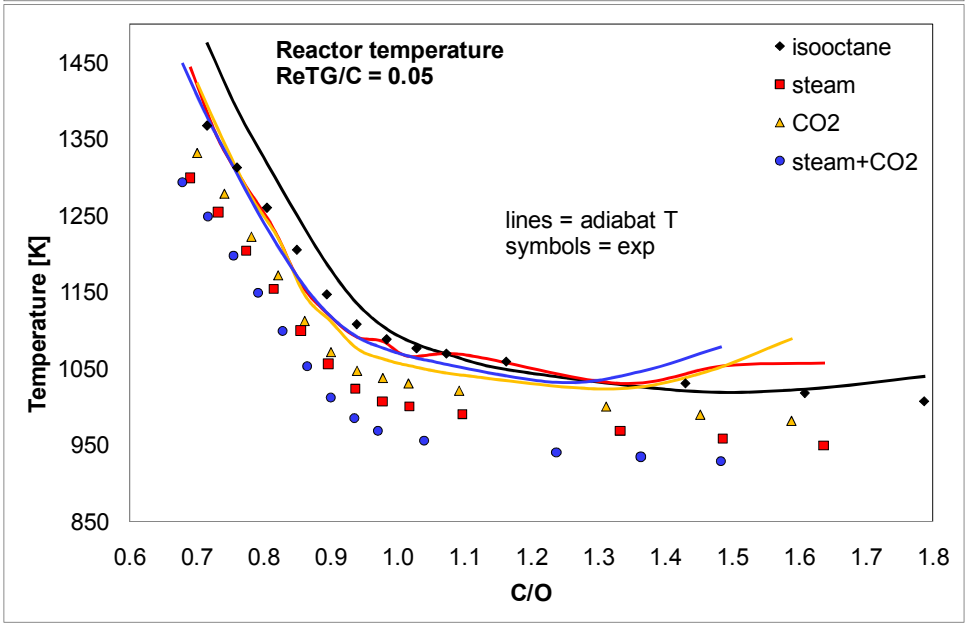
Reactor temperature
ReTG/C = 0.05
isooctane
steam
CO2
steam+CO2
lines = adiabat T
symbols = exp
Temperature [K]
1450
1350
1250
1150
1050
950
850
0.6
0.7
0.8
0.9
1.0
1.1
1.2
1.3
1.4
1.5
1.6
1.7
1.8
C/O

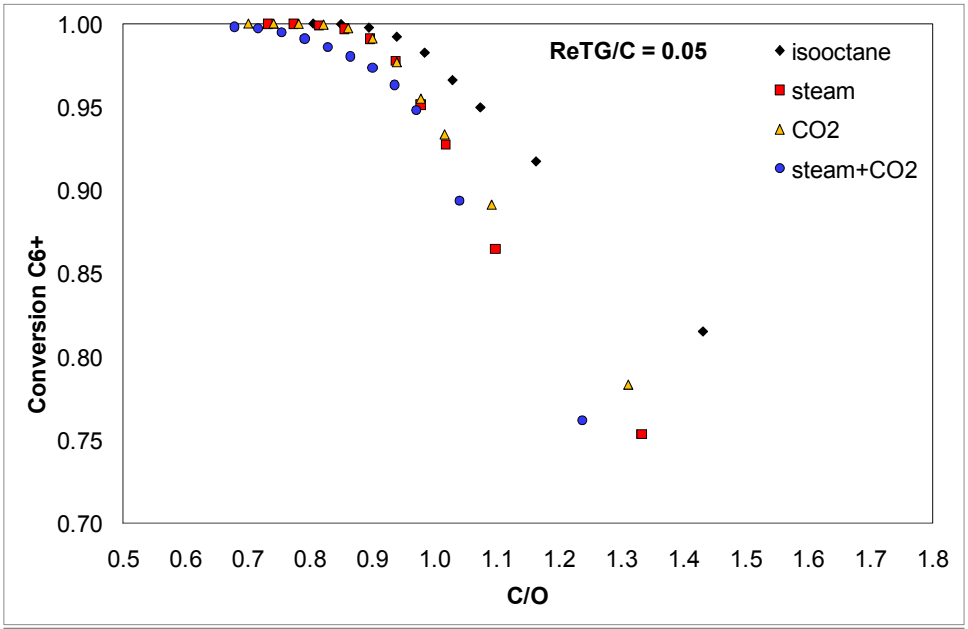
ReTG/C = 0.05
isooctane
steam
CO2
steam+CO2
Conversion C6+
1.00
0.95
0.90
0.85
0.80
0.75
0.70
0.5 0.6 0.7 0.8 0.9 1.0 1.1 1.2 1.3 1.4 1.5 1.6 1.7 1.8
C/O

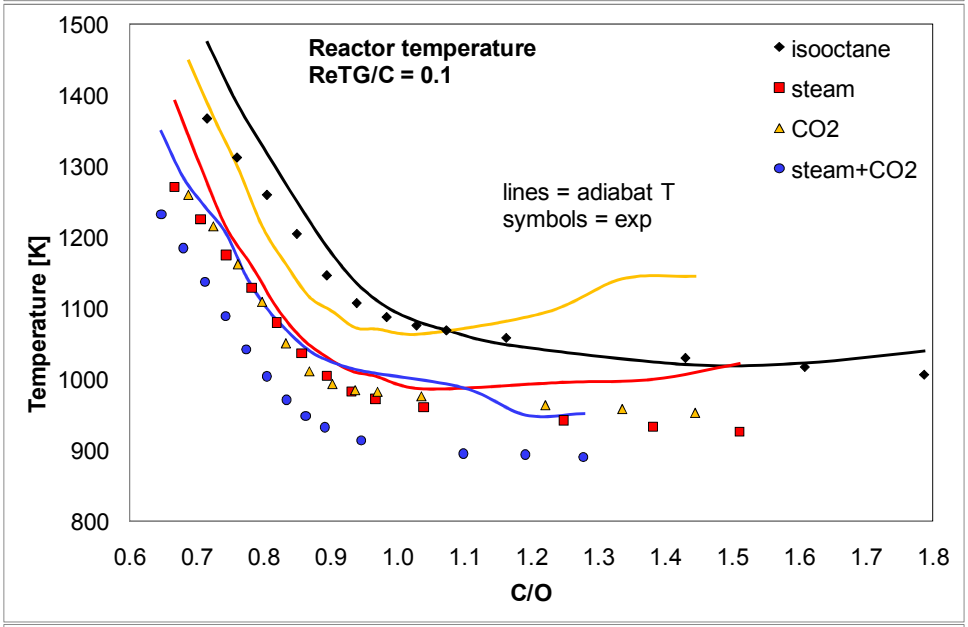
Reactor temperature
ReTG/C = 0.1
isooctane
steam
CO2
steam+CO2
lines = adiabat T
symbols = exp
Temperature [K]
1500
1400
1300
1200
1100
1000
900
800
0.6 0.7 0.8 0.9 1.0 1.1 1.2 1.3 1.4 1.5 1.6 1.7 1.8
C/O

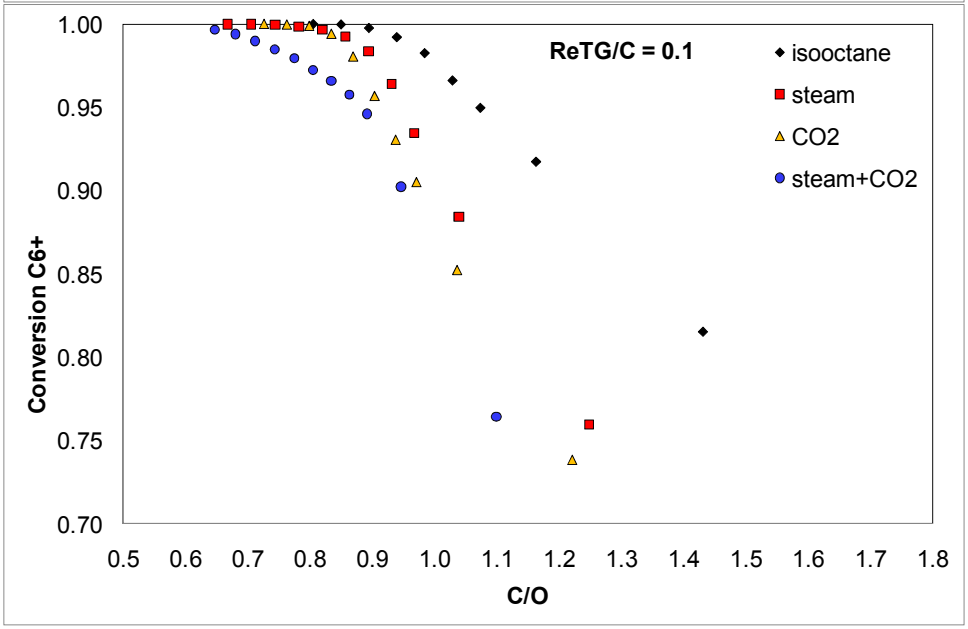
ReTG/C = 0.1
isooctane
steam
CO2
steam+CO2
Conversion C6+
1.00
0.95
0.90
0.85
0.80
0.75
0.70
0.5 0.6 0.7 0.8 0.9 1.0 1.1 1.2 1.3 1.4 1.5 1.6 1.7 1.8
C/O

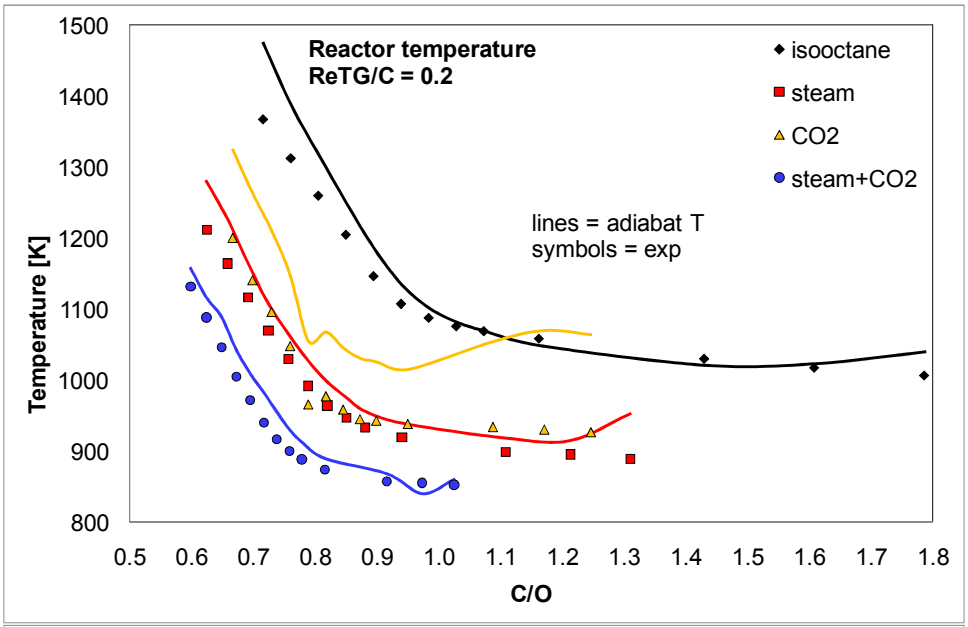
Reactor temperature
ReTG/C = 0.2
isooctane
steam
CO2
steam+CO2
lines = adiabat T
symbols = exp
Temperature [K]
1500
1400
1300
1200
1100
1000
900
800
0.5 0.6 0.7 0.8 0.9 1.0 1.1 1.2 1.3 1.4 1.5 1.6 1.7 1.8
C/O

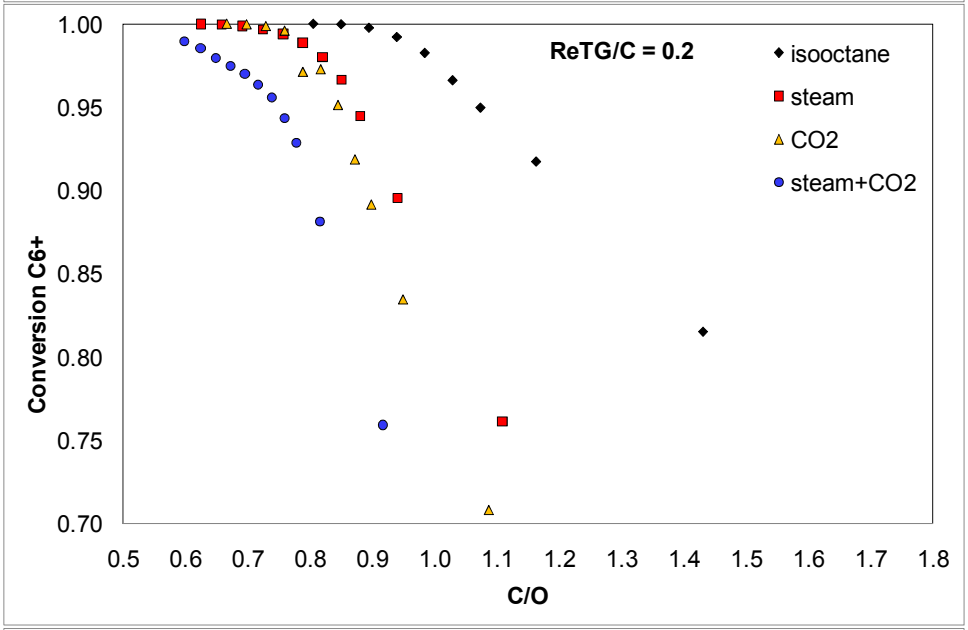
ReTG/C = 0.2
isooctane
steam
CO2
steam+CO2
Conversion C6+
1.00
0.95
0.90
0.85
0.80
0.75
0.70
0.5 0.6 0.7 0.8 0.9 1.0 1.1 1.2 1.3 1.4 1.5 1.6 1.7 1.8
C/O

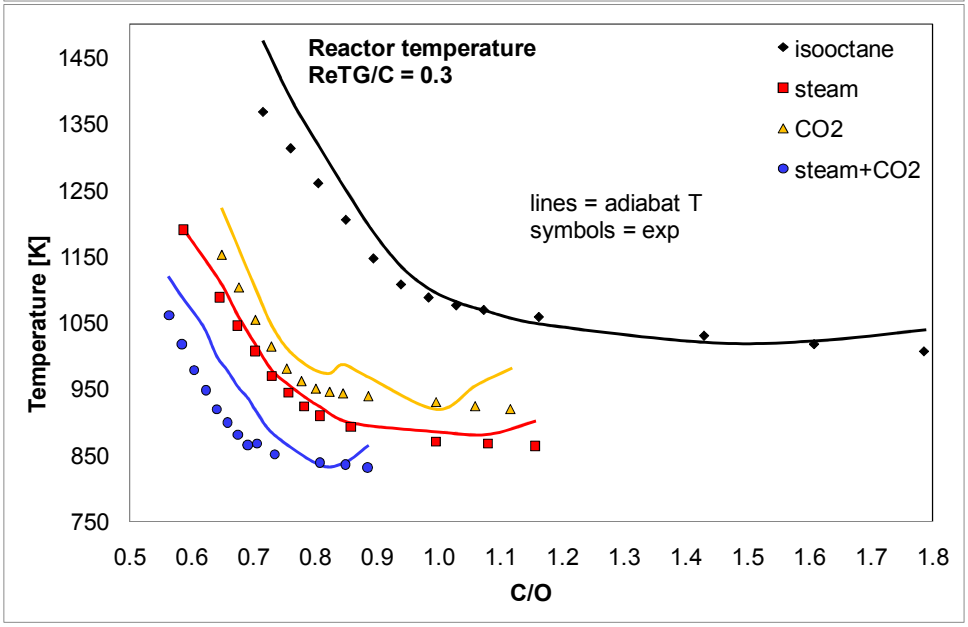
Reactor temperature
ReTG/C = 0.3
isooctane
steam
CO2
steam+CO2
lines = adiabat T
symbols = exp
Temperature [K]
1450
1350
1250
1150
1050
950
850
750
0.5 0.6 0.7 0.8 0.9 1.0 1.1 1.2 1.3 1.4 1.5 1.6 1.7 1.8
C/O

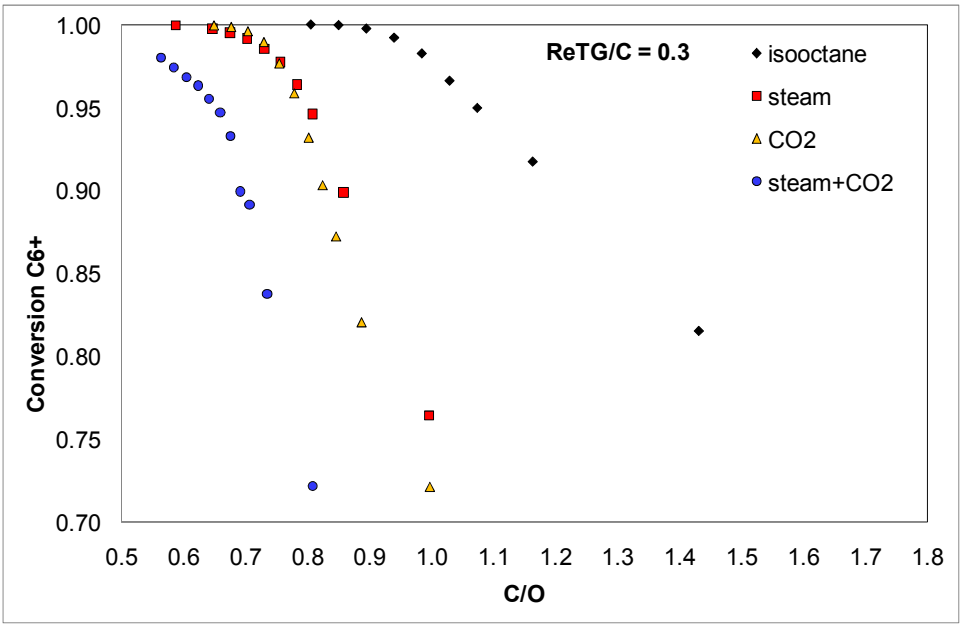

Figure 6-3: Catalyst outlet temperature and fuel conversion for cases 1-3 and the five ReTG/C ratios.

6.2.2 Effect of CO_2 as a Co-feed – Case 2

The effect of CO_2 added to the reactor inlet was also investigated for five different CO_2/C ratios. The same ratios as for the steam experiments of 0.01, 0.05, 0.1, 0.2 and 0.3 CO_2/C were chosen. Analogous to the steam experiments, CO_2/C was kept constant while C/O was varied. In all figures of Chapter 6, the addition of CO_2 is visualized as a yellow line or symbol.

CO_2 addition has a negative impact on hydrogen yield. In cases of CO_2/C 0.01 – 0.1, nearly the same amounts of hydrogen were reached compared to the reference experiment, but hydrogen yield drops with rising CO_2 content in the inlet feed. Only in case of CO_2/C = 0.1, a net carbon monoxide production was observed, as CO yield (fuel-based) exceeds 100 %. With rising CO_2 content in the feed, CO yields decrease but still reach values above 90 % (**Figure 6-1**). In terms of total oxidation products (**Figure 6-2**), the yields of H_2O and CO_2 rise with increasing CO_2/C ratio. The catalyst outlet temperature decreases with rising CO_2/C but shows the same trend as the reference, being comparable to the temperature profile of case 1 (**Figure 6-3**).

Concerning soot precursors, the addition of carbon dioxide leads to higher yields for ethylene and propylene, but lowers the methane yield compared to the steam addition experiments. Nevertheless, for all cases, lower yields in C_1 - C_3 hydrocarbons were detected than for to the pure isooctane reference, as shown in **Figure 6-5**. The conversion of isooctane is similar to the conversion achieved with steam addition. Formation of C_2 and C_3 hydrocarbons starts at C/O of 0.8 - 0.9, while methane and acetylene formation shifts to lower C/O ratios with increasing CO_2/C,as observed for rising S/C ratios.

6.2.3 Effect of H_2O and CO_2 as a Co-feed – Case 3

Analogous measurements have been performed with both steam and carbon dioxide in the inlet feed for the five ReTG/C ratios of 0.01, 0.05, 0.1, 0.2 and 0.3. Experimental procedures were the same as mentioned in cases 1 and 2. In all figures of Chapter 6, the simultaneous addition of steam and CO_2 is visualized as blue lines or symbols.

For all measurements, lower yields in H_2 and CO were detected, especially at lean conditions, and the yields decrease further with increasing ReTG/C ratio (**Figure 6-1**). No net production of syngas was observed, not even for the 0.01 case. Therefore, total oxidation products have the highest yields in all conducted experiments, namely up to 15 - 35 % (**Figure 6-2**). The temperature profile looks like the ones in cases 1 and 2 and also like those in the reference. However, the offset drops by 10 to 100 K more than in the other two cases (**Figure 6-3**).

For soot precursors, results are different compared to separate steam and CO_2 addition. Methane yields have a maximum in the range of ReTG/C = 0.1, while, for ethylene and propylene, the same order of magnitude in yield was found over the entire ReTG/C range. A noticeable fact in case 3 is that the formation of all C_1-C_3 hydrocarbons shifts to lower C/O ratios with increasing ReTG/C. In case of ethylene and propylene, the maximum even shifted to the lowest C/O ratio considered. This behavior is also revealed through the molar flow rates of the product stream (**Figure 6-6**). Regarding fuel conversion, increasing the ReTG/C ratio leads to a significant conversion drop even in the lean regime and falls below 80 % for an ReTG/C >0.1 and a C/O < 1 (**Figure 6-3**).

6.3 Discussion

The interpretation of the presented data is not straight-forward because, aside from catalytic fuel conversion on the Rh surface, gas-phase reactions in the fluid phase and coke deposition superimpose the catalytic cycle, and these interactions are also influenced by mass and heat transport and vary along the length of the reactor [124]. Also, gas phase chemistry downstream of the catalyst has to be considered and has influence on the measured values as long as unconverted fuel exits the catalyst, which is already discussed in Study 1 of this work and by Burke *et al.* [41, 59].

6.3.1 Effect on Reactor Outlet Temperature

The catalyst outlet temperatures for all case studies are shown in **Figure 6-3**. The reactor is operated nearly adiabatically, which is shown by the relatively small differences between measured and adiabatic reactor temperature, taking the high operating temperatures and the associated temperature uncertainties into account. As for both H_2O and/or CO_2 addition, the temperature drops below the reference for all ReTG/C ratios. Since all experiments used the same total flow rate of 4 SLPM, the co-feeds obviously reduce the catalyst exit temperatures because the total amount of fuel that can be exothermally oxidized (partial and total oxidation) decreases. Furthermore, heat capacities of H_2O and CO_2 are higher than that of nitrogen, leading to an increased heat capacity of the mixture and, hence, requiring more chemical heat release to reach the temperature of the reference case.

Nonetheless, all exothermic and endothermic reactions (fuel combustion, steam reforming, hydrogenation of olefins, gasification, carbon formation, shift reactions, etc.) contribute to the overall temperature and, thus, to the temperature measured at the catalyst exit. Hence, the temperature drop with co-feeding steam and carbon dioxide compared to the reference case is not only caused by varied heat capacity and heat transport properties. Tavazzi *et al.* described a method to validate the thermal efficiency α of a CPOx reactor using the adiabatic reactor temperature (given as lines in **Figure 6-3**). The thermal efficiency α is defined as a quotient of the difference between the measured gas out- and inlet

temperatures, T_{exp}^{out} and, T_{exp}^{in} and the difference between the calculated adiabatic reactor temperature, $T_{adiabat}^{out}$, and the gas inlet temperatures [125]:

$$\alpha = \frac{T_{exp}^{out} - T_{exp}^{in}}{T_{adiabat}^{out} - T_{exp}^{in}}$$

Equation 6-1

Thermal efficiency is calculated for the isooctane reference experiment in the range of 0.89 – 0.99 depending on the C/O ratio, and is comparable to the one mentioned in literature, even though the reported range was presented for CPOx of methane. Smaller thermal efficiencies are observed in case of tail-gas recycling. For steam addition, a thermal efficiency of 0.8 – 0.99, depending on the amount of steam, was calculated, which is about 10 % less than the reference, especially in the fuel-rich area. For CO_2 addition, α reaches values between 0.71 – 0.99 (mainly between 0.85 – 0.95), and for ReTG, between 0.75 – 0.99 (mainly between 0.8 – 0.9). Using identical thermal insulation in all three case studies, an increasing heat loss is observed in relation to the co-feed, implying a superimposition of chemical and physical effects on the reactor exit temperature.

In a technical realization, the recycled gas would usually have higher temperatures than the inlet fuel/air mixture, and hence, the drastic effect on temperature is likely to be compensated. Nevertheless, the understanding of the effect of recycled gas on the reactor temperature is crucial for reactor design and optimization of operating conditions because there are two opposing trends: higher temperatures do not only increase hydrogen yields due to thermodynamics, but also boost gas-phase reactions leading to coke precursors. In this work, the focus was on to the investigation of the direct chemical influence of the co-feed and, therefore, the same inlet temperatures were chosen for fuel, synthetic air and recycled gas.

6.3.2 Effect on Main Product Distribution

In spite of decreasing fuel conversion and accompanying temperature drop, the addition of steam to the inlet feed results in a higher net hydrogen yield compared to the reference

experiment for all S/C ratios. As shown in literature by utilization of spatial profiling, in case of CPOx of CH_4, H_2O concentrations have no effect on the initial total oxidation zone of the catalyst and the downstream catalyst reforming zone [65]. The overall reaction sequence is very likely to be similar to the ones observed for CPOx of hydrocarbons without steam and CO_2 addition, first (upstream) total oxidation and afterwards (downstream) reforming and shifting. Hence, the final product composition is strongly influenced by the amount of the shift reaction, which, of course, also depends on the contact time. The shift reaction is the slowest among these three reactions [126]. Consequently, hydrogen production slightly increases on the expense of CO by WGS.

Furthermore, carbon deposition on the catalyst surface can be prevented. This is also indicated by the comparison of the molar flow rates of H_2O for in - and output, as shown in **Figure 6-4**. Dashed lines show the constant input steam feed while full lines show the measured steam production. At S/C = 0.01, steam is a net product at all conditions, however, for an S/C of 0.05, a net H_2O consumption is observed around the C/O stoichiometric point for syngas production of 1.0. The C/O region in which a net consumption of steam is observed increases with rising S/C quickly covering the entire fuel rich regime of C/O > 1.0. At very low C/O, where total oxidation is favored, steam remains a net product.

Nevertheless, unconverted fuel and smaller hydrocarbon species can also be reformed by steam in homogeneous gas-phase reactions in the post catalyst zone at temperatures above 873 K, as hydrogen and carbon monoxide yields are higher than in the reference, especially for an S/C of 0.01 and 0.05. This effect was not observed in case of carbon dioxide recycling (case 2) as H_2 yields remain below the reference. Consequently, as already discussed for methane in literature, dry reforming can be neglected in CPOX reformers [123]. In case 2, the WGS reaction is observed: CO yields exceed the reference experiment, more water is detected, and H_2 yields remain low. In **Figure 6-4**, the molar in- and output flow rates of CO_2 are shown. A net consumption of CO_2 is only barely noticeable for CO_2/C = 0.3 around C/O = 0.8, while for the other ReTG/C ratios, more CO_2 is detected at the exit than fed to the reactor inlet for all conditions.

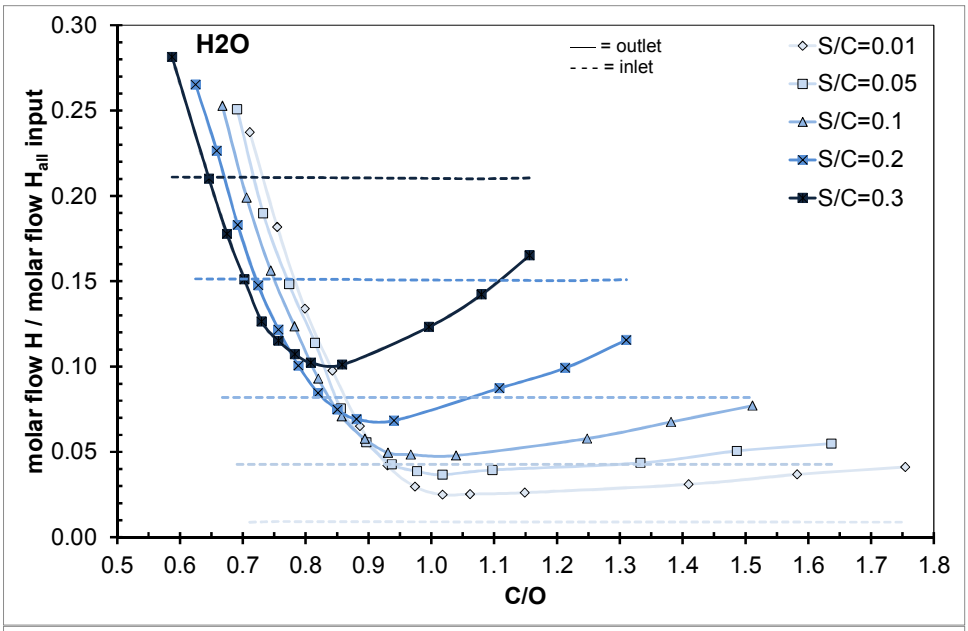
H2O
= outlet
= inlet
S/C=0.01
S/C=0.05
S/C=0.1
S/C=0.2
S/C=0.3
molar flow H / molar flow H$_{all}$ input
C/O

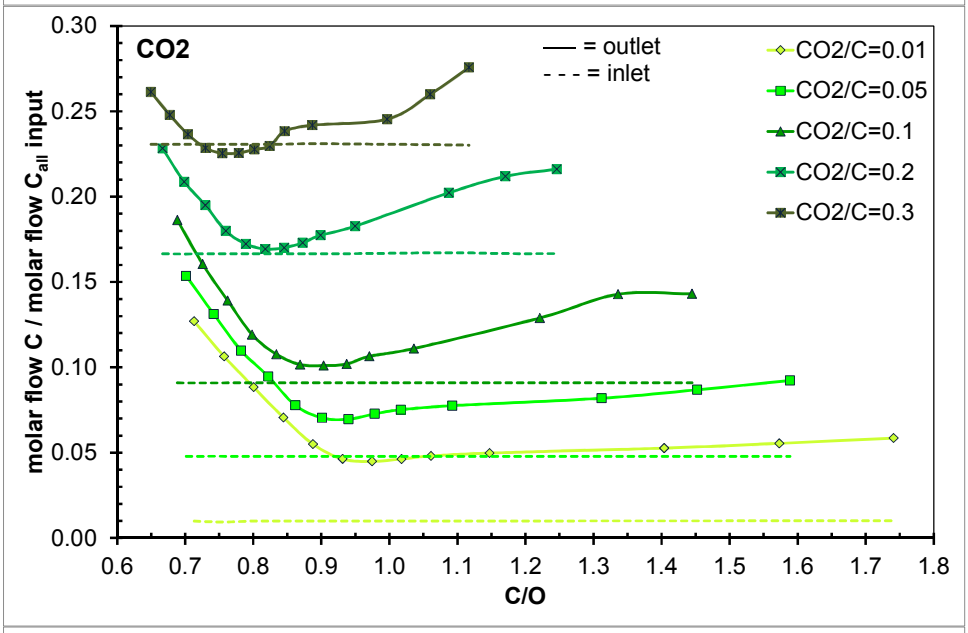
CO2
= outlet
= inlet
CO2/C=0.01
CO2/C=0.05
CO2/C=0.1
CO2/C=0.2
CO2/C=0.3
molar flow C / molar flow C$_{all}$ input
C/O

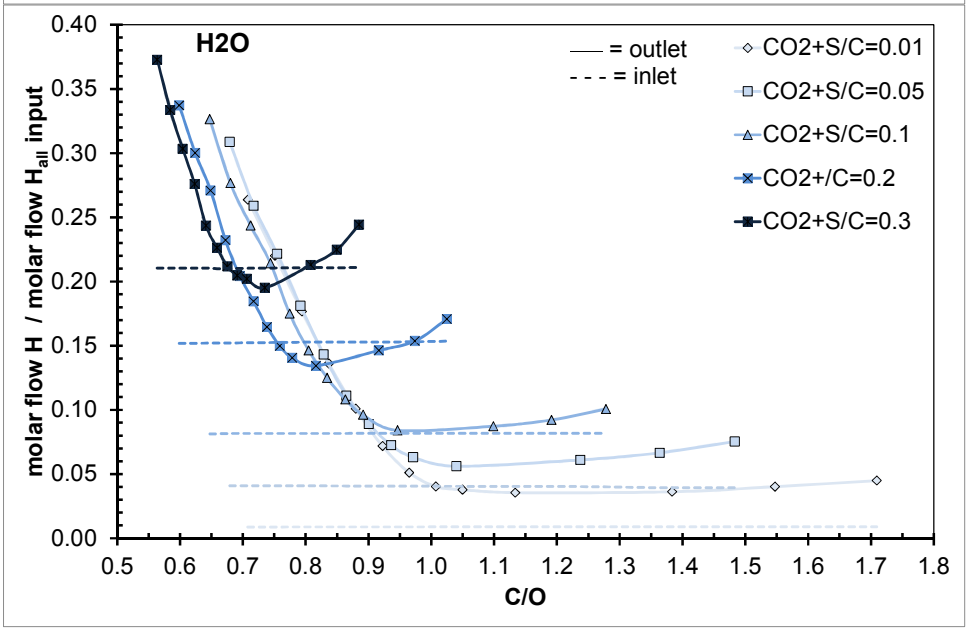
H2O
= outlet
= inlet
CO2+S/C=0.01
CO2+S/C=0.05
CO2+S/C=0.1
CO2+/C=0.2
CO2+S/C=0.3
molar flow H / molar flow H$_{all}$ input
C/O

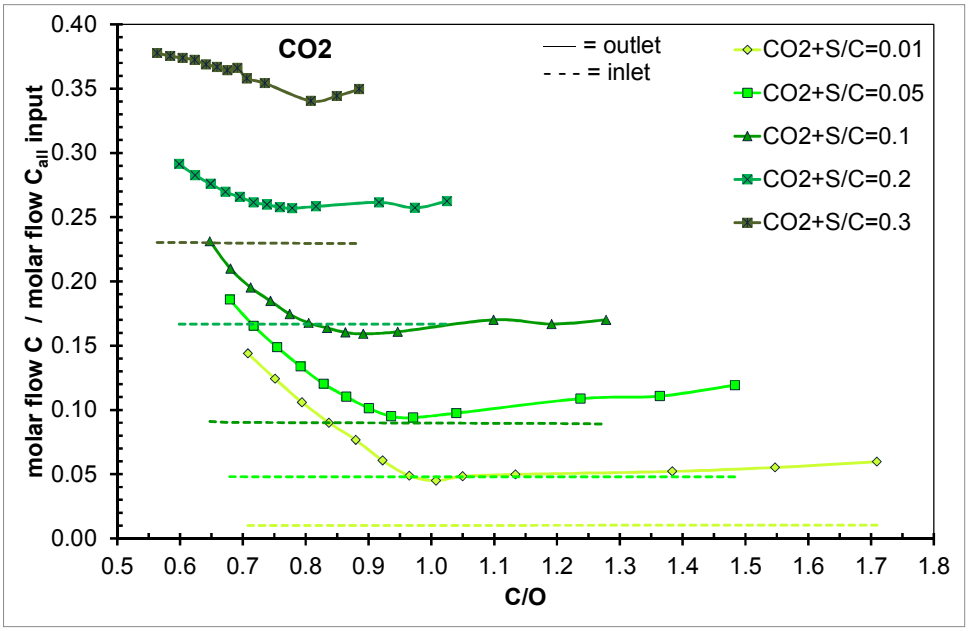

Figure 6-4: Input-referenced molar flow rates for H_2O and CO_2 input (dashed lines) and output (full lines) of the reactor. Upper first = case 1, second = case 2, last two = case 3.

In case 3, i.e., addition of steam and CO_2, a different behavior becomes obvious. Yields in H_2 and CO always remain below the reference; especially for small ReTG/C ratios, the influence in the lean area is very strong. Here, the addition of ReTG in the inlet competes with the total oxidation of the fuel at the initial catalyst zone. As reactor outlet temperatures drop very fast to levels below 1250 K, resulting from less total oxidation (see Chapter 6.3.1), a loss of syngas production (ReTG/C = 0.01) is the consequence. However, in the range of ReTG/C 0.05 - 0.1, the hydrogen yield reaches similar values as the reference (for fuel base yields), which indicate that either steam reforming or WGS or both increase the syngas yield again. For ReTG/C = 0.01, too little ReTG is in the inlet mixture and, thus, the lack of temperature cannot be compensated. Compared to the other case studies, the production of H_2O and CO_2 is favored for both species in case 3. **Figure 6-4** exhibits slight net water consumption for ReTG/C > 0.1 only, while CO_2 is a net product in all cases. The fuel conversion in case 3 strongly depends on the amount of ReTG. For ReTG/C = 0.1, even in the lean area, conversion is already not complete and precipitous drops to values below 0.8. For ReTG/C > 0.1, full conversion is never reached in the examined C/O ratios.

6.3.3 Effect on Formation of Side-Products (Methane, Ethylene, Propylene)

Side products, formed by thermal cracking of unconverted fuel, have been observed, in particular, at higher C/O ratios in CPOx of higher hydrocarbons [34]. The side products ethylene, propylene, and acetylene are well-known to serve as precursors for the formation of soot particles and solid carbon deposits [59].

Feeding ReTG to the reformer inlet stream significantly decreases the temperature and, consequently, fuel conversion (**Figure 6-3**). Here, fuel conversion is reduced and shifted towards lower C/O ratios with increasing ReTG/C compared to the reference feed. A larger amount of unconverted fuel rather increases the formation of soot precursors while, in general, a lower temperature slows down gas-phase reactions. As long as the temperature still exceeds 850 K over the entire C/O regime, thermal cracking of unconverted fuel leads to the appearance of olefins, even in the lean area. **Figure 6-5** exhibits the yields of the three major side-products methane, ethylene, and propylene.

In case of steam addition (case 1), compared to the reference, yields of all the three species are reduced by up to S/C = 0.1. Ethylene and propylene continuously decrease with increasing S/C although conversion of the fuel decreases, too. Once formed, the increasing amount of steam available in the reformate may lead to additional steam reforming of olefins. Only methane increases with increasing steam content in the inlet, exceeding the reference for S/C > 0.1. One possible explanation for rising methane yields could be gasification of carbon layers formed on the catalytic surface, thus leading to CO and H_2, followed by methanation of CO and / or CO_2 with available H_2. Furthermore, direct methanation of surface carbon with H_2 could be another possibility. Experimental data from in-situ analyses are needed to verify this explanation.

Comparable results are obtained by addition of carbon dioxide (case 2): the ethylene and propylene formation follows the same trends, and only the absolute amount of formation of these olefins is higher than in case 1. Since steam reforming in case 2 can only be realized by steam produced in total oxidation of the fuel, and since dry reforming is rather slow in terms of residence time, WGS is the best path for the CO_2 co-feed to interact with CPOx.

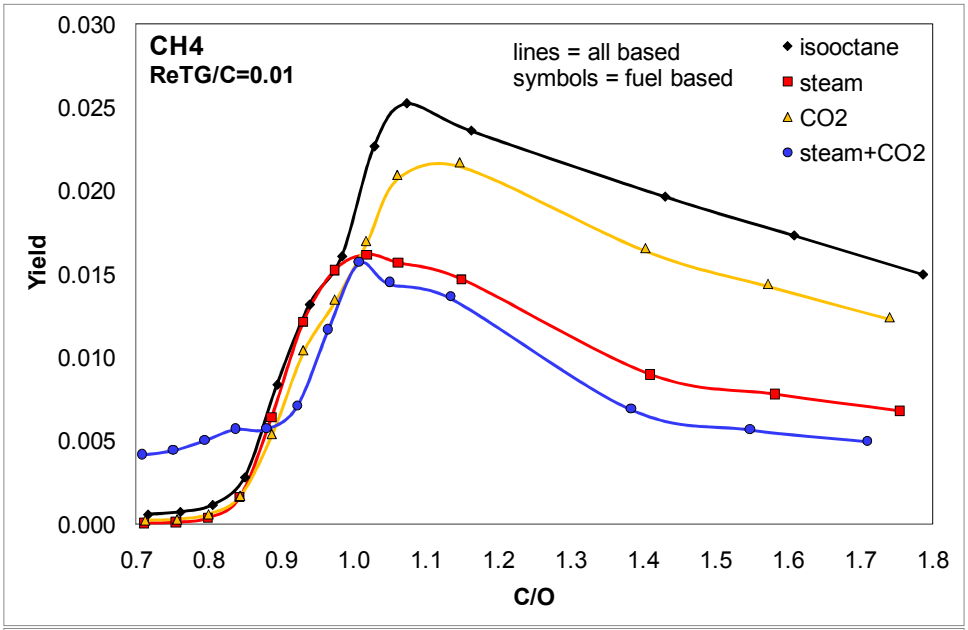
CH4
ReTG/C=0.01
lines = all based
symbols = fuel based
isooctane
steam
CO2
steam+CO2
Yield
0.030
0.025
0.020
0.015
0.010
0.005
0.000
0.7 0.8 0.9 1.0 1.1 1.2 1.3 1.4 1.5 1.6 1.7 1.8
C/O

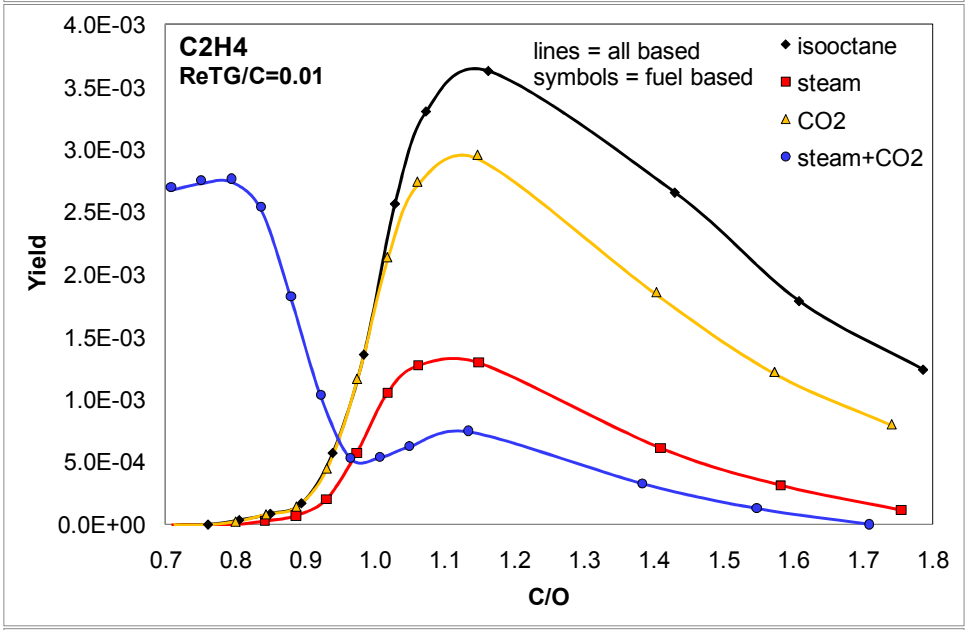
C2H4
ReTG/C=0.01
lines = all based
symbols = fuel based
isooctane
steam
CO2
steam+CO2
Yield
4.0E-03
3.5E-03
3.0E-03
2.5E-03
2.0E-03
1.5E-03
1.0E-03
5.0E-04
0.0E+00
0.7 0.8 0.9 1.0 1.1 1.2 1.3 1.4 1.5 1.6 1.7 1.8
C/O

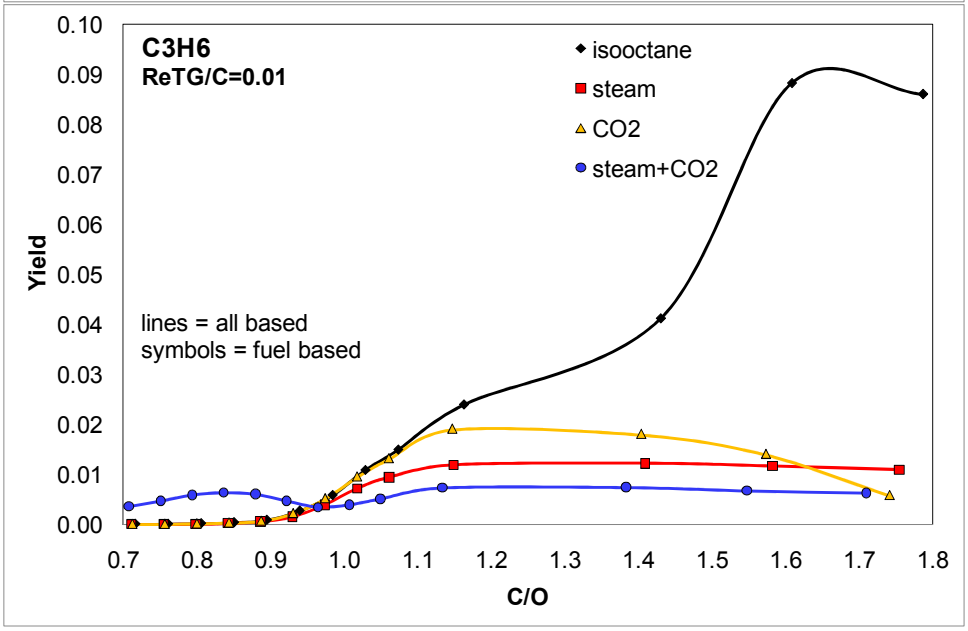
C3H6
ReTG/C=0.01
isooctane
steam
CO2
steam+CO2
lines = all based
symbols = fuel based
Yield
0.10
0.09
0.08
0.07
0.06
0.05
0.04
0.03
0.02
0.01
0.00
0.7 0.8 0.9 1.0 1.1 1.2 1.3 1.4 1.5 1.6 1.7 1.8
C/O

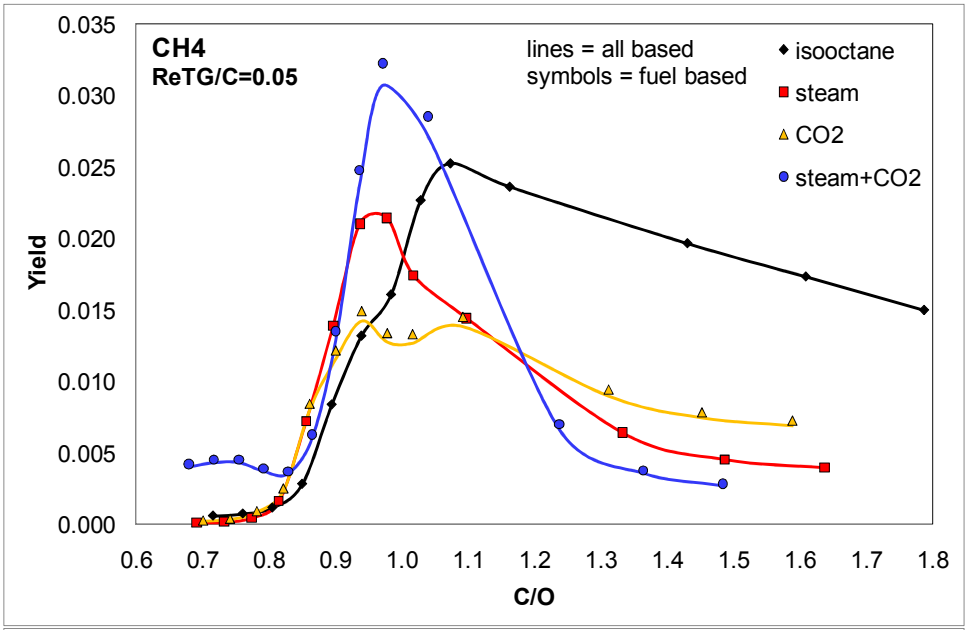
CH4
ReTG/C=0.05
lines = all based
symbols = fuel based
isooctane
steam
CO2
steam+CO2
Yield
0.035
0.030
0.025
0.020
0.015
0.010
0.005
0.000
0.6 0.7 0.8 0.9 1.0 1.1 1.2 1.3 1.4 1.5 1.6 1.7 1.8
C/O

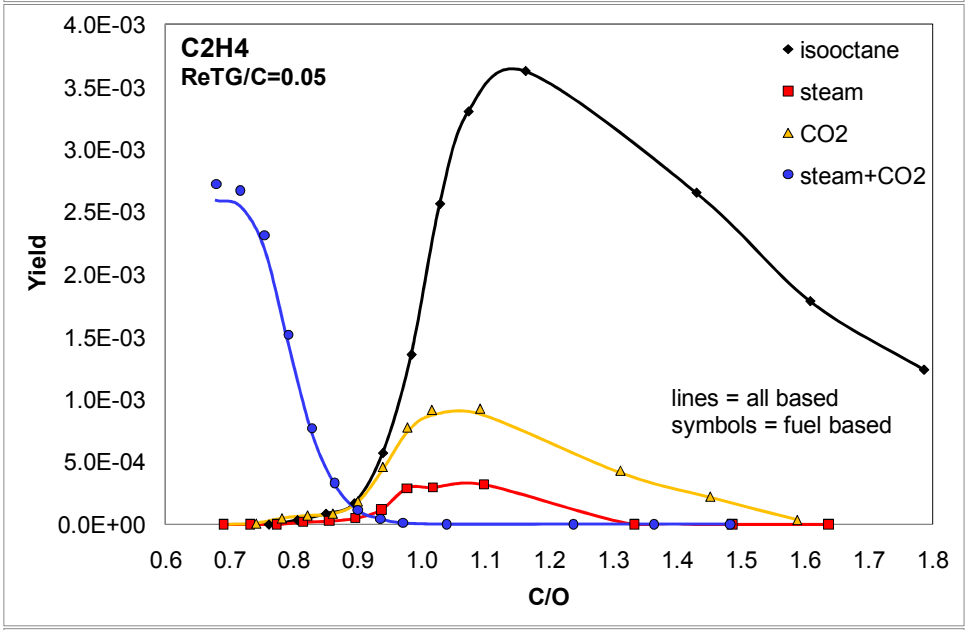
C2H4
ReTG/C=0.05
isooctane
steam
CO2
steam+CO2
lines = all based
symbols = fuel based
Yield
4.0E-03
3.5E-03
3.0E-03
2.5E-03
2.0E-03
1.5E-03
1.0E-03
5.0E-04
0.0E+00
0.6 0.7 0.8 0.9 1.0 1.1 1.2 1.3 1.4 1.5 1.6 1.7 1.8
C/O

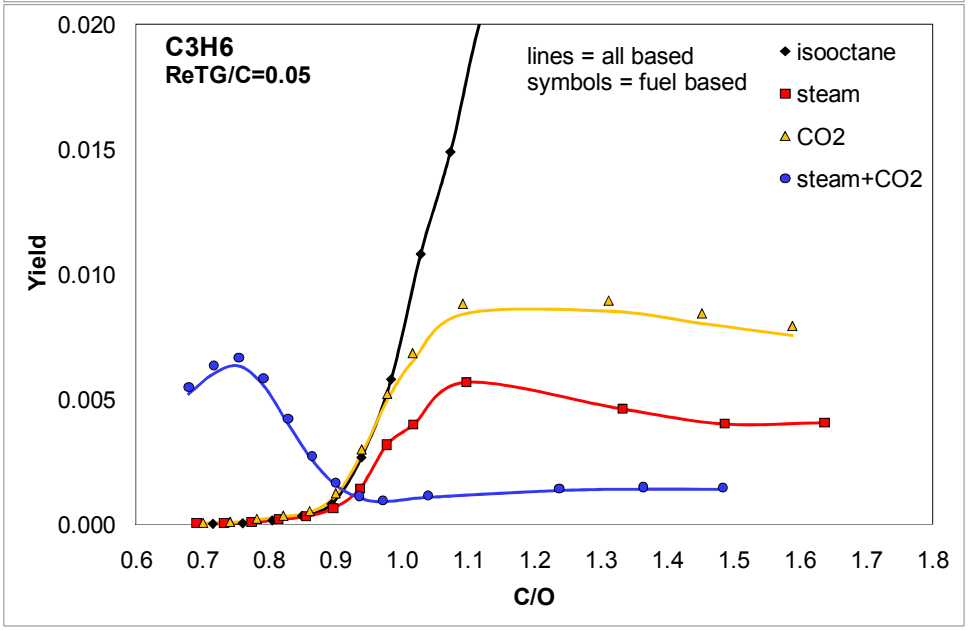
C3H6
ReTG/C=0.05
lines = all based
symbols = fuel based
isooctane
steam
CO2
steam+CO2
Yield
0.020
0.015
0.010
0.005
0.000
0.6 0.7 0.8 0.9 1.0 1.1 1.2 1.3 1.4 1.5 1.6 1.7 1.8
C/O

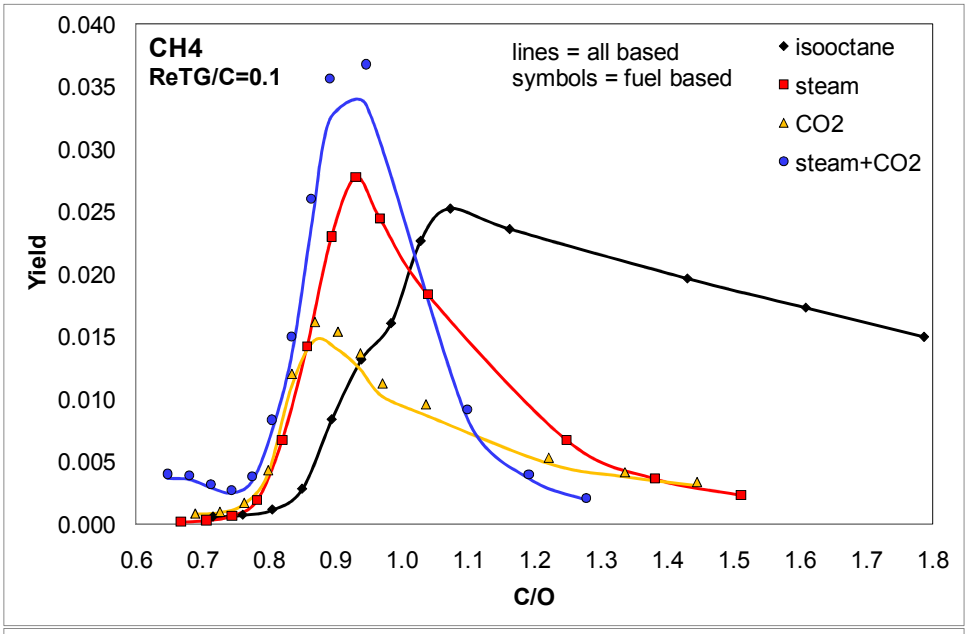
CH4
ReTG/C=0.1
lines = all based
symbols = fuel based
isooctane
steam
CO2
steam+CO2
Yield
0.040
0.035
0.030
0.025
0.020
0.015
0.010
0.005
0.000
0.6 0.7 0.8 0.9 1.0 1.1 1.2 1.3 1.4 1.5 1.6 1.7 1.8
C/O

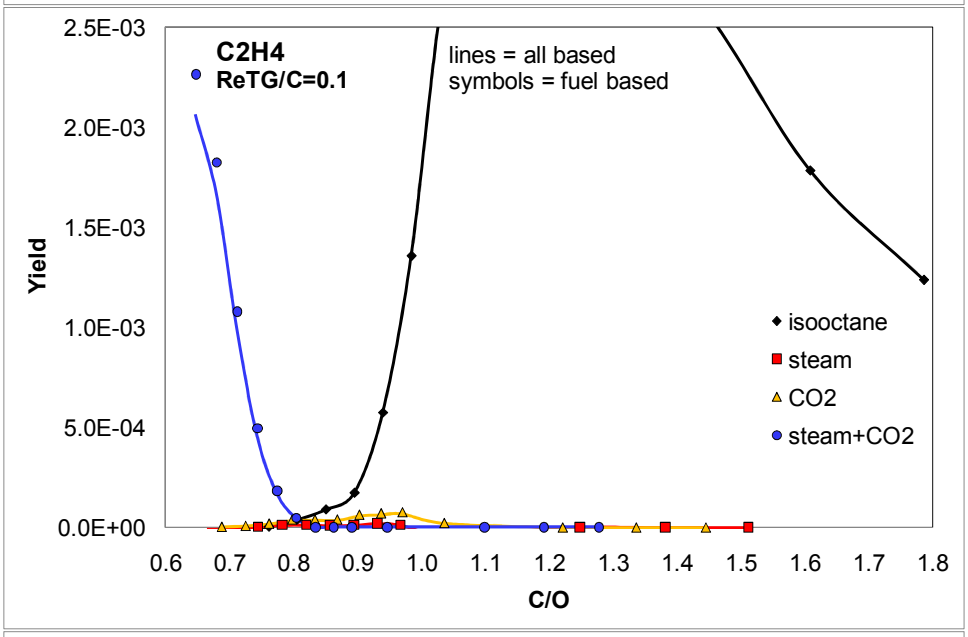
C2H4
ReTG/C=0.1
lines = all based
symbols = fuel based
isooctane
steam
CO2
steam+CO2
Yield
2.5E-03
2.0E-03
1.5E-03
1.0E-03
5.0E-04
0.0E+00
0.6 0.7 0.8 0.9 1.0 1.1 1.2 1.3 1.4 1.5 1.6 1.7 1.8
C/O

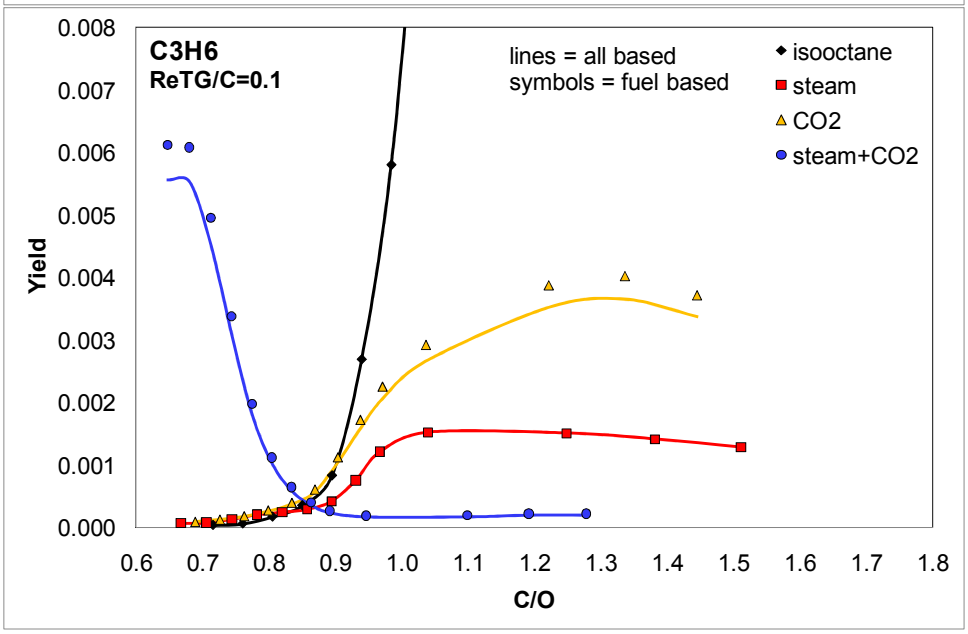
C3H6
ReTG/C=0.1
lines = all based
symbols = fuel based
isooctane
steam
CO2
steam+CO2
Yield
0.008
0.007
0.006
0.005
0.004
0.003
0.002
0.001
0.000
0.6 0.7 0.8 0.9 1.0 1.1 1.2 1.3 1.4 1.5 1.6 1.7 1.8
C/O

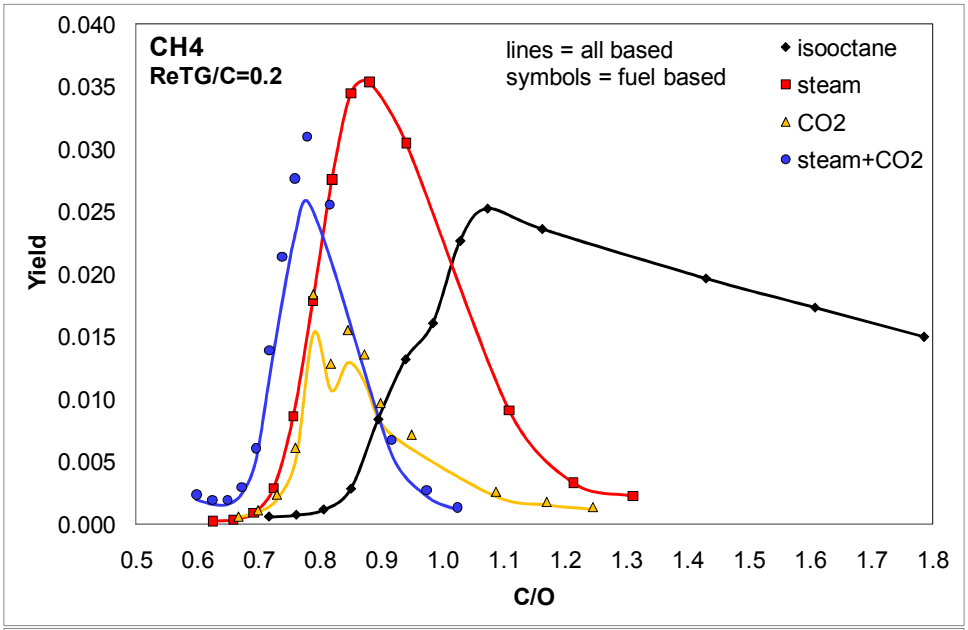
CH4
ReTG/C=0.2
lines = all based
symbols = fuel based
isooctane
steam
CO2
steam+CO2
Yield
0.040
0.035
0.030
0.025
0.020
0.015
0.010
0.005
0.000
0.5 0.6 0.7 0.8 0.9 1.0 1.1 1.2 1.3 1.4 1.5 1.6 1.7 1.8
C/O

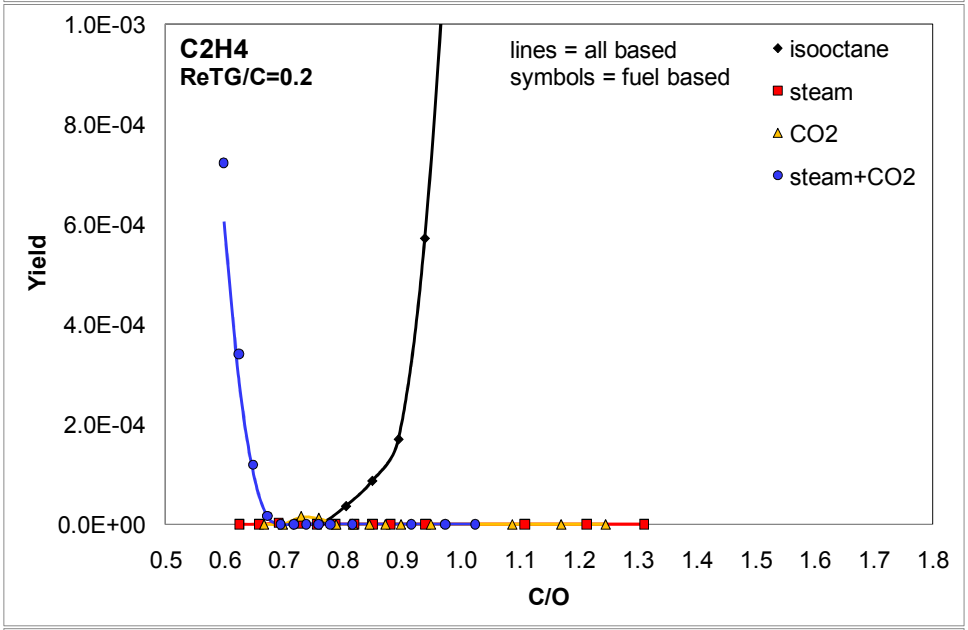
C2H4
ReTG/C=0.2
lines = all based
symbols = fuel based
isooctane
steam
CO2
steam+CO2
Yield
1.0E-03
8.0E-04
6.0E-04
4.0E-04
2.0E-04
0.0E+00
0.5 0.6 0.7 0.8 0.9 1.0 1.1 1.2 1.3 1.4 1.5 1.6 1.7 1.8
C/O

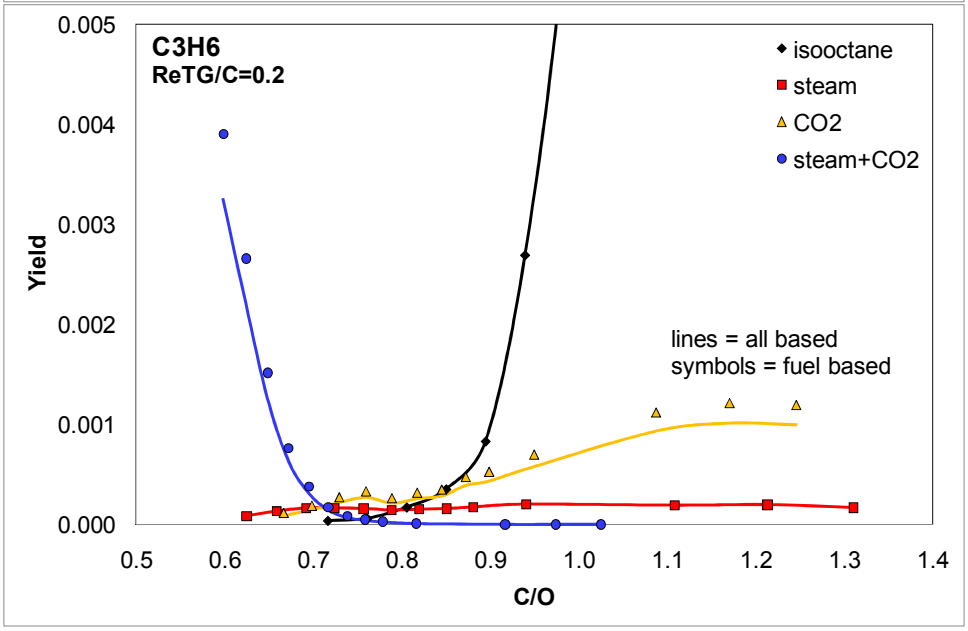
C3H6
ReTG/C=0.2
lines = all based
symbols = fuel based
isooctane
steam
CO2
steam+CO2
Yield
0.005
0.004
0.003
0.002
0.001
0.000
0.5 0.6 0.7 0.8 0.9 1.0 1.1 1.2 1.3 1.4
C/O

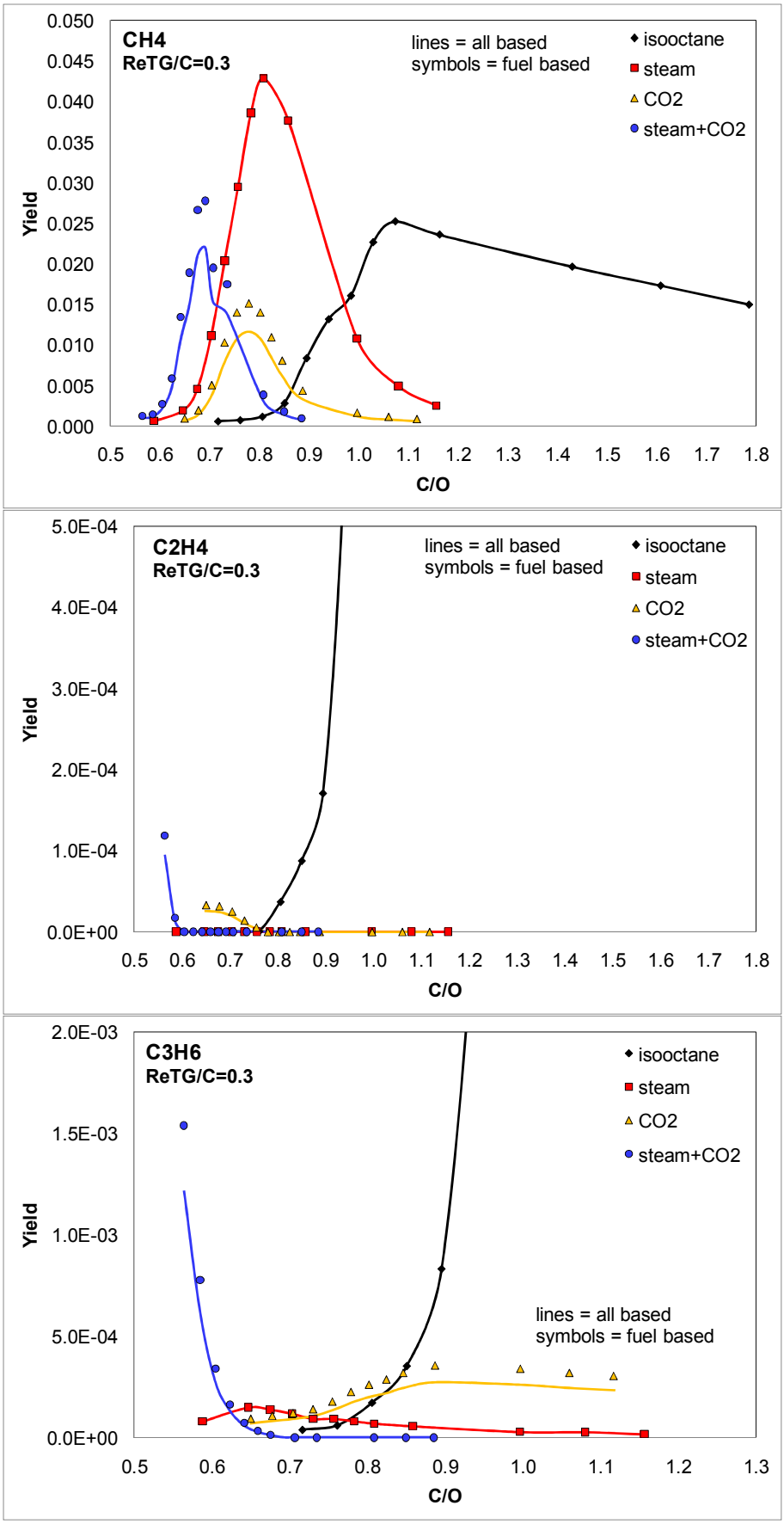

Figure 6-5: Yield of CH_4, C_2H_4 and C_3H_6 for case 1-3 and the five different ReTG/C ratios. Full lines = all based C/H yield, symbol = fuel based C/H yield.

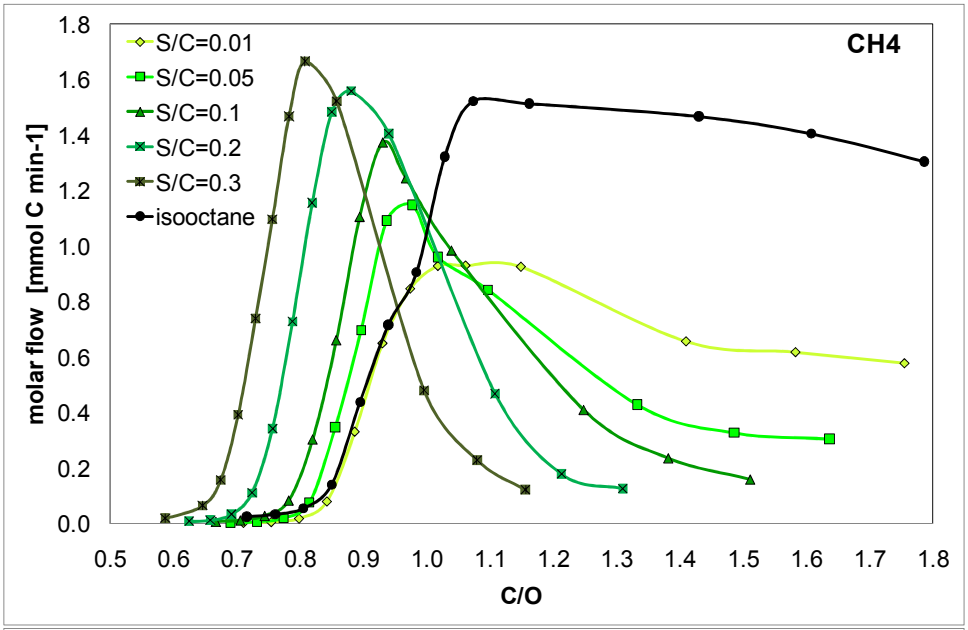
CH4
S/C=0.01
S/C=0.05
S/C=0.1
S/C=0.2
S/C=0.3
isooctane
molar flow [mmol C min-1]
C/O

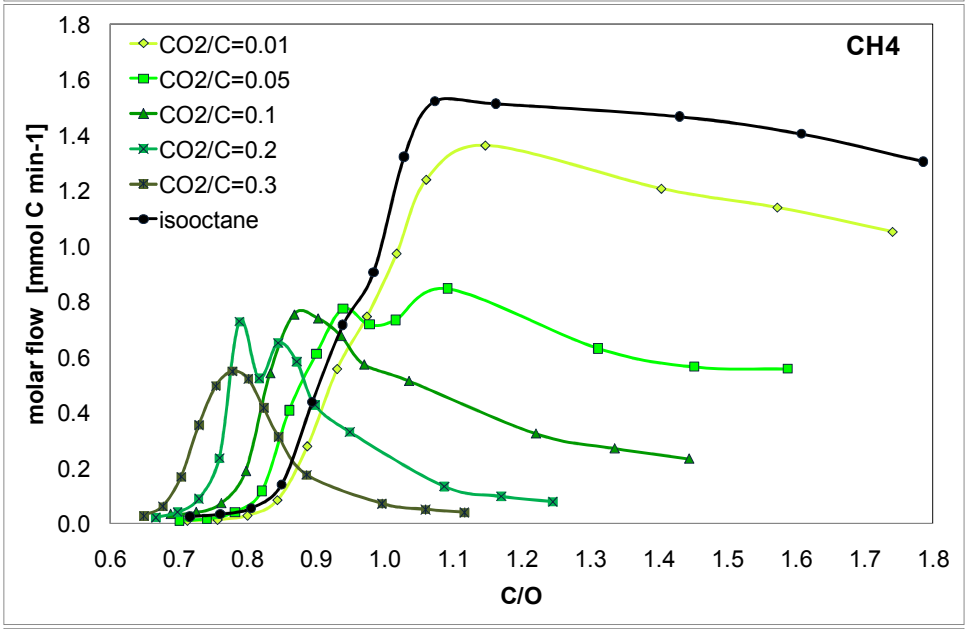
CH4
CO2/C=0.01
CO2/C=0.05
CO2/C=0.1
CO2/C=0.2
CO2/C=0.3
isooctane
molar flow [mmol C min-1]
C/O

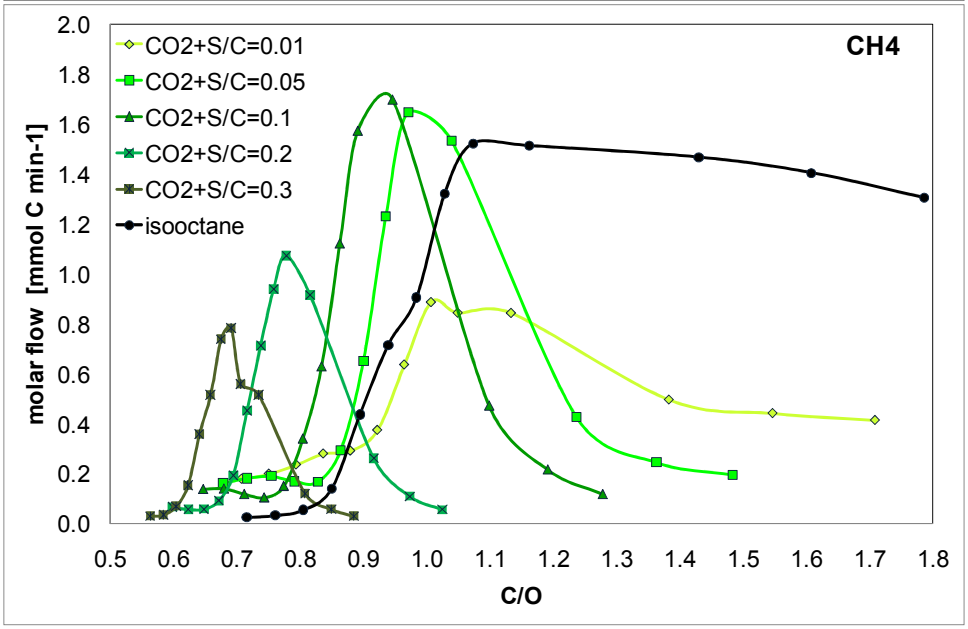
CH4
CO2+S/C=0.01
CO2+S/C=0.05
CO2+S/C=0.1
CO2+S/C=0.2
CO2+S/C=0.3
isooctane
molar flow [mmol C min-1]
C/O

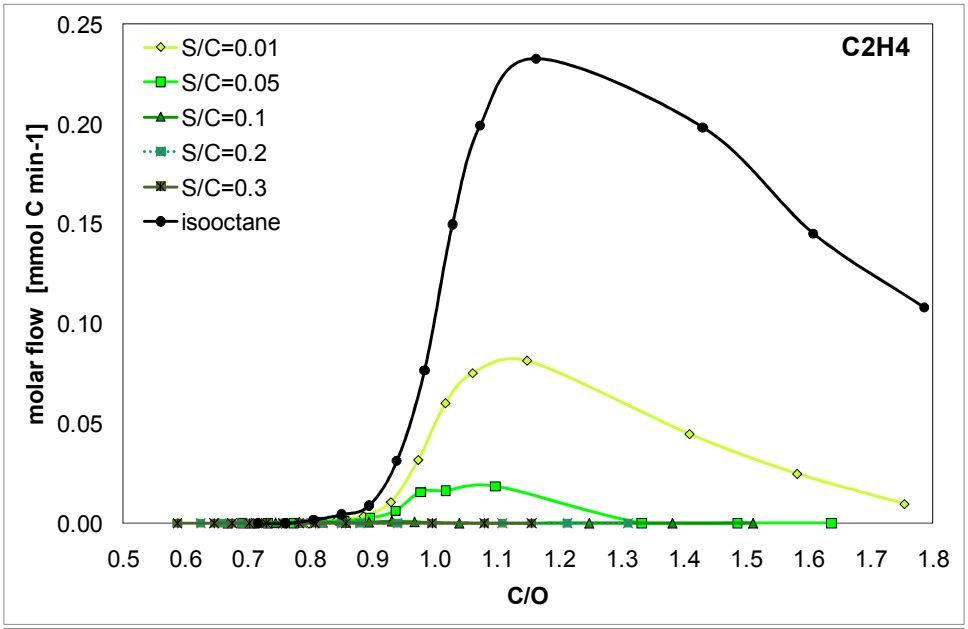
C2H4
S/C=0.01
S/C=0.05
S/C=0.1
S/C=0.2
S/C=0.3
isooctane
molar flow [mmol C min-1]
0.25
0.20
0.15
0.10
0.05
0.00
0.5 0.6 0.7 0.8 0.9 1.0 1.1 1.2 1.3 1.4 1.5 1.6 1.7 1.8
C/O

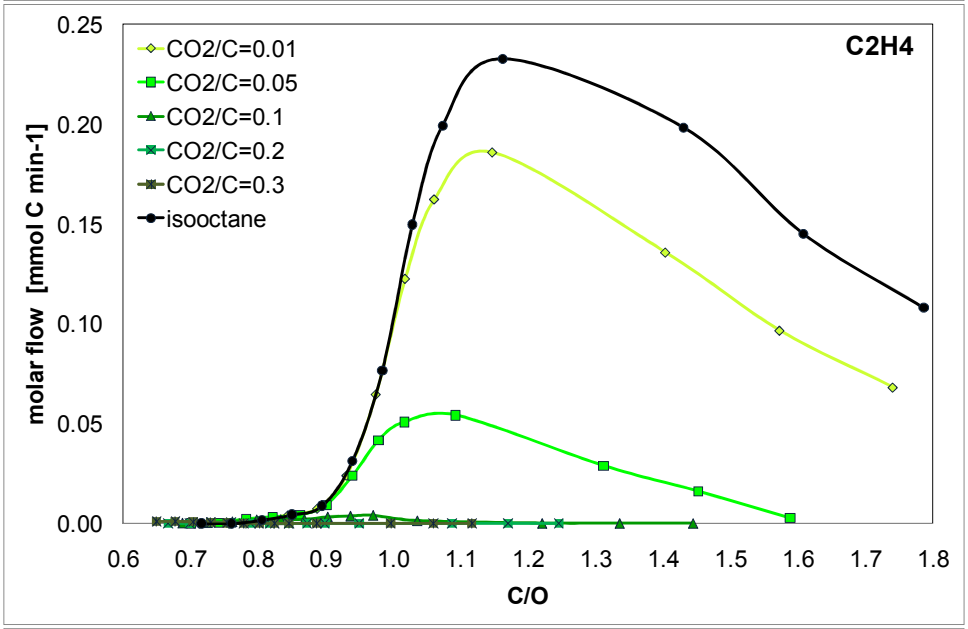
C2H4
CO2/C=0.01
CO2/C=0.05
CO2/C=0.1
CO2/C=0.2
CO2/C=0.3
isooctane
molar flow [mmol C min-1]
0.25
0.20
0.15
0.10
0.05
0.00
0.6 0.7 0.8 0.9 1.0 1.1 1.2 1.3 1.4 1.5 1.6 1.7 1.8
C/O

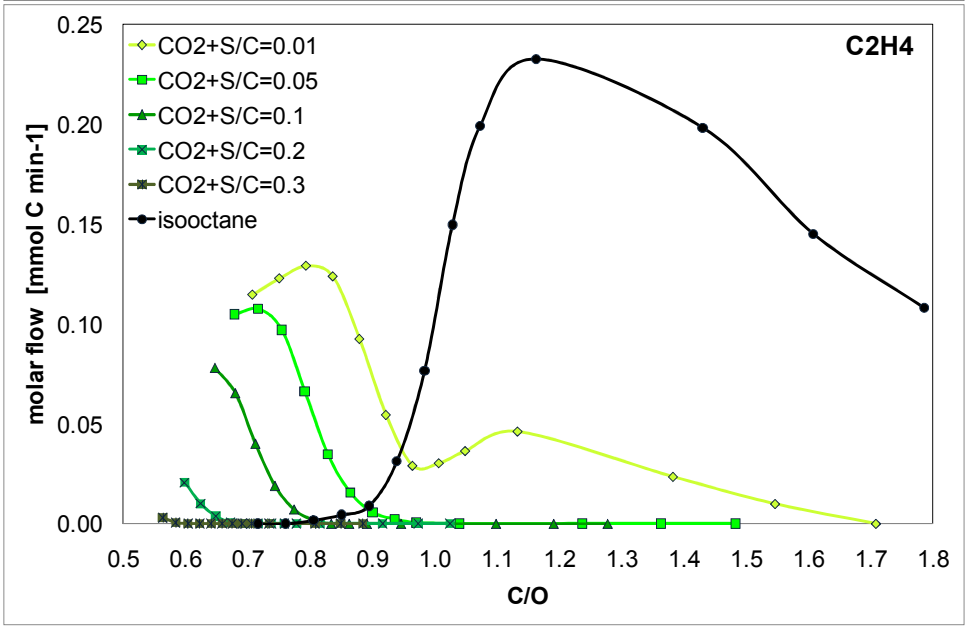
C2H4
CO2+S/C=0.01
CO2+S/C=0.05
CO2+S/C=0.1
CO2+S/C=0.2
CO2+S/C=0.3
isooctane
molar flow [mmol C min-1]
0.25
0.20
0.15
0.10
0.05
0.00
0.5 0.6 0.7 0.8 0.9 1.0 1.1 1.2 1.3 1.4 1.5 1.6 1.7 1.8
C/O

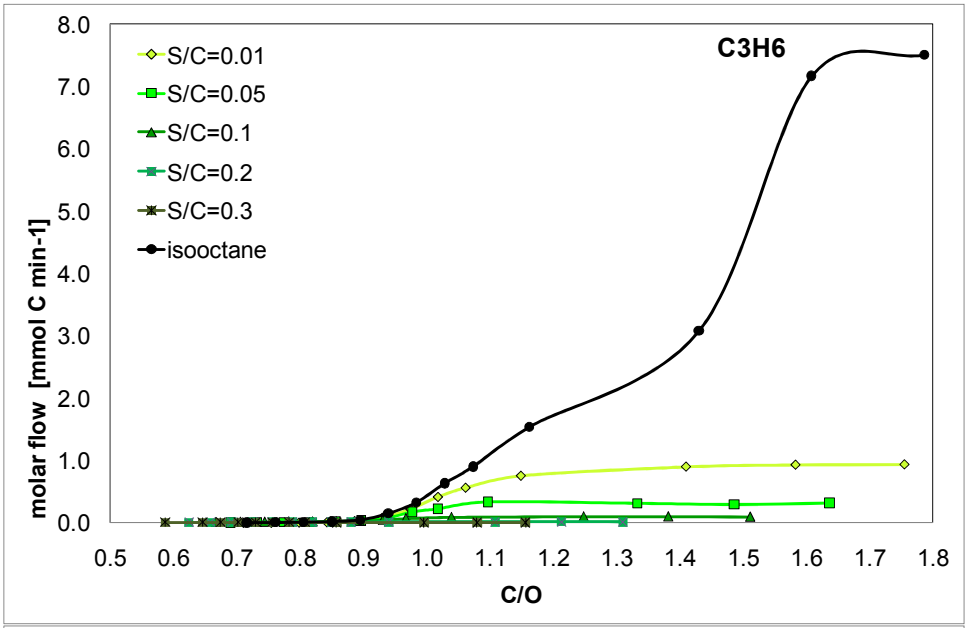
C3H6
S/C=0.01
S/C=0.05
S/C=0.1
S/C=0.2
S/C=0.3
isooctane
molar flow [mmol C min-1]
C/O

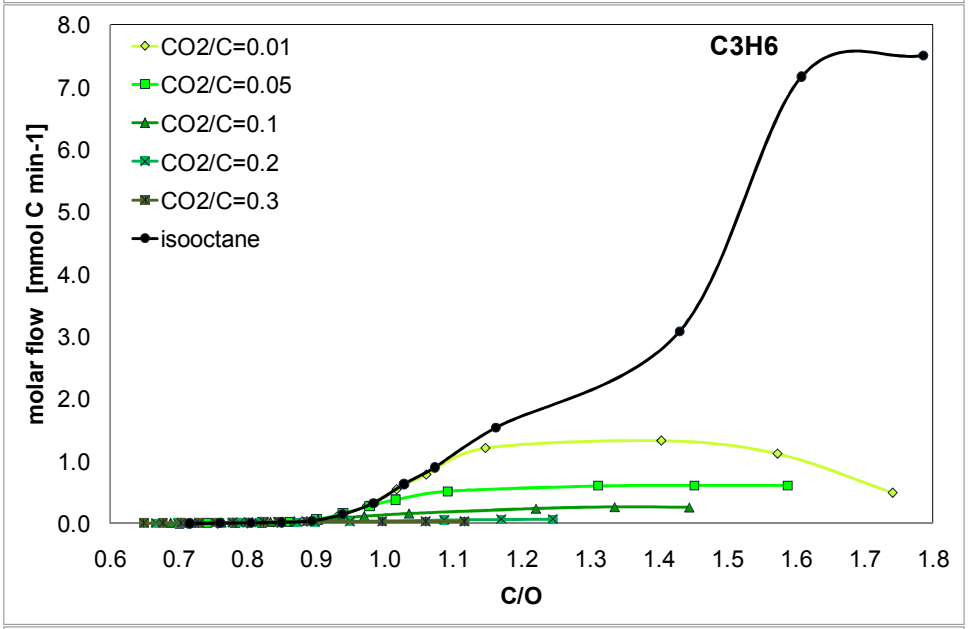
C3H6
CO2/C=0.01
CO2/C=0.05
CO2/C=0.1
CO2/C=0.2
CO2/C=0.3
isooctane
molar flow [mmol C min-1]
C/O

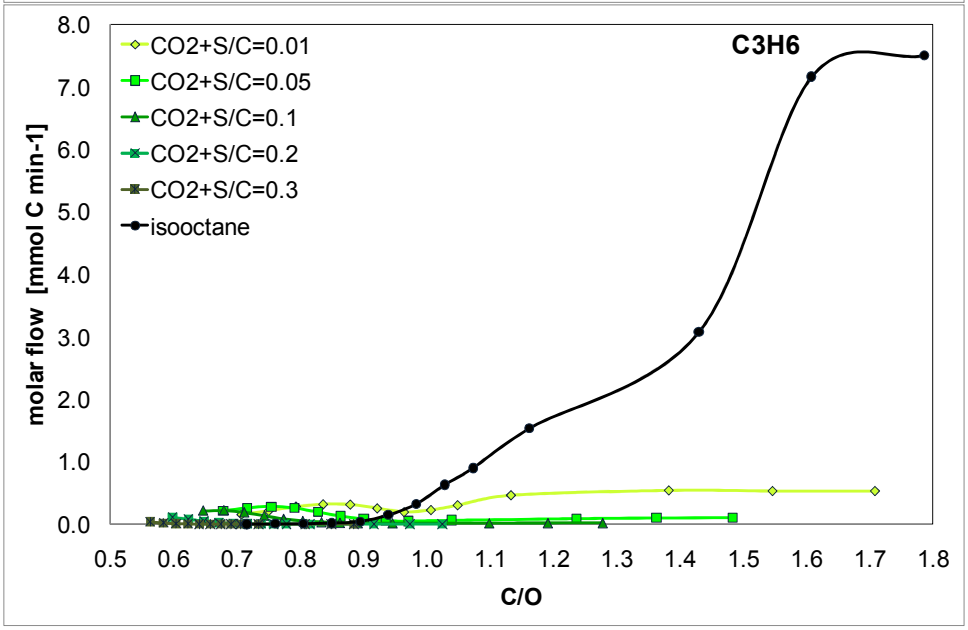
C3H6
CO2+S/C=0.01
CO2+S/C=0.05
CO2+S/C=0.1
CO2+S/C=0.2
CO2+S/C=0.3
isooctane
molar flow [mmol C min-1]
C/O

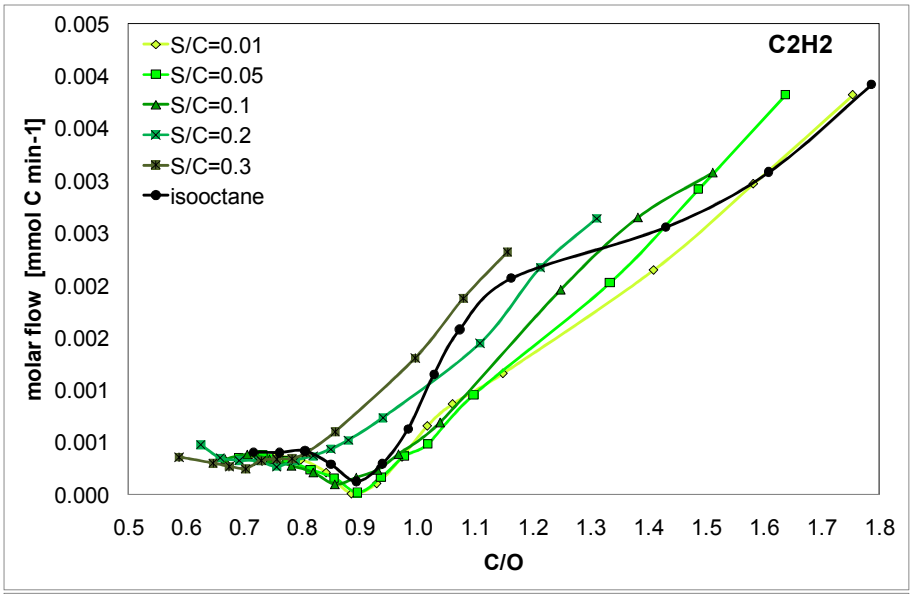

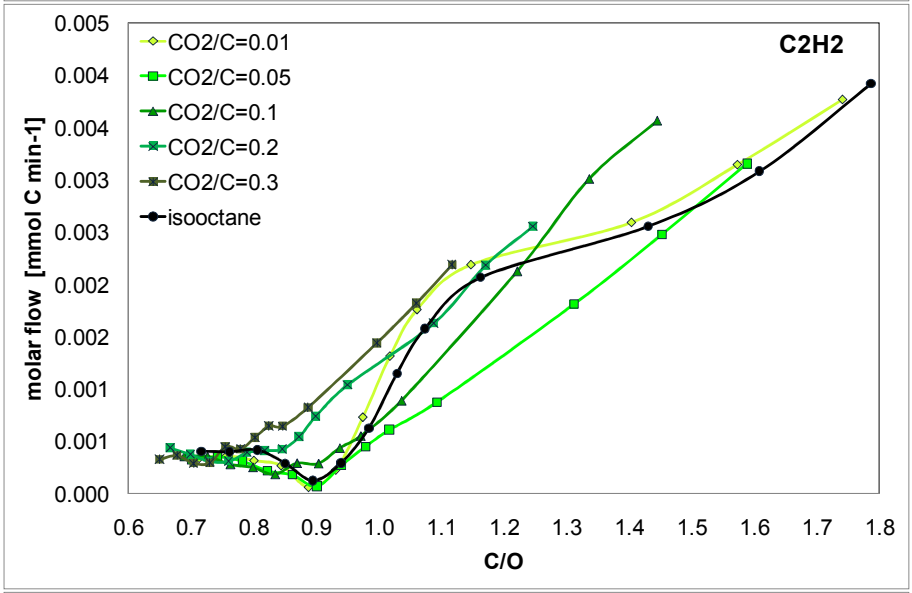

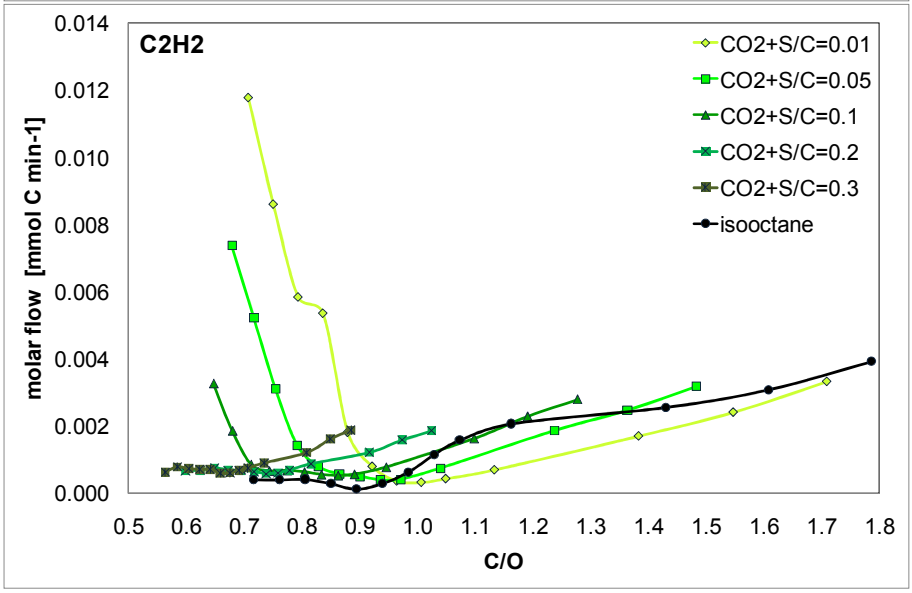

Figure 6-6: Molar flow rates of C_1-C_3 byproducts for case 1-3 and the five ReTG/C ratios.

The addition of both steam and carbon dioxide (case 3) exhibits a very different behavior. The yields of ethylene and propylene are qualitatively different, although a reduction in yield for both olefins is observed with increasing ReTG/C. The maxima, however, are shifted towards low C/O, and very small amounts of olefins are observed at C/O > 0.9. In case of ReTG/C > 0.2, the maxima are shifted to very lean conditions, thus, only the right shoulder of the peak can be seen. These large amounts of olefins are correlated to the incomplete conversion of the fuel in a high ReTG feed even at lower C/O.

The different reactivities of oxygen in molecular oxygen, steam, and carbon dioxide in conversion of hydrocarbons seem to lead to a rather complex behavior. As both recycling species are present, chemistry competes between steam reforming, WGS reaction, and, of course, total and partial oxidation. While the formation of olefins drastically changes, the formation of methane is similar to the first two cases, even though the maximum in methane yield is produced at lower C/O ratios at high ReTG/C ratios. For ReTG/C < 0.1, CH_4 yield curves are similar to the ones for steam co-feed. For ReTG/C > 0.1 the dependence of the methane yield on the C/O is similar to the one for the CO_2 co-feed. Concerning the formation of olefins in a fairly adiabatic reactor operation, tail-gas recycling leads to a reduction of these coke precursors in all cases studied for C/O > 0.9. On the other side, significant amounts of olefins are now seen at low C/O in case of steam and CO_2 addition, i.e., in a regime where they are not formed in high-temperature CPOx reactors without tail-gas recycling for model fuel surrogates. Concerning diesel fuel CPOx, Study 3 reveals that, even at C/O ratios < 1.0, significant amounts of by-products are obtained. This can be explained by the fact that the C/H content in a logistic fuel is much higher than that in model fuels and, therefore, the reaction behavior of the reformer is altered. This issue is discussed more in detail in Chapter 7.2.1.

6.3.4 Effect on Coke Formation

Attention has also been given to the total amount of carbon deposited on the catalyst surface. Carbon burn-offs were conducted after each full set of measurements over the C/O range of 0.72 to 1.79. Unfortunately, the detected amounts of carbon deposits represent the

entire amount of C on the surface for this measurement cycle and do not separately show the carbon amount of the defined C/O ratio. The detected CO and CO_2 signals were quantified to molar flow rates and integrated over time, and values are given in mmol of C in **Figure 6-7**.

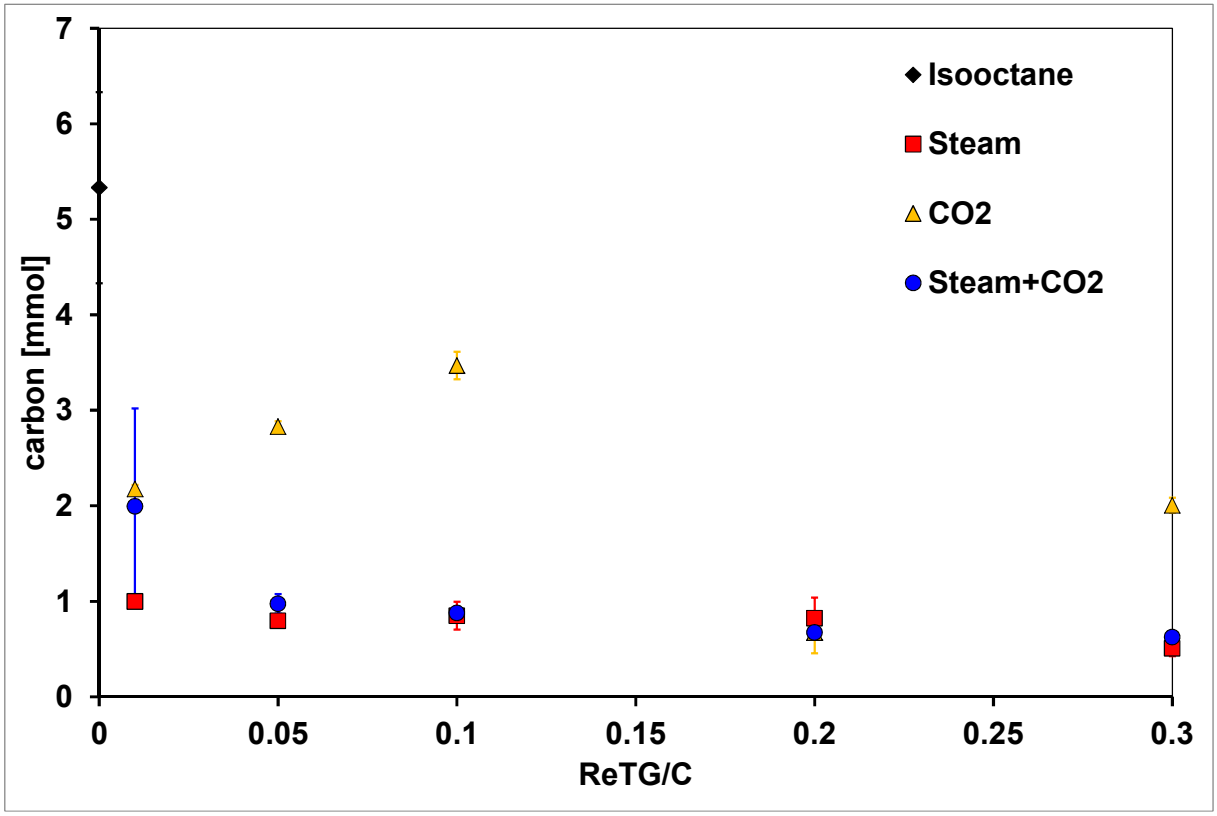

Figure 6-7: Calculated amount of carbon deposition from carbon burn-off experiments for each ReTG/C ratio and isooctane reference. Each value represents the overall carbon amount for C/O 0.72 – 1.79. Error margins are calculated from the total amount of C detected in the carbon burn-off experiments performed after each measurement and its rerun.

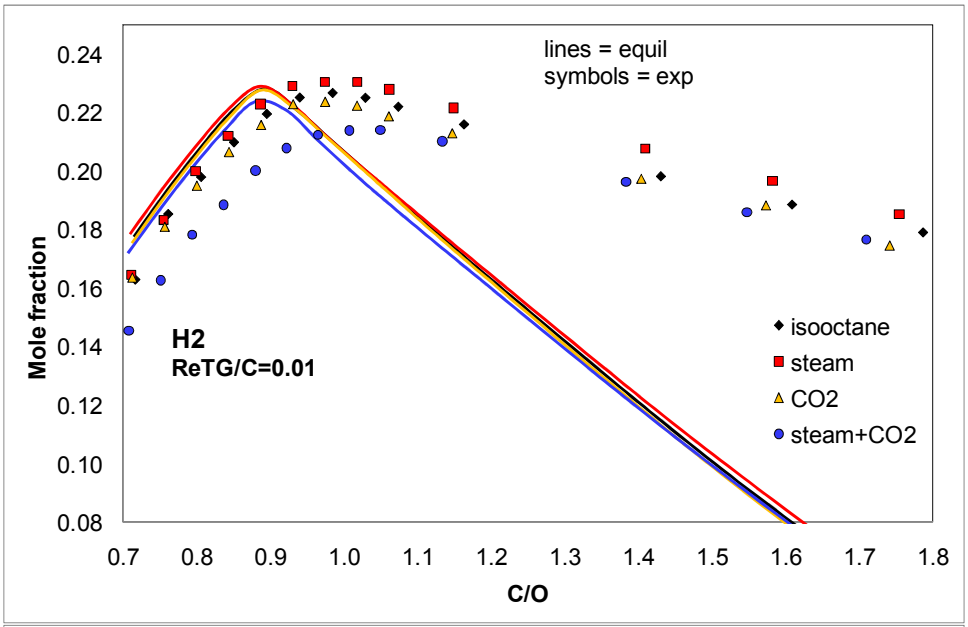
lines = equil
symbols = exp
H2
ReTG/C=0.01
isooctane
steam
CO2
steam+CO2
Mole fraction
C/O
0.24
0.22
0.20
0.18
0.16
0.14
0.12
0.10
0.08
0.7
0.8
0.9
1.0
1.1
1.2
1.3
1.4
1.5
1.6
1.7
1.8

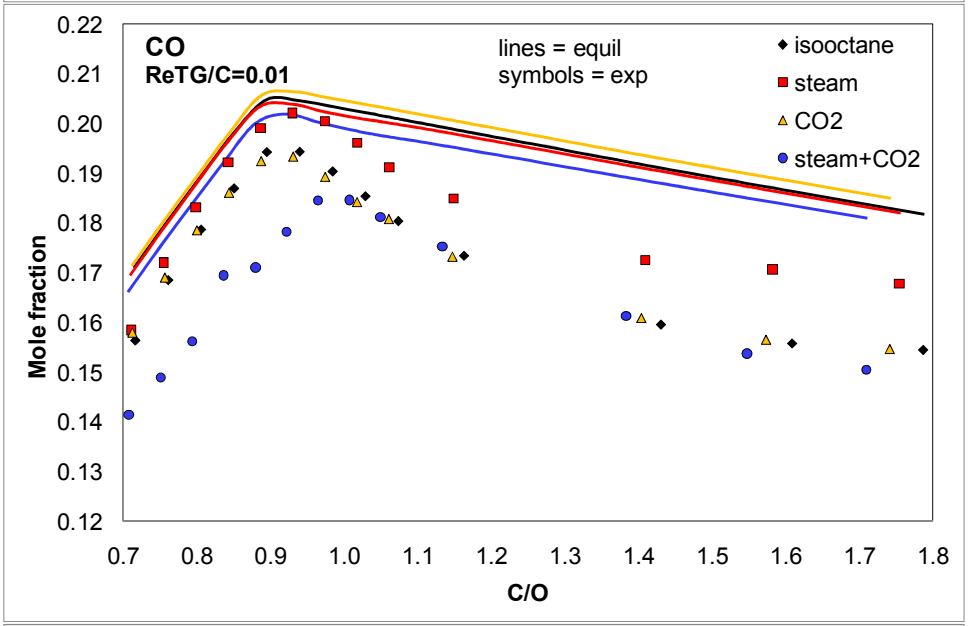
CO
ReTG/C=0.01
lines = equil
symbols = exp
isooctane
steam
CO2
steam+CO2
Mole fraction
C/O
0.22
0.21
0.20
0.19
0.18
0.17
0.16
0.15
0.14
0.13
0.12
0.7
0.8
0.9
1.0
1.1
1.2
1.3
1.4
1.5
1.6
1.7
1.8

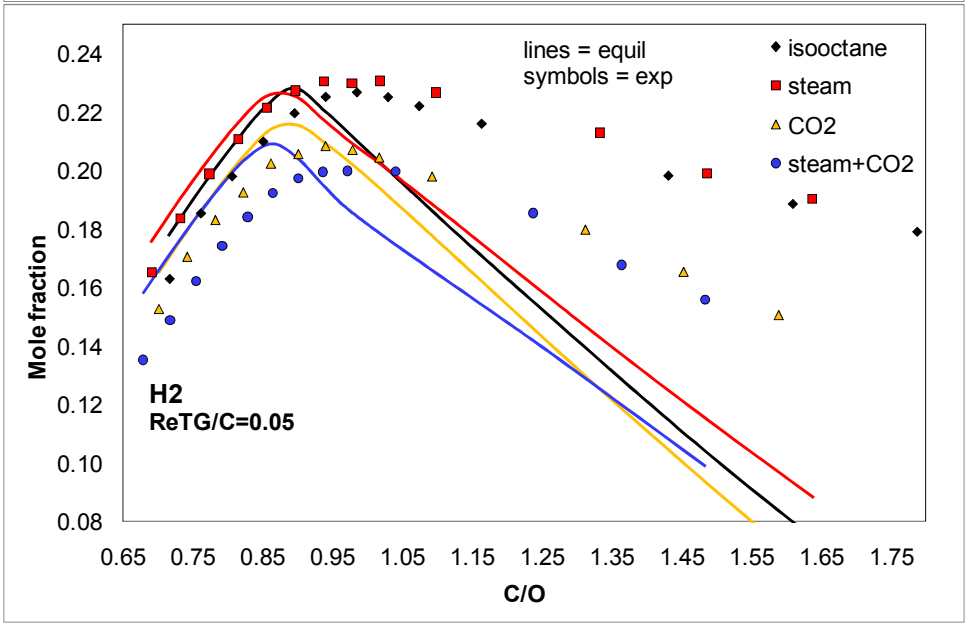
lines = equil
symbols = exp
isooctane
steam
CO2
steam+CO2
H2
ReTG/C=0.05
Mole fraction
C/O
0.24
0.22
0.20
0.18
0.16
0.14
0.12
0.10
0.08
0.65
0.75
0.85
0.95
1.05
1.15
1.25
1.35
1.45
1.55
1.65
1.75

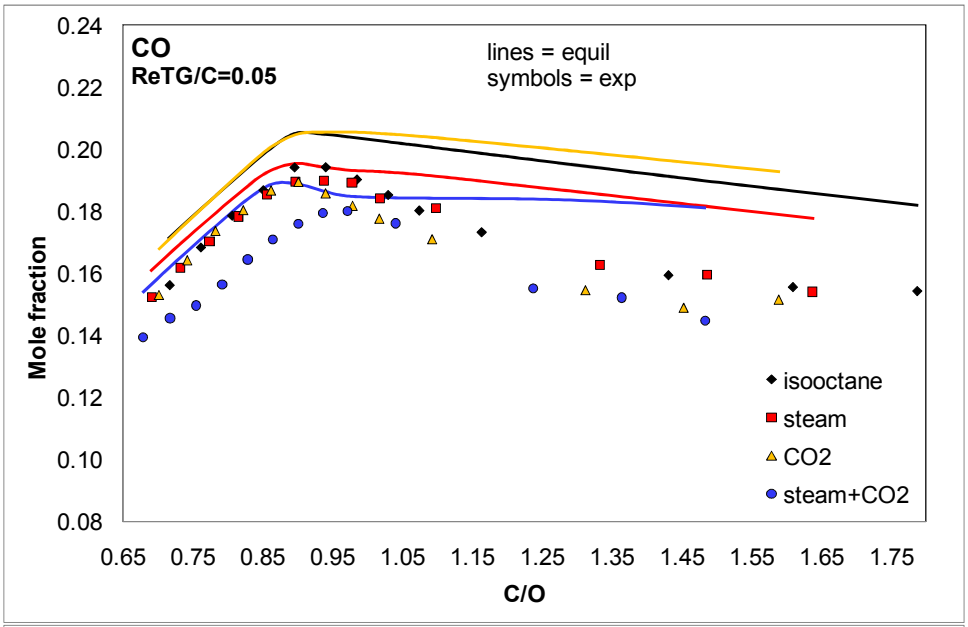
CO
ReTG/C=0.05
lines = equil
symbols = exp
isooctane
steam
CO2
steam+CO2
Mole fraction
C/O
0.24
0.22
0.20
0.18
0.16
0.14
0.12
0.10
0.08
0.65 0.75 0.85 0.95 1.05 1.15 1.25 1.35 1.45 1.55 1.65 1.75

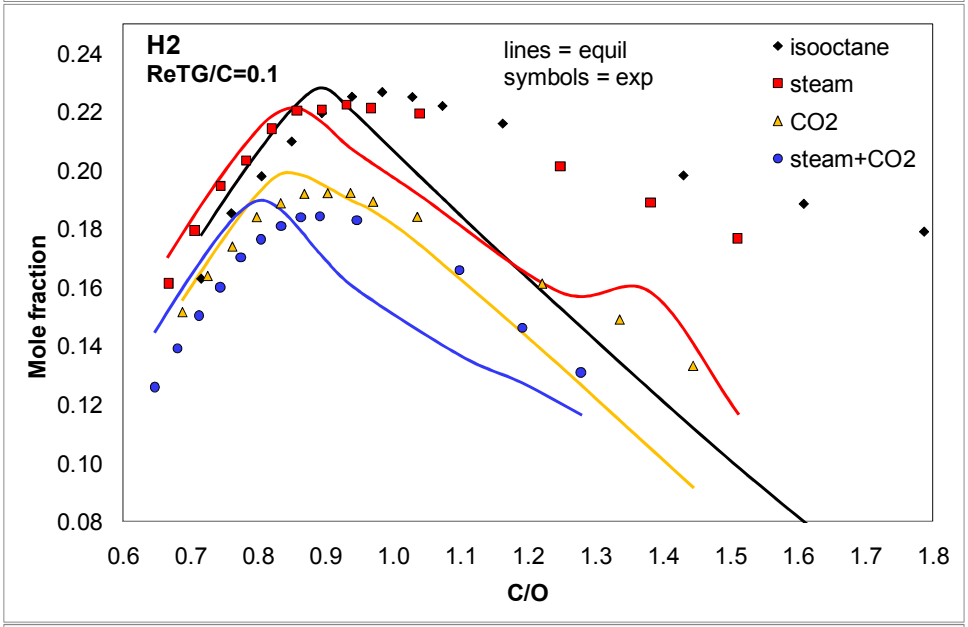
H2
ReTG/C=0.1
lines = equil
symbols = exp
isooctane
steam
CO2
steam+CO2
Mole fraction
C/O
0.24
0.22
0.20
0.18
0.16
0.14
0.12
0.10
0.08
0.6 0.7 0.8 0.9 1.0 1.1 1.2 1.3 1.4 1.5 1.6 1.7 1.8

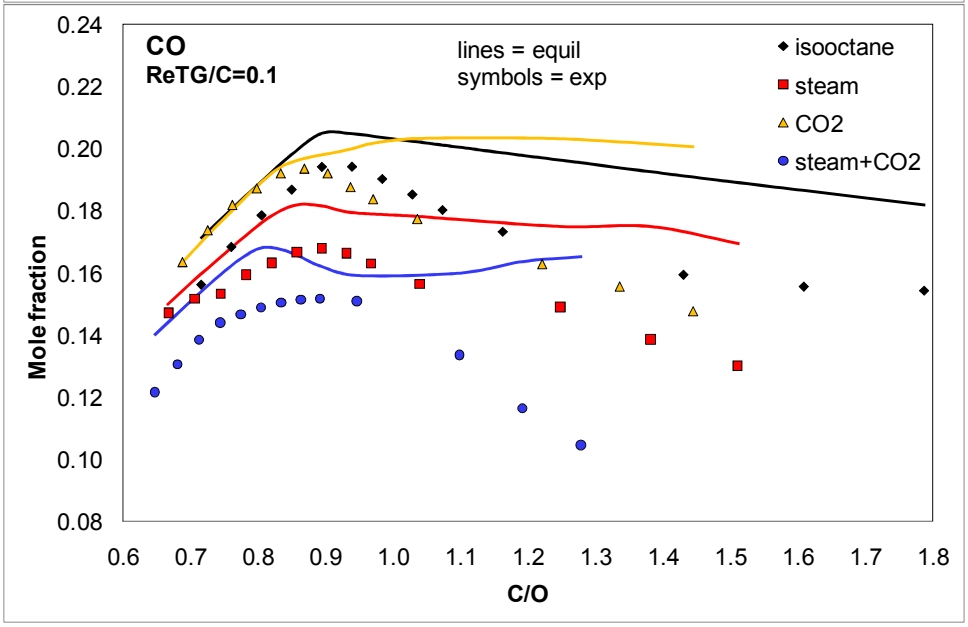
CO
ReTG/C=0.1
lines = equil
symbols = exp
isooctane
steam
CO2
steam+CO2
Mole fraction
C/O
0.24
0.22
0.20
0.18
0.16
0.14
0.12
0.10
0.08
0.6 0.7 0.8 0.9 1.0 1.1 1.2 1.3 1.4 1.5 1.6 1.7 1.8

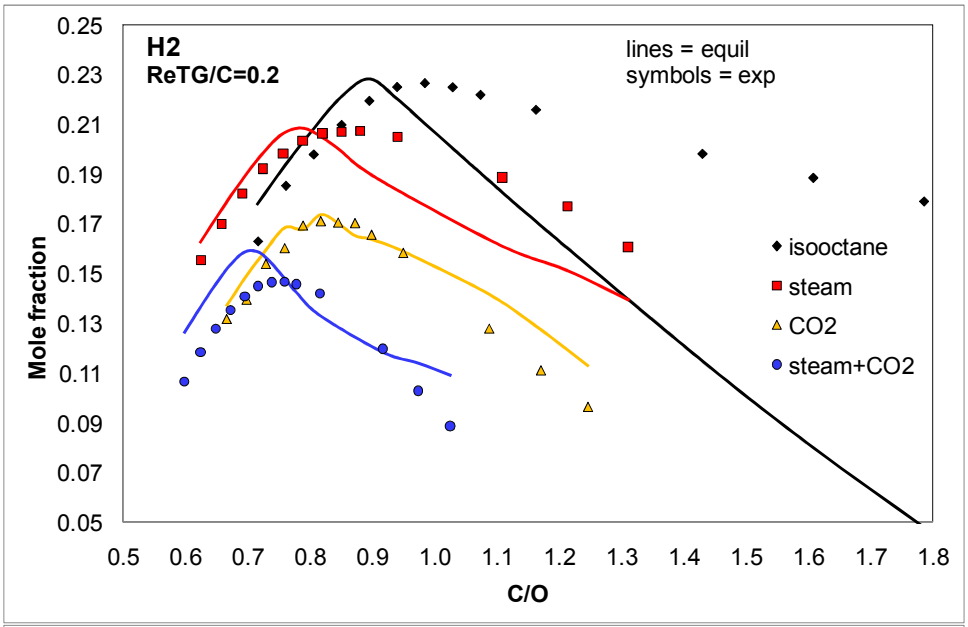
H2
ReTG/C=0.2
lines = equil
symbols = exp
isooctane
steam
CO2
steam+CO2
Mole fraction
C/O
0.25
0.23
0.21
0.19
0.17
0.15
0.13
0.11
0.09
0.07
0.05
0.5 0.6 0.7 0.8 0.9 1.0 1.1 1.2 1.3 1.4 1.5 1.6 1.7 1.8

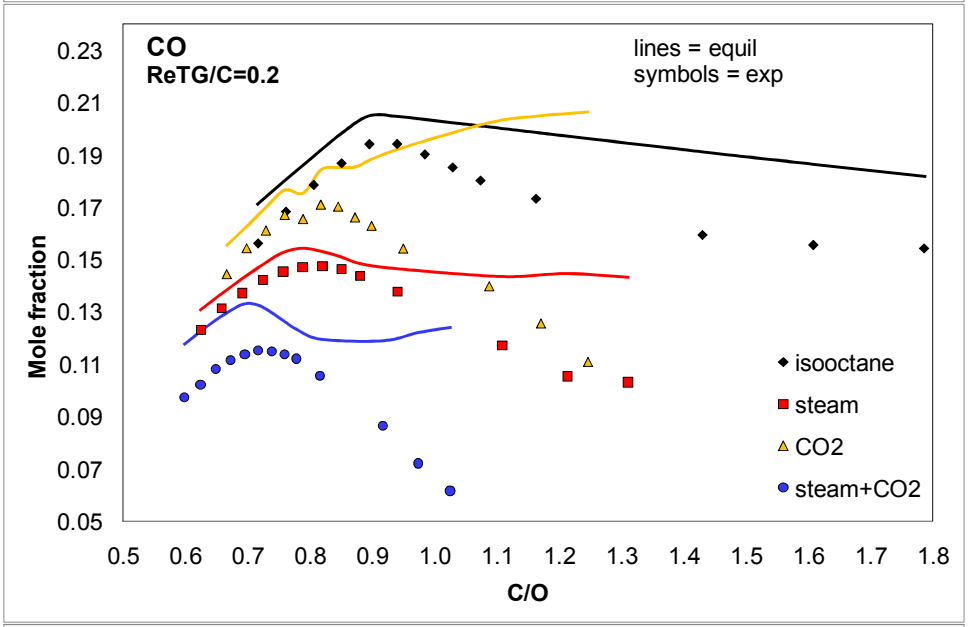
CO
ReTG/C=0.2
lines = equil
symbols = exp
isooctane
steam
CO2
steam+CO2
Mole fraction
C/O
0.23
0.21
0.19
0.17
0.15
0.13
0.11
0.09
0.07
0.05
0.5 0.6 0.7 0.8 0.9 1.0 1.1 1.2 1.3 1.4 1.5 1.6 1.7 1.8

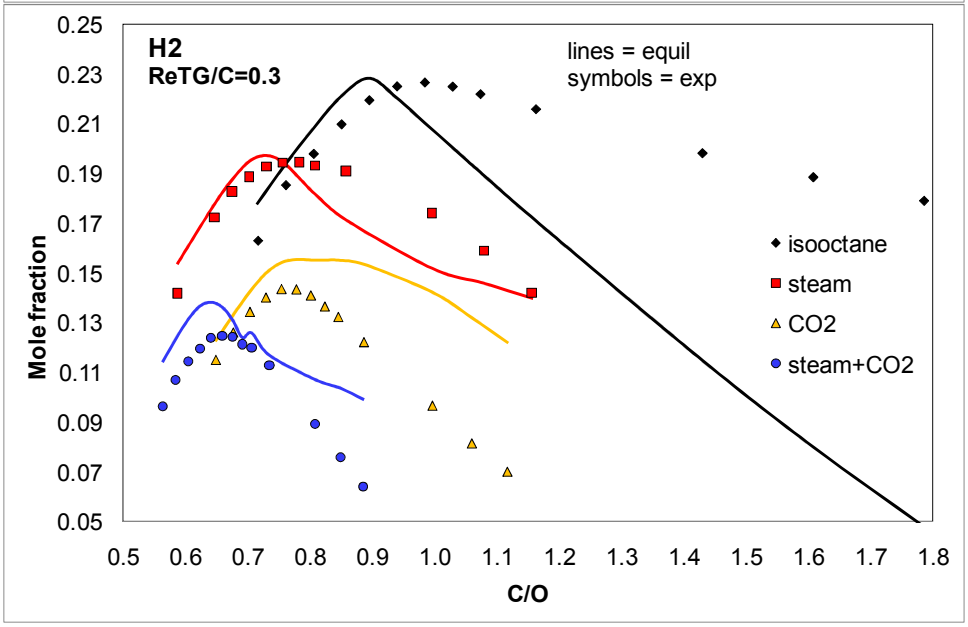
H2
ReTG/C=0.3
lines = equil
symbols = exp
isooctane
steam
CO2
steam+CO2
Mole fraction
C/O
0.25
0.23
0.21
0.19
0.17
0.15
0.13
0.11
0.09
0.07
0.05
0.5 0.6 0.7 0.8 0.9 1.0 1.1 1.2 1.3 1.4 1.5 1.6 1.7 1.8

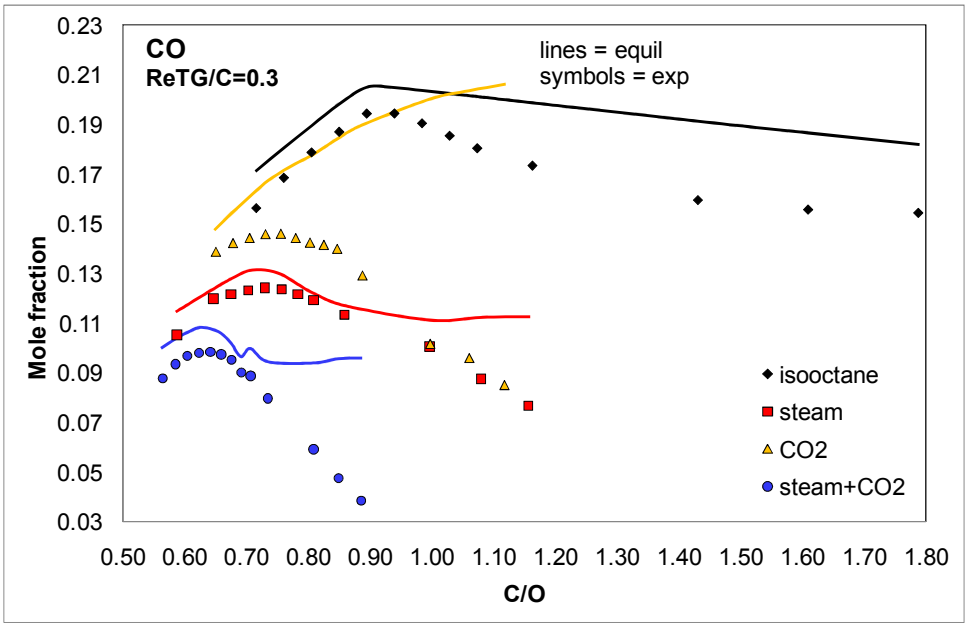

Figure 6-8: Mole fractions of H_2 and CO for case study 1-3 and the five different ReTG/C ratios. Full lines = calculated mole fractions at equilibrium for measured outlet temperatures, symbol = experiment.

The reference experiment (ReTG/C = 0) displays the largest amount of deposited C. CO_2 co-feed leads to less carbon deposition for all ReTG/C ratios and reveals a maximum at medium recycling rates. Steam and ReTG addition (cases 1 and 3) lead to clearly less carbon deposits on the catalyst and values are very similar for all ReTG/C ratios. Even though CO_2 co-feed still reduces the total amount of carbon deposited on the surface compared to the reference, however, significantly more deposits are formed. But these are still much less than without any co-feed. It is remarkable that even very small amounts of steam and/or CO_2 co-feed significantly reduce the formation of coke.

Due to a network of competing reactions both on the surface and in the gas-phase and their interaction with mass and heat transfer, a purely experimental study analyzing the exit feed only cannot satisfactorily explain the intrinsic processes leading to the product distribution observed. Also, it is not possible to eventually distinguish between chemical and thermal effects due to their strong coupling in CPOx reactors. The results discussed indicate that the reduction of olefin production is, at least to a certain extent, related to steam reforming and water-gas shift reactions, because the addition of steam and CO_2 has a strong impact on the rate and direction of these reactions. However, for all cases studied, a drop in reactor

temperature is observed due to tail-gas recycling, but the reactor temperature is still sufficiently high to thermally crack unconverted isooctane in the gas-phase, leading to the formation of olefins. At this point, investigations of spatially-resolved profiles over the reactor, both experimentally and numerically, are needed for a full understanding of the chemical and thermal effects on the formation of olefins and carbonaceous overlayers.

6.4 Summary and Conclusion for Study 2

The impact of H_2O and/or CO_2 addition to a reformer for oxidative conversion (CPOx) of isooctane over Rh/alumina-based honeycomb catalysts to hydrogen-rich synthesis gases was studied for five different amounts of H_2O, CO_2, and H_2O+CO_2 added over a broad range of C/O ratios. Feeding these tail-gas components to the reactor alters fuel conversion, product composition, reactor temperature, and coke formation rates. In case of simultaneous steam and CO_2 addition from all other cases, the formation of olefins differs quantitatively. Coking of the catalyst is reduced by tail-gas recycling. The co-feed influences the reactor performance mainly because of steam reforming and the forward and reverse WGS reaction in the fuel-lean area with C/O ratios of up to 0.9. Since all fuel is converted, reforming and WGS reactions are close to equilibrium as reaction temperature remains at a high value. Once unconverted fuel breaks through the monolithic catalyst, deviations from equilibrium are observed (**Figure 6-8**), and the appearance of smaller hydrocarbon species, such as ethylene and propylene, is noticeable even at low C/O. Nevertheless, the co-feed of either H_2O or CO_2 can significantly reduce the amount of soot precursors produced due to thermal cracking reactions. Tail-gas recycling in the studied CPOX reformer exhibits only small influence on the production of the major products hydrogen and carbon monoxide. Steam addition leads to a higher net hydrogen production over most of the C/O and S/C ratios studied. While simultaneous steam and carbon dioxide addition (recycling of the anode exhaust of a SOFC) is not beneficial to hydrogen production, it can reduce the formation of the soot precursors ethylene and propylene at higher C/O ratios. However, an increase in olefin production is observed at low C/O ratios. Integrating over all C/O ratios studied, the total amount of coke deposited is reduced with any addition of steam and/or CO_2.

The effects of steam addition and the effects of CO_2 addition do not allow extrapolation to the effects of both steam and CO_2 addition on the reactor behavior. The results shown reveal a complexity of interaction between surface and gas-phase kinetics as well as mass and heat transport that is difficult to understand by integral data. Spatially resolved species and temperature profiles are needed to eventually elucidate these interactions and explain the impact of chemical and thermal effects on product distribution of the reformer.

7 Catalytic Partial Oxidation of Diesel Fuel (Study 3)

The results presented show the first experimental investigations of diesel fuel CPOx with the introduced tube-in-tube configuration. The major challenge of diesel fuel CPOx or ATR is the defined evaporation of the fuel and homogeneous mixing with air without pre-ignition or carbon formation upstream of the catalyst (cf. Chapter 2.3). The reactor configuration works well for the investigated C/O ratios. However, when pacing concentration regimes close to total combustion, pre-ignition was sometimes observed. The ignition was initiated at the high surface temperature of the front-shield, where temperature exceeds the auto-ignition point. This is qualitatively shown in **Figure 7-1**. Tremendous coke depositions on the catalyst and in the filter, protecting the analytical set-up, were found and underline the statement for defined inlet conditions given by several authors working on diesel fuel reforming [7, 14]. But, for the C/O regimes that are of interest for CPOx operation, the same trends in diesel CPOx were observed as for isooctane and other single-component surrogate fuels. Therefore, the introduced reactor inlet configuration is suitable for the investigation of higher hydrocarbon fuels, such as diesel and kerosene, with respect to a more chemical investigation, because the inlet boundary conditions can be realized as for single component model surrogate fuels.

Figure 7-1: Flame propagation in a pre-igniting diesel fuel CPOx reformer. Inlet stream from right to left for a C/O < 0.7. The reactive diesel/air mixture ignites directly in front of the first heat-shield and propagates upstream up to the point where oxygen and diesel are mixed together. Pre-ignition leads to tremendous coke formation on the catalyst, and the exit temperature does not exceed 800°C (typically >950°C for lean conditions).

7.1 Accomplishment of Study 3

All experiments in Study 3 were carried out in a CPOx reactor with the catalyst configuration described in Chapter 4.3.2, without any further modification.

The annular slit at the nozzles tip is adjusted in width in a way that a 3 SLPM nitrogen carrier gas stream is only just pressed through the slit. Further narrowing of the slit would results in a decrease in the carrier gas flow rate. This was the optimum configuration for a homogeneous, nebulized diesel stream. Oxygen, remaining nitrogen and other gaseous components were provided to the outer tube. The complete inlet configuration was preheated to 523 K. The diesel fuel was not pre-heated before entering the nozzle to avoid thermal decomposition and evaporation of the low-boiling components. The feed gas stream was preheated to a temperature of 463 K before entering the inlet section, which was preheated further to 523 K. The furnace/catalyst section has been preheated up to a temperature of 673 K, helping the nebulized diesel stream to evaporate into the gaseous bulk phase directly upstream of the catalyst.

All experiments were performed with commercially-available diesel fuel. For the calculation of the C/O ratio, an assumed molecular formula of $C_{12}H_{22.4}O_{0.11}$ with a molecular weight M = 168.41 g/mol was used. The calculation is based on an elementary analysis revealing an average C, H, and O content of 85.6 wt%, 13.4 wt%, and 1 wt%, respectively. **Table 7-1** shows the calculated molar flow rates for all experiments accomplished.

Experiments with 80 % nitrogen dilution (case 1): The system was preheated to the temperatures given in the section above. C/O ratios have been calculated ranging from 0.6 – 0.9 for a total inlet flow of 4 SLPM with 80 vol% nitrogen dilution. In the beginning, all nitrogen inlet streams have been adjusted and were quantified with the method of internal standards. Next, the oxygen was mixed into the inlet stream. When oxygen was detected in the online analysis at the exit of the reactor, the diesel fuel flow rate was adjusted.

Two different measuring methods were used for the investigation of diesel fuel:

First, the continuous operation of the reformer was used, while the C/O ratio was varied between 0.6 and 0.9 with an increment of $\Delta = 0.05$ (in the following referred to as “continuous run”) without any carbon burn-off performed in-between the different

operating points. After a full run from C/O = 0.6 – 0.9, a carbon burn-off was performed to remove deposited carbon from the catalyst surface.

Second, each C/O ratio was measured independently with a carbon burn-off performed in-between each operating point (in the following referred to as “single step run”). Furthermore, the ignition of the reaction was initially performed at C/O = 0.75 to avoid a temperature overshoot during the first seconds of the reaction in case the fuel/oxygen mixing is not sufficient enough in this time window (except for the single-step runs, where the ignition was performed on the investigated C/O ratio).

Additionally to the continuous run, a second continuous run was performed with additional insulation of the catalyst inside the furnace. Therefore, the section (8 cm in length) of the quartz glass tube where the catalyst is located was surrounded with BC TEX fleece (HORST GmbH) with about 1.5 cm in thickness. The fleece is temperature stable up to 1000 °C. The total flow determination for each C/O operating point was also quantified with the method of internal standards.

Experiments with synthetic air mixture (case 2): The system was preheated to temperatures analogous to the 80% nitrogen dilution experiments. C/O ratios were calculated as ranging from 0.6 – 0.9 for an inlet flow of 4 SLPM synthetic air with a constant oxygen content of 20.9 vol%. According to this calculation, the total inlet flow varies between 4.08 – 4.12 SLPM, depending on the adjusted C/O ratio, as the fuel flow rate has to be added on top of the 4 SLPM syngas flow. This variance in the total flow rate, compared to the case 1 experiments in Study 3 as furthermore to the experiments in Study 2, is explained in that way, that the carrier flow rate for the two-substance nozzle was kept constant at 3 SLPM. Since a constant percentage of oxygen had to be present in the inlet mixture for the synthetic air mixture, the amount of nitrogen had to be reduced with increasing C/O ratio with an overall total inlet stream of 4 SLPM. In the given calculations, this would have meant a reduction of the nitrogen flow rate below 3 SLPM for C/O ratios > 0.7, and thus, an adaption of the two-substance nozzles slit. Therefore, the spray behavior of the nozzle a with 3 SLPM carrier flow rate has been found to be more important than the boundary condition of a 4 SLPM total flow rate.

At the beginning, all nitrogen inlet streams were adjusted and quantified with the method of internal standards. Next, the oxygen was mixed into the inlet stream. When oxygen was

detected in the online analysis at the exit of the reactor, the diesel fuel flow rate was adjusted.

In case 2, only the continuous run method was investigated with an additionally insulated catalyst (BC TEX fleece, cf. Chapter 7.1, case 1) inside the furnace. The total flow determination for each C/O operating point was also quantified with the method of internal standards.

Table 7-1: Inlet compositions given in mole fractions.

Experiments with 80 vol% nitrogen dilution							
C/O	0.6	0.65	0.7	0.75	0.8	0.85	0.9
x Diesel	0.018	0.020	0.021	0.022	0.024	0.025	0.026
x O_2	0.182	0.180	0.179	0.178	0.176	0.175	0.174
x N_2	0.800	0.800	0.800	0.800	0.800	0.800	0.800
Experiments with synthetic air mixture							
C/O	0.6	0.65	0.7	0.75	0.8	0.85	0.9
x Diesel	0.021	0.022	0.024	0.026	0.027	0.029	0.031
x O_2	0.205	0.204	0.204	0.204	0.203	0.203	0.203
x N_2	0.775	0.773	0.772	0.771	0.769	0.768	0.767

7.2 Results and Discussion

In the following, results for the two investigated cases 1 and 2 are presented. While, for case 2, an additionally insulated catalyst was always used, only in case 1 a distinction is made between an additionally-insulated (w/, indicated by dotted lines) and a not additionally-insulated (w/o, indicated by full lines) catalyst.

Table 7-2: Overview of experiments accomplished in case 1 and case 2.

Case 1	dilution	total flow rate
w/o additional insulation		
single-step run	80 vol% N_2	4 SLPM
continuous run	80 vol% N_2	4 SLPM
w/ additional insulation		
continuous run	80 vol% N_2	4 SLPM
Case 2		
w/ additional insulation		
continuous run	80 vol% N_2	4 SLPM
continuous run (AIR)	79.1 vol% N_2	4.08 SLPM

First, single-step runs for diesel fuel were performed, which are compared to a continuous run experiment to investigate the influence of the catalytic activity of the surface for fresh and used surface conditions as a function of the C/O ratio. In this case, fresh surface condition refers to the nature of the surface after a carbon burn-off was performed.

Afterwards, a continuous run with additionally-insulated catalyst was performed to reveal the temperature deviations compared to the non-insulated catalyst. These results are then compared to the results of the second case, in which diesel fuel was reformed under synthetic air conditions, as it is done likewise in the technical application, for instance in an APU. **Table 7-2** gives an overview of the experiments in case 1 and 2.

7.2.1 Experiments with 80 % Nitrogen Dilution – Case 1:

In **Figure 7-2**, the measured back-face temperature is shown for the single-step run (symbols) and for the continuous run (full lines). As is typical in CPOx reactions, temperature decreases with an increasing C/O ratio because there is less oxygen in the inlet stream and, therefore, less total oxidation in the initial high temperature oxidation zone of the catalyst [100, 124, 126]. But still, for a C/O ratio of 0.9, the temperature stays above 1200 K. With a temperature of about 1450 K at lean operating conditions (C/O = 0.6), the temperature reaches the structural integration limits of the cordierite structure of the monolith used. A further decrease in the C/O ratio would result in mechanical damage of the monolithic catalyst. Single-step runs show slightly higher temperatures for the C/O range of 0.6 – 0.7 than for the continuous run. This could be attributed to the fact that, for the continuous run, the ignition was performed at a C/O of 0.75 and, then, incrementally changed down to 0.6 (will be described later in more detail). Since, for a C/O of 0.75, no noticeable amounts of side products (except methane), such as olefinic hydrocarbons, were detected, no significant carbon layer deactivating the catalyst should have been formed on the surface. But since methane is detected for the entire fuel/oxygen range investigated, carbon depositions could arise from methane thermal decomposition.

Due to the way of driving the reactor described in 7.1, a carbon burn-off cannot provide quantitative information about carbon depositions on the catalyst, because diesel fuel is the first component taken out of the feed stream and oxygen is still available. Due to the still remaining high temperature, potential carbon depositions would burn-off within seconds after switching off the diesel fuel. In **Figure 7-3**, the process data measured for the C/O = 0.65 single-step run as function of time is shown. At the point where diesel fuel is switched off (t = 1100 s), infrequent temporal peaks in the back temperature are noticeable,

indicating the occurrence of an exothermal process. These peaks are accompanied by a temporal increase in CO_2 and a temporal consumption of O_2 (e.g., at t = 1270 S). This implies a combustion process and indicates that, even at lean C/O ratios, carbon depositions form on the catalyst during the reformation of commercial diesel fuel. Since carbon layers are formed on the catalytic surface in the fuel-lean operating regime, this could be an explanation for the decreased temperature measured in the continuous run compared to the single-step runs for a C/O of 0.6 – 0.7. Comparing the continuous run with the additionally-insulated continuous run (dotted line in **Figure 7-2**), the same trend in the temperature profile is noticeable. Only for C/O < 0.7, the profile does not increase with decreasing C/O. This effect could have the same explanation that was given for the discrepancies between single step and continuous run.

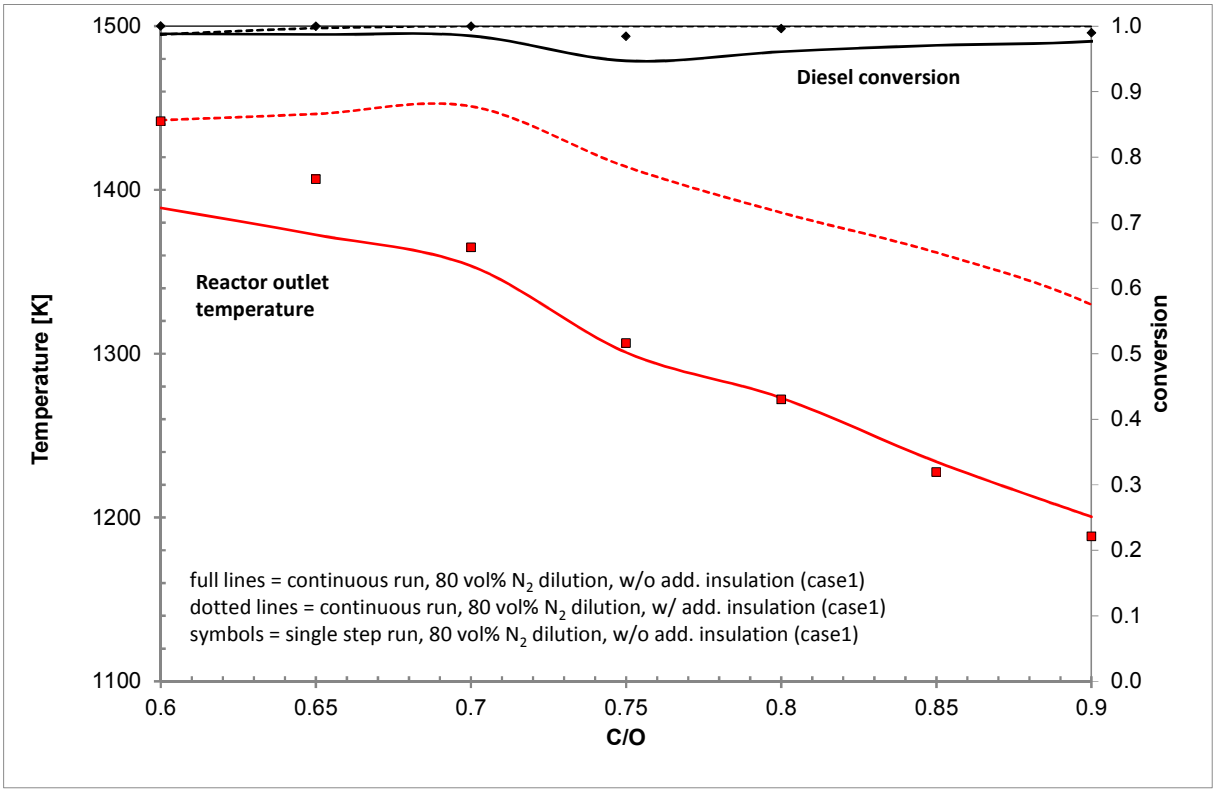

Figure 7-2: Diesel fuel conversion and reactor back-face temperature for case 1 over a C/O ranging from 0.6 – 0.9. Diesel conversion stays above 95% in all C/O operating conditions. Lines indicate the continuous-run operation (dotted lines with additional catalyst insulation), while symbols indicate single-step run results. In case of an additional insulation of the catalyst, the back-face temperature stays about 50 – 140K higher than without additional insulation and the conversion is almost complete over the entire regime.

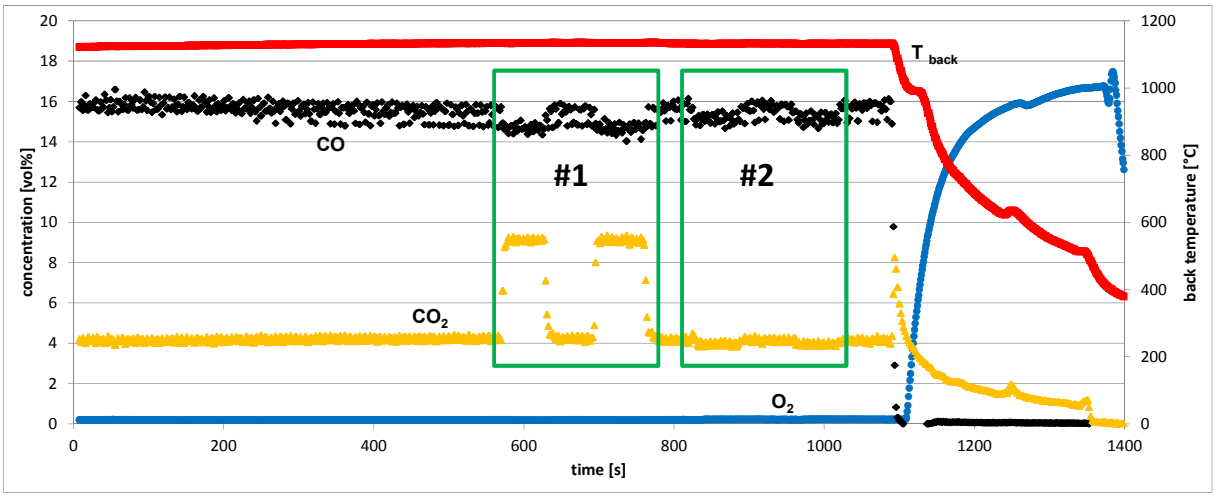

Figure 7-3: Measured process data in second time scale for the C/O = 0.65 single-step run of Study 1. Data acquisition started after the ignition procedure, only shutdown is shown (t > 1100 s). At the point where diesel fuel is shut off, T_{back} decreases and oxygen concentration increases. Noticeable local peaks in the profile of T_{back} indicate the occurrence of exothermal reactions, coming along with the production of CO_2 and the consumption of O_2 (t = 1270 s). #1: pulse sequence for CO_2 for total flow determination. #2: pulse sequence of H_2.

The ignition at C/O = 0.75 leads to carbon layers on the surface and, therefore, the performance of the catalyst is reduced, leading to a slightly more inefficient reforming behavior. Linear extrapolation of the temperature profile in the additional insulated case (dotted line) would result in temperatures above 1500 K and in mechanical damage of the catalyst. Nevertheless, for all cases, diesel conversion ranges between 95 – 99.9 %.

When paying attention to the main product distribution, typical trends that are known for CPOx of higher hydrocarbon fuels are observed [34]. The main products rise with increasing C/O ratio while total oxidation products decrease with increasing C/O (**Figure 7-5**, top), normally resulting in a local maximum for syngas production at a C/O of 1.0. In their diesel experiments, Krummenacher *et al.* [15] reported, that the maximum selectivities for syngas were achieved for a C/O = 0.35, which is quite close to the combustion ratio, and that they decrease with rising C/O. Due to the underlying chemistry, this behavior is quite abnormal. However, as they used a different technique for the fuel feeding, discrepancies could be explained by different reactor behavior in the entrance region. Thin-film evaporation with temperatures of up to 400 °C is used, leading to concentration gradients for low- and high-boiling components of the fuel inside the wall flow-field interface. Since olefinic species were

detected in their case even for a C/O of 0.4, the decrease in hydrogen selectivity could be attributed to the homogeneous gas-phase reactions occurring at these conditions at relatively high temperatures, which is extensively described in Study 1 of this work.

Nevertheless, it is apparent that, with about 70 – 90 %, the selectivity for CO is much higher than the selectivity for hydrogen, which is only about 40 – 80 %. This becomes obvious when attention is paid to the C/H ratio of the fuel. With a value of about $C/H_{diesel} = > 0.5$, the number of moles C compared to the number of moles H entering the reactor is nearly doubled. For comparison, isooctane as a reference fuel for gasoline has a $C/H_{isooctane}$ of 0.44, and methane a $C/H_{methane}$ of 0.25.

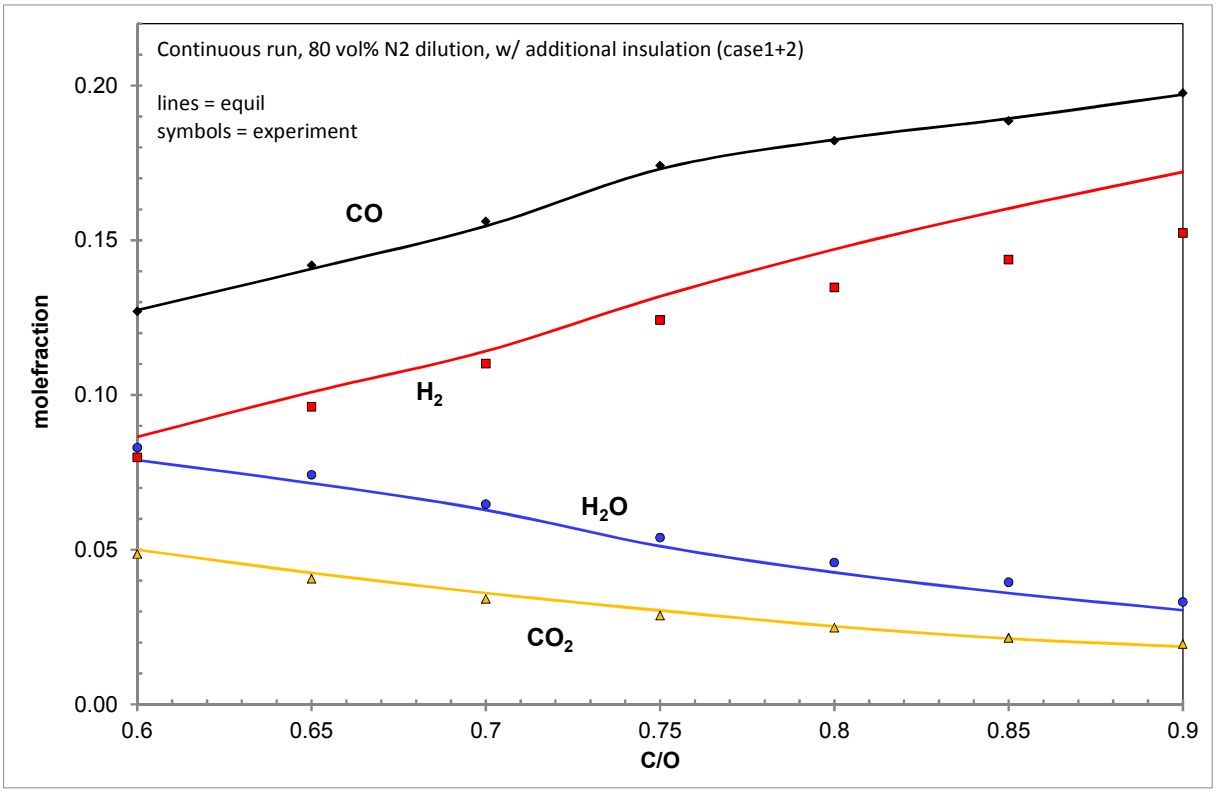

Figure 7-4: Mole fractions of H_2,H_2O, CO_2, and CO for case 1 with an additionally insulated catalyst. Full lines = calculated mole fractions at equilibrium for measured back-face temperatures, symbol = experiment.

Thermodynamic equilibrium data were calculated to get estimation on the main product distribution (Figure **7-4**). The calculations were performed for the continuous run with

80 vol% N_2 dilution with an additionally insulated catalyst using the DETCHEM^{TM} software code DETCHEM^{EQUIL} [109]. Molar flow rates of C, H, and O for each C/O ratio taken from the reactor exit composition were used for the calculations at the corresponding back-face temperature. The calculations show a good agreement with the experimental data, except for a decreasing molefraction in hydrogen with increasing C/O ratio.

Single-step and continuous-run experiments fit quite well in case of total oxidation product selectivities, only water is produced less in case 1 for a C/O > 0.75. Furthermore, for these operating conditions, higher selectivities in hydrogen, and in much slighter form for carbon monoxide, were achieved. Comparing the single step run results with the continuous run data, higher average selectivities are obtained for the main products H_2 and CO. In this case, a cleaned catalytic surface is more active towards reforming products although the temperature is quite similar. This effect becomes more obvious in the continuous run results for C/O ratios > 0.8. Desired reaction products start to decrease while total oxidation products rise again. At a point of C/O > 0.65, smaller hydrocarbons, such as ethylene and propylene, are formed and rise rapidly with increasing C/O ratio (**Figure 7-5**, bottom, continuous run w/o, full lines). At that point, diesel fuel breaks through the hot oxidation zone of the catalyst, underlies thermal decomposition, and is cracked down to these small hydrocarbons, as it could be shown in earlier works with isooctane as a model fuel surrogate [100]. Increasing the C/O ratio by $\Delta = 0.1$ up to 0.8, selectivities for C_2 and C_3 increase with exponential growth.

When the results for main and side products are compared to the continuous-run with additional catalyst insulation (w/, dotted lines in **Figure 7-2** and **Figure 7-5**), it is obvious that, over the entire investigated C/O regime, the selectivites are more stable with slightly smoothed profiles. Due to less thermal radiation loss inside the furnace, the measured temperature is about 50 to 140 K higher than that for the non-insulated catalyst results. Values for main and side products show similar trends compared to the continuous run but are also still below the single-step run results.

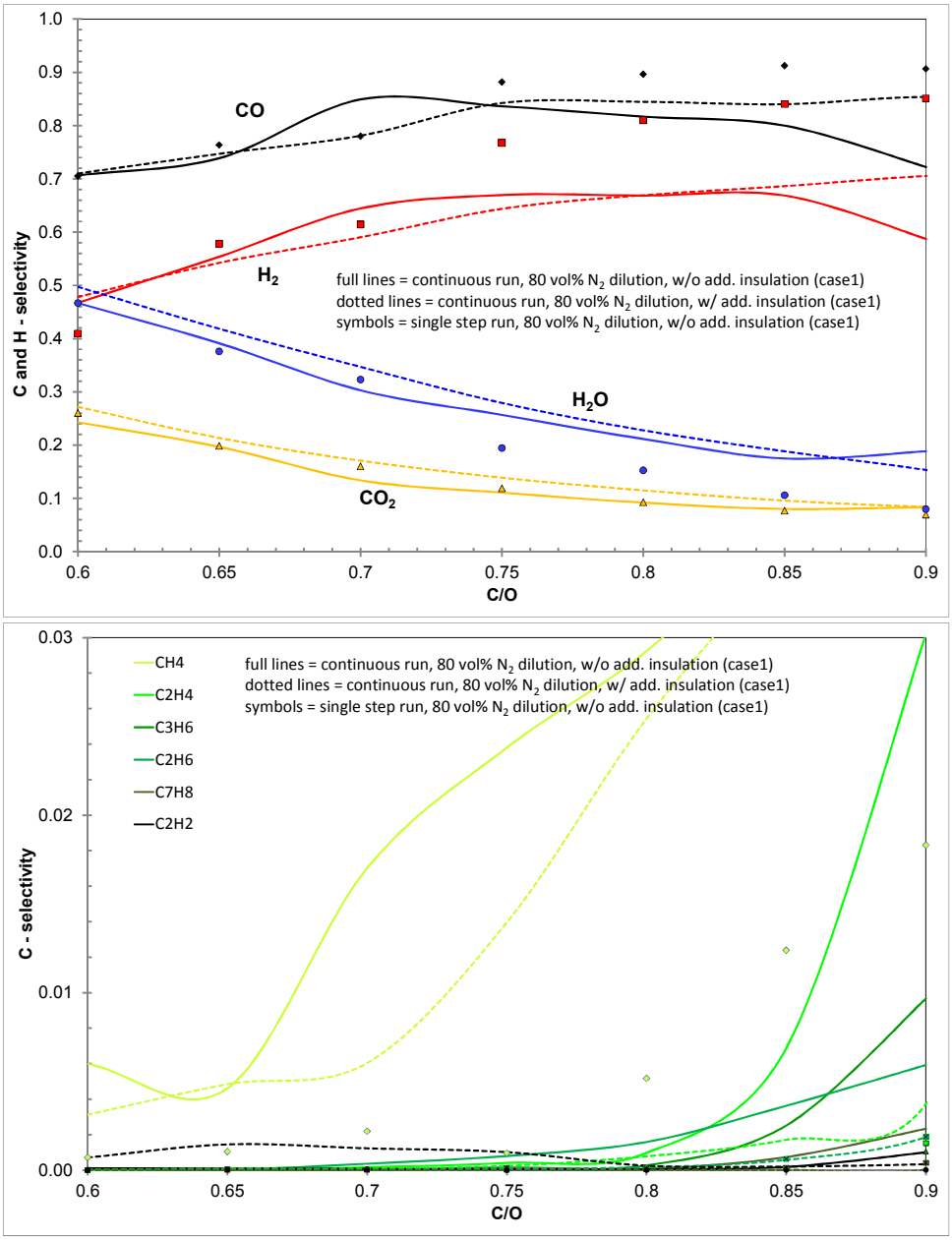

Figure 7-5: TOP: Main product distribution as function of the C/O ratio for Study 1 over a C/O ranging from 0.6 – 0.9. Trends are very similar for the single-step and continuous-run experiments (dotted lines with additional catalyst insulation). In case of an additional insulation of the catalyst, a more stable operation is noticeable regarding the production of syngas. Deviations from the single-step run experiments, especially for higher C/O ratios, could arise from the fact that, for the continuous runs, a carbon layer starts forming on the catalytic surface with increasing C/O, which slightly deactivates the catalytic activity. BOTTOM: Side product distribution as function of the C/O ratio for Study 1 over a C/O ranging from 0.6 – 0.9. Trends are very similar for the single-step and continuous-run experiments (dotted lines with additional catalyst insulation). In case of an additional insulation of the catalyst, side product formation is reduced. Since, for the single-step run experiments, even less C1 – C3 species were detected than for the continuous-run experiments, the actual condition state of the surface is imported for the interpretation of the measured results.

This indicates that a clean surface is more efficient in producing synthesis gas than the thermodynamically-favored higher temperature. Since both effects are strongly interlinked with each other, detailed numerical simulations have to be performed to validate this observation. Nevertheless, since diesel fuel is a mixture of several hundreds of hydrocarbon species, the complexity of the mixture makes it more difficult to find correct physical and thermodynamic data for detailed simulations.

Nonetheless, the higher temperature in the insulated catalyst case causes a shift of the point where smaller hydrocarbons are formed to higher C/O values. As described for the continuous run without further insulation, smaller hydrocarbons were formed starting at a C/O of 0.65. In the additionally-insulated catalyst case, smaller hydrocarbons are first formed at a C/O of about 0.8. When attention is now paid to temperature, both points, at which the formation of smaller hydrocarbon starts, correspond to a temperature of about 1400 K. This indicates an inefficient reforming zone in the catalytic channel, even for the high prevalent temperature. Again, an explanation can be given because of the high C/H_{diesel} ratio of 0.5. As less molar hydrogen enters the reactor that is oxidized within the initial hot oxidation zone of the catalyst to water, less molar water is available for the ongoing steam reforming directly following the hot oxidation zone and, therefore, more unconverted hydrocarbon species leave the catalyst channel. However, as temperature is still high enough, nearly all diesel fuel is cracked down and keeps the formally-calculated conversion at values above 95 %. So, even for a reformer operated in fuel-lean operation conditions, coke precursor products are detected and rise very quickly with increasing C/O ratio, when commercial diesel fuel is used. Therefore, coke depositions are expected even at $C/O < 0.85$, where only methane is detected in the reforming of isooctane. If diesel fuel is used in technical reformer applications, operation conditions have to be chosen carefully to prevent the formation of these small hydrocarbon species and, thus, the damager of coke depositions downstream of the catalyst. Fuel-lean C/O ratios (depending on the insulation effectiveness of the reformer itself) must be chosen for stable operation regarding long-term aspects. To validate these conclusions, a long-term run of 3 hours was performed at a C/O of 0.75 with additional insulation of the catalyst. No coke deposition could be found downstream the catalyst, even so, no significant deactivation of the catalyst was observed. Indeed, 3 hours of operation give no representative information on long-term stability for the technical application, but

within this time-scale important information with regard to chemical issues can be concluded.

Nevertheless, at these conditions, the hydrogen selectivity is less than 70 % and, therefore, the overall efficiency of, for instance, an APU is significantly decreased. Additional steam content in the inlet stream of the reformer could help improve the reforming behavior of the catalyst and further increase the hydrogen selectivity, as could be shown for isooctane operated with recycled tail-gas from an simulated SOFC exhaust gas [25].

7.2.2 Experiments with Synthetic Air Mixture – Case 2:

In the following, results are presented for a CPOx reformer operated with diesel fuel and a synthetic air mixture, consisting of 20.9 vol% O_2 and 79.1 vol% N_2, as it is performed in technical applications, such as the APU concept.

Figure 7-6 shows the comparison of the measured temperature and the conversion between the continuous run for an additionally insulated catalyst with 80 % N_2 dilution (dotted lines) and the continuous run with additionally insulated catalyst with the synthetic air mixture (symbols). For the synthetic air mixture experiment, the temperature profile looks quite similar to that for the 80 %-diluted experiments. Only a shift in the local temperature maximum from C/O = 0.7 to 0.8 is noticeable because of the higher oxygen content in the inlet stream. But still, for the higher oxygen content available, temperature stays at a maximum value of about 1450 K, even when the C/O ratio is decreased. This indicates a mass transport limitation of the oxygen molecules from the bulk gas-phase to the reactive wall [124].

In both cases, the diesel conversion stays at nearly 100 % for the entire C/O regime investigated. No data points were available for a C/O < 0.7 in case of the synthetic air mixture, which is due to pre-ignition of the diesel/oxygen mixture in the inlet upstream the catalyst. The fraction of oxygen reaches values, at which a flammable mixture of diesel and oxygen is generated. The ignition of this flammable mixture ignites directly upstream of the front shield, which is due to the hot surface of the alumina oxide foam arising from the

thermal radiation of the oxidation zone of the catalyst following directly afterwards. Since oxygen is mixed to the reactor in the outer tube of the inlet configuration (cf. **Figure 4-1**), the propagation of the flame stops immediately at the end of the inner tube, where oxygen and nebulized diesel get in contact for the first time.

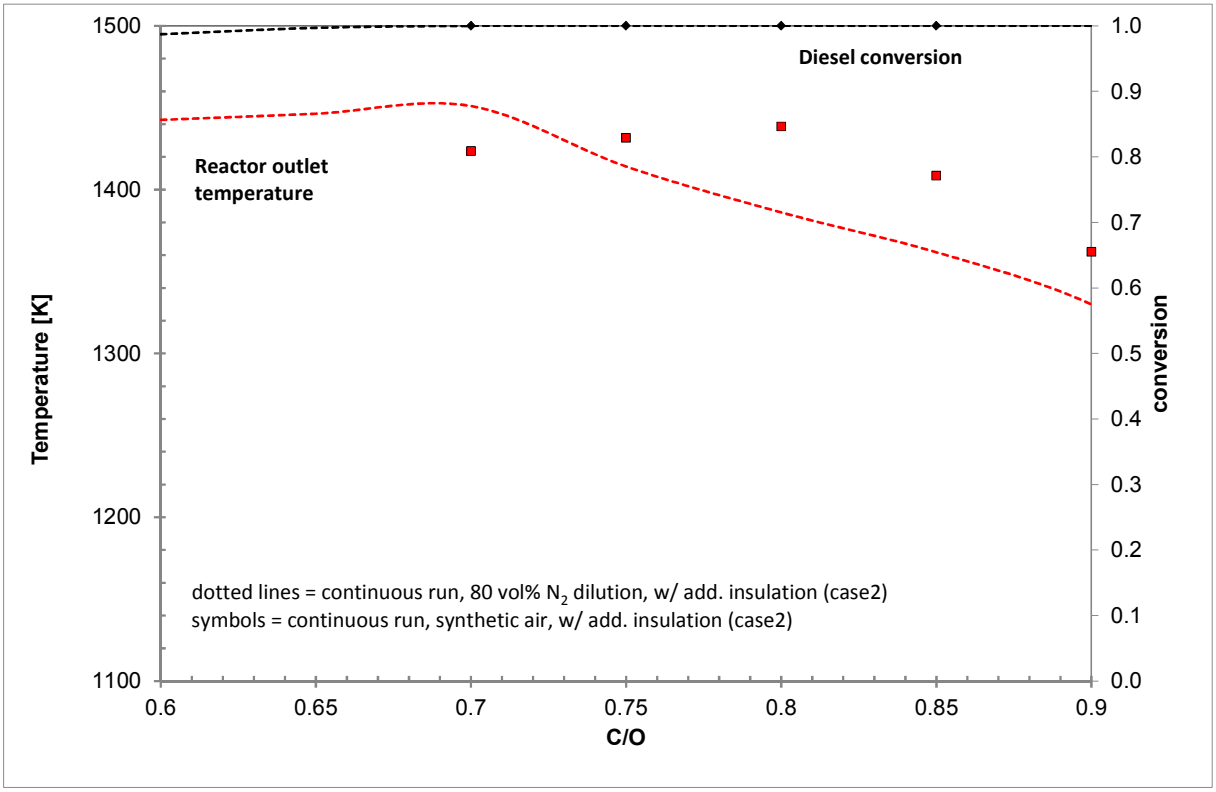

Figure 7-6: Comparison of the continuous run of Study 1 and Study 2 (both with additional insulation of the catalyst) of fuel conversion and back-face temperature. In both cases, full conversion is achieved over the entire C/O regime investigated (slight slope at C/O = 0.6 corresponds to less than 1.3 %, arising from the initial start-up at a C/O of 0.75 and then decreasing to 0.6). Back-face reactor temperatures show the same trend in profile, despite the decrease for Study 2, which is shifted slightly to higher C/O ratios. This is due to the higher oxygen content in the inlet stream. No data points were available for C/O < 0.7 in Study 2, as pre-combustion of the fuel started at that point. The oxygen content is too high, forming an incendive mixture that ignites directly in front of the alumina-oxide foam because of the thermal radiation of the catalyst.

Regarding main products (**Figure 7-7**, TOP), hydrogen and carbon monoxide selectivities are slightly increased (< 5 %) compared to the results of the experiment with 80 % dilution. For the total oxidation products steam and carbon dioxide, almost identical selectivities were

detected, despite the fact that there is more net oxygen available in the inlet stream (cf. **Table 7-1**) even for the same C/O ratio, arising from the higher oxygen content in the synthetic air mixture. Since temperatures and total oxidation products are quite similar and due to the slightly increased main products H_2 and CO, a more efficient reforming must occur. If this is the case, side products should be detected with less selectivities compared to case 1. And in-deed, **Figure 7-7** (bottom) reveals that only methane is detected over the entire C/O regime investigated, but is, analogous to the local maximum in temperature, shifted to higher C/O values. Short hydrocarbon species were first noticeably detected for a $C/O > 0.85$ (except acetylene, which is noticeably detected for $C/O > 0.8$, but with a selectivity still below 0.5 %).

To take up the results of case 1, a diesel fuel reformer used in a technical application has only a tight operating window available in terms of the C/O ratio. Downwards limitations are defined by the oxygen content in the inlet stream, which leads to pre-combustion and tremendous coke formation in the entire reformer. Upwards limitations exist due to the strong formation of coke precursors, even at fuel lean conditions.

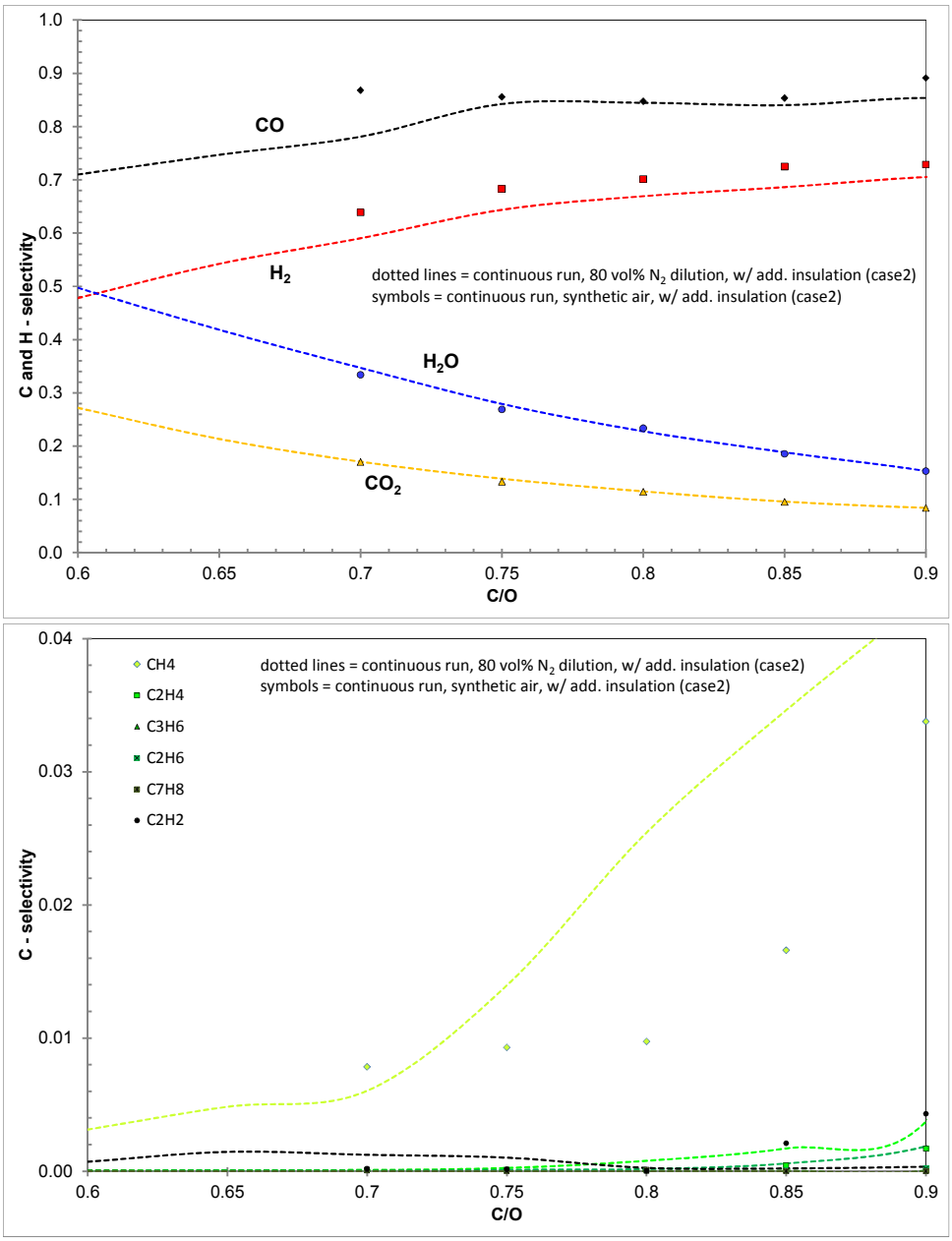

Figure 7-7: TOP: Comparison of the continuous run of Study 1 and Study 2 (both with additional insulation of the catalyst) with regard to main product distribution as function of the C/O ratio. Slightly higher selectivities in syngas production were detected in case of the synthetic air mixture. Total oxidation products stay at the same level as for the 80% nitrogen dilution case. BOTTOM: Comparison of the continuous run of study1 and Study 2 (both with additional insulation of the catalyst) with regard to side product distribution as function of the C/O ratio. Compared to Study 1 the higher oxygen content in Study 2 reduces the formation of smaller hydrocarbons. Significant reduction of CH_4 is observed.

7.3 Summary and Conclusions for Study 3

The investigation of commercial diesel fuel is presented in Chapter 7. For the realization of the discussed results, a new lab-scale reactor was established for the accurate handling of a commercially-available diesel fuel under defined boundary conditions. A two-substance nozzle setup delivers a pulse-free, nebulized diesel flow feed, guaranteeing reproducible reaction conditions. With the tube-in-tube configuration in the inlet section, the nebulized diesel feed stream is kept away from the reactor walls, resulting in a deposit-free operation upstream of the catalyst.

Two different cases were examined. First, experiments with an 80 % nitrogen dilution were performed for two different experimental methods. Single-step runs, in which a carbon burn-off was performed after each C/O operating point, are compared to a continuous run, in which a carbon burn-off was not carried out until the end of the entire C/O sequence. The results reveal that, for a freshly burned-off catalyst surface, higher selectivities towards the desired reaction products hydrogen and carbon monoxide are achieved because no carbon layer is present, arising from prior C/O operating points. Additional insulation of the catalyst inside the reactor furnace leads to higher reaction temperatures, shifted to higher values in C/O ratio, compared to the non-insulated case. However, the temperature that is achieved in both cases does not exceed a maximum value of about 1450 K.

The detection of higher selectivities for carbon monoxide than for hydrogen can be assigned to the higher value of C/H ratio for diesel fuel, which is about 0.5. The molar C input flow rate is higher compared to other hydrocarbon species, for instance, isooctane or methane. Since the molar H flow rate is small, less water is produced in the initial oxidation zone of the catalyst, and less water is provided for the reforming zone directly following in the catalytic channel. This, in turn, leads to an inefficient reforming behavior of the reactor and, even for fuel-lean operation conditions, significant amounts of coke precursors were detected. Increased insulation, leading to a higher reactor temperature, can demonstrably shift the occurrence of smaller hydrocarbon species toward higher C/O values.

Furthermore, the CPOx of diesel fuel with a synthetic air mixture was performed and reveals the same trends for main and side products as the 80 % nitrogen dilution case. Nevertheless, only for C/O ratios > 0.7, a stable operating reformer could be achieved, since for smaller

C/O ratios, pre-ignition of the diesel fuel/oxygen mixture takes place. However, in case of the synthetic air mixture, the higher oxygen content in the inlet stream shifts the appearance of coke precursors to C/O ratios > 0.85. Therefore, an operating window of a tight C/O range is revealed, which can be used in technical applications. Since C/O ratios which are too low lead to pre-combustion of the fuel/oxygen mixture, excessively high values accompany the formation of coke precursors with exponential growth for an increasing C/O ratio. To face these limitations and to widen the revealed operating window, the addition of steam might be a possibility. The added steam decreases the oxygen concentration in the inlet mixture, opening up the possibility for leaner fuel conditions. Furthermore, more steam in the reformer inlet improves the overall reforming efficiency, leading to higher selectivities in desired reaction products, as could be shown for other hydrocarbon species.

8 Summary and Overall Conclusions with Regard to the APU Concept

In this work, the catalytic partial oxidation was investigated for the production of hydrogen from a logistic fuel or fuel surrogate. Rhodium-containing monolithic honeycomb catalysts show excellent characteristics for the efficient conversion of a hydrocarbon species to hydrogen at millisecond contact times. Low pressure drop and high temperature stability of such monolithic catalysts enhance the development of fuel reformers for sufficient hydrogen production and make a more flexible engineering design possible. This allows the production of large quantities of hydrogen for the supply of stationary or, more particularly, in mobile fuel cell applications. Therefore, catalytic partial oxidation can pave the way for a more efficient utilization of the high energy content of a logistic fuel such as gasoline, diesel fuel, or kerosene. With the rising interest in fuel cell research during the last decades and the urgent calls for an alternative energy carrier in the near future, the production of hydrogen is brought more and more into focus of energy researchers.

The on-board generation of hydrogen for the direct usage in fuel cells is expected to be an efficient route for mobile electricity production. However, the conversion of a hydrocarbon fuel into hydrogen is challenging and there are certain problems deriving from both the physical and chemical properties of the fuel and the conversion process itself, especially when commercial logistic fuels are used as feedstock. The catalytic partial oxidation of a logistic fuel shows promising potential for a technical realization in APUs. However, most of the technical solutions reported in the literature have huge tendencies to the formation of carbon depositions in the fuel reformer and on the catalyst. Thus, mainly single component fuel surrogates are investigated by many researchers to gather a better understanding of the underlying chemistry of the conversion process and a better insight into the complex network structure of the chemical reactions involved, which is most challenging at high temperatures and dynamic reactor behavior.

In the first part, this work deals with the investigation of chemical processes occurring during the catalytic reforming of isooctane as a model fuel surrogate and focuses both on the understanding and identification of important chemical interactions and on their impact on a

technical operating reformer system. In the second part of this work, the investigation of a logistic diesel fuel from a more chemical point of view is the main intention. Therefore, a novel fuel-providing system was established, that allows accurate boundary conditions for fuel evaporation and mixing with further reactants for a detailed investigation of the complex chemistry networks that occur during the catalytic reforming of the fuel and to identify crucial boundary conditions for safe operation related to the underlying chemistry. Furthermore, the set-up can handle several types of fuel, either liquid or gaseous, under precise conditions with time-resolved monitoring of a broad variety of main and side products by different analytical methods. The generation of large datasets at short measuring-times helps to screen through a huge number of interesting chemical fuels and catalysts and provides experimental information for the development and validation of detailed reaction mechanisms and models. Computer-assisted control ensures the reproducibility at a high precision level, nearly eliminating careless mistakes, and allows the investigation of important reaction parameters such as feed composition and contact time with less effort.

For catalytic partial oxidation, the highest yields in hydrogen are obtained for a carbon to oxygen ratio close to unity. At this point, stoichiometric full conversion is achieved, only producing the desired reaction products hydrogen and carbon monoxide. In real operating systems, the conversion of the hydrocarbon feedstock is not completely achieved because of a lack of oxygen occurring from the partly total oxidation reaction. The presence of unconverted fuel downstream the initial total oxidation zone in the catalytic channel immediately leads to thermal cracking reactions and the build-up of a carbon layer downstream of the point at which all oxygen is consumed on the catalytic surface. The thermal cracking reactions lead to the formation of smaller radicals which cannot be quenched by the active sites due to carbon coverage, and gas-phase chemistry becomes important. These circumstances have been investigated with a simulated reformate gas mixture, typically in isooctane catalytic partial oxidation for selected fuel-rich conditions. At high temperatures, typically in oxidative operating reformers, the radicals undergo further degradation, mainly followed by β-hydrogen elimination, and thus, form unsaturated olefinic species, in particular C_2-C_4 olefines, which are determined by the constitution of the initial hydrocarbon molecule. These olefinic species were identified to form larger molecules such

as aromatic rings, leading to the formation of large polyaromatic molecules, and finally resulting in carbon depositions as a function of the reactor length or residence time. These formation progresses were identified, and two different zones of carbon depositions in the reactor were distinguished and reproduced with detailed numerical simulations. The first zone occurs initially at the reactor entrance, which derives from large amounts of short-chain olefins, the second one occurs more downstream due to the accumulation of large polyaromatic hydrocarbon species. Furthermore, at the reaction conditions present, hydrogen and parts of carbon monoxide are reduced in their yields due to hydrogenation, methanation, and gas-phase (reverse) water-gas shift chemistry as a function of the reactor temperature and, thus, decrease the reformer efficiency [7]. The results offer a minimum required temperature for initiating the cracking reactions and carbon formation for a given residence time. The results reveal that fuel breakthrough through the catalyst has to be avoided, as, otherwise, coke formation is inevitable. For the technical application, high demands are made on the engineering design as the identified coke formation is a function of temperature and residence time and, furthermore, coupled to the amount of hydrocarbon present in the effluent gas downstream of the catalyst. Therefore, short and straight interlink sections between the APU's components, with a sophisticated thermal management in-between, have to be realized, avoiding large recirculation zones and dead volume that lead to prolonged residence times and deductive carbon deposition. Fast quenching of the reformate can avoid gas-phase reactions but is not practicable due to minimum required temperatures of > 1000 K for SOFC operation. LT-SOFCs would be preferable due to operating temperatures of 600 °C. However, these are not available yet and PEMFCs have high demands on CO removal, which is contrary to compact and light-weight APU design. From a chemical point of view, water can be added to the reformer inlet to be steam reformed with the excessive hydrocarbon species in the gas-phase, and help to avoid carbon formation.

The flue gas of a high-temperature fuel cell or a thermal post-combustor mainly contains steam and carbon dioxide. In terms of steam availability and for improved thermal management, the flue gas of such devices is partly recycled to the reformer inlet for practical reasons. However, providing additional reactant species in the inlet stream results in a more complex reaction mixture and, as a consequence, in a more complex reaction network,

leading to a changed reactor behavior. The influence of the species water and carbon dioxide in the inlet stream of a CPOx reformer has been examined under defined boundary conditions in a broad variety of inlet concentrations, and the chemical interaction of each species differ. The results reveal that only water enhances the overall hydrogen production due to steam reforming, while carbon dioxide generally remains a diluent. Both interact with regard to the water-gas shift reactions but do not significantly affect the syngas composition, as it was already reported for the catalytic partial oxidation of methane. However, independently from the species added, the overall fuel conversion and the reactor temperature decrease as a function of the amount of recycled tail-gas and, thus, decrease the overall reformer efficiency, which is undesired in the practical application. With a lowered fuel conversion, larger amounts of unconverted fuel exit the catalytic channels and, according to the examined gas-phase reactions, tendencies towards thermal cracking reactions increase but are slightly hindered due to the lower reactor temperature. As could be proven in this work, this fact becomes more important when higher hydrocarbon fuels are used. Here, the reactor temperature shows two opposite trends: increased temperature would favor hydrogen production due to thermodynamics but also increase gas-phase reaction kinetics. The presence of larger amounts of methane in the reformate compared to the non-recycling case is attributed to methanation of carbon monoxide and carbon deposits formed on the catalytic surface after gasification due to the higher steam content. As already mentioned, LT SOFCs would be preferable due to lower operation temperature and, from a more practical point of view, because of less trouble with side products.

The recycling of a certain amount of tail-gas was found to be practical but strongly depends on the target operating conditions for the reformer. The easy control of reactor temperature by means of tail-gas recycling can be useful in the prevention of hot spots or accelerated gas-phase reactions and, in a certain way, contributes to the thermal integration with regard to the balance of plant. The reduction of the amount of smaller hydrocarbons, such as ethylene and propylene, which contribute to coke formation, can help protect the downstream parts following the reformer unit and improve long-term stability. Due to the ability of internal reforming into hydrogen, the increased methane content is only of less interest when HT fuel cells are supplied or can serve as fuel for the post-combustor. However, when recycling tail-gas, individual reactor behavior is assured due to the complex interaction of catalytic partial oxidation, total oxidation, steam reforming, and water-gas shift chemistry. The

occurrence of soot precursors is shifted dramatically towards leaner operating conditions and can lead to reformer failure, even at low C/O ratios. Medium recycling rates have shown the most efficient reduction of carbon depositions and must be defined with regard to decreasing fuel conversion and temperature drop for the highest reformer efficiency.

Increasing the complexity of the hydrocarbon feedstock towards a logistic fuel, technical challenges increase and engineering issues have to be given more attention than chemical ones. Typically for logistic fuels, the boiling point exceeds the auto-ignition point by far, leading to pre-combustion of the fuel which usually leads to reformer failure. However, the investigation of logistic fuels on a chemical basis is necessary as, due to non-additive reaction behavior of the single components with regard to the catalytic partial oxidation, the investigation of single or multi surrogate fuel mixtures can only provide an estimation of the suitability of a certain logistic fuel. The developed novel concept for fuel feeding for high-boiling liquids combined with the established tube-in-tube configuration for efficient mixing with the gaseous components allows the investigation of diesel fuel for desired C/O regimes in the catalytic partial oxidation. The set-up allows the defined chemical investigation with high accuracy and delivers comparable results and trends for single component fuels. In general, no pre-combustion was observed, except that flammable mixtures ignite at the front face of the catalyst due to extremely high temperatures, confirming that accurate fuel feeding is the key condition for a working and stable logistic-fuel reformer. A three hours run demonstrated the reliability of the concept without any failure under stable reaction conditions with no indication for residue formation in the feed mixing inlet section or the downstream part of the reactor tube.

Commercial diesel fuel was examined with regard to C/O ratio variation, influence of the catalyst temperature towards reforming performance, and the use of synthetic air. The results reveal that diesel fuel has a rather small operation C/O regime, limited either by pre-combustion on the fuel-lean side or by the formation of tremendous amounts of by-products and carbon deposits close to the stoichiometric point in C/O. Depending on the amount of oxygen available, methane is the only side product observed, followed rapidly by ethylene and propylene with increasing C/O. Cracking of methane could be identified to form carbon layers on the catalytic surface even for the lowest C/O ratios, influencing the conversion efficiency and lowering the yields of desired reaction products. For diesel CPOx,

temperatures close to the melting point of the honeycomb material were detected, implying precise reaction control or further heat management. In practical applications, the presented tail-gas recycling or the addition of steam can help to regulate the reactor temperature or to widen the operating regime and, therefore, improve the hydrogen yield, coming along with further advantages, such as additional increase in hydrogen yields and/or significant carbon deposition reduction.

From the point of view of this work, with regard to the APU concept using diesel fuel for mobile electricity production, the defined evaporation and accurate mixing of the fuel with the oxidizer is crucial for stable operation. Straight reactor geometries and designs are recommendable due to the elimination of recirculation and dead zones that increase the residence time, which is a significant parameter in coke formation. The presence of methane is non-critical due to internal reforming in SOFCs, but high temperatures are less favorable because of costly insulation materials and boosting gas-phase reactions when the fuel conversion is not complete. Low temperature solid oxide fuel cells would be preferable due to operation at a minimum temperature level required for thermal cracking at short residence times and the plain handling of methane and carbon monoxide without any pre-treatment. Furthermore, methane can serve as fuel for the post-combustor and the fuel cell's exhaust gas, producing heat, can be recuperated with regard to a sophisticated thermal management.

Additional feeding of steam or, if not directly available, recycling of tail-gas helps to adjust the reactor temperature while simultaneous reducing coke depositions. However, since the overall reactor behavior is defined by the overall heat and mass transport both inside the catalytic channel on a molecular level and in the reformer design on a more macroscopic scale, stepwise investigation of the catalytic partial oxidation is needed for a more detailed understanding. Combined with detailed numerical simulations including the geometric boundary conditions of the reformer design, these investigations can help to accelerate technical developments of such systems for a better integration into today's infrastructure and pave the way for the use of alternative energy carriers in the near future.

9 References

[1] A. Züttel, A. Borgschulte, L. Schlapbach, Hydrogen as a Future Energy Carrier, Wiley-VCH, Weinheim, 2008.

[2] B. Johnston, M.C. Mayo, A. Khare, Hydrogen: the energy source for the 21st century, Technovation, 25 (2005) 569-585.

[3] S. Dunn, Hydrogen Futures: Toward a Sustainable Energy System, in: J.A. Peterson (Ed.) WorlWatch Paper 157, WorldWatch Institute, Massachusetts, 2001.

[4] T.I. Sigfusson, Pathways to hydrogen as an energy carrier, Philos. Trans. R. Soc. A-Math. Phys. Eng. Sci., 365 (2007) 1025-1042.

[5] A. Borgschulte, A. Züttel, U. Wittstadt, Hydrogen Production, in: A. Züttel, A. Borgschulte, L. Schlapbach (Eds.) Hydrogen as a Future Energy Carrier, Wiley-VCH, Weinheim, 2008, pp. 149-164.

[6] T.K. Mandal, D.H. Gregory, Hydrogen: a future energy vector for sustainable development, Proc. Inst. Mech. Eng. Part C-J. Eng. Mech. Eng. Sci., 224 (2010) 539-558.

[7] B. Lindstrom, J.A.J. Karlsson, P. Ekdunge, L. De Verdier, B. Haggendal, J. Dawody, M. Nilsson, L.J. Pettersson, Diesel fuel reformer for automotive fuel cell applications, International Journal of Hydrogen Energy, 34 (2009) 3367-3381.

[8] R. Peters, Fuel Processors, in: H.K. G. Ertl, F. Schüth, J. Weitkamp (Ed.) Handbook of Heterogeneous Catalysis, Wiley-VCH, Weinheim, 2008, pp. 3045-3080.

[9] S. Ahmed, M. Krumpelt, Hydrogen from hydrocarbon fuels for fuel cells, International Journal of Hydrogen Energy, 26 (2001) 291-301.

[10] K. Föger, K. Ahmed, Fuel Cell Systems, in, 2005.

[11] D. Mogensen, J.D. Grunwaldt, P.V. Hendriksen, K. Dam-Johansen, J.U. Nielsen, Internal steam reforming in solid oxide fuel cells: Status and opportunities of kinetic studies and their impact on modelling, Journal of Power Sources, 196 (2011) 25-38.

[12] S. Yoon, J. Bae, A diesel fuel processor for stable operation of solid oxide fuel cells system: I. Introduction to post-reforming for the diesel fuel processor, Catalysis Today, 156 (2010) 49-57.

[13] H. Timmermann, W. Sawady, R. Reimert, E. Ivers-Tiffee, Kinetics of (reversible) internal reforming of methane in solid oxide fuel cells under stationary and APU conditions, Journal of Power Sources, 195 (2010) 214-222.

[14] K. Ahmed, K. Foger, Fuel Processing for High-Temperature High-Efficiency Fuel Cells, Industrial & Engineering Chemistry Research, 49 (2010) 7239-7256.

[15] J.J. Krummenacher, K.N. West, L.D. Schmidt, Catalytic partial oxidation of higher hydrocarbons at millisecond contact times: decane, hexadecane, and diesel fuel, Journal of Catalysis, 215 (2003) 332-343.

[16] M. Wei, Y.H. Wang, L. Reh, Experimental investigation of the prevaporized premixed (vpl) combustion process for liquid fuel lean combustion, Chemical Engineering and Processing, 41 (2002) 157-164.

[17] T. Aicher, L. Griesser, Novel process to evaporate liquid fuels and its application to the catalytic partial oxidation of diesel, Journal of Power Sources, 165 (2007) 210-216.

[18] C. Palm, P. Cremer, R. Peters, D. Stolten, Small-scale testing of a precious metal catalyst in the autothermal reforming of various hydrocarbon feeds, Journal of Power Sources, 106 (2002) 231-237.

[19] P.K. Cheekatamarla, A.M. Lane, Catalytic autothermal reforming of diesel fuel for hydrogen generation in fuel cells - I. Activity tests and sulfur poisoning, Journal of Power Sources, 152 (2005) 256-263.

[20] M. Sgroi, G. Bollito, G. Saracco, S. Specchia, BIOFEAT: Biodiesel fuel processor for a vehicle fuel cell auxiliary power unit - Study of the feed system, Journal of Power Sources, 149 (2005) 8-14.

[21] L. Hartmann, K. Lucka, H. Kohne, Mixture preparation by cool flames for diesel-reforming technologies, Journal of Power Sources, 118 (2003) 286-297.

[22] T. Aicher, B. Lenz, F. Gschnell, U. Groos, F. Federici, L. Caprile, L. Parodi, Fuel processors for fuel cell APU applications, Journal of Power Sources, 154 (2006) 503-508.

[23] J. Larminie, A. Dicks, Fuel Cell Systems Explained, Wiley VCH, England, 2001.

[24] A.D. Qi, B. Peppley, K. Karan, Integrated fuel processors for fuel cell application: A review, Fuel Process Technol, 88 (2007) 3-22.

[25] T. Kaltschmitt, C. Diehm, O. Deutschmann, Catalytic Partial Oxidation of Isooctane to Hydrogen on Rhodium Catalysts: Effect of Tail-Gas Recycling, Industrial & Engineering Chemistry Research, 51 (2012) 7536-7546.

[26] http://www.vda.de/de/meldungen/archiv/2006/12/15/1470/.

[27] F. Birkhold, Selektive katalytische Reduktion von Stickoxiden in Kraftfahrzeugen: Untersuchung der Einspritzung von Harnstofflösung, Doctoral thesis, Fakultät für Chemie und Biowissenschaften, Universität Karlsruhe (TH), 2007.

[28] A. Tsolakis, R. Torbati, A. Megaritis, A. Abu-Jrai, Low-Load Dual-Fuel Compression Ignition (CI) Engine Operation with an On-Board Reformer and a Diesel Oxidation Catalyst: Effects on Engine Performance and Emissions, Energ Fuel, 24 (2010) 302-308.

[29] A. Tsolakis, A. Megaritis, Partially premixed charge compression ignition engine with on-board H_2 production by exhaust gas fuel reforming of diesel and biodiesel, International Journal of Hydrogen Energy, 30 (2005) 731-745.

[30] J.J. Chong, A. Tsolakis, S.S. Gill, K. Theinnoi, S.E. Golunski, Enhancing the NO_2/NO_x ratio in compression ignition engines by hydrogen and reformate combustion, for improved aftertreatment performance, International Journal of Hydrogen Energy, 35 (2010) 8723-8732.

[31] Y.S. Seo, A. Shirley, S.T. Kolaczkowski, Evaluation of thermodynamically favourable operating conditions for production of hydrogen in three different reforming technologies, Journal of Power Sources, 108 (2002) 213-225.

[32] G.J. Panuccio, B.J. Dreyer, L.D. Schmidt, A comparison of the catalytic partial oxidation of C-1 to C-16 normal paraffins, Aiche J, 53 (2007) 187-195.

[33] A. Tsolakis, A. Megaritis, Catalytic exhaust gas fuel reforming for diesel engines—effects of water addition on hydrogen production and fuel conversion efficiency, International Journal of Hydrogen Energy, 29 (2004) 1409-1419.

[34] M. Hartmann, T. Kaltschmitt, O. Deutschmann, Catalytic partial oxidation of higher hydrocarbon fuel components on Rh/Al_2O_3 coated honeycomb monoliths, Catalysis Today, 147 (2009) S204-S209.

[35] C.E. Thomas, B.D. James, F.D. Lomax, I.F. Kuhn, Fuel options for the fuel cell vehicle: hydrogen, methanol or gasoline?, International Journal of Hydrogen Energy, 25 (2000) 551-567.

[36] T. Kaltschmitt, M. Hartmann, C. Diehm, O. Deutschmann, Catalytic Partial Oxidation of Iso-Octane on Rh Catalysts: Effect of Tail Gas Recycling on Hydrogen Yield, 21st International Symposium on Chemical Reaction Engineering, Philadelphia, PA, USA, 2010.

[37] J. Lawrence, M. Boltze, Auxiliary power unit based on a solid oxide fuel cell and fuelled with diesel, Journal of Power Sources, 154 (2006) 479-488.

[38] V.M. Janardhanan, O. Deutschmann, CFD analysis of a solid oxide fuel cell with internal reforming: Coupled interactions of transport, heterogeneous catalysis and electrochemical processes, Journal of Power Sources, 162 (2006) 1192-1202.

[39] V.M. Janardhanan, V. Heuveline, O. Deutschmann, Performance analysis of a SOFC under direct internal reforming conditions, Journal of Power Sources, 172 (2007) 296-307.

[40] D.A. Hickman, L.D. Schmidt, Synthesis gas -formation by direct oxidation of methane over Pt monoliths, Journal of Catalysis, 138 (1992) 267-282.

[41] N. Burke, D. Trimm, Coke formation during high pressure catalytic partial oxidation of methane to syngas, Reaction Kinetics and Catalysis Letters, 84 (2005) 137-142.

[42] R. Schwiedernoch, S. Tischer, C. Correa, O. Deutschmann, Experimental and numerical study on the transient behavior of partial oxidation of methane in a catalytic monolith, Chem Eng Sci, 58 (2003) 633-642.

[43] C. Appel, J. Mantzaras, R. Schaeren, R. Bombach, A. Inauen, N. Tylli, M. Wolf, T. Griffin, D. Winkler, R. Carroni, Partial catalytic oxidation of methane to synthesis gas over rhodium: in situ

Raman experiments and detailed simulations, Proceedings of the Combustion Institute, 30 (2005) 2509-2517.

[44] A. Schneider, J. Mantzaras, R. Bombach, S. Schenker, N. Tylli, P. Jansohn, Laser induced fluorescence of formaldehyde and Raman measurements of major species during partial catalytic oxidation of methane with large H2O and CO2 dilution at pressures up to 10 bar, Proceedings of the Combustion Institute, 31 (2007) 1973-1981.

[45] R. Horn, N.J. Degenstein, K.A. Williams, L.D. Schmidt, Spatial and temporal profiles in millisecond partial oxidation processes, Catal. Lett., 110 (2006) 169-178.

[46] R. Schwiedernoch, S. Tischer, H.R. Volpp, O. Deutschmann, Towards a better understanding of transient processes in catalytic oxidation reactors, in: X. Bao, Y. Xu (Eds.) Stud Surf Sci Catal, Elsevier Science Bv, Amsterdam, 2004, pp. 511-516.

[47] K.A. Williams, R. Horn, L.D. Schmidt, Performance of mechanisms and reactor models for methane oxidation on Rh, Aiche J, 53 (2007) 2097-2113.

[48] M. Hartmann, S. Lichtenberg, N. Hebben, D. Zhang, O. Deutschmann, Experimental investigation of catalytic partial oxidation of model fuels under defined constraints, Chem-Ing-Tech, 81 (2009) 909-919.

[49] M. Hartmann, L. Maier, H.D. Minh, O. Deutschmann, Catalytic partial oxidation of iso-octane over rhodium catalysts: An experimental, modeling, and simulation study, Combust Flame, 157 (2010) 1771-1782.

[50] R. Horn, K.A. Williams, N.J. Degenstein, A. Bitsch-Larsen, D. Dalle Nogare, S.A. Tupy, L.D. Schmidt, Methane catalytic partial oxidation on autothermal Rh and Pt foam catalysts: Oxidation and reforming zones, transport effects, and approach to thermodynamic equilibrium, Journal of Catalysis, 249 (2007) 380-393.

[51] I. Tavazzi, A. Beretta, G. Groppi, A. Donazzi, M. Maestri, E. Tronconi, P. Forzatti, Catalytic partial oxidation of CH_4 and C_3H_8: experimental and modeling study of the dynamic and steady state behavior of a pilot-scale reformer, in: F.B. Noronha, M. Schmal, E.F. SousaAguiar (Eds.) Natural Gas Conversion Viii, Proceedings of the 8th Natural Gas Conversion Symposium, Elsevier Science Bv, Amsterdam, 2007, pp. 319-324.

[52] C. Cellier, D.L. Clef, C. Mateos-Pedrero, P. Ruiz, Influence of the co-feeding of CO, H2, CO2 or H2O in the partial oxidation of methane over Ni and Rh supported catalysts, Catalysis Today, 106 (2005) 47-51.

[53] A. Bitsch-Larsen, R. Horn, L.D. Schmidt, Catalytic partial oxidation of methane on rhodium and platinum: Spatial profiles at elevated pressure, Appl Catal A-Gen, 348 (2008) 165-172.

[54] S. Cimino, L. Lisi, G. Russo, R. Torbati, Effect of partial substitution of Rh catalysts with Pt or Pd during the partial oxidation of methane in the presence of sulphur, Catalysis Today, 154 (2010) 283-292.

[55] S. Cimino, R. Torbati, L. Lisi, G. Russo, Sulphur inhibition on the catalytic partial oxidation of methane over Rh-based monolith catalysts, Appl Catal A-Gen, 360 (2009) 43-49.

[56] R. Torbati, S. Cimino, L. Lisi, G. Russo, The Effect of Support on Sulphur Tolerance of Rh Based Catalysts for Methane Partial Oxidation, Catal. Lett., 127 (2009) 260-269.

[57] A.M. DeGroote, G.F. Froment, The role of coke formation in catalytic partial oxidation for synthesis gas production, Catalysis Today, 37 (1997) 309-329.

[58] B.J. Dreyer, I.C. Lee, J.J. Krummenacher, L.D. Schmidt, Autothermal steam reforming of higher hydrocarbons: n-Decane, n-hexadecane, and JP-8, Applied Catalysis A: General, 307 (2006) 184-194.

[59] T. Kaltschmitt, L. Maier, M. Hartmann, C. Hauck, O. Deutschmann, Influence of gas-phase reactions on catalytic reforming of isooctane, P Combust Inst, 33 (2011) 3177-3183.

[60] H. Timmermann, W. Sawady, D. Campbell, A. Weber, R. Reimert, E. Ivers-Tiffee, Coke formation and degradation in SOFC operation with a model reformate from liquid hydrocarbons, Journal of the Electrochemical Society, 155 (2008) B356-B359.

[61] A. Tarancon, Strategies for Lowering Solid Oxide Fuel Cells Operating Temperature, Energies, 2 (2009) 1130-1150.

[62] J.S. Lee, N.D. Quan, J.M. Hwang, S.D. Lee, H.G. Kim, H.J. Lee, H.S. Kim, Polymer Electrolyte Membranes for Fuel Cells, J. Ind. Eng. Chem., 12 (2006) 175-183.

[63] G. HOOGERS, Fuel Cell Technology Handbook (Book), Sci-Tech News, 57 (2003) 51.

[64] C. Cellier, B. Blangy, C. Mateos-Pedrero, P. Ruiz, Modification of catalytic performances due to the co-feeding of hydrogen or carbon dioxide in the partial oxidation of methane over a $NiO/\gamma\text{-}Al_2O_3$ catalyst, Catalysis Today, 112 (2006) 112-116.

[65] B.C. Michael, A. Donazzi, L.D. Schmidt, Effects of H_2O and CO_2 addition in catalytic partial oxidation of methane on Rh, Journal of Catalysis, 265 (2009) 117-129.

[66] R. Subramanian, G.J. Panuccio, J.J. Krummenacher, I.C. Lee, L.D. Schmidt, Catalytic partial oxidation of higher hydrocarbons: reactivities and selectivities of mixtures, Chem Eng Sci, 59 (2004) 5501-5507.

[67] J. Thormann, L. Maier, P. Pfeifer, U. Kunz, O. Deutschmann, K. Schubert, Steam reforming of hexadecane over a Rh/CeO_2 catalyst in microchannels: Experimental and numerical investigation, International Journal of Hydrogen Energy, 34 (2009) 5108-5120.

[68] J. Thormann, P. Pfeifer, U. Kunz, K. Schubert, Reforming of diesel fuel in a micro reactor, International Journal of Chemical Reactor Engineering, 6 (2008) P1.

[69] J. Thormann, P. Pfeifer, K. Schubert, U. Kunz, Reforming of diesel fuel in a micro reactor for APU systems, Chem Eng J, 135 (2008) S74-S81.

[70] M. Huff, P.M. Torniainen, D.A. Hickman, L.D. Schmidt, Partial Oxidation of CH_4, C_2H_6, and C_3H_8 on Monoliths at Short-Contact Times, in: Natural Gas Conversion Ii, 1994, pp. 315-320.

[71] A.G. Dietz, A.F. Carlsson, L.D. Schmidt, Partial oxidation of C-5 and C-6 alkanes over monolith catalysts at short contact times, Journal of Catalysis, 176 (1998) 459-473.

[72] G.J. Panuccio, K.A. Williams, L.D. Schmidt, Contributions of heterogeneous and homogeneous chemistry in the catalytic partial oxidation of octane isomers and mixtures on rhodium coated foams, Chem Eng Sci, 61 (2006) 4207-4219.

[73] R.P. O´Connor, E.J. Klein, L.D. Schmidt, High yields of synthesis gas by millisecond partial oxidation of higher hydrocarbons, Catal. Lett., 70 (2000) 99-107.

[74] R.P. O´Connor, L.D. Schmidt, Catalytic Partial Oxidation of Cyclohexane in a Single-Gauze Reactor, Journal of Catalysis, 191 (2000) 245-256.

[75] M. Hartmann, Erzeugung von Wasserstoff mittels katalytischer Partialoxidation höherer Kohlenwasserstoffe an Rhodium. Doctoral thesis. , Erzeugung von Wasserstoff mittels katalytischer Partialoxidation höherer Kohlenwasserstoffe an Rhodium. Doctoral thesis. Fakultät für Chemie und Biowissenschaften, Universität Karlsruhe (TH), 2009.

[76] C. Diehm, T. Kaltschmitt, O. Deutschman, Hydrogen production by partial oxidation of ethanol/gasoline blends over Rh/Al_2O_3, Catalysis Today, 197 (2012) 90-100.

[77] J.G. Speight, Fuels for Fuel Cells, in: D. Shekhawat, J. Spivey, D.A. Berry (Eds.) Fuel Cells: Technologies for Fuel Processing, Elsevier, Amsterdam, 2011, pp. 29-48.

[78] N. Mota, M.C. Alvarez-Galvan, J.A. Villoria, F. Rosa, J.L.G. Fierro, R.M. Navarro, Reforming of Diesel Fuel for Hydrogen Production over Catalysts Derived from $LaCo_{1-x}M_xO_3$ (M = Ru, Fe), Topics in Catalysis, 52 (2009) 1995-2000.

[79] B.J. Dreyer, I.C. Lee, J.J. Krummenacher, L.D. Schmidt, Autothermal steam reforming of higher hydrocarbons: n-decane, n-hexadecane, and JP-8, Appl Catal A-Gen, 307 (2006) 184-194.

[80] S. Tischer, Simulation katalytischer Monolithreaktoren unter Verwendung detaillierter Modelle für Chemie und Transport, Naturwissenschaftliche-Mathematische Gesamtfakultät, Ruprecht-Karls-Universität, Heidelberg, 2004.

[81] F. Schüth, Heterogene Katalyse. Schlüsseltechnologie der chemischen Industrie, Chemie in unserer Zeit, 40 (2006) 92-103.

[82] I. Chorkendorff, J.W. Niemantsverdriet, Concepts of Modern Catalysis and Kinetics, 2nd, Revised and Enlarged Edition, Wiley VCH Verlag GmbH & CoKGaA, 2007.

[83] J.W. Erisman, M.A. Sutton, J. Galloway, Z. Klimont, W. Winiwarter, How a century of ammonia synthesis changed the world, Nat. Geosci., 1 (2008) 636-639.

[84] W. Boll, Korrelation zwischen Umsatzverhalten und katalytischer Oberfläche von Dieseloxidationskatalysatoren unter Variation von Beladung und Alterungszustand, Fakultät für Chemie und Biowissenschaften, Karlsruhe Institute of Technology (KIT), Karlsruhe, 2011.

[85] O. Deutschmann, Interactions between transport and chemistry in catalytic reactors. Habilitationsschrift, Fakultät für Chemie, Ruprecht-Karls-Universität, Heidelberg, 2001.

[86] O. Deutschmann, Modeling and Simulation of Heterogeneous Catalytic Reactions: From the molecular process to the technical system, Wiley-VCH Weinheim, 2012.

[87] O. Deutschmann, in: H.K. G. Ertl, F. Schüth, J. Weitkamp (Ed.) Handbook of Heterogeneous Catalysis, Wiley-VCH, Weinheim, 2008, pp. 1811-1828.

[88] R.J. Kee, M.E. Coltrin, P. Glarborg, Chemically Reacting Flow, Wiley-Interscience, 2003.

[89] R. Kissel-Osterrieder, F. Behrendt, J. Warnatz, Detailed Modeling of the Oxidation of CO on Platinum: A Monte-Carlo Model, Proceedings of the Combustion Institute, 27 (1998) 2267-2274.

[90] R. Kissel-Osterrieder, F. Behrendt, J. Warnatz, Dynamic Monte Carlo simulations of catalytic surface reactions, Proceedings of the Combustion Institute, 28 (2000) 1323-1330.

[91] S. Volkening, J. Wintterlin, CO oxidation on Pt(111) - Scanning tunneling microscopy experiments and Monte Carlo simulations, Journal of Chemical Physics, 114 (2001) 6382-6395.

[92] M.E. Coltrin, R.J. Kee, F.M. Rupley, SURFACE CHEMKIN (Version 4.0): A Fortran Package for Analyzing Heterogeneous Chemical Kinetics at a Solid-Surface - Gas-Phase Interface, SAND91-8003B, Sandia National Laboratories, 1991.

[93] S.J. Lombardo, A.T. Bell, A Monte Carlo model for the simulation of temperature-programmed desorption spectra, Surface Science, 206 (1988) 101-123.

[94] F.M. Kuhn, Kinetische Monte Carlo Simulationen von Reaktionen auf geträgerten Nanopartikeln, Fakultät für Chemie und Biowissenschaften, Karsruhe Institut of Technology (KIT), Karlsruhe, 2011.

[95] L.W.H. Kunz, Entwicklung eines Computerprogramms zur kinetischen Monte Carlo Simulation von Oberflächenreaktionen auf Nanopartikeln. , Fakultät für Chemie und Biowissenschaften, Universität Karlsruhe (TH), Karlsruhe, 2006.

[96] L.W.H. Kunz, L. Maier, S. Tischer, O. Deutschman, Modeling the Rate of Heterogeneous Reactions, in: O. Deutschman (Ed.) Modeling of Heterogeneous Catalytic Reactions: From the molecular process to the technical system, Wiley-VCH, Weinheim, 2011.

[97] T. Kaltschmitt, M. Hartmann, O. Deutschmann, Hydorgen Production from commercial fuel by Catalytic Partial Oxidation on Rhodium, 122nd BASF International Summer Course, Ludwigshafen, Germany, 2011.

[98] T. Kaltschmitt, S. Lichtenberg, L. Maier, O. Deutschmann, Hydorgen Production from commercial fuel by Catalytic Partial Oxidation on Rhodium, 45th Jahrestreffen Deutscher Katalytiker, Weimar, Germany, 2012.

[99] T. Kaltschmitt, O. Deutschmann, Fuel Processing for Fuel Cells, in: K. Sundmacher (Ed.) Fuel Cell Engineering - Model-based Approaches for Analysis, Control and Optimization, Elsevier, 2012.

[100] T. Kaltschmitt, L. Maier, M. Hartmann, C. Hauck, O. Deutschmann, Influence of gas-phase reactions on catalytic reforming of isooctane, Proceedings of the Combustion Institute, 33 (2011) 3177-3183.

[101] A. Freund, G. Friedrich, C. Merten, G. Eigenberger, Pulsation-poor laboratory vaporiser for small liquid streams, Chem-Ing-Tech, 78 (2006) 577-580.

[102] R.M. Heck, S. Gulati, R.J. Farrauto, The application of monoliths for gas phase catalytic reactions, Chem Eng J, 82 (2001) 149-156.

[103] T. Giroux, S. Hwang, Y. Liu, W. Ruettinger, L. Shore, Monolithic structures as alternatives to particulate catalysts for the reforming of hydrocarbons for hydrogen generation, Applied Catalysis B: Environmental, 56 (2005) 95-110.

[104] G. Groppi, E. Tronconi, Honeycomb supports with high thermal conductivity for gas/solid chemical processes, Catalysis Today, 105 (2005) 297-304.

[105] G. Schwedt, Analytische Chemie, 2nd, reviesed Edition ed., Wiley-VCH, Weinheim, 2008.

[106] P.W. Atkins, Physikalische Chemie, 2nd ed., VCH Verlagsgesellschaft mbH, Weinheim, 1996.

[107] J. Hoffmann, Taschenbuch der Messtechnik, 3rd ed., Fachbuchverlag Leipzig, 1997.

[108] http://www.ms4.info/datenblaetter/hsense.pdf.

[109] O. Deutschmann, S. Tischer, S. Kleditzsch, V.M. Janardhanan, C. Correa, D. Chatterjee, N. Mladenov, H.D. Minh, DETCHEM^{TM} software package, www.detchem.com, 2008.

[110] O. Deutschmann, R. Schwiedernoch, L.I. Maier, D. Chatterjee, Natural gas conversion in monolithic catalysts: interaction of chemical reactions and transport phenomena, Studies in Surface Science and Catalysis, 136 (2001) 251-258.

[111] D.K. Zerkle, M.D. Allendorf, M. Wolf, O. Deutschmann, Understanding homogeneous and heterogeneous contributions to the platinum-catalyzed partial oxidation of ethane in a short-contact-time reactor, Journal of Catalysis, 196 (2000) 18-39.

[112] H.D. Minh, H.G. Bock, S. Tischer, O. Deutschmann, Optimization of two-dimensional flows with homogeneous and heterogeneously catalyzed gas-phase reactions, Aiche J, 54 (2008) 2432-2440.

[113] L.L. Raja, R.J. Kee, O. Deutschmann, J. Warnatz, L.D. Schmidt, A critical evaluation of Navier-Stokes, boundary-layer, and plug-flow models of the flow and chemistry in a catalytic-combustion monolith, Catalysis Today, 59 (2000) 47-60.

[114] H.J. Curran, P. Gaffuri, W.J. Pitz, C.K. Westbrook, A comprehensive modeling study of iso-octane oxidation, Combust Flame, 129 (2002) 253-280.

[115] http://www-cms.llnl.gov/combustion/combustion_home.html.

[116] P. Dagaut, G. Pengloan, A. Ristori, Oxidation, ignition and combustion of toluene: Experimental and detailed chemical kinetic modeling, Physical Chemistry Chemical Physics, 4 (2002) 1846-1854.

[117] J. Andrae, D. Johansson, P. Bjornbom, P. Risberg, G. Kalghatgi, Co-oxidation in the auto-ignition of primary reference fuels and n-heptane/toluene blends, Combust Flame, 140 (2005) 267-286.

[118] C.A. Mims, R. Mauti, A.M. Dean, K.D. Rose, Radical Chemistry in Methane Oxidative Coupling: Tracing of Ethylene Secondary Reactions with Computer Models and Isotopes, Journal of Physical Chemistry, 98 (1994) 13357-13372.

[119] K.M. Walters, A.M. Dean, H.Y. Zhu, R.J. Kee, Homogeneous kinetics and equilibrium predictions of coking propensity in the anode channels of direct oxidation solid-oxide fuel cells using dry natural gas, Journal of Power Sources, 123 (2003) 182-189.

[120] E. Ranzi, T. Faravelli, P. Gaffuri, A. Sogaro, A. D'Anna, A. Ciajolo, A wide-range modeling study of iso-octane oxidation, Combust Flame, 108 (1997) 24-42.

[121] P.A. Vlasov, J. Warnatz, Detailed kinetic modeling of soot formation in hydrocarbon pyrolysis behind shock waves, Proceedings of the Combustion Institute, 29 (2003) 2335-2341.

[122] P.S. Barbato, G. Landi, Partial Oxidation and CO_2-ATR of Methane over Rh/$LaMnO_3$ Honeycomb Catalysts, Catal. Lett., 137 (2010) 16-27.

[123] A. Donazzi, M. Maestri, A. Beretta, G. Groppi, E. Tronconi, P. Forzatti, Microkinetic analysis of CH_4 CPO tests with CO_2-diluted feed streams, Appl Catal A-Gen, 391 (2011) 350-359.

[124] L. Maier, M. Hartmann, S. Tischer, O. Deutschmann, Interaction of heterogeneous and homogeneous kinetics with mass and heat transfer in catalytic reforming of logistic fuels, Combust Flame, 158 (2011) 796-808.

[125] I. Tavazzi, M. Maestri, A. Beretta, G. Groppi, E. Tronconi, P. Forzatti, Steady-state and transient analysis of a CH_4-catalytic partial oxidation reformer, Aiche J, 52 (2006) 3234-3245.

[126] M. Hartmann, L. Maier, O. Deutschmann, Hydrogen production by catalytic partial oxidation of iso-octane at varying flow rate and fuel/oxygen ratio: From detailed kinetics to reactor behavior, Applied Catalysis A: General, 391 (2011) 144-152.

[127] N. Muradov, Emission-free fuel reformers for mobile and portable fuel cell applications, Journal of Power Sources, 118 (2003) 320-324.

[128] B. Lenz, T. Aicher, Catalytic autothermal reforming of Jet fuel, Journal of Power Sources, 149 (2005) 44-52.

[129] X.M. Liu, G.Q. Lu, Z.F. Yan, J. Beltramini, Recent advances in catalysts for methanol synthesis via hydrogenation of CO and CO_2, Industrial & Engineering Chemistry Research, 42 (2003) 6518-6530.

[130] X.K. Phan, H. Bakhtiary-Davijany, R. Myrstad, P. Pfeifer, H.J. Venvik, A. Holmen, Preparation and performance of Cu-based monoliths for methanol synthesis, Applied Catalysis A: General, 405 (2011) 1-7.

[131] S. Basri, S.K. Kamarudin, Process system engineering in direct methanol fuel cell, International Journal of Hydrogen Energy, 36 (2011) 6219-6236.

[132] Z. Zhu, D.K. Li, J. Liu, Y.J. Wei, S.H. Liu, Investigation on the regulated and unregulated emissions of a DME engine under different injection timing, Appl Therm Eng, 35 (2012) 9-14.

[133] S.H. Yoon, J.P. Cha, C.S. Lee, An investigation of the effects of spray angle and injection strategy on dimethyl ether (DME) combustion and exhaust emission characteristics in a common-rail diesel engine, Fuel Process Technol, 91 (2010) 1364-1372.

[134] P. Courty, P. Chaumette, C. Raimbault, P. Travers, Production of Methanol-Higher Alcohol Mixtures from Natural-Gas Via Syngas Chemistry, Rev I Fr Petrol, 45 (1990) 561-578.

[135] M. Gupta, M.L. Smith, J.J. Spivey, Heterogeneous Catalytic Conversion of Dry Syngas to Ethanol and Higher Alcohols on Cu-Based Catalysts, Acs Catalysis, 1 (2011) 641-656.

[136] J.J. Spivey, A. Egbebi, Heterogeneous catalytic synthesis of ethanol from biomass-derived syngas, Chemical Society Reviews, 36 (2007) 1514-1528.

[137] V. Subramani, S.K. Gangwal, A review of recent literature to search for an efficient catalytic process for the conversion of syngas to ethanol, Energ Fuel, 22 (2008) 814-839.

[138] W.N. Zhang, Automotive fuels from biomass via gasification, Fuel Process Technol, 91 (2010) 866-876.

[139] A.R. Knight, A. Verma, Measurement of Odorant Levels in Natural Gas, Product R&D, 15 (1976) 59-63.

[140] G. Alptekin, S. DeVoss, M. Dubovik, J. Monroe, R. Amalfitano, G. Israelson, Regenerable sorbent for natural gas desulfurization, J Mater Eng Perform, 15 (2006) 433-438.

[141] P.J. de Wild, R.G. Nyqvist, F.A. de Bruijn, E.R. Stobbe, Removal of sulphur-containing odorants from fuel gases for fuel cell-based combined heat and power applications, Journal of Power Sources, 159 (2006) 995-1004.

[142] S. Chunshan, An overview of new approaches to deep desulfurization for ultra-clean gasoline, diesel fuel and jet fuel, Catalysis Today, 86 (2003) 211-263.

[143] S. Hernandeza, L. Solarino, G. Orsello, N. Russo, D. Fino, G. Saracco, V. Specchia, Desulfurization processes for fuel cells systems, International Journal of Hydrogen Energy, 33 (2008) 3209-3214.

[144] O. van Rheinberg, K. Lucka, H. Kohne, About the process improvement of adsorptive desulphurisation by adding hydrogen donators as additives in liquid fuels, Journal of Power Sources, 196 (2011) 8983-8993.

[145] G. Kolb, Fuel Porcessing for Fuel Cells, WILEY-VCH, Weinheim, 2008.

[146] S.K. Gangwal, Desulfurization for Fuel Cells, in: D. Shekhawat, J. Spivey, D.A. Berry (Eds.) Fuel Cells: Technologies for Fuel Processing, Elsevier, Amsterdam, 2011, pp. 317-360.

[147] B. Guichard, M. Roy-Auberger, E. Devers, C. Pichon, C. Legens, P. Lecour, Influence of the promoter's nature (nickel or cobalt) on the active phases 'Ni(Co)MoS' modifications during deactivation in HDS of diesel fuel, Catalysis Today, 149 (2010) 2-10.

[148] S.A. Hanafi, M.S. Mohamed, Recent Trends in the Cleaning of Diesel Fuels via Desulfurization Processes, Energ Source Part A, 33 (2011) 495-511.

[149] R.L. Borup, M.A. Inbody, T.A. Semelsberger, J.I. Tafoya, D.R. Guidry, Fuel composition effects on transportation fuel cell reforming, Catalysis Today, 99 (2005) 263-270.

[150] N. Muradov, K. Ramasamy, C. Linkous, C.P. Huang, I. Adebiyi, F. Smith, A. T-Raissi, J. Stevens, Combined pre-reforming-desulfurization of high-sulfur fuels for distributed hydrogen applications, Fuel, 89 (2010) 1221-1229.

[151] J.R. Rostrup-Nielsen, Catalytic Steam Reforming, in: J.R. Anderson, M. Boudart (Eds.) Catalysis Science and Technology, Springer-Verlag, New York, 1984.

[152] Q. Zhuang, Y. Qin*, L. Chang, Promoting effect of cerium oxide in supported nickel catalyst for hydrocarbon steam-reforming, Applied Catalysis, 70 (1991) 1-8.

[153] D.L. Trimm, Catalysts for the control of coking during steam reforming, Catalysis Today, 49 (1999) 3-10.

[154] B. Schädel, Wasserdampfreformierung von Erdgas mit Rhodiumkatalysatoren: Aktivität und Deaktivierung. Doctoral thesis., Department of Chemistry and Biosciences, University of Karlsruhe, Karlsruhe, 2008.

[155] J.R. Rostrup-Nielsen, Sulfur-passivated nickel catalysts for carbon-free steam reforming of methane, Journal of Catalysis, 85 (1984) 31-43.

[156] J.R. Rostrup-Nielsen, Catalysis and large-scale conversion of natural gas, Catalysis Today, 21 (1994) 257-267.

[157] D.L. Trimm, Coke formation and minimisation during steam reforming reactions, Catalysis Today, 37 (1997) 233-238.

[158] S. Sa, H. Silva, L. Brandao, J.M. Sousa, A. Mendes, Catalysts for methanol steam reforming-A review, Appl Catal B-Environ, 99 (2010) 43-57.

[159] A. Birot, F. Epron, C. Descorme, D. Duprez, Ethanol steam reforming over $Rh/Ce_xZr_{1-x}O_2$ catalysts: Impact of the $CO\text{-}CO_2\text{-}CH_4$ interconversion reactions on the H_2 production, Appl Catal B-Environ, 79 (2008) 17-25.

[160] M. Ni, D.Y.C. Leung, M.K.H. Leung, A review on reforming bio-ethanol for hydrogen production, International Journal of Hydrogen Energy, 32 (2007) 3238-3247.

[161] N. Laosiripojana, S. Assabumrungrat, Catalytic steam reforming of ethanol over high surface area CeO_2: The role of CeO_2 as an internal pre-reforming catalyst, Appl Catal B-Environ, 66 (2006) 29-39.

[162] E.C. Wanat, K. Venkataraman, L.D. Schmidt, Steam reforming and water-gas shift of ethanol on Rh and Rh-Ce catalysts in a catalytic wall reactor, Appl Catal A-Gen, 276 (2004) 155-162.

[163] S. Cavallaro, Ethanol steam reforming on Rh/Al_2O_3 catalysts, Energ Fuel, 14 (2000) 1195-1199.

[164] I. Fishtik, A. Alexander, R. Datta, D. Geana, A thermodynamic analysis of hydrogen production by steam reforming of ethanol via response reactions, International Journal of Hydrogen Energy, 25 (2000) 31-45.

[165] B.C. Enger, R. Lodeng, A. Holmen, A review of catalytic partial oxidation of methane to synthesis gas with emphasis on reaction mechanisms over transition metal catalysts, Appl Catal A-Gen, 346 (2008) 1-27.

[166] O. Deutschmann, L.D. Schmidt, Modeling the partial oxidation of methane in a short-contact-time reactor, American Institute of Chemical Engineering Journal, 44 (1998) 2465-2477.

[167] O. Deutschmann, L.D. Schmidt, Two-Dimensional Modeling of Partial Oxidation of Methane on Rhodium in a Short Contact Time Reactor, Proc. Combust. Inst., Pittsburgh, 1998, pp. 2283-2291.

[168] R. Horn, K.A. Williams, N.J. Degenstein, A. Bitsch-Larsen, D.D. Nogare, S.A. Tupy, L.D. Schmidt, Methane catalytic partial oxidation on autothermal Rh and Pt foam catalysts: Oxidation and reforming zones, transport effects, and approach to thermodynamic equilibrium, Journal of Catalysis, 249 (2007) 380-393.

[169] R. Horn, K.A. Williams, N.J. Degenstein, L.D. Schmidt, Syngas by catalytic partial oxidation of methane on rhodium: Mechanistic conclusions from spatially resolved measurements and numerical simulations, Journal of Catalysis, 242 (2006) 92-102.

[170] A. Beretta, G. Groppi, M. Lualdi, I. Tavazzi, P. Forzatti, Experimental and Modeling Analysis of Methane Partial Oxidation: Transient and Steady-State Behavior of Rh-Coated Honeycomb Monoliths, Industrial & Engineering Chemistry Research, 48 (2009) 3825-3836.

[171] A. Donazzi, A. Beretta, G. Groppi, P. Forzatti, Catalytic partial oxidation of methane over a 4% Rh/α-Al_2O_3 catalyst: Part I: Kinetic study in annular reactor, Journal of Catalysis, 255 (2008) 241-258.

[172] C.L. Li, Y.C. Lin, Catalytic Partial Oxidation of Methanol over Copper-Zinc Based Catalysts: A Comparative Study of Alumina, Zirconia, and Magnesia as Promoters, Catal. Lett., 140 (2010) 69-76.

[173] N. Hebben, C. Diehm, O. Deutschmann, Catalytic partial oxidation of ethanol on alumina-supported rhodium catalysts: An experimental study, Appl Catal A-Gen, 388 (2010) 225-231.

[174] J.P. Kopasz, D. Applegate, L. Miller, H.K. Liao, S. Ahmed, Unraveling the maze: Understanding of diesel reforming through the use of simplified fuel blends, International Journal of Hydrogen Energy, 30 (2005) 1243-1250.

[175] D. Shekhawat, D.A. Berry, D.J. Haynes, J.J. Spivey, Fuel constituent effects on fuel reforming properties for fuel cell applications, Fuel, 88 (2009) 817-825.

[176] I. Kang, H.H. Carstensen, A.M. Dean, Impact of gas-phase reactions on SOFC systems operating on diesel and biomass-derived fuels, Thermec, Pts 1-4, 638-642 (2009) 1118-1124.

[177] A.M. Dean, S.M. Villano, J. Hoffmann, H.H. Carstensen, Selective Removal of Ethylene, a Deposit Precursor, from a "Dirty" Synthesis Gas Stream via Gas-Phase Partial Oxidation, J Phys Chem A, 114 (2010) 6502-6514.

[178] T.V. Choudhary, D.W. Goodman, Methane activation on Ni and Ru model catalysts, Journal of Molecular Catalysis A-Chemical, 163 (2000) 9-18.

[179] D. Haynes, D. Shekhawat, Oxidative Steam reforming, in: D. Shekhawat, J. Spivey, D.A. Berry (Eds.) Fuel Cells: Technologies for Fuel Processing, Elsevier, Amsterdam, 2011, pp. 129-190.

[180] C.-C. Chang, C.-T. Chang, S.-J. Chiang, B.-J. Liaw, Y.-Z. Chen, Oxidative steam reforming of methanol over $CuO/ZnO/CeO_2/ZrO_2/Al_2O_3$ catalysts, International Journal of Hydrogen Energy, 35 (2010) 7675-7683.

[181] O. Akdim, W.J. Cai, V. Fierro, H. Provendier, A. Van Veen, W.J. Shen, C. Mirodatos, Oxidative Steam Reforming of Ethanol over $Ni-Cu/SiO_2$, Rh/Al_2O_3 and Ir/CeO_2: Effect of Metal and Support on Reaction Mechanism, Topics in Catalysis, 51 (2008) 22-38.

[182] V. Fierro, O. Akdim, C. Mirodatos, On-board hydrogen production in a hybrid electric vehicle by bio-ethanol oxidative steam reforming over Ni and noble metal based catalysts, Green Chem, 5 (2003) 20-24.

[183] C. Ratnasamy, J.P. Wagner, Water Gas Shift Catalysis, Catalysis Reviews-Science and Engineering, 51 (2009) 325-440.

[184] K.-O. Hinrichsen, K. Kochloefl, M. Muhler, Water Gas Shift and COS Removal, in: H.K. G. Ertl, F. Schüth, J. Weitkamp (Ed.) Handbook of Heterogeneous Catalysis, Wiley-VCH, Weinheim, 2008, pp. 2905-2920.

[185] A.F. Ghenciu, Review of fuel processing catalysts for hydrogen production in PEM fuel cell systems, Curr Opin Solid St M, 6 (2002) 389-399.

[186] W. Ruettinger, X.S. Liu, R.J. Farrauto, Mechanism of aging for a Pt/CeO_2-ZrO_2 water gas shift catalyst, Appl Catal B-Environ, 65 (2006) 135-141.

[187] R.A. Dagle, A. Platon, D.R. Palo, A.K. Datye, J.M. Vohs, Y. Wang, PdZnAl catalysts for the reactions of water-gas-shift, methanol steam reforming, and reverse-water-gas-shift, Appl Catal A-Gen, 342 (2008) 63-68.

[188] F. Zane, V. Trevisan, F. Pinna, M. Signoretto, F. Menegazzo, Investigation on gold dispersion of Au/ZrO_2 catalysts and activity in the low-temperature WGS reaction, Appl Catal B-Environ, 89 (2009) 303-308.

[189] S.D. Senanayake, D. Stacchiola, P. Liu, C.B. Mullins, J. Hrbek, J.A. Rodriguez, Interaction of CO with OH on Au(111): HCOO, CO(3), and HOCO as Key Intermediates in the Water-Gas Shift Reaction, J Phys Chem C, 113 (2009) 19536-19544.

[190] N. Bion, F. Epron, M. Moreno, F. Marino, D. Duprez, Preferential Oxidation of Carbon Monoxide in the Presence of Hydrogen (PROX) over Noble Metals and Transition Metal Oxides: Advantages and Drawbacks, Topics in Catalysis, 51 (2008) 76-88.

[191] E.D. Park, D. Lee, H.C. Lee, Recent progress in selective CO removal in a H_2-rich stream, Catalysis Today, 139 (2009) 280-290.

[192] S.H. Oh, R.M. Sinkevitch, Carbon-Monoxide Removal from Hydrogen-Rich Fuel-Cell Feedstreams by Selective Catalytic-Oxidation, Journal of Catalysis, 142 (1993) 254-262.

[193] G. Avgouropoulos, T. Ioannides, Effect of synthesis parameters on catalytic properties of CuO-CeO_2, Appl Catal B-Environ, 67 (2006) 1-11.

[194] S. Takenaka, T. Shimizu, K. Otsuka, Complete removal of carbon monoxide in hydrogen-rich gas stream through methanation over supported metal catalysts, International Journal of Hydrogen Energy, 29 (2004) 1065-1073.

[195] H.A. Gasteiger, J. Garche, Fuel Cells, in: H.K. G. Ertl, F. Schüth, J. Weitkamp (Ed.) Handbook of Heterogeneous Catalysis, Wiley-VCH, Weinheim, 2008, pp. 3081-3121.

[196] M.M. Mench, Fuel Cell Engines, John Wiley & Sons, Hoboken, Jew Jersey, 2008.

[197] K. Haga, S. Adachi, Y. Shiratori, K. Itoh, K. Sasaki, Poisoning of SOFC anodes by various fuel impurities, Solid State Ionics, 179 (2008) 1427-1431.

[198] K. Haga, Y. Shiratori, Y. Nojiri, K. Ito, K. Sasaki, Phosphorus Poisoning of Ni-Cermet Anodes in Solid Oxide Fuel Cells, Journal of the Electrochemical Society, 157 (2010) B1693-B1700.

[199] H.F. Oetjen, V.M. Schmidt, U. Stimming, F. Trila, Performance data of a proton exchange membrane fuel cell using H_2/CO as fuel gas, Journal of the Electrochemical Society, 143 (1996) 3838-3842.

[200] N.M. Markovic, P.N. Ross, Electrocatalysts by design: from the tailored surface to a commercial catalyst, Electrochimica Acta, 45 (2000) 4101-4115.

[201] J.D. Holladay, Y. Wang, E. Jones, Review of Developments in Portable Hydrogen Production Using Microreactor Technology, Chemical Reviews, 104 (2004) 4767-4790.

[202] S. Roychoudhury, R. Mastanduno, Balance of Plant, in: D. Shekhawat, J. Spivey, D.A. Berry (Eds.) Fuel Cells: Technologies for Fuel Processing, Elsevier, Amsterdam, 2011, pp. 517-526.

APPENDIX

A. List of abbreviations

°C	degree Celsius
µm	micrometer
APU	auxiliary power unit
BOP	balance of plant
C/O	carbon-to-oxygen ratio
cm	centimeter
COS	carbonyl sulfide
CPOx	catalytic partial oxidation
cpsi	channels per square inch
DIN	German industry standard
EGR	exhaust gas recirculation
EN	European standard
FTIR	Fourier transformation infrared spectroscopy
GHSV	gas hourly space velocity
GUI	graphical user interface
HDS	hydrodesulfurization
HT	high-temperature
ICE	internal combustion engine
ID	inner diameter
ISO	International Organization for Standardization
K	temperature in Kelvin
KIT	Karlsruhe Institute of Technology
LHV	lower heating value
LPG	liquefied natural gas
LT	low-temperature
m	meter
mm	millimeter
MS	mass spectrometry
NI	National Instruments
Nm	nanometer

$Ø_i$	inner diameter of reactor tube
PAH	polyaromatic hydrocarbons
PEM	proton exchange membrane
PEMFC	proton exchange membrane fuel cell
ppi	pores per inch
PTFE	polytetrafluoroethylene
REGR	reformed exhaust gas recirculation
RON	research octane number
S/C	steam-to-carbon ratio
SCR	selective catalytic reduction
SelOx	selective oxidation of carbon monoxide
SLPM	standard liters per minute
SMET	selective methanation of carbon monoxide
smlpm	standard milliliter per minute
SOFC	solid oxide fuel cell
SR	steam reforming
TIC	temperature indicator controller
vol%	percentage by volume
WGS	water –gas shift
wt%	percentage by weight

B. List of symbols

A	pre-exponential factor in Arrhenius equation	(mol, m, s)
A_i	symbol of species *i*	-
c_i	concentration of species *i*	[mol m^{-3}][mol m^{-2}]
D_s	effective diffusion coefficient	[m^2 s^{-1}]
E_a	activation energy	[J mol^{-1}]
$F_{cat/geo}$	ratio of catalytic active surface area to geometric surface area	[1]
H	enthalpy	[J]
$\bar{H}_i^0$	molar standard enthalpy of formation	[J mol^{-1}]

h	specific enthalpy		[J M^{-1}]
j_{si}	diffusion flux		[kg m^{-2} s^{-1}]
K_p	equilibrium constant at standard pressure p^0		[1]
k_f	rate constant of forward reaction		(mol, m, s)
k_r	rate constant of reverse reaction		(mol, m, s)
L	thickness of the porous medium (washcoat)		[m]
M	molecular weight		[g mol^{-1}]
M_s	molar mass of species *s*		[kg mol^{-1}]
$\bar{M}$	mean molar mass		[kg mol^{-1}]
N_g	number of species in the gas-phase		-
N_s	number of species adsorbed on the surface		-
N_b	number of species in the bulk phase		-
$\dot{n}_i$	molar flow rate of species *i*		[mol min^{-1}]
p	pressure		[Pa]
p_i	partial pressure of species *i*		[Pa]
p^0	pressure at standard conditions		[Pa]
q_i	heat flux density		[W m^{-2}]
R	gas constant	R = 8,3145	[J mol^{-1} K^{-1}]
R_g	amount of reactions in the gas-phase		-
R_s	amount of reactions on the surface		-
R_i^het	heterogeneous surface reaction rate of species *i*		[mol m^{-2} s^{-1}]
r	coordinate in radial direction		[m]
$\bar{S}_i^0$	molar standard entropy of formation		[J mol^{-1}]
$\dot{s}_i$	surface reaction rate of species *i*		[mol m^{-2} s^{-1}]
T	temperature		[K]
u	axial velocity		[m s^{-1}]
$\dot{V}_\mathrm{tot}$	total flow rate of the product stream		[mol min^{-1}]
X_s	mole fraction		[1]
Y_s	mass fraction of species *s*		[1]

a_i'	reaction order in species *i*	-
β	temperature exponent	[1]
Γ	Number of available adsorbates on the surface	[mol m^{-2}]
ϵ_{i_k}	reduced potential energy	[1]
η	laminar viscosity coefficient	[kg m^{-1} s^{-1}]
η_i	effectiveness factor of species *i*	[1]
η_k	transport effectiveness factor	[1]
θ_i	surface coverage of species *I*	[1]
λ	thermal conductivity coefficient	[W m^{-1} K^{-1}]
μ_{i_k}	change in reaction order	[1]
v_i	stoichiometric coefficient	[1]
v_i'	stoichiometric coefficient of species *i* on the educt side	[1]
v_i''	stoichiometric coefficient of species *i* on the product side	[1]
ρ	density	[kg m^{-3}]
σ_i	coordination number of species *i* on the surface	[1]
τ	residence time	[s]
τ_{ij}	friction tensor	[Pa]
v_i	velocity vector	[m s^{-1}]
Φ	Thile module	[1]
$\dot{\omega}_i$	reaction rate of species *i* in the gas-phase	[mol m^{-3} s^{-1}]

C. Auxiliary Power Unit

C.1. Fuel Requirements for APUs

A broad variety of different fuel cell types is available for producing electrical power from a chemical energy carrier. Hydrogen is the most common fuel type used in fuel cell applications. Since molecular hydrogen is not stored in nature, its production is necessary. Therefore, hydrogen has to be generated out of a primary fuel, mainly deriving from a fossil fuel, i.e., coal, crude oil, or natural gas. Biomass as a regenerative fuel source is of huge interest in the achievement of a carbon-neutral fuel processing step for the production of hydrogen.

In this work, the term “primary fuel” refers to the fuel that is the feedstock for the fuel processor, which converts the primary fuel to a hydrogen-rich gas mixture that can be used as a fuel for a fuel cell. Depending on the source of the primary fuel, further downstream processing of the reformate has to be accomplished as some compounds, such as sulfur and carbon monoxide, have poisoning effects on the active sites of the fuel cell and need to be removed. In **Table C-1**, some specifications for the most common types of fuel cells used today are summarized with regard to the fuel cell’s fuel quality. In all cases, hydrogen, which is converted to electricity, is the chemical energy carrier. For high-temperature fuel cells, such as the SOFC or molten carbonate fuel cell (MCFC), carbon monoxide can act as a fuel because of the water gas shift reaction with water and the formation of hydrogen. For low-temperature fuel cells, e.g., PEMFC, carbon monoxide acts as a poison because of the high sticky coefficients of CO on precious metals, e.g., platinum, that are commonly used in the anode material. In this case, the active sites are blocked for hydrogen adsorption, which leads to activity loss. When the hydrogen is produced from a logistic fuel, small hydrocarbon species can be present in the effluent stream of the reformer. Methane, for instance is less harmful to fuel cells and acts mainly as a diluent or as a further fuel source for internal reforming in high temperature fuel cells. Unsaturated hydrocarbons such as ethylene, however, cannot be converted in the fuel cell stack and tend to cause coke formation on the anode material and, finally, blockage of the fuel cell. This phenomenon even occurs in the ppm level range of ethylene and propylene. Therefore, it is mandatory to avoid their

formation in the fuel processor or to further process those before they enter the fuel cell stack. Sulfur must not be present in any type of fuel cell in order to avoid poisoning of the active sites and complete inactivity of the oxidation process of the hydrogen.

Table C-1: Fuel requirements for common fuel cell types, adapted from [23]

Type of FC:	**SOFC**	**MCFC**	**PEMFC**	**PAFC**
Syngas				
H_2	Fuel	Fuel	Fuel	Fuel
CO	Fuel (WGS to H_2 in the presence of H_2O)	Fuel (WGS to H_2 in the presence of H_2O)	Poison (@>10ppm)	Poison (@>1 %)
Hydrocarbons				
CH_4	Internal reforming with H_2O to syngas	Internal reforming with H_2O to syngas	Diluent	Diluent
$C_{>2}$ e.g. C_2H_4	Harmful due to coking	Harmful due to coking	Harmful due to coking	Harmful due to coking
Total oxidation products				
H_2O	Diluent / reactant	Diluent / reactant	Diluent	Diluent
CO_2	Diluent	Diluent	Diluent	Diluent
Sulfur				
H_2S / COS	Poison (@>1ppm)	Poison (@>0.5ppm)	Poison (@>1ppm)	Poison (@>50ppm)

All of this shows that the primary fuels and the conversion quality of the fuel processor system need to comply with a lot of important requirements. Since this work deals with the fundamental process investigation of the catalytic partial oxidation regarding the conversion of a primary fuel for the supply of a SOFC, fuel processor systems will be discussed in more detail in in Chapter C.2.

Today, nearly all commonly available primary fuels, for instance LPG, LNG, gasoline, or diesel fuel, are based on hydrocarbon fuels, which are mainly derived from fossil fuels. Due to legislative regulations, however, the share of biomass fuels, especially ethanol, has increased significantly over the last decade, even in the European market. Fossil fuels can be divided into three main categories: coal, crude oil, and natural gas. As mentioned above, hydrogen is the main fuel for fuel cell applications, and therefore, the primary fuel has to be processed further down towards hydrogen. **Figure C-1** gives a hypothetic chart of the fuel processing from the original feedstock source to the electro-chemical oxidized fuel cell´s fuel hydrogen.

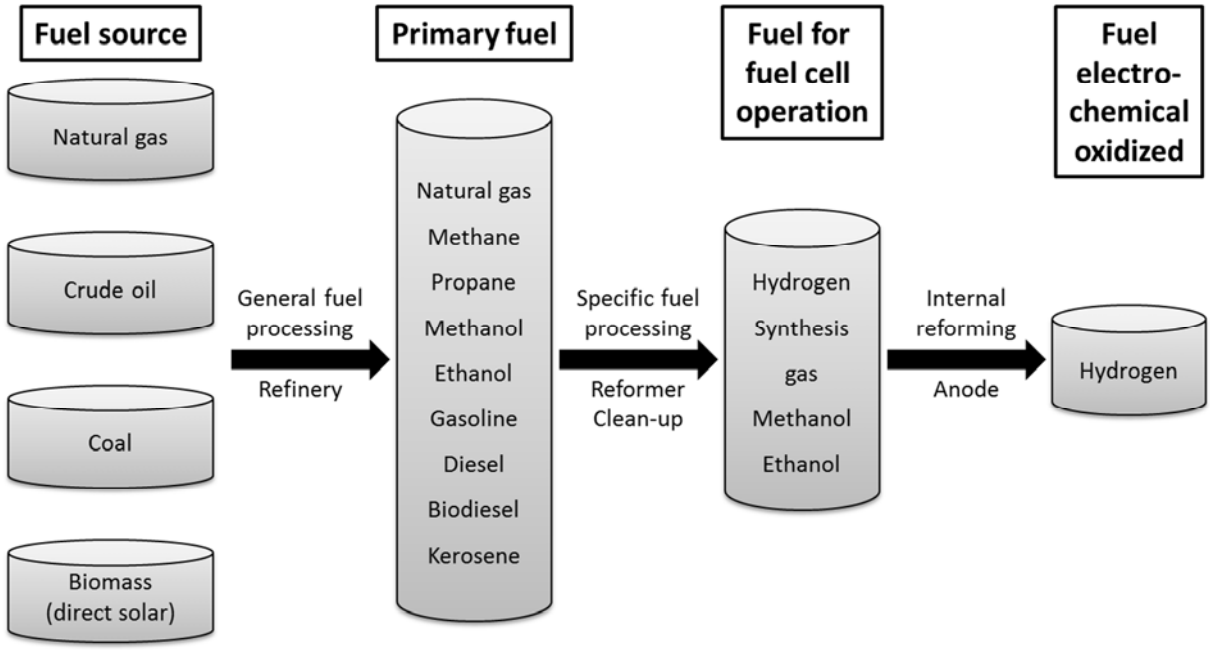

Figure C-1: Chart of fuel flow from source to hydrogen, taken from [99].

In the following sections, selected primary fuels that are derived from the four main feedstock sources will be discussed.

C.1.1. Primary Fuels Derived from Coal

For the chemical and petrochemical industry, coal is less attractive due to the amount of impurities. Furthermore, the carbon to hydrogen ratio of coal is very high and yields are limited by its hydrogen content. Today, coal is mainly burned in power plants for the generation of energy. The released heat is used for the production of steam that drives turbines for electricity generation. In most cases, the overall efficiency is below 35 %.
Instead of burning coal directly, a syngas can be produced via gasification reactions. The syngas has only low hydrogen content and is, also for power generation, in many cases burned in gas turbines. The produced syngas is not attractive for fuel cell applications as the content of hydrogen is low. Further downstream processing is needed, e.g., WGS reaction to increase the hydrogen content and to remove the undesired CO from the stream. For sulfur-containing compounds, such as H_2S, purification is necessary and makes the process more costly. Brown coal, for instance, has a sulfur content of up to 3 vol% that must be removed from the effluent. Only in places where coal is cheaply available, can the production of hydrogen out of coal pay off compared to the immense costs for the fuel processor. Typically, the syngas produced from coal is used for the synthesis of other primary fuels, such as ethanol, methanol, or Fischer-Tropsch liquids.

C.1.2. Primary Fuels Derived from Crude Oil

Crude oil is a hydrocarbon liquid, that is formed in the Earth´s crust in the course of millions of years. Due to local geologic differences, the composition of crude oils varies from source to source. The resulting primary fuels based on crude oil also vary in their composition depending on the oil field and the finishing processes in the refinery.
In the automotive and mobility sector, the main primary fuels from the refinery are gasoline, diesel fuel, and kerosene. Other products arising from crude oil, e.g., bitumen or vacuum gas oils, will not be dealt with in the present thesis. The primary fuels mentioned above are specially tailored for the usage in internal combustion engines or turbines, and therefore, they have to meet special physical properties, such as heating value, flash point, boiling range, and viscosity, as well as composition properties as limitations for maximum aromatics

content, maximum sulfur and water content. **Table C-2** gives a short general overview of the typical composition of the main common primary fuels derived from crude oil and biomass.

Table C-2: Typical composition of primary fuels in the automotive sector, adapted from [99].

	Gasoline	**Diesel**	**Kerosene**	**Biodiesel**
n-paraffines	4-7	40-70	10.13	
i-paraffines	25-40		60.37	
aromatics	20-50	<30	18.68	
naphthalines /olefines	6-16	10-30	0.03	
FAME	0	< 7	0	> 96
typical chain length	C4-C12	C8-C25	C10-C16	C12-C22

These properties are obtained by blending different refinery fractions and by further chemical processing, e.g., hydro-treating, hydro-cracking, and dehydrogenation. Since these fuels are commercially available on a large scale, fuel processors in mobile applications have to handle those as they are, which means that no further refinement will be provided that is especially tailored for the chemical conversion to hydrogen. Crude oil as a natural source contains certain amounts of sulfur. Nonetheless, the sulfur content in the derived primary fuel is determined by the degree of sulfur removal in the refineries and by legislative regulations. Since the desulfurization is a costly process step, the fuel processor must be designed to have a certain tolerance level towards sulfur, either by further purification of the primary fuel or by improved materials. Therefore, actual research is performed in the sulfur resistant reforming catalyst and, of course, in the fuel cell's active sites.

LPG, gasoline, diesel fuel and kerosene have been exemplary chosen as fuels derived from crude oil because of their existing logistic infrastructure and implementation for on-board fuel processing.

C.1.2.1. Liquefied Petroleum Gas

Liquefied petroleum gas (LPG) is a mixture of certain hydrocarbon species, mainly with three or four carbon atoms. The mixture stays in the liquid phase at room temperature and under moderate pressures, and is sold in tanks for heating issues and combustion in small utility vehicles, such as fork lifters.

Most of the LPG is derived from refinery processes, cracking of higher hydrocarbons, and from natural gas processing after separation and liquefaction (cf. Chapter C.1.3.1). The most common commercialized products for LPG are mixtures of propane and butane, which exhibit the highest specific hydrogen content among fossil fuels and, taking the weight of the hydrogen storage tank into account, could even exceed that of liquefied hydrogen [127].

C.1.2.2. Gasoline

In the sense of petro-chemistry, gasoline is a middle distillate fraction of the crude oil refinery process, which is blended with several additives to meet specified requirements regarding its physical properties. In the sense of chemistry, gasoline is a mixture of hundreds of hydrocarbons and oxygenates, mainly ethers and alcohols, with boiling points ranging between 25 and 200 °C. Due to the high combustion energy of the hydrocarbon mixture, gasoline has become the preferred fuel in the automobile industry. To improve the combustion behavior, which is defined by the research octane number (RON), oxygenates are added to avoid “knocking” of the engine that is specified in DIN EN ISO 5164.

At the refinery, gasoline is produces in a three-step process:

- Distillation and separation of the crude oil in different fractions by boiling range
- Refinement of certain fractions by means of cracking, branching/isomerization, and aromatizing
- Removal of undesired byproducts and desulfurization, tuning for physical properties and blending with additives

In Europe, the specifications for gasoline are stipulated by the EN 228 which allows a volumetric content of up to 5 % of bioethanol in the fuel to meet legislative regulations for the use of renewable energy sources. Further additives are added to the fuel to enhance certain performance characteristics or to provide characteristics, that are not inherent in the gasoline. Common additives are antioxidants, corrosion inhibitors, demulsifiers, dyes and markers, anti-icing agents, and drag reducers. Most of the additives are based on organic alcohols or acids, polymers, soluble solids and aromatic amines. Therefore, gasoline is a mixture of a broad variety of organic compounds which all contribute to the desired fuel properties. Since they are made for internal combustion engines, fuel processors have to handle these compounds in the conversion of, now more generally speaking, organic species to hydrogen, as well. Hartmann *et al.* [34] showed that different types of hydrocarbons have different reforming behaviors in case of catalytic partial oxidation, and thus influence the overall efficiency of the reformer.

C.1.2.3. Diesel Fuel

In general, diesel fuel can be compared to gasoline as it is aslo a distillation fraction of the refinery. Originally, diesel fuel was a straight-run product of the refinery. But with improving diesel engine technologies, demands on the diesel fuel have increased. Compared to gasoline, diesel fuel has more non-volatile compounds, resulting in a higher boiling range, typically ranging from 160 – 371 °C. The increase of the paraffin fraction of up to 70 % compared to gasoline fuel disables the evaporation of the fuel, and therefore, diesel fuel has to be sprayed. Evaporation of diesel in air with auto-ignition points below the boiling temperature results in pre-ignition of the mixture. Providing diesel fuel with sufficient air mixing and simultaneously avoiding pre-ignition is one of the major challenges for the use of diesel fuel in on-board reformer applications.

The production of diesel fuel is analogous to that of gasoline, first distillation, followed by refining and clean-up. Analogous to the criteria mentioned for gasoline, several additives are blended to the diesel fraction. However, there are two further main issues that are important with regard to the additives in diesel fuel. First, keeping the injector nozzles clean from coke depositions and second, preventing the fuel from gelling in cold winter weather.

In Europe, DIN EN 590 regulates the specification for an automotive diesel fuel, which is exemplarily shown in Table **C-3**. Up to 10 ppm sulfur content are allowed in the fuel, which is far too hight for today's reforming catalyst and fuel cell membrane technologies with respect to long-term operation. In the US, road diesel can contain up to 15 ppm sulfur, which leads to even faster deactivation of the fuel processor / fuel cell stack. To meet European biofuel directives, diesel fuel has been blended with up to 7 vol% fatty acid methyl ester (FAME) since 2010.

Reforming diesel fuel is considered to be an attractive option for providing fuel for auxiliary power unit systems, especially on transportation trucks and for fuel cells in military applications [24].

Table C-3: Requirements, test methods and threshold values for common diesel fuel (05/2010).

Specification	**Unit**	**Threshold values acc. to DIN EN 590**	**Test method**
Density at 15°	kg/m³	min. 820 max. 845	EN ISO 3675:1998 EN ISO 12185:1996
Cetane (acc. to CFR) number (acc. to BASF)	-	min. 51 min. 52.2	EN ISO 5165:1998 DIN 51773
Cetane index	-	min. 46	EN ISO 4264
Viscosity at 40 °C	mm²/s	2 - 4.5	EN ISO 3104
Flashpoint	°C	min. 55	EN 22719
Neutralisation number	mg KOH/g	-	DIN 51558 Part 1
Corrosive effect on copper (3h at 50 °C) degree	Corrosion	max. 1	EN ISO 2160
Total contamination, indicated as mass concentration	mg/kg	max. 24	EN 12662
Oxidation stability, indicated as mass concentration	g/m³	-	EN ISO 12205
Sulfur content	mg/kg	max. 10	EN ISO 20884 EN ISO 20846 ASTM D 5453 DIN 51400-T11
Carbon residue distillation residue	% (m/m)	max. 0.3	EN ISO 10370
Ash content	% (m/m)	max. 0.01	EN ISO 6245
Distillation at 250 °C 350 °C at 95%	vol.% vol.% °C	< 65 min. 85 max. 360	prEN ISO 3405:1998
Conductivity at 20 °C	pS/m	min. 50	DIN 51412-2 ASTM D 2624
Polycyclic aromatic hydrocarbons (PAH)	% (m/m)	max. 11	EN 12916 IP 391/95
Water content	mg/kg	max. 200	prEN ISO 12937:1996

Fatty acid methyl ester content (FAME)	% V/V	max. 7	EN 14078
Cold flow properties* 03/01-04/14 04/15-09/30 10/01-11/15 11/16-02/28	°C	CFPP -10 0 -10 -20	EN 116

C.1.2.4. Kerosene

Kerosene, just as diesel fuel, is a straight-run product made from petroleum in refineries. Kerosene is mainly used in the aeronautics sector as jet fuel and as fuel for domestic burners. Its boiling range varies within 150- 350 °C. The volatility lies in the range of those of gasoline and diesel fuel., Kerosene has to meet stricter regulations than gasoline and diesel fuel. In kerosene, less aromatics and no unsaturated hydrocarbons, and only very low sulfur concentrations are allowed [77]. Its composition mainly consists of saturated long-chain hydrocarbon species ranging from C_{10} to C_{16}, e.g., branched alkanes, n-alkanes, and alkyl benzenes. The distillation fraction of petroleum is hydro-treated to eliminate double bonds, and is completely desulfurized. No cracking processes are performed in the production of kerosene, which is another difference from the production route of gasoline and diesel. To further improve the physical properties of kerosene, additives, as was done in the cases of gasoline and diesel fuel, are added. Lenz *et al.* successfully used kerosene in a 15 kW autothermal reformer test rig for aircraft applications [128].

C.1.3. Primary Fuels Derived from Natural Gas

Natural gas occurs in porous rocks in the Earth´s crust or in reservoirs deep in the earth. It can also be found in crude oil fields, either as gas caps above the petroleum or dissolved in the liquid hydrocarbon mixture of the crude oil. Natural gas is a combustible gas and mainly

consists of methane (70 – 95 vol%), with varying fractions of ethane, propane and butane. Only few hydrocarbons with five or more carbon atoms can be found. The composition varies, just as for crude oil, depending on to the source and seasonal variations. Furthermore, natural gas contains quantities of nitrogen, carbon dioxide, and traces of other gases, e.g., helium. Sulfur is mainly present in the form of H_2S and has to be removed. **Figure C-2** shows a typical gas processing plant.

Depending on the gas consumer, natural gas can be blended with mixtures of $C_2 – C_4$ hydrocarbons in order to supply a more constant gas composition in case of source fluctuations. In many countries, a certain amount of odorant is added to the gas for safety reasons, as natural gas has no distractive odor. In Europe and the US, tetrahydrothiophene (THT) is commonly used, while in the UK, a cocktail mix of several mercaptanes and diethyl sulfide is used [23].

Natural gas is mainly burned for electricity production or steam reformed to produce a synthesis gas. This syngas can be used either directly in stationary fuel cell applications [8] for large-scale power generation or for further chemical processing and the production of other primary transportation fuels. The production of selected examples of the latter is described in the next section.

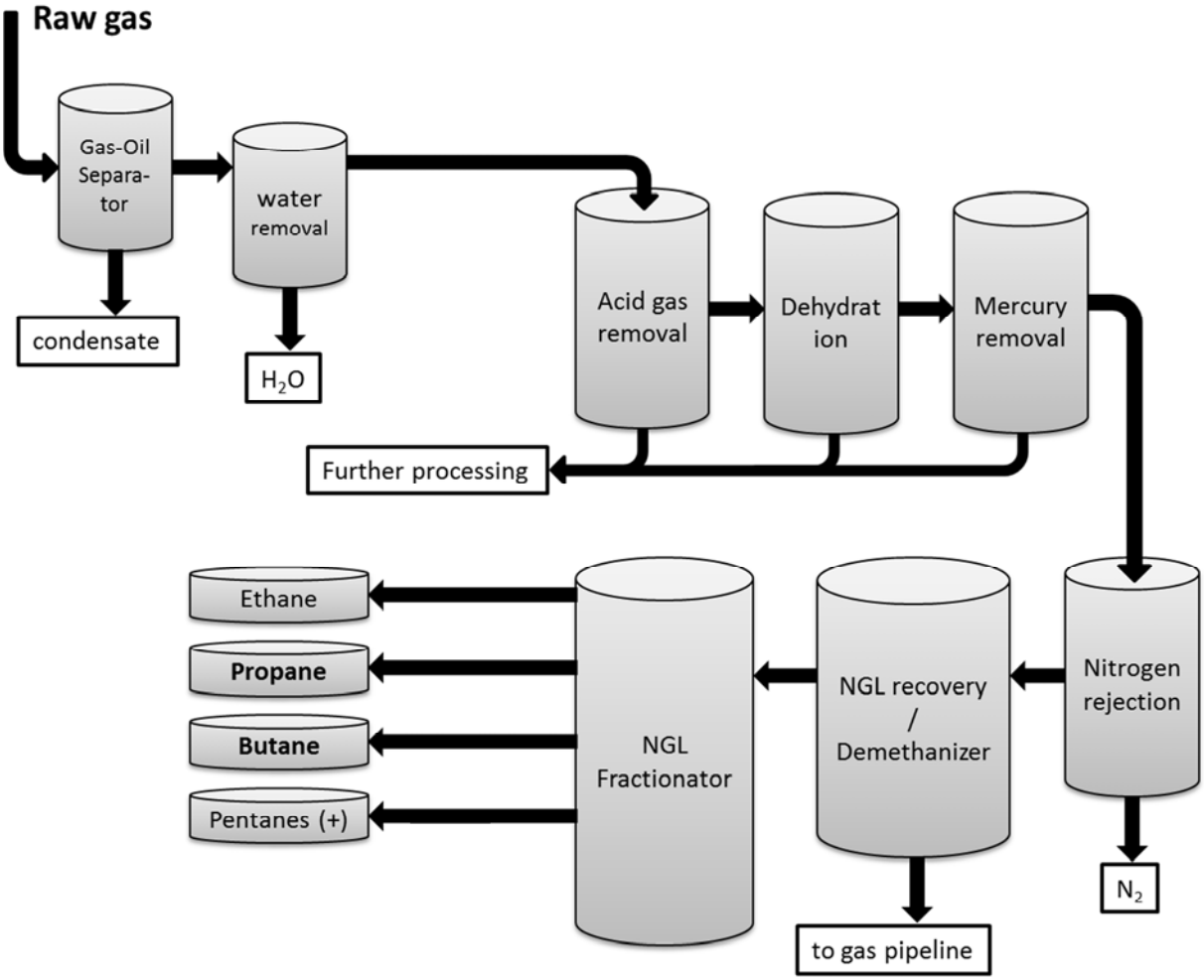

Figure C-2: Schematic gas processing of a natural raw gas, taken from [99].

C.1.3.1. Propane / Butane and LPG

As mentioned in the previous paragraph, natural gas contains certain amounts of light hydrocarbons, including propane and butanes. The main recovery technology used to enrich those for the production of LGP, is cryogenic liquefaction followed by low temperature distillation. The gas is cooled down to temperatures of about -51 °C with heat exchanges, where a gaseous and a liquid phase are formed that are separated. The liquid phase undergoes a throttling expansion and cools down to about -80 °C. The gas stream enters a turbo-expander system and is cooled down to about -90 °C. Both streams enter the demethanizer where $C_{>1}$ hydrocarbons are separated as a liquid and further processed to the individual hydrocarbon species, e.g., propane and butane. LPG is considered to be an

attractive fuel for hydrogen production due to large existing reserves and the conversion efficiencies [24].

C.1.3.2. Methanol

Today's industrial methanol production is based exclusively on the conversion of synthesis gas to methanol with certain catalysts. Well established catalysts are Cu/ZnO- or CuO/ZnO-based catalysts, mainly supported on Al_2O_3 [129, 130]. A synthesis gas of $H_2/CO = 2$ is needed for the catalytic process, which is carried out at pressures of about 50 - 100 bars and at temperatures in the range of 200 – 300 °C. Due to the slight exothermic formation of methanol in **Equation C-1** and **Equation C-2**, the synthesis is performed at low temperature under thermodynamic control:

$$CO + 2H_2 \rightarrow CH_3OH, \qquad \Delta H^0_{298} = -91\frac{kJ}{mol}$$

Equation C-1

$$CO_2 + 3H_2 \rightarrow CH_3OH + H_2O, \qquad \Delta H^0_{298} = -49.5\frac{kJ}{mol}$$

Equation C-2

$$CO + H_2O \rightarrow CO_2 + H_2, \qquad \Delta H^0_{298} = -41.2\frac{kJ}{mol}$$

Equation C-3

The water produced in **Equation C-2** is converted to additional hydrogen in the water-gas shift reaction (**Equation C-3**), resulting in a strong overall driving force of the reaction to the product side.

Despite its toxicity, methanol is particularly used as a transportation fuel and as a means of energy storage for fuel cell applications. Depending on the methanol's purity, it can be directly fed to direct methanol fuel cells (DMFC) which oxidize the methanol completely to CO_2 and H_2O. Up to now, DMFCs have had no significant relevance in the application of on-board fuel reforming. They are mainly used in the range of 1 mW – 20 W power output for

portable electronic devices [131] such as laptops or smart phones. Nevertheless, the general reforming of methanol is of great interest because of its mild reforming conditions (temperature between 200 – 450 °C) and high conversion efficiency [8, 24].

When a further process step is added to the methanol synthesis, dimethyl ether (DME) can easily be obtained. The catalytic reaction is carried out with special alumina oxide catalysts at temperatures of about 310 °C at 26 bars. DME can be used as a substituent for LPG and, due to its high oxygen content and high cetane number, it is attractive as a diesel fuel substituent.[132, 133]

C.1.3.3. Ethanol

Ethanol and higher alcohols have been identified to be a potential fuel or additive to fossil-based fuels. In many countries, ethanol is used as a fuel additive to increase the octane rating with a simultaneous reduction of pollutant emissions, e.g., NO_x and CO_2 [134].

Comparable to methanol, higher alcohols are often produced by the catalytic conversion of synthesis gas. However, two other processes are also established in industry, the hydration of ethylene and the fermentation of sugar. The latter is based on a biomass feedstock derived from vegetables and can interfere with food supplies. Nevertheless, attention will only be paid to the syngas route. The syngas can be generated from a variety of carbon sources, e.g., coal, natural gas, or biomass. The latter is of great interest for the production of fuel from renewable energy sources due to limited fossil fuel resources. Gupta *et al.* [135] gave a recent review on the production of higher alcohols out of syngas using Cu-based catalysts. Conventionally, rhodium-based catalysts, which have high selectivities towards C_{2+} oxygenates but are very costly, are used at temperatures around 275 °C and pressures of about 100 bars. Cu-based catalysts promoted with alkali, transition metals and their oxides, and rare earth oxides are in the focus of current research. Furthermore, apart from the Rh- and Cu-based catalysts, modified Fischer-Tropsch and Mo-based catalysts are under investigation [136, 137].

C.1.4. Primary Fuels Derived from Biomass

Due to the energy shortage crisis and global warming issues, there is a high necessity of using biomass as an alternative source for the production of automotive fuels. This is also indicated by the European guidelines for the enhancement of biofuels in all automotive fuels (gasoline and diesel fuel). In 2010, 5.75 % of the automotive fuel had to be produced from biofuel, rising up to 10 % in 2020. Today, only 1.4 % of all automotive fuels are produced from biomass [8, 138]. In general, two types of biofuels are distinguished, 1st and 2nd generation fuel. 1st generation biofuel is based on sugar crops for bioethanol, oil crops for biodiesel, and organic waste for biogas. Most of the feedstock used can be roughly divided into two different categories: feedstock containing sugar/starch and oil, in general various grain and vegetable crops, which are converted to liquid fuels using conventional technologies. In locations where there are high crop yields and low costs for labor and land , these types of fuels have large potential to be economic in costs compared to conventional production routes. Nevertheless, from an economic point of view with regard to the environment, the use of land, water, and fertilizer as well as the usage of food feedstock is not sustainable, and there is a strong demand for the usage of woody or grassy materials as feedstock for biofuel production [138]. Biofuels derived from agricultural feedstock and municipal waste are classified as 2nd generation biofuels. Here, mainly lignocellulosic biomass, originating, for instance, from forest, crops and agricultural residues, grasses and tree barks, is converted via hydrolysis, pyrolysis, or gasification. While hydrolysis pathways rely on enzymes, that convert the feedstock to sugar and then ferment it into ethanol, pyrolysis produces a poor volatile, highly viscose bio-oil with varying contents of ash, coke, and water. Since several problems arise due to its physical properties, the oil has to be upgraded for the application in automotive fuel and is therefore more costly. The pathways of gasification use a catalytic process including high temperature and a certain oxygen level to produce biofuels out of biomass. All pathways occupy the intermediate platform of synthesis gas, which is then further processed to the later fuel, for instance Fischer-Tropsch-diesel, biomethanol, bioethanol, dimethyl ether, or synthetic natural gas. A big advantage of the gasification process is the ability to also convert lignin which cannot be converted via the hydrolysis pathway [138]. The production of methanol and ethanol from syngas has already

been presented in the Chapter C.1.3.2 and C.1.3.3, and these paragraphs shall also be referred to with regard to a biomass feedstock.

C.1.4.1. Biodiesel

The physical characteristics of a biodiesel can be compared to those of the petroleum-based diesel as both are used for internal combustion engines. Generally, biodiesel is derived from biomass, however, two main aspects have to be distinguished regarding the production process. 1st generation biodiesel fuel is made of vegetable oils, e.g., soybeans and rapeseeds, by means of esterification with methanol or ethanol. 2nd generation biodiesel is also derived from biomass, but is produced from syngas via Fischer-Tropsch (FT) synthesis (cf. C.1.4) [138]. FT-diesel fuel has a high cetane number in the range of 73.5 – 75 [8] and is nearly free of sulfur and nitrogen contents. It therefore leads to very low emissions in hydrocarbons, NO_x, and particulates[138]. Two operation regimes are performed in the FT synthesis, one at temperatures around 200 – 240 °C using iron- or cobalt-based catalysts, which produces high molecular mass linear waxes for the hydrocracker. The other one is performed at temperatures in the range of 300 – 350 °C with iron-based catalysts and produces linear low molecular mass olefins. Due to its physical properties, e.g., flame point between 67 - 110 °C and aromatic content < 2.7 %, cetane number and low sulfur content, FT-diesel fuel is an ideal fuel for fuel processors [77].

1st generation biodiesel mainly consists of fatty acid alkyl esters and is a good lubricant. Therefore, biodiesel is blended with diesel fuel derived from petroleum to improve knocking and combustion performance of the latter [77]. Table **C-4** gives the specifications for biodiesel in the EU since 2005 compared to the German ones in 2003.

Table C-4: Specifications, test methods, and threshold values for biodiesel in DIN EN 14214 as of the year 2005.

Specification	**Unit**	**Threshold values acc. to DIN 51606 (2003)**	**Threshold values acc. to DIN EN 14214 (01/2005)**	**Test method**
Density at 15°	kg/m³	875-900	860-900	EN ISO 3675
Cetane number	-	min. 49	min. 51	EN ISO 5165
Viscosity at 40 °C	mm²/s	3.5-5.0	3.5-5.0	EN ISO 3104
Flashpoint	°C	min. 110	min. 101	EN 22719
Neutralization number	mg KOH/g		0.5	DIN EN 14104
Corrosive effect on copper (3h at 50 °C) degree	Corrosion	1	1	EN ISO 2160
Total contamination, indicated as mass concentration	mg/kg	max. 20	max. 24	EN 12662
Sulfur content	mg/kg	max. 10	max. 10	-
Carbon residue, distillation residue	% (m/m)	max. 0.03	max. 0.03	EN ISO 10370
Ash content	% (m/m)	-	0.02	ISO 3987
Conductivity at 20 °C	pS/m	-	-	-
Water content	mg/kg	max. 300	max. 300	EN ISO 12937
Iodine number	-	max. 115	120	Pr EN 14111
Phosphor	mg/kg	max. 10	max. 10	Pr EN 14105
Alkaline metals Na + K	mg/kg	max. 5	max. 5	DIN EN 14108
Methanol	% (m/m)	max. 0.3	max. 0.2	DIN EN 14110
Ester content	% (m/m)	min. 96.5	min. 96.5	Pr EN 14103

Monoglycerides	% (m/m)	max. 0.8	max. 0.8	DIN EN 14105
Diglycerides	% (m/m)	max. 0.4	max. 0.2	DIN EN 14105
Triglycerides	% (m/m)	max. 0.4	max. 0.4	DIN EN 14105
Free glycerol	% (m/m)	max. 0.02	max. 0.02	DIN EN 14105
Total glycerol	% (m/m)	max. 0.25	max. 0.25	DIN EN 14105
Linolenic acid methyl ester content	% (m/m)	-	max. 12	DIN EN 14103
Fatty acid methyl ester content with ≥4 double bonds	% (m/m)	-	max. 1	-
Cold flow properties* 03/01-04/14. 04/15-09/30 10/01-11/15 11/16-02/28	°C	-	CFPP -10 0 -10 -20	EN 116

C.2. Fuel Processing in APUs – Fuel Processors

As already mentioned in Chapter 1.2, converting hydrocarbon fuels to a hydrogen-rich gas mixture, including the pre-processing of the primary fuel and the post gas-cleanup, is a challenging task. In the following, the main steps of pre-processing, conversion, and post-processing are described. Please refer to **Figure 1-1** for the individual stages.

C.2.1. Pre-treatment of the Primary Fuel – Desulfurization and Pre-reforming

Primary fuels derive from fossil fuels and have a share of > 95% in today's fuel production. Depending on the source, the hydrocarbon feedstock contains a certain amount of inorganic sulfur components, e.g., H_2S and COS in natural gas and light organic sulfur components, such as mercaptanes, dimethyl sulfides, and thiophenes. As mentioned in Chapter C.1.3, organic sulfur compounds, mainly tetrahydrothiophene (THT) are added to natural gas in the range of 4 – 6 ppm for safety reasons [139, 140], up to 120 ppm can be added to LPG [141]. These sulfur compounds have poisoning effects on the reforming catalyst that typically contains precious metals such as rhodium, platinum, or ruthenium, and on the anode material of the fuel cell, e.g., nickel or platinum. When the sulfur content is not reduced to a level of a few parts per billion, deactivation of both the reformer and the fuel cell is predictable and a decline in conversion efficiency unavoidable [14]. Most fuel cell applications dictate sulfur contents below 0.1 ppm [142, 143] Apart from chemical issues, strict directives, regarding the reduction of sulfur dioxide emissions into the environment are dictated by the government [144]. Therefore, sulfur levels in primary fuels must be reduced and desulfurization is necessary prior to combustion or reforming.

Desulfurization is not needed when sulfur-free primary fuels are used in the fuel processor. In general, these fuels are alcohols, such as methanol and ethanol, or Fischer-Tropsch fuels made ofrom a sulfur-free synthesis gas. Nevertheless, for reasons mentioned above, sulfur has to be removed for the synthesis gas production. In principle, two main processes for desulfurization are used, hydrodesulfurization (HDS) and adsorptive desulfurization. The desulfurization can be carried out in the gas-phase, which is typically done for natural gas or

LPG cleaning, or in the liquid phase, which is of great interest for mobile, portable, or transportable applications using fossil fuels.

The hydrodesulfurization process is a large-scale process operated at the refinery to meet sulfur specifications for transportation fuels. The process is generally operated at temperatures between 200 – 400 °C and relevant pressures of 40 – 50 bars [145, 146]. HDS is a two-step process. In the first step, organic sulfur compounds are converted to H_2S and the corresponding hydrocarbon in the presence of hydrogen and a catalyst, based on Co-Mo or Ni-Mo or mixtures of these [14, 146-148]. The H_2S is then adsorbed by a metal oxide at moderate temperatures. The most common adsorbent is zinc oxide. The HDS process is characterized by reliable operation with high sulfur pickup. Nevertheless, it is not favorable for compact fuel processor integration because of its temperature operation range of up to 400 °C and the requirement of a certain amount of hydrogen for the hydrogenation process in the first step. In case of an APU, the hydrogen has to be recycled from the hydrogen stream for the fuel cell, lowering the overall conversion efficiency from fuel to electricity.

For small scale fuel cell applications, several technologies are available to provide an ultra-clean hydrocarbon primary fuel. Adsorptive desulfurization technologies have been stated to be attractive due to size and cost reduction, while providing sulfur levels below 1 ppm [144]. Adsorptive desulfurization is widely used for the removal of sulfur components because of its adaptability and simplicity, and can be carried out at nearly ambient temperatures when performed in the liquid phase [146]. Otherwise, the fuel has to be evaporated for gas-phase desulfurization first, which makes the process more bulky and costly. Up- and downscaling of the process is uncritical and can be easily adapted to the process's capacity. One big advantage of the adsorption technology is the abandonment of hydrogen. Nevertheless, adsorption selectivity for sulfur components increasingly competes with growing hydrocarbon species in the fuel and is a major challenge in today's research. A broad variety of sorbent materials are available on the market, ranging from activated carbon, catalysts containing transition and precious metals to metal oxides. ZnO, partly doped with copper, has improved adsorption tendencies for H_2S compared to activated carbon, but the pickup is slow and a longer residence time of the fuel is necessary. Advanced adsorbent materials are in the focus of actual research that targets specific sulfur containing species. Zeolithes and multi-metal oxides offer high quantities for sulfur pickup, with improved resident times. Therefore, desulfurization units become smaller in size and more long-term active [14]

compared to the commercial HDS process. Due to the variety of different sulfur components in the fuel, multi-stage adsorption beds are required because of different adsorption tendencies of the sorbents. Sorbents for small molecules such as H_2S and COS only have low capacities for bulkier molecules, e.g. 4,6 dimehtyl dibenzothiophene. Furthermore, the mechanism for sorption varies from polarity-based sorbents and sulfur-metal-based interaction sorbents, to π-complexation sorbents, each of which is appropriate for a certain type of sulfur component [146].

Oxidation-assisted adsorption is stated to be attractive for desulfurization in the liquid phase. Here, thiophenic sulfur components are selectively oxidized, for instance, with a peroxide or air, at mild conditions (25 – 90 °C), resulting in more polar sulfur components. Those can then be separated in a second step, e.g., liquid-liquid phase separation. Since this is a two-step process and liquid-liquid separation is impossible for compact fuel processors, it is less attractive for mobile applications. Only the approach of the selective oxidation followed by selective adsorption could be of interest for sulfur removal in future technologies.

Pre-reforming of the primary fuel is performed to convert heavy long-chain hydrocarbon species into smaller molecules, mainly ranging from C_1 to C_6 [14, 149]. These smaller hydrocarbon species tend to have better reforming characteristics in SR, ATR or CPOX, the main reforming routes applied in compact fuel processors. Borup *et al.* investigated the light-off behavior of various fuel components, typically found in logistic fuels, which is a critical parameter in mobile fuel processors start-up behavior and energy demand. Roughly, these components can be divided mainly into aliphatic hydrocarbons, further split up into straight, branched, long- and short-chain, aromatic hydrocarbons, and oxygenated hydrocarbons. They were able to show that short-chain aliphatic hydrocarbons tend to have a more favorable light-off temperature than long-chain or aromatic hydrocarbons. Straight-chain hydrocarbons have lower light-off temperatures compared to branched hydrocarbons of nearly the same length. When oxygenates such as methanol, ethanol, or DME are present in the mixture, the light-off temperature is even more decreased [149]. Therefore, pre-reforming can improve the fuel characteristics with regard to start-up and reforming behavior of the main reformer unit, and decrease coke formation as aromatics and long-chain hydrocarbons were identified to have higher coking tendencies than the shorter

hydrocarbons. When the primary fuel is converted down to almost C_1 species, these can directly be fed to a high-temperature fuel cell for direct internal reforming [11-13]. Furthermore, coke formation in the reformer unit and in downstream parts of the fuel processor is partly prevented as heavier hydrocarbons have been removed from the stream in the latter case.

Muradov *et al.* have recently reported about their investigations of a novel process that combines both pre-treatment methods, desulfurization and pre-reforming [150]. The process uses about 13 – 16 % hydrogen from the reformer outlet stream for the conversion of diesel fuel to $C_3 – C_4$ followed by adsorptive desulfurization of the pre-reformer effluent gas.

Selecting the most suitable fuel processor design, including pre-treatment and reforming technology, will depend on both the primary fuel and the fuel cell stack. Since primary fuels are directly convertible in common reformer technologies, only desulfurization is necessary to protect the reforming catalyst and the fuel cell. To make it attractive for mobile applications, positive aspects regarding lower start-up temperature and the reformer's energy demand have to be balanced with the increase in weight and cost for a further processor unit in case of pre-reforming.

C.2.2. Conversion of the Primary Fuels to Hydrogen

In literature, three routes for the conversion of hydrocarbon fuels to hydrogen are mainly claimed to be beneficial for the use in mobile applications. These are:

- Catalytic steam reforming (SR)

$$C_xH_yO_z \; + \; (x-z)H_2O \; \rightleftarrows \; x\,CO \; + \; \left(x-z+\frac{y}{2}\right)H_2, \qquad \Delta H^0_{298} \; > \; 0$$

Equation C-4

- Catalytic partial oxidation (CPOx)

$$C_xH_y + \frac{x}{2}O_2 \rightarrow x\,CO + \frac{y}{2}H_2, \qquad \Delta H^0_{298} < 0$$

Equation C-5

$$C_xH_yO_z + \frac{x-z}{2}O_2 \rightarrow x\,CO + \frac{y}{2}H_2, \qquad \Delta H^0_{298} < 0$$

Equation C-6

- Catalytic autothermal reforming (ATR)

$$C_xH_yO_z + n\,O_2 + (2x-z-2n)H_2O \rightarrow x\,CO_2 + \left(2x-z-2n+\frac{y}{2}\right)H_2, \qquad \Delta H^0_{298} \sim 0$$

Equation C-7

ATR can be seen as the combination of SR and CPOx, as the heat release of the partial oxidation reaction is used in the steam reforming reaction in one reactor. Since this work deals with the background of an APU, only these three reforming routes will be discussed in detail.

For a convenient way of characterizing the feed composition, which includes C, H, and O atoms from both, fuel and water/air, there is a common nomenclature of the C/O ratio. C/O describes the amount of C atoms in the feed stream divided by the number of O atoms in the feed. Furthermore, when steam is added to the inlet, the S/C ratio is commonly used.

$$\frac{C}{O} = \frac{x\,\dot{n}_{C_xH_yO_z}}{2\,\dot{n}_{O_2} + z\,\dot{n}_{C_xH_yO_z}},$$

Equation C-8

$$\frac{S}{C} = \frac{\dot{n}_{H_2O}}{x\,\dot{n}_{C_xH_yO_z}}.$$

Equation C-9

C.2.2.1. Steam Reforming (SR)

Due to the hydrogen content in the fuel and the S/C ratio used in practice, according to **Equation C-4**, steam reforming produces a hydrogen-rich gas mixture. The reaction can be considered as irreversible for higher hydrocarbons with $C_{>1}$. In general, during steam reforming, several side reactions occur which include the water-gas shift reaction (**Equation C-3**), the formation of methane out of syngas,

$$CO + 3H_2 \rightleftarrows CH_4 + H_2O, \qquad \Delta H^0_{298} < 0,$$

Equation C-10

and the formation of carbon via

$$CO + H_2 \rightleftarrows C + H_2O, \qquad \Delta H^0_{298} < 0,$$

Equation C-11

$$2CO \rightleftarrows C + CO_2, \qquad \Delta H^0_{298} < 0,$$

Equation C-12

$$CH_4 \rightleftarrows C + 2H_2, \qquad \Delta H^0_{298} > 0.$$

Equation C-13

An S/C = 1.0 is the minimum ratio needed for the thermodynamic conversion of all hydrocarbon species in the feed. According to **Equation C-3**, increasing the S/C ratio results in a net production of hydrogen at the expense of CO and, in parallel, decreases the methane content (**Equation C-10**). In concerns of thermodynamics, **Equation C-4** indicates that more H_2 is produced with increasing temperature. In many SR applications, heat for the reforming reaction is provided by the partial total combustion of the fuel.

$$C_xH_yO_z + \left(x + \frac{y}{4} - \frac{z}{2}\right) O_2 \rightarrow x\, CO_2 + \frac{y}{2}\, H_2O, \qquad \Delta H^0_{298} \ll 0.$$

Equation C-14

In practical steam reforming processes, according to **Equation C-11** - **Equation C-13**, S/C > 1 has to be provided to the reformer to avoid undesired carbon formation. In terms of natural gas reforming, S/C is practicable up to 3 and for heavier hydrocarbons even up to 7 [14].

However, one major advantage of SR is the fact that it does not rely on oxygen, and that only the fuel and steam are needed. Therefore, large amounts of nitrogen do not have to be heated in case of using air as an oxygen source.

Established steam reforming catalysts are based on group VIII metals, and among these, Ni is the most common and widely-used one. Precious metals such as Rh, Ru and Pt show higher activities in SR, but due to their high prize, they are not economical for large-scale processes. However, in small-scale applications, such as APUs, S/C ratios of 3 - 5, which are usually used to avoid coke formation, cannot be operated because of the high energy demand for water evaporation and water contend available. Furthermore, excess of water decreases the APUs overall electrical efficiency due to lowering the Nernst voltage trough steam dilution [14]. For carbon formation prevention, even at lower S/C ratios, alkali metals can be added to the Ni catalyst, which enhance steam adsorption and, therefore, lowers coke deposition [151]. Heavier rare-earth metals, such as ceria, enhance coke gasification as they keep the surface cleaner from coke depositions while not dramatically influencing the catalytic activity of nickel [152, 153]. Noble metals, such as Rh, have been shown to be very active in SR, and are less sensitive to coke formation than Ni [154], but not attractive due to their high prizes. Due to ensemble size control of the surface of nickel [153], a controlled, small amount of sulfur in the feed also reduces coke formation in Ni-SR, as was first mentioned by Rostrup-Nielsen [155]. However, sulfur content of a few ppm in the feed stream can lead to poisoning of Ni by the formation of nickel sulfide and rapid deactivation (cf. Chapter C.2.1).

SR of natural gas is the major route for producing large amounts of hydrogen and synthesis gas. The reaction is strongly endothermic and therefore has huge energy demands, which makes it more unattractive for small scale applications [9, 14]. **Equation C-15** exemplarily shows the SR of methane, which is the main component of natural gas

$$CH_4 + H_2O \longrightarrow CO + 3H_2, \qquad \Delta H^0_{298} = +207 \frac{kJ}{mol}.$$

Equation C-15

Nevertheless, SR is very efficient with yields close to the thermodynamic equilibrium, especially in large-scale facilities [151, 156]. S/C ratios above 3 are usually used to avoid coke formation in the reforming of fossil-based fuels [157].

With regard to fuel cell applications, the steam reforming of methanol (**Equation C-16**) is of rather little interest due to the fast developments in direct methanol fuel cells [8], that convert MeOH directly in the fuel cell and therefore do not need upstream reforming processes.

$$CH_3OH + H_2O \longrightarrow CO + 3H_2, \qquad \Delta H^0_{298} = +336\frac{kJ}{mol}.$$

Equation C-16

However, a large number of studies can be found about the development of new catalysts for SR of MeOH [158]. Ethanol has attracted much attention in SR [159-163], as it can be produced from renewable sources (cf. Chapter C.1.3.3)

$$C_2H_5OH + H_2O \longrightarrow 2CO + 4H_2, \qquad \Delta H^0_{298} = +255\frac{kJ}{mol}.$$

Equation C-17

Due to the higher reforming temperature needed and the occurrence of smaller hydrocarbons and by-products, e.g. ethylene and acetaldehyde, which leads to coke formation, the reforming of ethanol is more challenging than that of methanol [164]. SR of logistic fuel was investigated for model surrogates , as was isooctane for gasoline and hexadecane for diesel [67], but is less attractive due to the endothermicity and large steam requirement of S/C up to 7 (depending on the fuel) to prevent coke formation. CPOx and especially ATR are the more favored routes for logistic fuel reforming [7, 9, 14, 24, 149].

C.2.2.2. Catalytic Partial Oxidation (CPOx)

Under exothermic reaction conditions, the catalytic partial oxidation produces a hydrogen-containing gas mixture (**Equation C-5** and **Equation C-6**). About 17 % of the lower heating value (LHV) of the fuel is converted for the enthalpy increase of the feedstock, and therefore correlates with the increase in temperature from 298 K to about 1143 [8]. In comparison to SR, partial oxidation has the advantage of operating without steam addition. Only oxygen (air) is needed, which makes the process more flexible. Only substoichiometric amounts of oxygen are used (**Equation C-5**) to prevent full total oxidation of the fuel and the production of hydrogen and carbon monoxide. The conversion of the hydrocarbon to a syngas can be performed within milliseconds, when catalysts, mainly noble metals as Pt, Pd, Ru and Rh [14] supported on monolithic honeycombs or foams, are used (CPOx). Short contact times with high conversion rates and selectivities towards hydrogen [75] make CPOx attractive for small-scale applications. The CPOx of methane has gathered interest very in the late 1990s, starting with Ni-based catalysts originating from steam reforming, but showed high carbon formation tendencies compared to noble metals [165]

$$CH_4 + \frac{1}{2}O_2 \longrightarrow CO + 2H_2, \qquad \Delta H^0_{298} = -36\frac{kJ}{mol}.$$

Equation C-18

However, the option for an autothermally-operated reformer for the conversion of natural gas to a syngas for compact devices gathered larger interest than SR, and intensive research is performed in this field [45, 166-171]. However, for mobile applications, liquid fuels are more attractive due to their higher energy densities and the lower light-off temperatures of the reaction [149]. CPOx of methanol has been reported to be attractive for fuel cell application using non-noble metals, such as Cu/ZnO-based catalysts [172],

$$CH_3OH + \frac{1}{2}O_2 \longrightarrow CO + 2H_2, \qquad \Delta H^0_{298} = +95\frac{kJ}{mol}.$$

Equation C-19

However ethanol is of greater interest than methanol due to reasons already mentioned for SR. The production of hydrogen from ethanol is a slightly endothermic reaction

$$C_2H_5OH + \frac{1}{2}O_2 \longrightarrow 2CO + 3H_2, \qquad \Delta H^0_{298} = +13\frac{kJ}{mol}$$

Equation C-20

and has recently been studies by Hebben *et al.* [173]. CPOx of ethanol can be operated close to thermodynamic equilibrium, when C/O is below 0.8. For higher C/O ratios, significant amounts of hydrocarbons and oxygenates have been found, accompanied by a steady decrease in ethanol conversion. However, oxygen consumption stays high, indicating the formation of oxygenates, such as acetaldehyde and dimethyl ether [173].

For APUs, catalytic partial oxidation provides an attractive route for the conversion of logistic fuels, that are carried on-board, to hydrogen or a hydrogen-rich syngas. However, gasoline and diesel fuel consist of several hundreds of hydrocarbons, ranging over short- and long-chain, saturated, olefinic, aromatic, linear, cyclic, and branched hydrocarbon species. General constitutions of logistic fuels are discussed in Chapter C.1. In several studies in literature, it could be figured out that the structure of a hydrocarbon species plays a dominant role in its conversion to hydrogen and to by-products using noble metal catalysts [34, 149, 174, 175]. The CPOx of isooctane as a model surrogate for gasoline was already shown in **Equation 2-1**. Due to the broad variety of hydrocarbons in the feed, individual species are preferred in reforming reactions, others in total oxidation. Hartmann *et al.* [34] investigated archetypical constituents of logistic fuels and revealed that variations in the chain length of n-alkanes have no significant effect on fuel conversion and hydrogen yield, whereas changing the structure of comparable C_6 hydrocarbons showed a continuous decrease in hydrogen yield from branched, to cyclic and olefinic and to aromatic species. Furthermore, the formation of by-products is also dominated by the structure of the hydrocarbon fuel, leading to smaller hydrocarbons, such as ethylene, propylene, and acetylene, which were identified by Kang *et al.* [176], Dean *et al.* [177] , Burke *et al.* [41] ,and Kaltschmitt *et al.* [100] to be coke precursors. Acetylene, however, is the only by-product produced at fuel-lean (C/O < 0.8) conditions, especially for an aromatic hydrocarbon feedstock and high reaction temperatures. Concerning diesel fuel CPOx, strong propensity

for coke precursor formation is reported [15] and also found in this work (Chapter 7), even for CPOx with noble metal catalysts that have a low propensity for carbon formation.

Due to the increasing use of renewable fuels, ethanol blended gasoline has been investigated for CPOx hydrogen production by Diehm *et al.* [76]. Ethanol/isooctane mixtures, ranging from 0 – 100 vol% ethanol blends, have been investigated over Rh/Al_2O_3 catalysts and are compared to commercially-available gasoline (E5) and E85. E85 is a gasoline, blended with 85 vol% ethanol and gasoline has about 5 vol% ethanol content already included. The conversion of ethanol is favored compared to isooctane in all blends studied, while the conversion of isooctane decreases rapidly with increasing ethanol content and C/O ratio and starts even in the fuel-lean regime. Hydrogen selectivities decrease with increasing ethanol content, whereas selectivities towards ethylene increase. Untypically for CPOx of non-alcohol fuels, by-products appear with increasing ethanol content even at lower C/O ratios.

The complexity of the logistic fuel makes a prediction about the reactor performance more challenging. Model fuel surrogates help researchers to understand individual processes of the interaction of different species and allow them to reduce the complexity to a certain level. This makes it easier to develop detailed models for a better understanding of logistic fuel CPOx. However, as shown in case of ethanol-blended fuels, single components do not have additional behavior in the mixture but superimpose to the overall performance of the reactor.

C.2.2.3. Autothermal Reforming (ATR)

Autothermal reforming (**Equation C-7**) is attractive because of its nearly thermo-neutral operation conditions. In the ATR, the exothermic reaction of partial oxidation (**Equation C-6**) is combined with the endothermic reaction of steam reforming (**Equation C-4**). ATR has gathered much attention in the last decades because, in principle, no external heat is required, which makes the process suitable for the requirements of APU systems. Furthermore, its rapid start-up characteristics and the capability for dynamic condition changes due to the CPOx reaction can achieve high efficiencies even under non-steady operating conditions.

ATR catalysts with high efficiencies are generally based on, either group VIII transition metals, such as Pt, Rh, and Ni, which are also suitable for SR and CPOx, or non-noble metal catalysts with perovskite structure ABO_3 [14]. Apart from the catalytic demands, high demands are made to engineering aspects because the endothermic SR relies on the exothermic CPOx reaction. Heat integration is essential for high efficiencies.

ATR of natural gas is mainly performed for stationary approaches to hydrogen production. Due to the strong C-H bonds of methane, high temperatures are required, ranging from 700 – 900 °C [178].

$$CH_4 + \frac{1}{2}O_2 + H_2O \longrightarrow CO_2 + 3H_2, \qquad \Delta H^0_{298} = -76\frac{kJ}{mol}.$$

Equation C-21

With ATR, the CO content produced with CPOx is converted to CO_2 and hydrogen via WGS reaction, leading to the expression in **Equation C-21**. Ni-based catalysts are used in industry because of low cost and availability with an S/C ratio of about 2.5. An extensive overview of the research on metal- and non-metal-based catalysts for ATR of natural gas, and in particular methane, can be found in [179].

ATR of methanol is attractive due to low reforming temperatures of about 200 – 300 °C, and no extensive efforts are made concerning insulation and downstream heat exchangers in an integrated fuel processor system. CuO/ZnO based catalysts, partly supported on Al_2O_3, have been used in recent studies at S/C ratios of about 1.1-1.3 [179, 180].

$$2CH_3OH + O_2 + H_2O \longrightarrow 2CO_2 + 5H_2, \qquad \Delta H^0_{298} = -135.2\frac{kJ}{mol}.$$

Equation C-22

However, methanol conversion rates of 80 % at maximum are reported.

For ethanol, ATR is more challenging compared to methanol because of the cleavage of the C-C bond. Reaction temperatures of about 450 – 600 °C are required with mostly transition metals, such as Ni, Rh, Pt, and Ru, partly supported on La_2O_3 or Al_2O_3, at S/C ratios of about 1.3 – 1.6 [179, 181].

$$C_2H_5OH + O_2 + H_2O \longrightarrow CO_2 + 4H_2, \qquad \Delta H^0_{298} = -311.2\frac{kJ}{mol}.$$

Equation C-23

Non-noble metals, such as Ni-Cu, supported on SiO_2 and Al_2O_3 were reported to be very stable under ATR reaction conditions of ethanol [182]. Ethanol is still favored in contrast to methanol due to its lower toxicity and the possibility to produce it from renewable sources.
For logistic fuels, such as gasoline and diesel, in ATR, the same statements can be mentioned in comparison to CPOx. The reforming is quite difficult and high S/C ratios have to be provided to prevent or at least inhibit the high rates of carbon formation when higher hydrocarbon species are used. Compared to the optimum operating conditions of about 700 °C for maximum hydrogen yields, temperatures are usually kept above 800 °C to reduce carbon formation and the formation of metal sulfides that are derive from H_2S, which is formed from the sulfur content in the logistic fuel in the presence of steam [179].

As already mentioned, ATR efficiency relies on both, exothermic CPOx and endothermic SR reaction. The highest efficiency is achieved at the thermo-neutral point, $\Delta H_R = 0$.
Ahmed and Krumpelt [9] introduced a method for the determination of the optimum C/O and S/C ratios for ATR depending on the molecular formula for the fuel.
With regard to **Equation C-7**, **Equation C-24** is introduced including the nitrogen from air:

$$C_xH_yO_z + n\,(O_2 + 3.76\,N_2) + (2x - z - 2n)H_2O \rightarrow x\,CO_2 + \left(2x - z - 2n + \frac{y}{2}\right)H_2 + 3.76n\,N_2.$$

Equation C-24

In this case, n defines the oxygen to carbon molar ratio and determines the molar amount of water needed for full conversion of the fuel to CO_2, $2x - z - 2n$, the maximum achievable hydrogen yield, $2x - z - 2n + \frac{y}{2}$, the maximum hydrogen concentration in the product stream, $\frac{2x-z-2n+\frac{y}{2}}{x+\left(2x-z-2n+\frac{y}{2}\right)+3.76n}$, and the heat of reaction

$\Delta H_R = x\Delta H_{\mathrm{f},CO_2} - (2x - z - 2n)\Delta H_{\mathrm{f},H_2O} - \Delta H_{\mathrm{f},fuel}$. Rearrangement of the latter part determines the molar oxygen content n for thermoneutral operation $\Delta H_R = 0$ to

$$n_o = x - \frac{z}{2} - \frac{1}{2}\left(\frac{\Delta H_{\mathrm{f},fuel} - \Delta H_{\mathrm{f},CO_2}}{\Delta H_{\mathrm{f},H_2O}}\right).$$

Equation C-25

Equation C-25 is also valid for SR ($n = 0$), CPOx ($n = x - \frac{z}{2}$), and total combustion ($n = x + \frac{y}{4} - \frac{z}{2}$). Therefore, the fuel processors efficiency can be determined, which is defined as the usable energy produced, i.e., the yield of H_2, divided by the energy of the fuel used in the process. This can be expressed by the lower heating value (LHV) of hydrogen compared to the LHV of the fuel [9]

$$\eta_{\mathrm{fp}} = \frac{LHV_{hydrogen\ produced}}{LHV_{fuel\ used}},$$

Equation C-26

and was expressed by Lindström *et al*. [7] for an ATR diesel fuel processor as

$$\eta_{\mathrm{fp}} = \frac{\dot{h}_{produced}}{\dot{h}_{diesel}} = \frac{\left(n_{CO} + n_{H_2}\right) \cdot LHV_{H_2}}{n_{diesel} \cdot LHV_{diesel}}.$$

Equation C-27

It should be mentioned that the given efficiency is not the overall efficiency from the APU, since no efficiency for hydrogen conversion in the fuel cell stack is included. Here, only the fuel processor is considered.

C.2.3. Product Clean-up and Optimization – Water-gas Shift and CO Polishing

The three reforming methods described in Chapter C.2.2 produce a gas mixture that mainly consists of hydrogen, carbon monoxide, water vapor, and carbon dioxide, and shall be understood as the gas mixture for which the term “reformate” is used. Its composition depends on the reformer’s operating parameters, characterized by the C/O and S/C ratio, respectively. If no desulfurization of the primary fuel was performed upstream the reformer unit, sulfur-containing species, such as H_2S and COS, are also present in the reformate. Using such kinds of gas mixtures for fuel cell applications, further conditioning and gas clean-up has to be accomplished for maximum fuel cell power output.

In case of sulfur contamination of the reformate, COS hydrolysis can be performed, followed by a conventional liquid phase adsorption. Amine scrubbing is well-established in large-scale power plants. However, these methods lead to large-dimension process units and are impossible to realize in a compact fuel processor system. As indicated in the pre-treatment section, primary fuels are more likely desulfurized in the liquid phase upstream the reformer units, and no more attention is given to sulfur contamination in this chapter, except where it is worth mentioning.

Reducing the CO content of a reformate to the ppm level is vital for PEM fuel cells which can only convert hydrogen to electrical power. Typically, CO conditioning down to 10 ppm or lower is necessary because of the poisoning of the active sites in the anode material (often platinum) and the accompanying suspension of the oxidation reaction. High-temperature fuel cells, such as SOFCs and MCFCs, are insensitive to CO due to their high operating temperature of about 800 °C. At this temperature, the CO is internally shifted to hydrogen and carbon dioxide with steam present in the reformate and therefore provides a further fuel source for hydrogen.

For decreasing CO down to the ppm level, several process technologies are available that are presented in the following. In practice, certain technologies are combined to achieve desired concentrations of CO. The combination of the water-gas shift reaction for bulk CO removal, and preferential oxidation of CO or selective methanation of CO for final clean-up is well established.

The water-gas shift (WGS) reaction, **Equation C-3**, is a well-known, commercially available process technology performed in industrial scale. WGS reduces the CO concentration of a

hydrocarbon reformate from an initial 15 - 20 vol% down to 1 - 2 vol% [63] and, due to thermodynamic limitations at high temperatures, is performed in a two-step process consisting of a high-temperature (HTS) and a low-temperature (LTS) stage. The WGS is an equilibrium-controlled, mildly exothermic reaction and the conversion of CO is favored at temperatures < 200 °C. However, lower temperature favors lower reaction rates, leading to an approximately sixfold increased volume of the WGS catalyst compared to the reforming catalyst [24]. Since the reaction is equilibrium-controlled, the composition of the reformate has influence on the conversion of CO. Depending on the reforming route, higher S/C ratios lead to increased CO conversions, while higher hydrogen content decreases the conversion rate. Therefore, high- and low-temperature stages are necessary for efficient CO removal. HTS is usually performed at temperatures around 350 – 450 °C with catalysts based on Fe_2O_3 and Cr_2O_3 due to their low costs and long lifetime. The catalysts are reduced under reaction conditions and need stringent temperature conditions to form the active phase Fe_3O_4 [183] and to avoid sintering. Promoters, such as Cu and Al_2O_3, are added to conventional HTS catalysts to stabilize the active phase, whereas ZnO and MgO increase the selectivity with respect to methane formation, sulfur resistance, or mechanical strength [184]. Typically, HTS catalysts are not sensitive to sulfur compounds, such as H_2S and COS. Sulfur levels below 100 ppm are tolerated without affecting activity. Sulfur levels above 100 ppm lead to the formation of FeS, which is still WGS-active but with far less activity than Fe_3O_4.

LTS uses $Cu/Zn/Al_2O_3$-based catalysts at temperatures around 190 – 250 °C, since the Fe-based catalysts are less active at lower temperatures. LTS typically lowers the CO content in the effluent gas stream of the HTS down to 0.3 % [183]. Analogous to the HTS catalysts, LTS catalysts are reduced under reaction conditions, and because of the exothermicity of the reduction of initial copper oxides to metallic copper, a precise temperature control is needed to avoid sintering of the catalyst, which results in a lower Cu dispersion. Due to the moderate exothermicity of the reaction, heat removal in WGS is a challenge, and therefore, heat exchangers are implemented between HTS and LTS for temperature control. LTS catalysts are typically highly sensitive to sulfur in the stream, only about 0.1 ppm or less is tolerated. ZnO beds are placed upstream the LTS to remove sulfur components via the formation of ZnS [184].

In terms of mobile applications, conventional WGS reactors are large compared to the size of the fuel reformer and make a compact design more difficult. To reduce catalyst volume and

reactor size, precious metal catalysts are of great interest as they offer much higher activities in WGS. Ceria- and titanium-supported platinum catalysts, operating in a temperature round 250 – 400 °C, have been studied extensively [183, 185, 186]. Pd/Zn-based (250 – 300 °C) [187] and Au-based (150 – 250 °C) [183, 188, 189] catalysts are promising systems for WGS because of their lower operation temperatures at potential conversion rates. However, due to the thermodynamic limitations of the LTS's CO conversion, the content of CO is still far too high for the usage in PEMFCs and has to be further decreased. One technology to this end is preferential oxidation of carbon monoxide (PrOX), which provides good results for the removal of CO down to 10 ppm and below, and thus meets the requirements for PEMFCs in mobile applications [190]. Originally, Pt-based catalysts were used for the selective oxidation of CO in the presence of hydrogen [191], but were replaced by Ru/Al_2O_3 and Rh/Al_2O_3, which are more selective catalysts for PrOX [192]. Platinum tends to reverse WGS chemistry at temperatures above 150 °C, which hinders a full CO removal at these reaction conditions [190]. CuO/CeO_2 catalysts have been reported to be even more selective for the oxidation of CO in the presence of H_2, as a conversion of up to 99 % can be achieved. However, their preparation is quite difficult and precise preparation methods and preconditioning parameters have to be followed as the reduction/oxidation processes on both copper and ceria are responsible for the high activity [193]. Just as LTS, Au-based catalysts are under investigation for PrOX reaction at low temperature, but no stable catalysts has been reported yet to meet acceptable CO conversion over a longer period of time under realistic reaction conditions [190].

A further technology for CO polishing down to the ppm level is selective methanation of CO (SMET). SMET can be carried out over a broad range of hydrogenation catalysts in the presence of CO_2 and H_2, but temperature control is crucial due to the high exothermicity of the reaction and the occurrence of reverse WGS at longer resident times [191]. Ru/Al_2O_3 and Rh/Al_2O_3 are reported to be good catalysts even in the presence of carbon dioxide. Takenaka *et al.* [194] investigated Ni-based catalysts for SMET, but achieved only a removal of CO down to 20 ppm (they started at an initial concentration of 0.5 vol%), which is not sufficient for PEMFC operation.

C.3. Fuel cells in APUs

Fuel cells are a key technology for future energy production at a high electrical efficiency level, especially for mobile applications. Fuels cells convert an electro-chemical energy carrier to electrical power. The favored energy carrier of the current technology status is hydrogen. Hydrogen is oxidized with atmospheric oxygen, thereby forming electrical energy and water. Unlike the battery, fuel cells do not run down or require recharging. They operate as long as fuel is supplied to the cell, producing electricity and heat.

Fuels cells are very attractive for the concerns of APUs. The hydrogen, provided from a fuel processor which ordinary operates with a fossil-based primary fuel, is converted at higher efficiency with lower emissions compared to the commonly-used electrical generators that are driven by an internal combustion engine. As the fuel cell process relies on chemistry and not on combustion, emissions are lower than emissions from the cleanest fuel combustion process [2].

In general, fuel cells are divided into two main groups [14]:

- Low-temperature (LT) fuel cells, operating at temperatures below 300 °C
- High-temperature (HT) fuel cell, operating at temperatures above 600 °C

Electricity generation in the fuel cell is generally related to redox reactions that involve the migration of ionic species from the electrodes, cathode and anode, through the electrolyte membrane. The conversion of chemical energy into electrical energy occurs at the interface between electrodes that form the electric circuit with the power consumer, and the electrolyte [195]. A general overview over common types of fuel cells, including operation temperature, redox reactions, and electrical efficiencies, is given in **Table C-5**.

Depending on the underlying application, the specific characteristics of a fuel cell type determine if the fuel cell is suitable for the process, e.g., with regard to operating temperature, the used primary fuel, weight, start-stop characteristics, and costs.

Table C-5: Overview of common types of fuel cells for high- and low-temperature operation, adapted from [99, 195] and [14]. Electrical efficiency is referred to with respect to the lower heating value of the commonly-used type of fuel.

	SOFC	**MCFC**	**PEMFC**	**PAFC**	**DMFC**
Operating temperature	600 – 1000°C	~ 650°C	60 – 120°C (HT-PEM up to 170 – 180°C)	190 – 200°C	25 – 90°C
Electrolyte	Yttria stabilized ZrO_2	Li_2CO_3 K_2CO_3	Nafion (poly-benzimidazole)	H_3PO_4	Nafion
Anode material	Ni-ZrO_2	90% Ni, 10% Cr	Pt Pt/C	Pt/C	Pt Pt/C
Cathode material	Sr-doped $LaMnO_3$	Li-doped NiO	Pt Pt/C	Pt-alloy/C	Pt Pt/C
Anode reaction	$H_2 + O^{2-} \rightarrow H_2O + 2e^-$	$H_2 + {CO_3}^{2-} \rightarrow H_2O + CO_2 + 2e^-$	$H_2 \rightarrow 2H^+ + 2e^-$	$H_2 \rightarrow 2H^+ + 2e^-$	$CH_3OH + H_2O \rightarrow CO_2 + 6H^+ + 6e^-$
Cathode reaction	$O_2 + 4e^- \rightarrow 2O^{2-}$	$O_2 + 2CO_2 + 4e^- \rightarrow 2{CO_3}^{2-}$	$O_2 + 4H^+ + 4e^- \rightarrow 2H_2O$	$O_2 + 4H^+ + 4e^- \rightarrow 2H_2O$	$3/2\, O_2 + 6H^+ + 6e^- \rightarrow 3H_2O$
Cell electrical efficiency	45 - <70 % (CH_4, CO, H_2)	50 - <70 % (CH_4, H_2)	30 – 60 % (H_2, reformate)	35 – 60 % (H_2, reformate)	20 - 30 % (MeOH/water)

LT fuel cells are attractive because of their fast start-stop characteristics, which are important for mobile applications, but have much higher requirements on the quality of the fuel than the HT fuel cells. The latter are more fuel-flexible due to CO content and the capability to internally reform methane. This feature improves the overall efficiency when

the fuel cell stack and the reformer unit are thermally-coupled in an integrated stack design. Furthermore, HT fuel cells have higher electrical efficiencies than the LT fuel cells because of kinetic limitations at lower operation temperatures. However, longer start-up times are necessary as a certain temperature is necessary for sufficient ion migration and the provision of electrical power. Nevertheless, the higher energy demand of HT fuel cells is balanced with the LT fuel cell's energy requirements for reformate processing and CO removal. However, besides a specific type, fuel cells have only few moving parts and thus require less maintenance compared to electric generators and have furthermore high efficiencies even at part load.

Since both are of great interest in the APU concept, the SOFC and the PEMFC are explained in more detail in the following two chapters.

C.3.1. Solid Oxide Fuel Cells

Due to high efficiency and low emissions, SOFCs are mainly used in large, stationary power facilities. Their usage in mobile applications is quite low, because of their long start-up period. short term usage still causes problems for SOFCs because, due to micro cracks in the ceramic materials, frequent temperature cycles lead to material fatigue and failure. However, the ability of direct internal reforming of CO and methane make the SOFC very attractive for applications in which hydrogen is generated by a reforming process of a hydrocarbon fuel.

Hydrogen, carbon monoxide, and methane can be fed to the SOFC, whereas hydrogen is the actual converted fuel for electricity production. CO and methane are converted to hydrogen via WGS or internal reforming in the presence of water at operating temperatures of 800 – 1000 °C. Typical electrolytes are solid-state ZrO_2/Y_2O_3 membranes with O^{2-} as conducting ion. Ni/ZrO_2 cermet is commonly used as anode material, while the cathode is based on doped perovskites, mainly a doped lanthanum manganite ($LaMnO_3$, $LaSrMnO_3$, $LaCoO_3$). Cell power densities of about 0.2 – 0.3 W cm^{-2} can be reached at electrical efficiencies < 70 %, but typically > 50 % [14].

Due to the high operation temperature, lifetime and durability of SOFCs depends on the number of start-up and cool-down cycles. LT SOFCs with improved electrode materials for

sufficient ion conduction at temperatures around 600 °C are under development. Lower operating temperatures would result in less material stress and, due to metallic materials solutions instead of current high-cost materials, would simplify the system's sealing problem, [195, 196].

Thanks to internal reforming, SOFC have no limitation in CO and methane content. However, sulfur has to be removed from the stream to avoid poisoning of the Ni-sites ,cf. Chapter C.2.1 and [197]. Furthermore, Haga *et al.* showed that phosphorus content even in ppb levels leads to Ni phosphides in case of Ni-based anodes and cell performance degradation [198].

Two main cell designs exist, tubular and planar. Planar design is similar to the LT fuel cells and can be produced very simple and in a compact manner. However, sealing and external manifolds are the major limitations, but, compared to the tubular design, much higher power densities (up to 2 W cm^{-2}) can be achieved [196]. The tubular design was introduced by Westinghouse in 1980 and has the major advantage that the HT seals, which are needed for the planar design, are eliminated. Nevertheless, higher internal ohmic losses due to the tube length and the resulting long in-plane path of the electrons are a major drawback, resulting in lower power densities of about 0.25 - 0.3 W cm^{-2} [196].

Major advantages of the SOFC compared to LT fuel cells are the non-precious metal catalysts and the tolerance of CO-containing reformate. Furthermore, integrated heat recuperation has a potential for high overall system efficiency.

C.3.2. Proton Exchange Membrane Fuel Cells

PEM fuel cells are the most common type of fuel cells used in mobile applications. Hydrogen is the only fuel that can be converted by the PEMFC at a temperature operating range of 60 – 120 °C. Typical electrolytes are proton-conducting polymer electrolyte membranes, a so-called ionomer, with carbon-supported platinum metal catalyst electrodes and H^+ as conducting ion. The anode-membrane-cathode assembly is very thin, which makes the system compact. For the desired cell voltage of the stack, these assemblies are connected in series via bipolar plates. Cell power densities of about 0.5 – 1.0 W cm^{-2} can be reached at electrical efficiencies < 60 %. PEMFCs are operated at very high relative humidity values to

maintain the proton movability inside the membrane, which is related to the water content in the material [23]. This limits the temperature operating range to about 90 °C. If the pressure increases, slightly higher temperatures are reachable (< 120 °C) with modern, tuned membrane materials. Nevertheless, strong research activities are afforded to develop materials for higher temperature operation [195].

Conventional PEMFCs are sensitive to carbon monoxide due to the strong bonding of CO on Pt, and thus hinder the adsorption and dissociation of hydrogen. CO levels below 10 ppm are necessary to avoid poisoning of the Pt/C active sites, which results in anode overpotentials and decreased current densities. Pt/Ru-based catalysts show an improved tolerance towards CO and can handle concentrations of approximately 100 ppm without activity loss at high current densities [195, 199]. Exceeding a CO content of 10 ppm in the fuel feed necessitates further upstream purification, as there are no CO-tolerant anode catalysts available. Preferential oxidation, as already mentioned in Chapter C.2.3 in certain levels (about 100 ppm), can be performed directly on the anode by injecting about 2 vol% of air into the reformate stream. Newer CO-tolerant catalysts are based on Pt-alloys or Pt/Ru-alloys, which show higher activities in CO oxidation [200].

Other species besides CO have negative effects on the PEMFC anode. Sulfur poisoning is discussed in Chapter C.2.1. Furthermore, small concentrations of several ppm of oxygenates, such as formaldehyde and formic acid, which mainly derived from the reforming process, are harmful and can lead to irreversible damage of the electrodes.

C.4. Balance of Plant

In the previous chapters, the concept on an auxiliary power unit was presented, and the main operational parts, such as fuel processor and the fuel cell stack, were introduced. For stable long-term operation of a fuel processor and of course the fuel cell stack, a precise control of the various parameters for optimum performance is essential. Therefore, not only the reformer and the fuel cell stack need to be considered, but also multiple other components such as sensors, electronic controls, pumps, start-up power sources, burners, heat exchangers, steam generators, sulfur removal units, water recovery units, thermal

insulation, and filters. All parts contribute to the overall processor assembly and shape the balance of plant (BOP) [201, 202].

Depending on the parts integrated in a certain reformer unit, more or less challenges have to be faced. Fuel processors are sensitive to a constant flow rate and a precise and a well-defined mixture of fuel, air and steam to achieve high conversion efficiencies. Therefore, high demands are made on each component, especially at high temperatures, when an accurate flow control is essential to avoid temperature drifts or peaks in order to observe material limits and safety issues [145].

The balance of plant can roughly be divided into three different sections: the fuel feed management, the thermal management, including reformer / stack heat-up, cool down, and heat exchangers for different temperature zones, and the control system. The fuel feed management consist of the fuel pumping, atomization, evaporation, air control, and the homogeneous mixing of the reactants. In case of gaseous species, the accurate flow control is quite easy, but it becomes considerably more challenging when liquid fuels are used. Issues such as the defined atomization, evaporation, mixing with air below the auto-ignition point, and the avoidance of pre-combustion are still in the focus of the present research. Fuel breakthrough must also be avoided, otherwise coking of the reformer and the downstream fuel cell stack is the consequence, ending up in system failure. Reformers are usually operated at temperatures between 800 – 1000 °C. Therefore, depending on the used fuel cell stack, a heat management system is necessary. The temperature has to be controlled for downstream WGS shift and PrOX reactors and for fuel cells operating at lower temperatures. Several heat exchangers can be implemented in a fuel processor system, which makes it possible to recycle energy by preheating inlet flows or steam generation. Furthermore, steam can be condensed from the anode´s exhaust gas or the burners for water recycling. When high-temperature fuel cells are used, even the cathode air stream must be preheated to avoid thermal shocks in the stack. But in parallel, heat has to be removed from the stack to avoid thermal hot spots and overheating. High temperature handling also makes high demands on the thermal insulation materials, as most technical and electronic parts are not design for a high-temperature environment. Commonly-used insulation materials are based on ceramic materials such as zirconia, alumina, and silica, because of their low thermal conductivity and weight. Due to the dynamic behavior of the fuel processor, electronic components have to be resistive enough for on-board

environment but must also provide precise control with a minimum variance of error. Therefore, a sophisticated balance of plant is essential for a successful commercial implementation of such systems.

D. Mechanism M1 and M2, Surface Mechanism

The mechanisms M1 and M2 used in Study 1 (Chapter 5) are publicly accessible on www.detchem.com.

The surface mechanism for the catalytic experiment simulation is shown below (taken from [49] and publicly accessible on www.detchem.com):

Reaction	A (cm,mol,s)	Ea kJ/mol
H2 +2Rh(s) --> H(s) +H(s)	0.010E-00[a]	0.0
O2 +2Rh(s) --> O(s) +O(s)	0.010E-00[a]	0.0
C3H8 +Rh(s) --> C3H8(s)	5.800E-03[a]	0.0
CH4 +Rh(s) --> CH4(s)	8.000E-03[a]	0.0
H2O +Rh(s) --> H2O(s)	1.000E-01[a]	0.0
CO2 +Rh(s) --> CO2(s)	1.000E-05[a]	0.0
CO +Rh(s) --> CO(s)	5.000E-01[a]	0.0
H(s) +H(s) --> Rh(s) +Rh(s) +H2	3.000E+21	77.8
O(s) +O(s) --> Rh(s) +Rh(s) +O2	1.300E+22	$355.2\text{-}280\theta_{O(S)}$[b]
H2O(s) --> H2O +Rh(s)	3.000E+13	45.0
CO(s) --> CO +Rh(s)	3.500E+13	$133.4\text{-}15\theta_{CO(S)}$[b]
CO2(s) --> CO2 +Rh(s)	1.000E+13	21.7
C3H8(s) --> C3H8 +Rh(s)	1.000E+13	30.1
CH4(s) --> CH4 +Rh(s)	1.000E+13	25.1
C3H8(s) +Rh(s) --> C3H7(s) +H(s)	3.700E+21	55.0
C3H7(s) +H(s) --> C3H8(s) +Rh(s)	3.700E+21	56.6
C3H7(s) +Rh(s) --> C3H6(s) +H(s)	3.700E+24	73.4
C3H6(s) +H(s) --> C3H7(s) +Rh(s)	3.700E+21	75.9
C3H8(s) +O(s) --> C3H7(s) +OH(s)	1.700E+24	71.5
C3H7(s) +OH(s) --> C3H8(s) +O(s)	3.700E+21	31.3
C3H7(s) +O(s) --> C3H6(s) +OH(s)	3.700E+24	88.7
C3H6(s) +OH(s) --> C3H7(s) +O(s)	3.700E+21	45.3
C3H6(s) +Rh(s) --> C2H3(s) +CH3(s)	3.700E+24	83.7
CH3(s) +C2H3(s) --> C3H6(s) +Rh(s)	3.700E+21	55.8
C2H3(s) +Rh(s) --> C(s) +CH3(s)	3.700E+21	35.6
C(s) +CH3(s) --> C2H3(s) +Rh(s)	3.700E+21	118.7
H(s) +O(s) --> OH(s) +Rh(s)	5.000E+22	83.7
OH(s) +Rh(s) --> H(s) +O(s)	3.000E+20	37.7

H(s) +OH(s) --> H2O(s) +Rh(s)	3.000E+20	33.5
H2O(s) +Rh(s) --> H(s) +OH(s)	5.000E+22	106.4
OH(s) +OH(s) --> H2O(s) +O(s)	3.000E+21	100.8
H2O(s) +O(s) --> OH(s) +OH(s)	3.000E+21	171.8
C(s) +O(s) --> CO(s) +Rh(s)	5.200E+23	97.9
CO(s) +Rh(s) --> C(s) +O(s)	2.500E+21	169.0
CO(s) +O(s) --> CO2(s) +Rh(s)	5.500E+18	121.6
CO2(s) +Rh(s) --> CO(s) +O(s)	3.000E+21	115.3
CO(s) +H(s) --> HCO(s) +Rh(s)	5.000E+19	108.9
HCO(s) +Rh(s) --> CO(s) +H(s)	3.700E+21	$0.0+50\theta_{CO(S)}$ [b]
HCO(s) +Rh(s) --> CH(s) +O(s)	3.700E+24	59.5
CH(s) +O(s) --> HCO(s) +Rh(s)	3.700E+21	167.5
CH4(s) +Rh(s) --> CH3(s) +H(s)	3.700E+21	61.0
CH3(s) +H(s) --> CH4(s) +Rh(s)	3.700E+21	51.0
CH3(s) +Rh(s) --> CH2(s) +H(s)	3.700E+24	103.0
CH2(s) +H(s) --> CH3(s) +Rh(s)	3.700E+24	44.0
CH2(s) +Rh(s) --> CH(s) +H(s)	3.700E+24	100.0
CH(s) +H(s) --> CH2(s) +Rh(s)	3.700E+24	68.0
CH(s) +Rh(s) --> C(s) +H(s)	3.700E+21	21.0
C(s) +H(s) --> CH(s) +Rh(s)	3.700E+21	172.8
CH4(s) +O(s) --> CH3(s) +OH(s)	1.700E+24	80.34
CH3(s) +OH(s) --> CH4(s) +O(s)	3.700E+21	24.27
CH3(s) +O(s) --> CH2(s) +OH(s)	3.700E+24	120.31
CH2(s) +OH(s) --> CH3(s) +O(s)	3.700E+21	15.06
CH2(s) +O(s) --> CH(s) +OH(s)	3.700E+24	114.5
CH(s) +OH(s) --> CH2(s) +O(s)	3.700E+21	36.82
CH(s) +O(s) --> C(s) +OH(s)	3.700E+21	30.13
C(s) +OH(s) --> CH(s) +O(s)	3.700E+21	136.0

[a] Value initial sticking coefficient

E. Scientific publications and conferences

E.1. Publications

[1] Torsten Kaltschmitt and Olaf Deutschmann, **Fuel Processing for Fuel Cells**, *Fuel Cell Engineering - Model-based Approaches for Analysis, Control and Optimization*, (Ed: K. Sundmacher), Elsevier, **2012**.

[2] Torsten Kaltschmitt, Claudia Diehm, and Olaf Deutschmann, **Catalytic Partial Oxidation of Isooctane to Hydrogen on Rhodium Catalysts: Effect of Tail-Gas Recycling**, *Industrial & Engineering Chemistry Research, dx.doi.org/10.1021/ie201712d*

[3] Torsten Kaltschmitt, Lubow Maier, Marco Hartmann, Christian Hauck, Olaf Deutschmann, **Influence of gas-phase reactions on catalytic reforming of isooctane**, *Proceedings of the Combustion Institute*, *Volume 33, **2011**, 3177-3183*

[4] Claudia Diehm, Torsten Kaltschmitt, and Olaf Deutschmann, **Hydrogen production by partial oxidation of ethanol/gasoline blends over Rh/Al2O3**, *Catalysis Today, **2012***
(submitted)

[5] Marco Hartmann, Torsten Kaltschmitt, Olaf Deutschmann, **Catalytic partial oxidation of higher hydrocarbon fuel components on Rh/Al_2O_3 coated honeycomb monoliths**, *Catalysis Today*, *Volume 147, **2009**, S204-S209*

E.2. Conference oral presentations

Torsten Kaltschmitt, Marco Hartmann, Lubow Maier, Claudia Diehm, and Olaf Deutschmann, *1st International Symposium on Chemistry of Energy Conversion and Storage*, Fritz-Haber-Institute, Berlin, Germany (**2011**).

Torsten Kaltschmitt, Lubow Maier, Marco Hartmann, Christian Hauck, Olaf Deutschmann, *33th International Symposium on Combustion*, Tsinghua University, Beijing, China (**2010**).

Claudia Diehm, Torsten Kaltschmitt, Olaf Deutschmann, *22nd North American Catalysis Society, National American Meetings*, Detroit Michigan, USA (**2011**).

E.3. Poster presentations

Torsten Kaltschmitt, Sven Lichtenberg, and Olaf Deutschmann, *15th International Conference on Catalysis*, München, Germany (**2012**).

Torsten Kaltschmitt, Sven Lichtenberg, Lubow Maier, and Olaf Deutschmann, *45th Jahrestreffen Deutscher Katalytiker*, Weimar, Germany (**2012**).

Alexander Zellner, Lea Burger, Torsten Kaltschmitt, and Olaf Deutschmann, *45th Jahrestreffen Deutscher Katalytiker*, Weimar, Germany (**2012**).

Claudia Diehm, Torsten Kaltschmitt, and Olaf Deutschmann, *45th Jahrestreffen Deutscher Katalytiker*, Weimar, Germany (**2012**).

Torsten Kaltschmitt, Marco Hartmann, and Olaf Deutschmann, *122nd BASF International Summer Course*, Ludwigshafen, Germany (**2011**).

Claudia Diehm, Torsten Kaltschmitt, and Olaf Deutschmann, *EuropaCat X*, Glasgow, United Kingdom (**2011**).

Torsten Kaltschmitt, Marco Hartmann, Claudia Diehm and Olaf Deutschmann, *21st International Symposium on Chemical Reaction Engineering*, Philadelphia, USA (**2010**).

Marco Hartmann, Torsten Kaltschmitt and Olaf Deutschmann, *21st International Symposium on Chemical Reaction Engineering*, Philadelphia, USA (**2010**).

F. Curriculum vitae

Personal information

Name	Torsten Kaltschmitt
Date of Birth	July 16th, 1981
Citizenship	German
Personal status	single

Work

05/2012	**hte company AG**, Heidelberg Project manager R&D Solutions - Refinery

PhD study

10/2007 - today (till 05/2012)	**PhD study**, Karlsruhe Institute of Technology (KIT) Institute for chemical technology and polymer chemistry Institute for Nuclear and Energy Technologies Group of Prof. Dr. Olaf Deutschmann PhD thesis topic: „ Catalytic Reforming of Higher Hydrocarbon Fuels to Hydrogen: Process Investigations with Regard to Auxiliary Power Units “

Tertiary education

10/2001 - 10/2007	**Ruprecht-Karls-Universität,** Heidelberg Course of studies: Chemistry Topic of diploma thesis „Catalyst development for the conversion of dimethylether to hydrocarbons“

Education

1992 - 2001	**Friedrich-Ebert-Gymnasium**, Sandhausen Degree: general qualification for university entrance
1988 - 1992	**Geschwister-Scholl-Grundschule**, St.Ilgen

Scientific internships and activities

08/2011 – 08/2011	**BASF SE**, Ludwigshafen *Participant*, 122nd International Summer Course
Since 12/2010	**BASF SE**, Member of the European Talent Pool
08/2006 - 03/2007	**hte AG**, Heidelberg *Assistant, Reseach and Development*
05/2006 - 07/2006	**hte AG**, Heidelberg *Student apprentice, Research and Development*
02/2006 - 02/2006	**DECHEMA**, Frankfurt Chemical technology II (chemical reaction engineering)
10/2004 - 10/2004	**DECHEMA**, Frankfurt Chemical technology I (basic process engineering operations)

Danksagung

Für das Gelingen dieser Arbeit möchte ich mich bei allen bedanken, die maßgeblich meine Arbeiten unterstützt haben. Mein Besonderer Dank gilt im Besonderen

Prof. Dr. Olaf Deutschmann für die interessante Aufgabenstellung und die Betreuung meiner Arbeit, sowie das Vertrauen und die Freiheiten bei der Ausübung und Darstellung meiner wissenschaftlichen Arbeiten.

Dr. Marco Hartmann und Sven Lichtenberg für die interessanten Diskussionen und Anregungen, die mentale und physische Unterstützung, sowie die unzähligen Kaffeediskussionen im Chicco. Danke! War echt eine spitze Zeit! Und natürlich Sven für die komplette elektrische Planung und Konstruktion von CPOX II.

Dr. Lubow Maier für die Simulationen zu meiner Arbeit und die Diskussionen über Experiment und Theorie.

der Umicore AG & Co. KG für die Bereitstellung des Modelkatalysators.

der DFG für die finanzielle Unterstützung.

Prof. Dr. Jan-Dierk Grunwaldt für die Übernahme des Korreferats

allen Beteiligten der Werkstätten vom KIT CS, ins besondere Andreas Wagner, Alexander Jaks und Richard von Budberg, für die Fertigung meiner manchmal auch etwas absonderlichen Konstruktionsplanungen. Ohne euch würde CPOX II nicht laufen!

Dr.-Ing. Matthias Hettel, M.A. Yvonne Dedecek und Jutta Heil für die Verwaltungsarbeiten und die Unterstützung außerhalb des Labors.

M.A. Yvonne Dedecek und Rebecca Klinkig für das Korrekturlesen in Englisch.

Ich möchte mich ganz herzlich bei allen Kollegen am CS und CN für die Unterstützung (besonders Steffen, Angi und Kathrin im CT Grundpraktikum), Diskussionen und schönen Stunden sowie bei meinen Kollegen vom CN für die herzliche Aufnahme bei meinem Wechsel vom KIT CS nach CN bedanken. Danke auch an Jutta, Dunja, Kurt, Nadja und Martin für die morgendliche Kaffeerunde. Was haben wir gelacht…

Ich wünsche meinen beiden Nachfolgern Dipl.-Chem. Claudia Diehm und Dipl.-Chem. Alexander Zeller viel Erfolg bei ihrer weiteren Promotion und danke euch für die tolle Zeit während eurer Diplomarbeiten.

Zuletzt möchte ich ganz besonders Daniela und meiner Familie für die liebevolle Unterstützung in den letzten Jahren danken. Deren Rückhalt hat meine Arbeit in dieser Form erst möglich gemacht.

Erklärung:

Ich versichere hiermit, dass ich die vorliegende Dissertation selbst verfasst habe und mich keiner anderen als der von mir ausdrücklich bezeichneten Quellen und Hilfsmittel bedient habe.

Karlsruhe, den 02. Juni 2012 _____

(Torsten Kaltschmitt)